# Dispersal dynamics and connectivity-driven conservation strategies for kelp and mangrove ecosystems


by

Gabriela Thompson Saud

B.Sc., Pontifical Catholic University of Chile; M.Sc., University of Queensland


In December 2024

For the degree of Doctor in Philosophy (PhD)

In the College of Science and Engineering

James Cook University

## Acknowledgments

I am deeply grateful for all the support I received during my PhD, which made the journey of writing this thesis an incredible experience. My deepest thanks go to Dr. Alana Grech, my primary advisor and an extraordinary mentor. Her encouragement to pursue my ideas and her unwavering support throughout the process have meant the world to me. I am also immensely thankful to Dr. Severine Choukroun, who worked closely with Alana to guide me, showing endless patience as I developed my programming skills. A special thanks to Dr. Andres Ospina-Alvarez, who also taught me invaluable programming skills and introduced me to network analysis, a key component of my thesis. I am so grateful for the months I spent in his lab, where he provided guidance and shared his expertise side by side with.

I also want to acknowledge the early support I received from the ARC Centre of Excellence for Coral Reef Studies, particularly Janet Swanson and Vivian Doherty, as well as the College of Science and Engineering, especially Tammy Walsh, who was always there to quickly help me with travel paperwork. My thanks also go to Melissa Joyce and Melissa Cowan for their assistance and to the Fisheries Planning & Assessment Unit of the Queensland Government for granting me the permits needed to carry out my fieldwork.

My sincere thanks go to everyone who contributed to my journey. Prof. Alistair Robertson, for his invaluable guidance during my mangrove fieldwork and experiments—his expertise made it all possible. Dr. Murray Logan and Dr. Erin Graham, for their help with statistics and programming. Sebastian Vazquez and Douchan Hanuise, for assistance with the biophysical models for the kelp and mangrove chapters. Dr. Mirjam Van Der Mheen and Dr. Adam Canning, for their invaluable expertise, which greatly supported my mangrove modelling and understanding of mangrove conditions in the Great Barrier Reef. Dr. Alejandra Mora-Soto and Dr. Erasmo Macaya, for sharing their insights on *Macrocystis pyrifera* distribution and ecology. To my friends and fieldwork volunteers—Chieh Lin, Emily Webster and Dr. Kyana Pike—who made the fieldwork such an enjoyable experience.

Finally, I want to thank my family and friends, whose support has been a constant source of strength. My deepest gratitude goes to my parents, Luis Thompson and Evelyn Saud, for their endless support and trust in me. Thank you to my siblings, Camila and Juan Pablo Thompson, who were there for all the important moments and took such good care of my beloved dog, Baltasar, during my absence. I'm grateful for my friends all over the world—especially those back in Chile, who have been with me since the beginning and those in Townsville, who supported me through every step of this journey. Your support made my time here so much better.

## Statement of contribution of others

Funding for this thesis was provided by James Cook University, the Australian Government Research Training Program (RTP) Scholarship and the Australian Research Council Centre of Excellence for Coral Reef Studies (CE140100020). I also received support for conference attendance and travel from the ARC Centre of Excellence for Coral Reef Studies, the College of Science and Engineering and TropWATER.

All chapters of my thesis received conceptual guidance and editorial assistance from my primary advisor, Dr. Alana Grech. In **Chapters 2 and 3**, Dr. Alana Grech and Dr. Andres Ospina-Alvarez contributed to the conceptualization of the papers, while Dr. Cristian Salas and Sebastian Vazquez contributed to the development of the hydrodynamic model and Dr. Alana Grech, Dr. Andres Ospina-Alvarez, Dr. Severine Choukroun, Dr. Cristian Salas and Sebastian Vazquez provided statistical and editorial assistance. In **Chapter 4**, Dr. Alana Grech and Prof. Alistair Robertson were involved in the conceptualization of the paper, Dr. Murray Logan contributed to the statistical analysis and Dr. Alana Grech, Prof. Alistair Robertson, Dr. Andres Ospina-Alvarez, Dr. Severine Choukroun and Dr. Mirjam Van Der Mheen provided statistical and editorial assistance. In **Chapter 5**, Dr. Alana Grech contributed to the conceptualization of the paper, Douchan Hanuise and Dr. Severine Choukroun contributed to the development of the biophysical model, Dr. Adam Canning contributed to the NDVI analysis and Dr. Alana Grech, Dr. Severine Choukroun, Douchan Hanuise, Dr. Andres Ospina-Alvarez and Dr. Adam Canning provided statistical and editorial assistance.

## Abstract

Dispersal and connectivity are fundamental processes that enhance ecosystem resilience and support species persistence by maintaining ecological linkages between habitat patches. Marine macrophytes, such as kelp and mangroves, form highly interconnected systems. However, challenges in assessing and integrating dispersal and connectivity often lead to these aspects being overlooked in management plans. This thesis explores species-specific dispersal patterns and the incorporation of connectivity objectives in management through two case studies: *Macrocystis pyrifera* in the Southeast Pacific and mangroves in the central Great Barrier Reef (GBR), Australia.

In Chapter 2, I developed a biophysical model to predict the dispersal patterns of giant kelp along the western coast of South America. Using a combination of hydrodynamic and individual-based models, I simulated kelp fragment movements over a 12-year period, focusing on the role of environmental factors in shaping dispersal patterns within the Humboldt Current System. The findings highlight a key settlement area in southern Chile, where favourable ocean currents and environmental conditions increase the likelihood of reaching a suitable habitat. Shorter dispersal distances—typically around 50 km—enhance settlement probability, underscoring the role of local environmental dynamics in sustaining kelp populations. I identified complex northward dispersal pathways for kelp fragments, shaped by the combined influence of wind and ocean currents. The findings also underscore the importance of seasonal changes—particularly in autumn and winter, when favourable winds facilitate reaching a settlement area. The influence of El Niño-Southern Oscillation (ENSO) cycles is also apparent, with fragments dispersing farther during El Niño phases. The results of Chapter 2 provide insight into the dynamic dispersal patterns governing kelp populations and how different environmental drivers affect them.

In Chapter 3, I used the biophysical model outputs from Chapter 2 to analyse the connectivity of *M. pyrifera* populations, aiming to identify key connectivity areas to prioritise them for conservation. Applying graph theory and network analysis, I identified critical connectivity nodes, particularly in the southern region (36–43°S), which serves as a primary source area supporting both local and long-distance dispersal. Central regions exhibit more pronounced fluctuations in connectivity due to seasonal and ENSO variability, impacting kelp replenishment patterns. Based on these findings, I recommend establishing no-take zones in the southern region to protect this important and well-connected area, as well as adaptive seasonal closures to accommodate temporal changes in connectivity in the central populations. Additionally, community detection analysis revealed clusters with high internal connectivity, allowing the identification of key source areas within each community to protect connectivity. Chapter 3's connectivity-driven framework illustrates how regional dynamics

shape kelp dispersal, highlighting the importance of incorporating connectivity insights into sustainable management strategies for kelp forests.

In Chapter 4, I assessed the dispersal and connectivity of mangroves in the central GBR. I employed an experimental approach to evaluate buoyancy traits and salinity responses across 13 mangrove species over a 90-day period. My analysis revealed significant interspecies variability in the effects of varying salinity on propagule buoyancy and early growth characteristics. Most species exhibited buoyancy traits at some point during the experiment with some able to float for extended durations, indicating their potential for long-distance dispersal. Morphological and buoyancy traits unique to each species provided crucial data, such as windage and drift factors, to parametrise biophysical models which are essential for refining dispersal predictions. These findings highlight the importance of incorporating species-specific parameters into biophysical models, as different mangrove propagules exhibited varying behaviours. Overall, Chapter 4 highlights the complexities of mangrove dispersal and offers data to enhance the accuracy of dispersal modelling, which is crucial for understanding connectivity within mangrove ecosystems.

In Chapter 5, I utilized the experimental outputs from Chapter 4 to parameterize biophysical models for the mangrove species *Rhizophora stylosa* and *Bruguiera gymnorhiza* in the central GBR. In the biophysical model, I incorporated species-specific parameters like propagule buoyancy to simulate dispersal patterns over a 90-day period, with hourly outputs to capture the complexity of their movement within the central GBR. I then applied network analysis to the model outputs to evaluate their connectivity. I mapped habitat patches based on five connectivity-driven management objectives and combined this information with data from the 2023 *Southern Great Barrier Reef Mangrove and Saltmarsh Condition Survey* to develop an urgency index for prioritising management. My results identified critical areas, such as replenishment sources and key connectivity corridors, which face increasing threats from climatic and anthropogenic pressures. These findings underscore the necessity of integrating connectivity into management strategies, particularly under initiatives like the Blue Carbon Initiative and the Emission Reduction Fund, aimed at reducing emissions and enhancing carbon sequestration through ecosystem protection and restoration. Chapter 5's framework identifies priority areas where protection and restoration efforts can strengthen mangrove resilience and connectivity, thereby supporting both biodiversity conservation and climate mitigation initiatives. Furthermore, it has the potential to be applied to study dispersal and connectivity in other ecosystems and locations worldwide.

Overall, this thesis underscores the importance of incorporating dispersal dynamics and connectivity into conservation strategies for marine macrophytes. It demonstrates the value of employing robust

biophysical models that incorporate site- and species-specific information to accurately represent connectivity. By accounting for environmental variability, including ENSO events and seasonal changes, management efforts can better align with ecological processes and support ecosystem resilience. The recommendations provided in this thesis for both kelp and mangrove ecosystems advocate for connectivity-informed management measures such as no-take zones, adaptive harvest closures and protection of key connectivity habitats. This work provides a framework for using connectivity to guide spatial planning and policy, ultimately enhancing the long-term sustainability of these critical marine ecosystems.

# Table of Contents

# List of tables

# List of figures

# Chapter 1: General introduction

The dispersal and connectivity of coastal and marine organisms are important functions in the replenishment and recovery following disturbance events, maintaining population structure, supporting genetic diversity and responding to invasive species and transmission of diseases (Cowen et al., 2007). Marine dispersal refers to the movement of organisms (or propagules) from their natal place to a new location, driven by currents, tides and wind, and in some cases by biological vectors, such as organisms carrying propagules, while connectivity refers to how populations or habitats are linked through this dispersal (Balbar and Metaxas, 2019). Oceanic and wind driven currents as drivers of dispersal are especially important during the first stage of life (e.g. propagule, spores and larval) where units can passively travel with currents for short or long distances. For some sessile species, this drift in an early stage of their life represents the only mechanism of dispersal. Therefore, identifying dispersal corridors is critical when managing marine species with a pelagic phase (Steneck et al., 2009, Van der Stocken et al., 2019b). Ensuring the protection of key areas of supply and connectivity enhance population viability (Beger et al., 2010). Nevertheless, quantitative information on dispersal and connectivity is rarely incorporated in management plans (but see, Balbar and Metaxas (2019), Ospina-Alvarez et al. (2020b), mainly due to the significant time and financial resources required to obtain empirical data on dispersal and connectivity (Magris et al., 2014).

Connectivity assessments during early life stages are typically performed by observing the age of drifting individuals (Shanks, 2009, Macaya et al., 2005), studying larval behaviour in the water column (Paris et al., 2008) and analysing parental DNA (Hedgecock, 2017, Palumbi, 2003, Weersing and Toonen, 2009, Castorani et al., 2015). While these techniques can provide useful insights, they often fail to capture the full extent of species distribution and are typically limited to short observation periods. Due to the impracticality of tracking millions of propagules in the field, researchers have developed indirect methods to estimate probable dispersal pathways, overcoming these challenges. One of these approaches are biophysical models that use hydrodynamic models of ocean circulation to drive individual based models (IBMs) of propagule transport (Werner et al., 2007) (Figure 1). The IBM contains the biological parameters of the organism (e.g. size, buoyancy, vertical movement, orientation, reproductive time and mortality). The hydrodynamic model integrates currents, tides and winds information, which interact among them. The output of the biophysical model is the potential dispersal pathways of organisms.

Dispersal data from biophysical models can be used to construct connectivity matrices, which are then applied in network analysis and graph theory to explore ecological linkages (Figure 1). Graph theory is the study of the mathematical component of graphs and network analysis is a branch of graph theory

that applies these theories to understand real-world networks. Networks are the graphical representations of habitat connectivity (Treml et al., 2008) and both matrices and networks provide key information about connectivity. Using network analysis, emergent properties of each habitat patch and dispersal routes can be obtained (Treml et al., 2008, Rayfield et al., 2011, Ospina-Alvarez et al., 2020b). Network analysis quantifies habitat connectivity by representing networks as nodes, which represent habitat patches, and links between nodes, which indicate potential dispersal routes. Weights can be assigned to nodes and links to provide information about the strength of the connections and the importance of each habitat patch within the network. Network analysis enables a series of measures to infer the attributes of the connectivity between habitats (Rayfield et al., 2011, Ospina-Alvarez et al., 2020b, Pastor et al., 2022, Grech et al., 2018, Treml et al., 2008, Van der Stocken et al., 2019a).

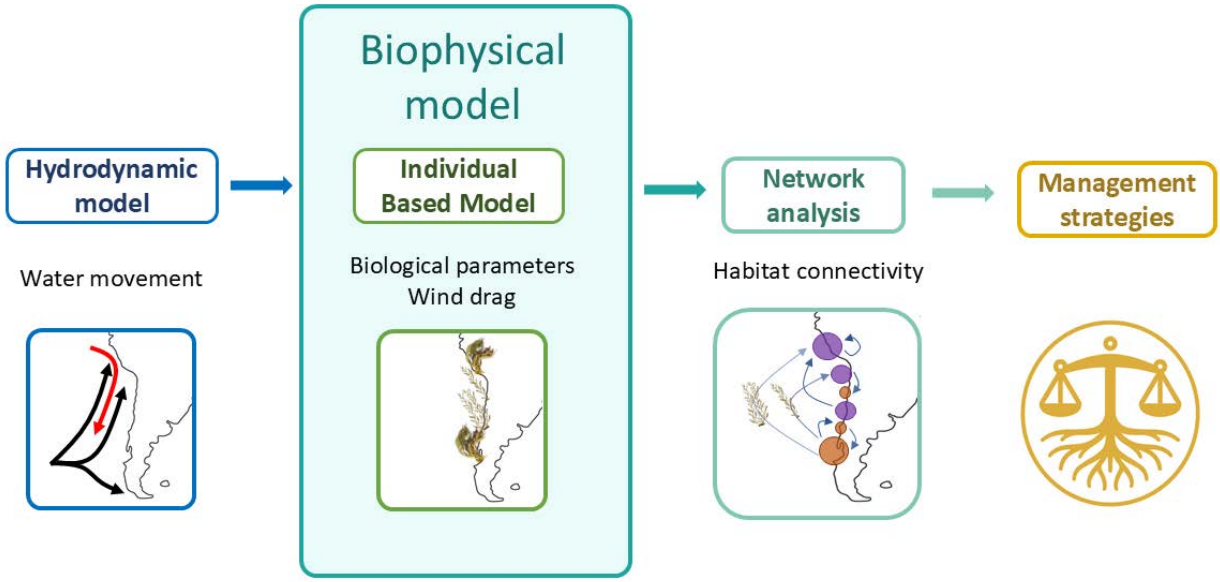


**Figure 1.** Diagram illustrating the analytical approach applied in this thesis. The hydrodynamic model provides input to the individual-based (biophysical) model, which generates the dispersal pattern of the organism. These dispersal outputs are then used with network analysis to assess connectivity, with insights informing management strategies.

Marine macrophytes, such as kelps and mangroves, form highly interconnected ecosystems, with their dispersal and connectivity largely driven by hydrodynamic processes. Ocean currents and circulation patterns play a crucial role in shaping population dynamics across various spatial scales. Propagules can travel for short (e.g. within bays) or long distances (e.g. transoceanic). The long-distance dispersal capacity of sessile species, such as some kelps and mangroves, suggests the existence of metapopulations, where discrete habitat patches or groups of patches form subpopulations that interact at some level (Castorani et al., 2015, Van der Stocken et al., 2019a, Grech et al., 2018). Particular patches or groups of patches may perform important roles for the metapopulation, acting as sources that provide recruits to other locations or as steppingstones that maintain connectivity

throughout the population. This emphasises the importance of understanding the effect of propagule dispersal and connectivity in population structure at the scale of the distributional range to inform the conservation and management of marine plants. Despite growing recognition of the importance of marine connectivity, a significant knowledge gap remains regarding the connectivity of marine plants, particularly kelp and mangrove forest (Bryan-Brown et al., 2017) (Figure 2). While there have been some efforts to integrate connectivity into management practices, there has been limited progress in directly linking connectivity to specific management objectives, which remains a critical challenge (Beger et al., 2022). In this thesis, I focus on developing biophysical models of the dispersal of *Macrocystis pyrifera* in the Southeast Pacific and mangroves in the central Great Barrier Reef to inform the management of connectivity.

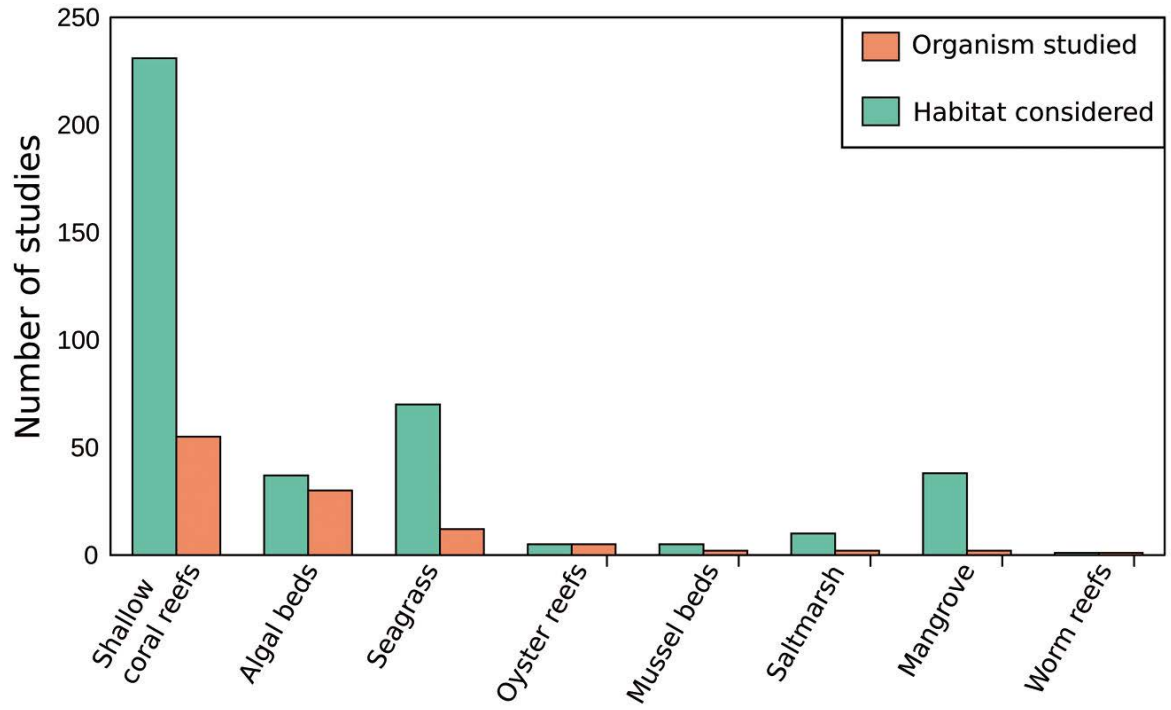


**Figure 2.** Graph from Bryan-Brown et al. (2017) showing the number of studies on connectivity, categorized into those that explicitly consider habitat and those focusing on connectivity between populations of organisms. This graph clearly illustrates that kelp and mangrove forests have received disproportionately less attention than ecosystems such as coral reefs, underscoring the need for more research on the dispersal and connectivity of these habitats.

## *Macrocystis pyrifera* along the Southeast Pacific region

*Macrocystis pyrifera* or giant kelp is a brown alga that has a predominantly antitropical distribution in temperate regions. The giant kelp typically grows in the subtidal zone and can reach lengths of up to 40 metres, making it the largest alga and benthic organism in the world. *M. pyrifera* forms submarine kelp forest on rocky or thick sand substratum (Graham et al., 2007). Along the Chilean coast and parts of the Peruvian coast, *M. pyrifera* is distributed from 6°S (northern Peru) to 55°S (Patagonia). Two

ecomorphs exist within this range: *intergrifolia*, found in the northern population (6-32°S), and *pyrifera*, present in the southern population (37-55°S; Figure 3) (Buschmann et al., 2004).


**Figure 3.** Distribution of *Macrocystis pyrifera* in the Southeast Pacific. a) Kelp distribution along the Chilean and Peruvian coast. b) South America with the Southeast Pacific region shown on the left side.

The giant kelp plays an important ecological role in the Southeast Pacific region. As an ecosystem engineer, it forms dense kelp forests that provide habitat and shelter for numerous species. Additionally, *M. pyrifera* significantly contributes to the economy, primarily through alginate extraction and as a food source for the abalone industry (*Haliotis rufescens*) (Villegas et al., 2019). Over the past two decades, kelp forest extraction has increased significantly, driven by high international demand for raw seaweed (Villegas et al., 2019). Most of this extraction is carried out by

small-scale fisheries, which harvest kelp from natural forests (Porras, 2019). For a decade, kelp forests were harvested indiscriminately in the Southeast Pacific region due to a lack of regulations, leading to overexploitation. This is particularly concerning in northern Chile and Peru, where most of the extraction occurs (Porras and Vásquez, 2020).

In response to concerns about overexploitation, regulations were implemented in both Chile and Peru. In Chile, a local-level management plan for the giant kelp was introduced—the first seaweed in the country to receive such a plan. Then, in 2013, a new law was enacted to regulate all seaweed extraction along the Chilean coast, incorporating both regional and local strategies. Harvesting is controlled through TURF (Territorial Use Rights in Fisheries), a co-management strategy designed to sustainably extract and protect common resources (Albornoz and Glückler, 2020). Similarly, in Peru, regulations for giant kelp have been in place since 2009, prohibiting kelp removal without the necessary permits (Avila-Peltroche and Padilla-Vallejos, 2020). While these measures have helped curb the indiscriminate extraction of *M. pyrifera*, the current state of kelp populations remains a concern (Steneck et al., 2002). A deeper understanding of ecosystem processes is needed to improve conservation strategies at multiple scales. For example, well-connected populations of *M. pyrifera* contribute to a healthy metapopulation by enhancing resilience during disturbance events (Hughes et al., 2005). Protecting key areas that supply propagules and maintain connectivity could enhance population viability. However, connectivity patterns and long-distance dispersal trajectories of *M. pyrifera* in the Southeast Pacific region are still largely unknown.

Understanding the ecology and life history of giant kelp is crucial for protecting the species and its ecosystem services. The reproductive period of *M. pyrifera* varies significantly depending on environmental conditions and nutrient availability (Carney and Edwards, 2010, Buschmann et al., 2006a). It has a heteromorphic life cycle, consisting of a macroscopic sporophyte stage and a microscopic gametophyte stage. The gametes are produced in specialized blade clusters near the holdfast, with a single blade capable of generating up to 12 million spores per day. Typically, these spores move short distances using their two flagella before settling (Kinlan et al., 2003b). However, due to their aerocyst structures, which provide buoyancy, kelp fragments and the spores contained within the sporophyte's sorus can float and drift with ocean currents and winds, allowing them to passively travel long distances, sometimes exceeding 100 or even 1,000 kilometres (Gaines et al., 2007). Floating fertile fragments of *M. pyrifera* could drift up to 2,700 kilometres (Bernardes-Batista et al., 2018). The detached plant can survive for up to 125 days and the spores remain viable during this period (Hernández-Carmona et al., 2006, Hobday, 2000, Macaya et al., 2005).

Biophysical models have been employed to analyse the dispersal and connectivity of *M. pyrifera* primarily in the northern hemisphere. In southern California (USA), population connectivity was estimated using a three-dimensional ocean model (ROMS) alongside Lagrangian particle tracking to monitor kelp dispersal. By complementing the biophysical model with genetic information, researchers found that demographic connectivity of kelp forests significantly influences population dynamics, with well-connected populations reducing the probability of extinction (Castorani et al., 2015). A similar study was conducted in the Santa Barbara Channel (USA), where researchers also utilized a biophysical model and genetic data to explain the connectivity of *M. pyrifera* along the channel, finding that ocean currents predominantly influence the connectivity patterns (Alberto et al., 2011). These studies highlight the potential of employing a biophysical model along the Southeast Pacific coast to understand critical ecosystem processes associated with giant kelp. The outputs of such models will aid in identifying key areas of connectivity and supply, which can inform management practices. By protecting areas that play a vital role in population dynamics, the viability of kelp populations can be enhanced. Furthermore, the information on dispersal and connectivity can be utilized to prioritise regions for restoration and to implement more sustainable harvesting practices.

## Mangroves of the Great Barrier Reef region, Australia

Mangroves are halophytic trees uniquely adapted to thrive in intertidal saltwater environments, where they regulate water uptake and exclude salt through a combination of physiological and structural mechanisms (Reef and Lovelock, 2015). Often saturated with water and subject to anoxic environments, these trees are distributed across tropical and subtropical regions worldwide, with estimates suggesting around 80 species of mangroves exist globally. In the central Great Barrier Reef (GBR), mangroves are found along the entire coastline (Figure 4), with 41 species documented in the GBR, covering an area of approximately 1,240 km² (Duke, 2006). Mangroves adjacent to the GBR are among the healthiest mangrove communities globally, providing habitat and sustenance for a diverse array of species. These ecosystems support numerous invertebrates, including crustaceans, molluscs and insects, while also sheltering vertebrates such as juvenile fish, mammals, reptiles and birds (Goudkamp and Chin, 2006). By fostering such biodiversity, mangrove communities play a crucial role in maintaining the ecological balance of coastal environments. Additionally, mangroves provide essential coastal protection by reducing erosion, buffering against storm surges and acting as natural barriers to extreme weather events, thereby enhancing climate resilience (Othman, 1994, Marois and Mitsch, 2015, Maza et al., 2021, Asari et al., 2021). In addition to their ecological importance and role in protecting coastlines, mangroves are recognised as critical carbon sinks (Bouillon et al., 2008), thus contributing to climate mitigation and adaptation by sequestering large amounts of carbon in their

biomass and soils (Lovelock and Reef, 2020). Given their capacity to store carbon, initiatives like the Blue Carbon framework have prioritised the restoration and protection of mangrove ecosystems (Alongi, 2020, Zeng et al., 2021). This global effort invests significantly in conserving these areas, not only to safeguard biodiversity but also to enhance carbon sequestration as part of broader climate change mitigation strategies. Protecting these carbon-rich ecosystems is vital for both local communities and global efforts to reduce greenhouse gas emissions.


**Figure 4.** a) Distribution of Mangroves in the central Great Barrier Reef (GBR) developed by Dunning (2010). b) Australia with Queensland (QLD) highlighted in brown and the Great Barrier Reef World Heritage Area (GBRWHA) highlighted in red.

Even though various legal frameworks, such as the *Queensland Fisheries Act* 1994, Fish Habitat Areas and the *Great Barrier Reef Marine Park Zoning Plan* 2003, aim to protect mangroves in the GBR, these ecosystems continue to face significant threats from both human activities and natural disturbances.

Land development, coastal pressures and declining water quality are major drivers of habitat loss, while storms, cyclones and invasive species also contribute to the degradation of mangrove forests (Duke et al., 2003, Houston, 1999, McKillup and McKillup, 1997, Dutta Roy et al., 2024, Adame and Reef, 2020). Over the last four decades, mangrove distribution in the GBR has been significantly altered, with some areas experiencing expansion while others face contraction (Duke et al., 2003, Hamylton et al., 2023, Chamberlain et al., 2020, Canning and Duke, 2013). To enhance conservation efforts, it is crucial to deepen our understanding of the ecological processes that sustain these habitats. For instance, understanding the dispersal and connectivity pathways of mangroves can help identify critical propagule sources that replenish populations following disturbances. This knowledge can guide management decisions to preserve key areas that contribute to the ecological resilience of mangrove ecosystems, ensuring long-term conservation success.

Reproduction in mangroves is a key process that must be understood to protect mangrove forests and the ecosystem services that they provide. The reproductive cycle begins with flowering, which varies across mangrove species. In the GBR, most mangroves bloom in warmer months, typically spring to early summer, with pollination facilitated by insects, birds, mammals or wind. After successful pollination, the flowers develop into seeds, usually during the summer months. Mangrove species exhibit two reproductive strategies: viviparous and non-viviparous. In viviparous species, the seed remains attached to the tree until it germinates into a propagule before detaching. In contrast, non-viviparous species release their seeds, which germinate separately from the parental tree (Tomlinson, 2016). Once detached, propagules might settle near the parental tree or travel long distances. Long-distance dispersal is facilitated by the propagules' positive buoyancy, which allows them to float for extended periods, driven by ocean currents, tides and winds (Van der Stocken et al., 2019b). Propagules can remain afloat for an average of 75 days, although this period can vary depending on the species (Van der Stocken and Menemenlis, 2017).

While mangrove connectivity has been studied in several regions (Van der Stocken et al., 2019a, Hamilton et al., 2017, Di Nitto et al., 2013, Van der Stocken and Menemenlis, 2017, Gouvêa et al., 2023, Ngeve et al., 2016, Proisy et al., 2016, Zainol et al., 2022, Kennedy et al., 2017), it has received disproportionately less attention compared to other ecosystems like coral reefs (Bryan-Brown et al., 2017). This is mostly because there is a lack of intertidal oceanographic connectivity models. Most of these models resolve offshore currents and do not extend into the surf zone. However, there are some studies on mangrove dispersal and connectivity. For instance, a notable global study by Van der Stocken et al. (2019a) combined an ocean model and IBM to track propagule transport, finding that propagule transport can be along the coasts, but also transoceanic (i.e. Atlantic, Pacific and Indian Oceans). They also found that there are islands that work as key areas of connectivity across the

Pacific. Several local biophysical studies have examined mangrove connectivity in specific regions (Hamilton et al., 2017, Di Nitto et al., 2013, Van der Stocken and Menemenlis, 2017, Proisy et al., 2016), all highlighting the significant influence of ocean currents and winds on propagule dispersal and population dynamics. Some studies also integrated genetic data with biophysical models. For example, Ngeve et al. (2016) in Cameroon found that ocean currents and historical sea-level rise shaped the local mangrove communities, while Kennedy et al. (2017) in Florida demonstrated the role of ocean circulation changes in determining community structure. These studies underscore the importance of understanding ocean dynamics in mangrove dispersal. Applying biophysical models to the GBR with accurate parameters based on empirical data could reveal key dispersal pathways and vital population dynamics, which would significantly enhance mangrove management. By identifying critical patches and dispersal routes, conservation strategies could prioritise areas for protection and restoration. Such insights are also valuable for decision-making when assessing the ecological impact of mangrove removal.

## Thesis goal and outline

Dispersal and connectivity are essential for promoting ecosystem resilience and ensuring species persistence by maintaining ecological links between habitat patches. Although kelps and mangroves form highly interconnected ecosystems, dispersal and connectivity processes are rarely incorporated in their management strategies.

The primary goal of my thesis is to inform and enhance management strategies for marine and coastal ecosystems by improving the accuracy and reliability of dispersal and connectivity estimates. These improved estimates will support the implementation of measures that protect kelp and mangrove connectivity, thereby enhancing their resilience to natural and anthropogenic pressures. This is achieved through the integration of species-specific traits into biophysical models, which allows for a more refined understanding of how environmental factors and biological characteristics influence dispersal. By focusing on key species such as giant kelp and mangroves, this research aims to provide actionable insights that promote ecosystem resilience, support biodiversity and guide management and restoration efforts in the face of climate change and anthropogenic pressures. To achieve this goal, the following objectives were identified:

1. Assess dispersal of *Macrocystis pyrifera* in the Southeast Pacific using biophysical models;
2. Investigate connectivity patterns of *M. pyrifera* to derive management lessons;
3. Assess species-specific traits (e.g. buoyancy) for mangrove propagules in the GBR to improve the performance of biophysical models;

4. Assess dispersal and connectivity of mangroves to create an urgency index to prioritise management actions.

This thesis aligns each objective to four data chapters, each presented in the format used for submission to peer-reviewed journals (Figure 5). Contributions for each chapter are detailed within their respective sections.

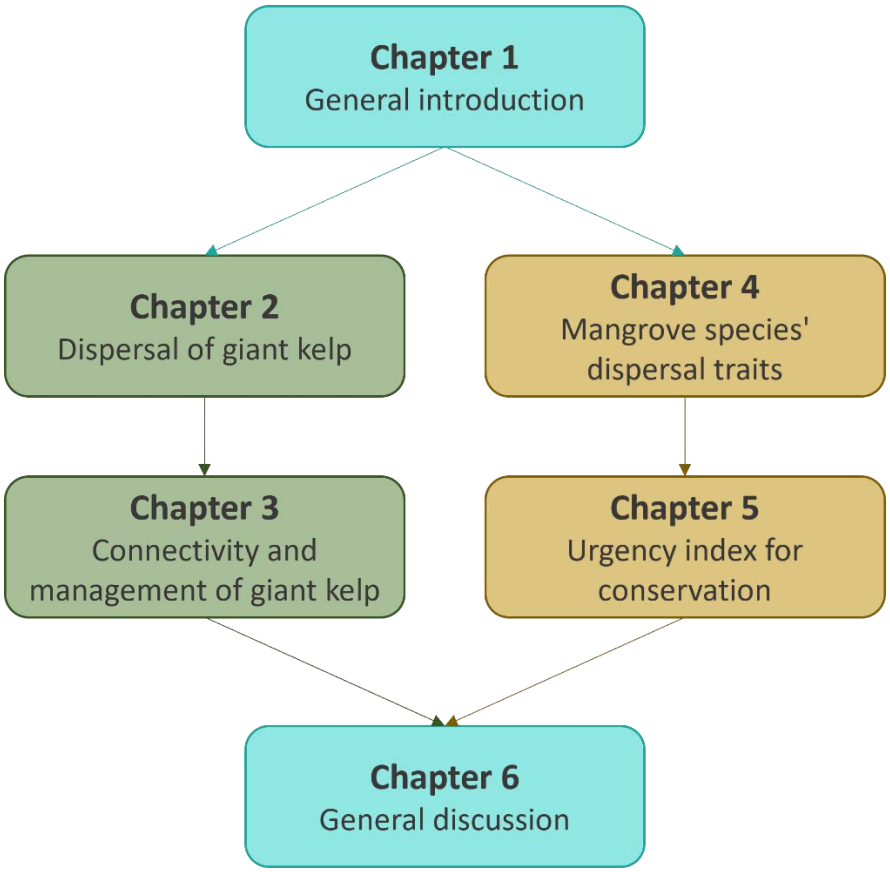


**Figure 5.** Thesis structure.

Understanding the population dynamics of giant kelp is crucial because this species plays a foundational role in marine ecosystems, supporting biodiversity and contributing to ecological balance. By studying how environmental factors, such as ocean currents and climatic variations like seasons and ENSO, affect the dispersal and settlement of kelp, I can uncover patterns that inform conservation efforts. In Chapter 2, I assessed the dispersal of *Macrocystis pyrifera* along the western coast of South America, highlighting the impact of environmental variables and ocean currents within the Humboldt Current System. The analysis employs hydrodynamic and individual-based models over 12 years to delineate dispersal patterns, identify key settlement areas and quantify the effects of seasonal and ENSO changes on kelp dispersal dynamics.

Understanding the dispersal and connectivity of *Macrocystis pyrifera* is critical due to the threats posed by intensive harvesting and climate change. A well-connected population is vital for recovery and replenishment. Identifying key source and sink areas, along with connectivity corridors and well-connected areas, is essential for developing conservation measures to protect this important species. In Chapter 3, I evaluated the connectivity of giant kelp populations in the Southeast Pacific, providing insights for conservation strategies. Outputs from biophysical models and network analysis identify critical source-sink areas and connectivity corridors across spatial and temporal scales. The findings reveal the significance of the southern population for management and highlighted adaptive strategies to address seasonal and ENSO variability in connectivity.

Mangrove forests rely on propagule movement to expand, recover from disturbances and maintain connectivity between populations. However, the dispersal potential of mangrove species is highly variable and depends on specific traits, such as buoyancy and tolerance to different salinity levels, which directly affect how far propagules can travel and their survival during dispersal. By focusing on the buoyancy and morphological traits of 13 different species, this objective sought to provide empirical data that could refine biophysical models, allowing for more accurate predictions of dispersal pathways. In Chapter 4, I investigated the dispersal potential of mangrove propagules by employing an experimental approach involving 13 mangrove species from the central Great Barrier Reef. The study examines the influence of salinity and buoyancy on propagule traits over a 90-day period. Results showcase interspecies variations in buoyancy and responses to environmental factors, offering species-specific parameters for biophysical modelling of mangrove dispersal trajectories.

Connectivity in mangrove ecosystems is crucial for maintaining biodiversity and enhancing resilience against environmental changes. By prioritising connectivity in management frameworks, I can identify critical habitats and corridors for protection and restoration. This approach aids in conservation efforts and aligns with broader initiatives, such as the Blue Carbon Initiative, which seeks to maximize carbon sequestration and mitigate climate impacts. Understanding and incorporating connectivity into management strategies is essential for fostering resilient ecosystems and sustaining their ecological functions. In Chapter 5, I developed a biophysical model to predict the dispersal of *Rhizophora stylosa* and *Bruguiera gymnorhiza*, enhancing the understanding of their connectivity. By mapping habitat patches based on connectivity-driven management objectives and integrating data from the 2023 *Southern Great Barrier Reef Mangrove and Saltmarsh Condition Survey*, along with remote sensing imagery, an urgency index is created for prioritising management actions. The findings underscore the importance of protecting critical areas to enhance mangrove resilience against climate change and anthropogenic impacts.

# Chapter 2: The biophysical dynamics of giant kelp, *Macrocystis pyrifera*: seasonal patterns and dispersal mechanisms in the southeast Pacific [1]


## Abstract

Dispersal and connectivity play important roles in shaping the population structure of giant kelp, *Macrocystis pyrifera,* across the western coast of South America. Its high potential dispersal capacity suggests the existence of metapopulations, where discrete habitat patches or groups of patches form subpopulations that interact at some level. However, the dispersal patterns of giant kelp in this region have not been quantified. Chapter 2 assesses the dispersal and settlement of *Macrocystis pyrifera* in the Southeast Pacific, specifically focusing on the impact of environmental variables and ocean currents within the Humboldt Current System. Using a combination of Hydrodynamic and Individual-Based Models, I analysed kelp fragment movements over 12 years, with a particular emphasis on the effects of the El Niño-Southern Oscillation (ENSO) and seasonal changes. My results highlight a key settlement area in the southern Chilean region. I found that shorter travel distances of kelp fragments increased the likelihood of reaching a suitable habitat, underscoring the importance of local environmental conditions. I delineated intricate northward dispersal paths for kelp fragments, which appear to be governed by the interplay of wind and ocean current dynamics. Seasonal variations, notably in autumn and winter, favour the likelihood of reaching a settlement area due to favourable winds. Furthermore, ENSO events appear to influence dispersal distances, with fragments travelling the longest distances during El Niño phases. These findings are essential for informing kelp conservation strategies in the context of climate change, emphasizing the necessity of considering local and seasonal environmental factors alongside ENSO impacts.



Keywords: *Macrocystis pyrifera,* Humboldt Current System, biophysical modelling, individual-based modelling, kelp, ENSO (El Niño-Southern Oscillation), dispersal


[1] Published as:
Thompson-Saud, G., Grech, A., Choukroun, S., Vásquez, S. I., Salas, C., & Ospina-Alvarez, A. (2024). The biophysical dynamics of giant kelp, *Macrocystis pyrifera*: Seasonal patterns and dispersal mechanisms in the southeast Pacific. Journal of Biogeography, 51(11), 2198-2210.

## Introduction

The effective dispersal and connectivity of coastal and marine organisms are critical for the resilience of marine ecosystems in the face of environmental changes and in sustaining their ecological functions. Dispersal (the movement of organisms or their propagules from their natal place to a new location) and connectivity (the process linking separate populations through dispersal, play essential roles in maintaining genetic diversity and ecological stability (Balbar and Metaxas, 2019, Cowen et al., 2007, Steinberg et al., 2016). Marine currents, including oceanic, coastal and tidal, are key in driving this dispersal, particularly during the first stage of life (e.g., spores, seeds, fruits, eggs, larvae, etc.) as they enable these entities to travel passively with the prevailing currents. For some sessile species, early-stage drift represents the only mechanism of dispersal. The identification of dispersal pathways is critical when managing marine species with a pelagic phase (Steneck et al., 2009, Van der Stocken et al., 2019b) because the protection of key areas of supply and connectivity can enhance population viability (Beger et al., 2010, Pastor et al., 2023). Nevertheless, quantitative information on dispersal and connectivity is often overlooked in management plans (but see (Pastor et al., 2023, Balbar and Metaxas, 2019, Ospina-Alvarez et al., 2020b) due to the challenges in assessing it and the significant costs (both financial and time consuming) associated with gathering empirical data on the scale of dispersal (Magris et al., 2014).

Focusing on giant kelp, *Macrocystis pyrifera*, understanding its dispersal and connectivity is key to comprehending its population dynamics and distribution along the Southeast Pacific coast (Figure 6). This brown alga is widely dispersed in temperate regions, exhibiting a predominantly antitropical distribution and can be found in both the west and east of South America, west coast of North America, South Atlantic, South Africa, central and southern New Zealand and South Australia. The erect plant typically grows in the subtidal zone and can reach up to 40 metres in length, making it the largest algae and benthic organism in the world. *M. pyrifera* forms dense submarine kelp forests on rocky or thick sand substratum (Graham et al., 2007). The giant kelp plays a crucial ecological role along the Southeast Pacific coast, serving as an ecosystem engineer species by creating extensive kelp forests that offer habitat and shelter to a myriad of marine organisms. Additionally, *M. pyrifera* holds significant economic importance, as it is used for alginate extraction and serves as a primary food source for the abalone industry (*Haliotis rufescens*) (Villegas et al., 2019). Most of the seaweed extraction is carried out by small-scale fisheries, which harvest from natural kelp forests, representing an important resource for numerous coastal communities reliant on fisheries (Márquez Porras, 2019). For a decade, the indiscriminate extraction of kelp forests, due to the absence of regulations, led to a high level of exploitation. Despite the current implementation of marine conservation measures by Chile and Peru, such as the establishment of five marine protected areas and 799 Territorial Use Rights

in Fisheries (TURF) in Chile and six MPAs in Peru aimed at promoting sustainable extraction of marine resources, the giant kelp has continued to be indiscriminately harvested, resulting in significant deterioration.

The reproductive period of the kelp varies significantly depending on environmental conditions and nutrient availability (Carney and Edwards, 2010, Buschmann et al., 2006b). It has a complex life cycle with macroscopic sporophyte and microscopic gametes. Spores can move short distances by using their two flagella before settling (Kinlan et al., 2003a). This mode of dispersal via flagella is considered the primary mechanism for spore dispersal (Gaylord et al., 2004). Typically, the dispersal ranges of *M. pyrifera* spores, along with those of other marine macroalgae, are confined temporally and spatially, amounting to durations of hours to days and spanning a few tens of kilometres (Gaines et al., 2007, Reed et al., 1992, Wanner et al., 2024). Nevertheless, under severe weather and oceanic conditions, the spatial extent of dispersal can dramatically increase, enabling the transport of kelp fragments that contain spores over distances surpassing 100 and even 1000 kilometres (Gaines et al., 2007). Taking kelp fragments into consideration, *M. pyrifera* emerges as an organism with the capacity for Long Pelagic Dispersion Phases (LPDP) - extended periods of pelagic dispersal lasting beyond four months (Ramirez-Romero et al., 2023). With aerocysts providing buoyancy, kelp rafts and the spores contained in sorus of the sporophyles, which are located near the base of the kelp, just above the holdfast, remain afloat and are carried by currents and winds. The buoyant nature of *M. pyrifera* significantly influences its distribution, rendering it a pivotal factor in shaping the geographic range of this species. Floating fertile fragments of *M. pyrifera* can drift up to 2700 km (Bernardes-Batista et al., 2018). The detached plant survives up to 125 days, during which time the spores can remain reproductive (Hernández-Carmona et al., 2006, Hobday, 2000, Macaya et al., 2005). In the Southeast Pacific region, Macaya and Zuccarello (2010) documented a notable low haplotype variability relative to other macroalgal species, suggesting a pronounced genetic connectivity within the population. Additionally, Macaya et al. (2005) recovered fertile kelp rafts, underscoring the potential role of dispersal in fostering genetic interconnectedness among individuals within the species. These findings collectively imply that dispersal mechanisms may play a key role in shaping the genetic structure of the Southeast Pacific population of giant kelp.

The long-distance dispersal capacity of *M. pyrifera* suggests the existence of metapopulations, where discrete habitat patches or groups of patches form subpopulations that interact at some level (Castorani et al., 2015, Van der Stocken et al., 2019b). Biophysical models have been demonstrated as a useful tool to assess dispersal and connectivity of *M. pyrifera* in other regions. For instance, Alberto et al. (2011) used biophysical modelling in the Santa Barbara Channel to investigate *M. pyrifera*

populations, revealing that ocean currents are a primary factor in explaining connectivity patterns. Similarly, Castorani et al. (2015) observed that well-connected kelp populations exhibited reduced extinction risk, highlighting the role of enhancing demographic connectivity. These studies underscore the potential utility of biophysical models in deepening the understanding of critical ecosystem processes involving giant kelp. Yet, there is a notable absence of biophysical models to elucidate the dynamics of the giant kelp in the South American region.

This Chapter aims to evaluate the potential dispersal of *M. pyrifera* along the Southeast Pacific coast using a biophysical model. My goal is to explain dispersion of the giant kelp along the Humboldt Current System (HCS) to improve understanding of population dynamics. To achieve this, I implemented a coupled Hydrodynamic-Individual Based Model to simulate the movement of giant kelp fragments, which release spores. I assessed factors (e.g. season and ENSO) that influence changes in the dynamics of the coastal ocean and subsequently affect the transport and dispersion of giant kelp fragments in this eastern boundary upwelling system, noted for its exceptionally high primary productivity. The output of the biophysical model was used to assess the key determinants that impact kelp dispersal distance and the likelihood of successfully reaching a suitable habitat.

## Methods

### Study area

The study area, as discussed in Chapter 1, is situated in the HCS of the Southeast Pacific basin (Figure 6.b), spans from approximately 10 to 43°S. It encompasses the extensive coastlines of Chile (6,435 km) and Peru (3,080 km) which fall within the HCS. *M. pyrifera* distribution stretches along most of the Chilean coast and parts of the Peruvian coast, from 6 to 55°S. In this region, ocean temperatures near the equator (at 6°S) typically range from 19°C to 23.5°C in summer and 15.9°C to 18.2°C in winter, while further south (at 55°S), summer temperatures range from 8.5°C to 10.5°C and in winter, they drop to 5.4°C to 6.6°C. However, the optimal temperature range for *M. pyrifera*, where the majority of plants are found, generally falls between 10°C to 20°C. Two distinct ecomorphs are identified: *intergrifolia*, representing the northern population (6-32°S), and *pyrifera,* the southern population (37-55°S) (Buschmann et al., 2004), divided by a notable upwelling area around 37°S (Aguirre et al., 2012). The distinction between the two ecomorphs lies in the morphology of their holdfasts: while *pyrifera* is characterized by tall holdfasts, *intergrifolia* exhibits flattened ones.

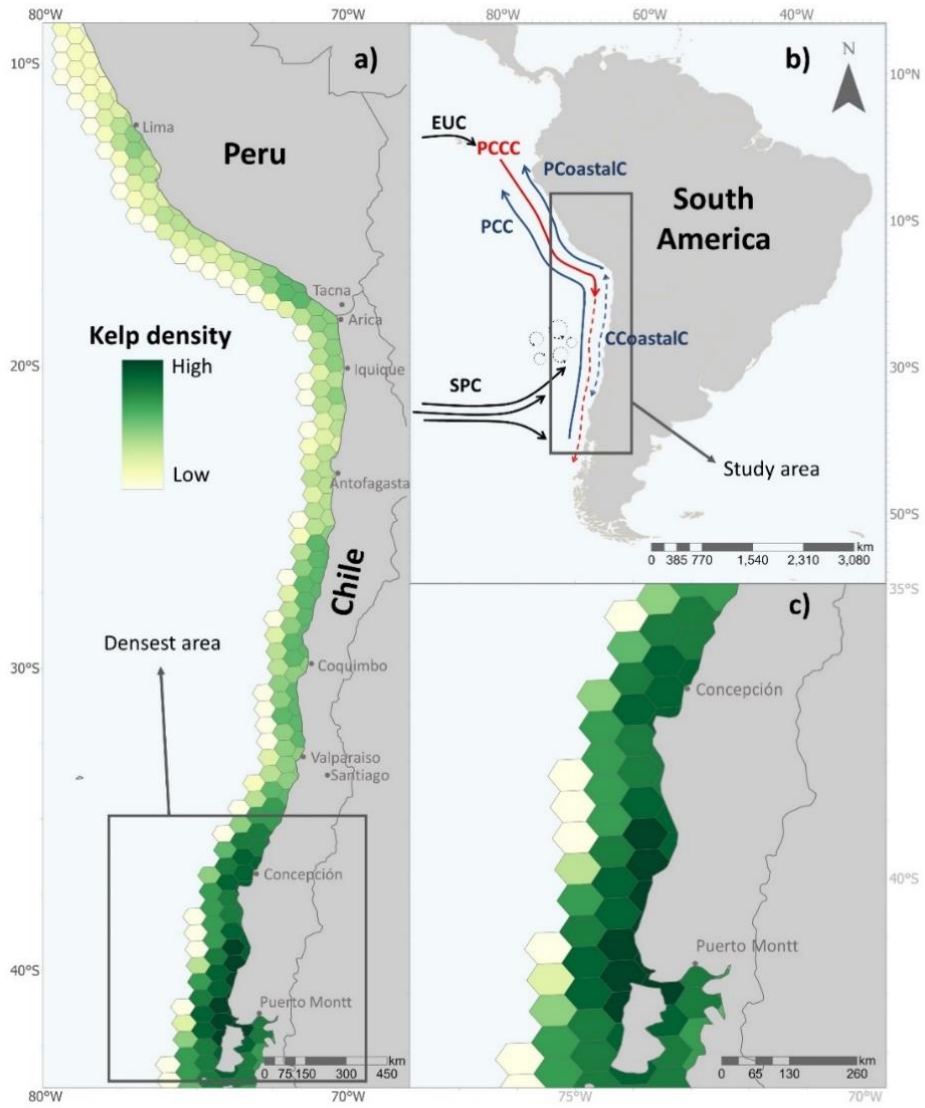


**Figure 6.** Distribution and oceanographic influences on *Macrocystis pyrifera* in the Southeast Pacific. a) Kelp density gradient along the Chilean and Peruvian coast, with darker green indicating higher density kelp forests and lighter green indicating sparser populations. The kelp inhabits primarily in the coastal areas, with lower resolution extending further into the ocean. The density of giant kelp patches was calculated using a kernel density estimation in ArcGIS, with results expressed as the number of kelp patches per square kilometre. b) South America and the prevailing surface currents of the Southeast Pacific. Red and blue arrows denote warm and cold currents, respectively, including the Chile Coastal Current (CCoastalC), Peru Coastal Current (PCoastalC), Peru-Chile Counter Current (PCCC) and Peru-Chile Current (PCC), with their origins traced back to the South pacific Current (SPC) and Equatorial Under Current (EUC). Arrows circled in black signify regions of eddy formation. c) The southern Chilean coast highlighting the area with the densest kelp forest populations relative to other regions. All the maps are in Transverse Cylindrical Equal Area projection.

## Coastal conditions

The HCS, originating from the South Pacific Current, is characterized by its cold, low-salinity, nutrient-rich waters, flowing northward along South America's western coast from southern Chile (~42°S) to northern Peru and Ecuador (~4°S). The upper ocean flow, the Peru-Chile Current System (PCCS), features the equatorward movement of cooler Sub-Antarctic Surface Water (SASW) north of 45°S (Chaigneau and Pizarro, 2005, Montecino and Lange, 2009). The PCCS is significantly influenced by the south-eastern Pacific atmospheric anticyclone, leading to intense upwelling and high productivity.

From 1997 to 2008, the study period, El Niño and La Niña events notably affected the region's oceanography (Figure A1.1), impacting the strength and behaviour of the Humboldt Current and upwelling patterns. Seasonal variations, driven by the South Pacific Anticyclone, also influenced the Humboldt Current, with varying intensity and upwelling in different seasons. For a comprehensive background on the oceanographic conditions, refer to Appendix A1 in the Supporting Information.

### Kelp distribution

The kelp forest distribution map (Figure 6.a) was obtained from a dataset derived from Mora-Soto et al. (2020), which used satellite imagery from Google Earth Engine (Gorelick et al., 2017). This methodology facilitated the detection of *M. pyrifera* canopies that extend to the ocean surface, as well as identifying submerged portions within open ocean waters, typically ranging from the intertidal zone down to depths of about 30 to 40 metres. The dataset represents the mean kelp coverage from 2015 to 2019. However, it should be noted that the map also includes green algae due to limitations in their algorithm, which cannot distinguish between giant kelp and green algae (*Ulvophyceae*) (Mora-Soto et al., 2020). I extracted the map distribution and further refined it in ArcGIS Pro 2.8.0. For enhanced accuracy, polygons indicating kelp presence in habitats where kelp does not grow, such as rivers or sandy beaches, were meticulously vetted and removed. Conversely, regions known for kelp harvesting yet absent in the initial dataset, particularly along the southern Peruvian coast, were added to the kelp density map to reflect actual conditions. To further evaluate the accuracy of the map, I conducted a comparison with the locations of TURFs where giant kelp harvesting is claimed, checking for the presence or absence of kelp. This analysis revealed a high level of accuracy in the map's depiction of kelp distribution. Subsequently, a kelp density map was generated using a grid of 321 hexagons. Each hexagon has a side length of 34 km, yielding an area of around 3000 $km^2$. The grid resolution was selected to balance spatial detail and computational efficiency, ensuring a clear representation of kelp dynamics. This map highlights the kelp distribution along the coastline with varying density using the kelp distribution extracted from Mora-Soto et al. (2020). Notably, the southern regions of Chile exhibit denser kelp populations compared to other areas (Figure 6.c).

### Coupled Hydrodynamic-Individual Based model

Ocean circulation along the Peru-Chile system was modelled using a three-dimensional hydrodynamic framework based on the Regional Ocean Modelling System (ROMS), which was modified to better represent the dynamics of the HCS. The ROMS configuration has a 10 km horizontal resolution spanning 10°N to 50°S and 68°W to 132°W. For this Chapter, the domain was delimited at 43°S as areas beyond this latitude require nested models due to complex hydrodynamics, particularly among the fjords. The model incorporates hydrographic forcings, such as temperature, salinity, wind stress, surface heat flux and transport and freshwater flux, along with initial and lateral boundary conditions,

including temperature, salinity, currents and sea surface elevation. Bathymetric data with a 4 km resolution informed the seafloor contours of the model. Simulations spanned from 1996 to 2008, providing daily outputs, with 1996 serving as a spin-up year excluded from the analysis.

This hydrodynamic model was coupled with a customized version of Ichthyop (Lett et al., 2008), an Individual-Based Model (IBM) tool that incorporates daily ROMS outputs to simulate the physical and biological influences on *M. pyrifera* floating fragments (Table 1). These fragments were represented in the model as virtual particles, representing fertile kelp fragments, such as fronds with aerocysts and sporophylls and emulating their dispersal mechanism (Macaya et al., 2005). However, it is important to note that the model does not explicitly represent the physical characteristics of the kelp fragments, such as their size, morphology or arrangement of fronds and sporophylls. Instead, the focus is on simulating the dispersal of virtual particles representing floating fragments in response to hydrodynamic forces. Each virtual particle embodying an average spore count of 11,200 spores, as this is the average number of spores per gram of sporophyll tissue per hour that kelp fragments have after detachment (Hernández-Carmona et al., 2006). In accordance with the experiments conducted by Hernández-Carmona et al. (2006), a decay rate (Eq. 1) was incorporated to model the decrease in spore numbers over time.

$$N_{(t)} = 13{,}321.2 \times e^{-0.000509 \times t} - 2121.1$$

*Equation 1*

where: *N(t)* is the number of spores at time, *t* (hours), 13321.17 is the initial number of spores (adjusted for the decay curve), 0.000509 is the decay rate, −2121.06 is the constant to fit the curve to the data.

The virtual particles remained afloat for up to 125 days, aligning with evidence of their reproductive capacity duration (Hernández-Carmona et al., 2006), or until beaching, at which point they were removed from the model. Although exposure to water temperatures above 20°C has been linked to reduced reproductive capacity and that spore and germling development is constrained within a temperature range of 21.7°C to 23.8°C (Le et al., 2022, Rothäusler et al., 2009), this was not integrated into the model because most of the particles were in cooler waters. A sensitivity analysis was run to determine the minimum number of particles that can be released to obtain stable results and determined that by releasing 5,000 particles at 5 metres depth per simulation run was effective. The particles were released according to the density map (Figure 6.a). Therefore, in areas of higher density more particles were released. The particles were not released in waters deeper than 500 metres, given that kelp forests are typically confined to coastal regions. This choice was based on the understanding that, for the resolution of the model, a depth of 500 metres serves as the limit for the coastal system.

The model dynamically adjusts the release of virtual particles based on local density conditions, with higher kelp densities resulting in the release of additional particles to reflect increased particle dispersal in crowded areas. While the model does not directly address the physical characteristics of the fragments, the incorporation of density-dependent particle release allows for a realistic representation of the dispersal dynamics observed in natural kelp populations. From 1997 to 2008, there were 10,685,141 recorded spores released.

**Table 1.** Summary of the main input parameters used for the biophysical model of *M. pyrifera* in the Southeast Pacific region.

| Category | Parameters | State / Description |
|---|---|---|
| *Particle-tracking model* | Total number of particles released per simulation | 5000 for each release |
| | Particle types/classes | Particles representing floating fronds/fragments releasing spores |
| *Initiation of pelagic phase* | Release location | Known location of *M. pyrifera* forests (Figure 6.a) |
| | Release events coverage | From 1997 to 2008 |
| | Frequency of release events | Once a week all year round |
| *Transport and movement* | Maximum length of pelagic phase | 125 days |
| | Horizontal dispersion | 10 $m^2s^{-1}$ |
| | Buoyancy | Positive |
| | Vertical migration | No |
| | Direct wind drift | Yes, included as forcing |
| *Settlement* | Settlement rate | Decay rate (Eq. 1) |

The IBM was operational from 1997 to 2008, a period marked by significant El Niño and La Niña events, with weekly particle releases. Due to computational constraints, particle positions were evaluated on specific days post-release (1, 5, 10, 15, 20, 30, 45, 60, 90 and 125). Dispersal distances were calculated using sea distance metrics, a measurement similar to the Euclidean distance but adjusted to account for geographical features along the coastline, using the Haversine formula and the geosphere package in R. I reported the distance travelled based on measurements taken on day 30, as nearly 90% of the spores that eventually settled had already reached the settlement area by that time.

## Statistical analysis

Generalized Additive Model (GAM) was used to evaluate the factors affecting the likelihood of a virtual particle, representing a kelp fragment releasing spores, reaching a suitable habitat (defined as within 500 metres of water depth). I chose the GAM to explore and visualize the complex relationships between environmental variables and particle transport rather than to test specific hypotheses or derive inferential statistics about natural phenomena. Unlike simpler methods such as ANOVA, which are critiqued by White et al. (2014) for their over-reliance on p-values in ecological simulation studies,

GAMs allow for the modelling of nonlinearities and interactions in a flexible, non-parametric framework. This approach is particularly suited to the data, where the goal is to understand complex patterns and relationships rather than to make inferential claims based on controlled sample sizes. The dataset included all particle trajectories. The analysis was performed using the "mgcv" package (Wood, 2017) within the R language and environment for statistical computing (Team, 2010).

Different model families and configurations were tested to ascertain the optimal fit for the study's data. The "DHARMA" package (Hartig, 2020) was used to evaluate overdispersion, selecting the family that most effectively mitigated this issue. A range of model structures was considered, from simpler forms without splines to more complex ones that incorporated multiple splines and interactions among variables. Model performance was evaluated by examining the deviance explained, checking for convergence and employing the Akaike Information Criteria (AIC) from the "MuMIn" package (Barton and Barton, 2015).

The primary response variable "settlement success" (the likelihood of arriving to kelp habitat) was analysed in relation to ENSO phases (El Niño, La Niña and neutral), seasonal periods (summer, autumn, winter and spring), particle travel durations and the geographical coordinates (longitude and latitude) of particle release points. An identification variable (ID) was also included to address the potential autocorrelation in data from repeated measures of the particles' positions.

## Results

### Settlement of kelp spores

A total of 8,158,121 spore arrived to kelp forests patches between 1997 to 2008. This Chapter's findings suggest that virtual particles with shorter drift periods have a higher likelihood of releasing spores that reach settlement areas. Specifically, 45.7% of particles successfully reached settlement areas within the first five days, 35% within the next 15 days and the remaining 19.3% over the subsequent 105 days. Notably, 1.5% of kelp fragments reached settlement areas on the last 35 days of viability and reproductive capability, indicating that most settlement occurred earlier in the dispersal period. A significant northward drift was observed in 82% of cases (excluding local settlement), with a noted southward shift from approximately 37°S. The primary settlement zones were identified between 45 and 35°S in southern Chile (Figure 7 and 8), whereas the zones between 26 to 13°S exhibited the lowest kelp fragments arrival rates.

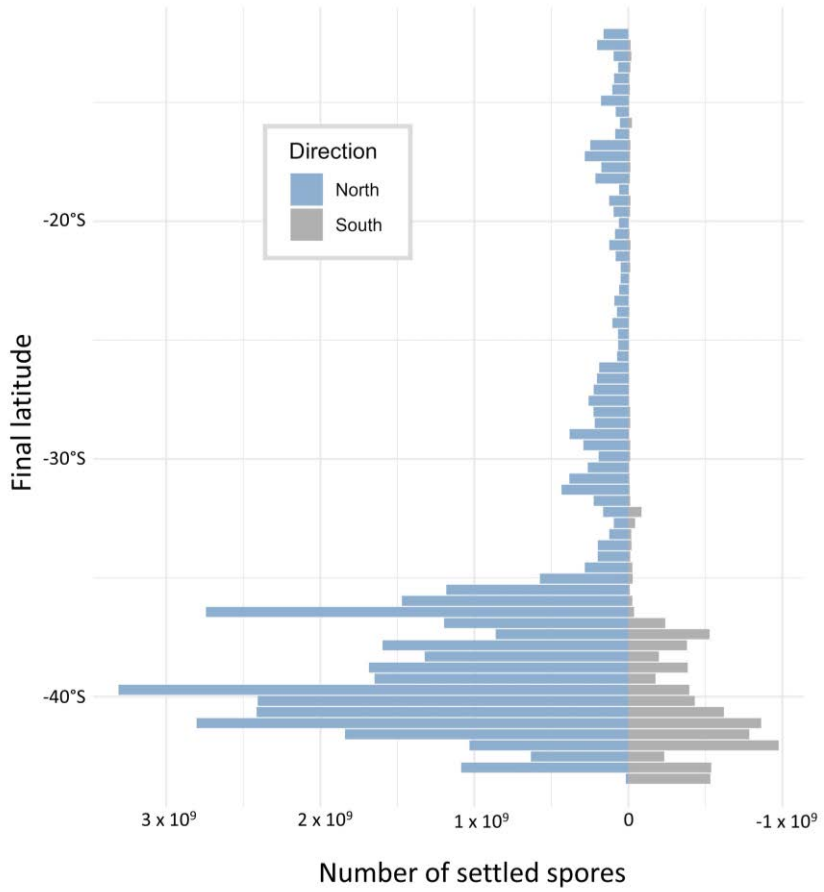


**Figure 7.** Histogram of kelp fragment spore settlement (spores that arrived to kelp forest patches) along latitudinal gradients in the Humboldt Current System (1997-2008). The y-axis represents the final latitude of kelp fragment settlement, ranging from 10 to 45°S. The x-axis quantifies the number of settled particles, scaled in billions. Colour coding distinguishes the direction of fragment drift: northward drift is depicted in blue, while southward drift is shown in grey.

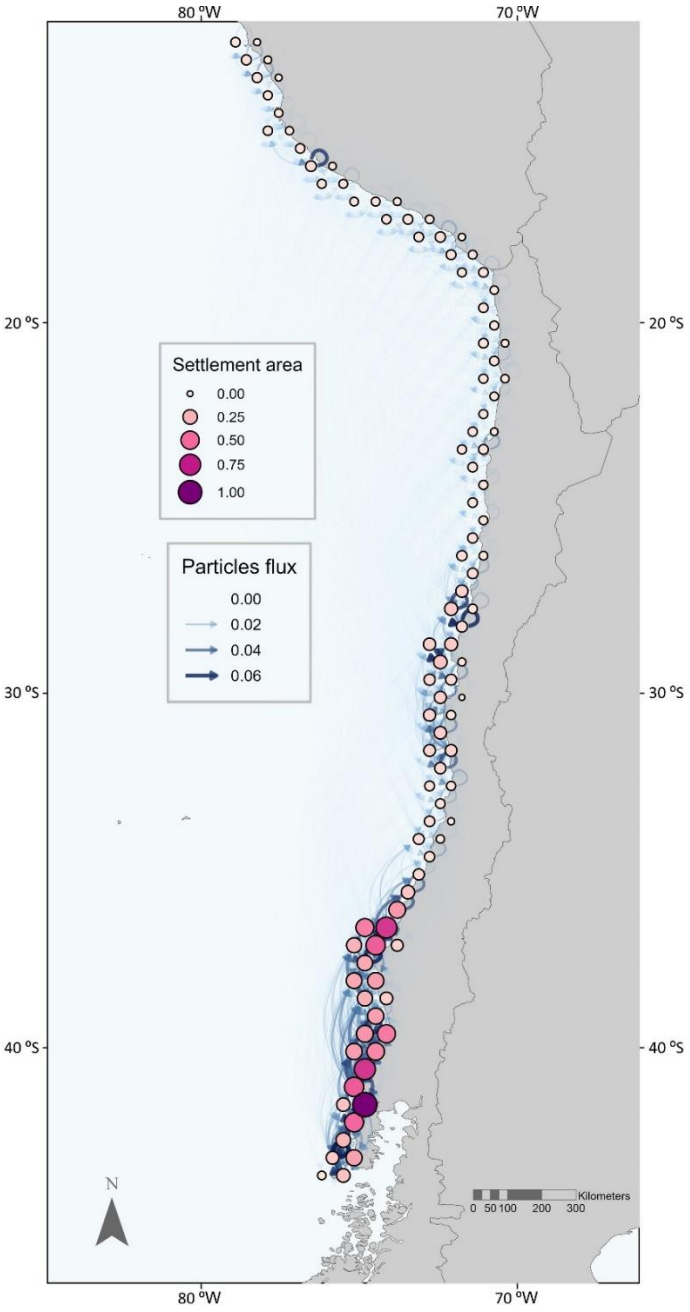


**Figure 8.** Map of kelp fragment settlement and dispersal pathways in the southeast Pacific. Circles indicate settlement density of kelp fragments spores, which is the normalized number of spores reaching a suitable habitat, across the region, with the size and colour gradient representing the normalised concentration from low (small, light pink) to high (large, dark purple). Arrows illustrate the normalised flux of kelp fragments, with direction and thickness indicating the movement and relative quantity of fragments travelling from their release points to settlement areas. In regions of minimal flux, the arrows are nearly transparent to emphasize areas with significant flux.

The model to assess the likelihood of reaching a settlement area operates with binary outcomes, classifying them as either “true” (in coastal area) or “false” (outside of coastal area). The analysis of this binary nature involved logistic regression within a GAM, utilizing a binomial family. This resulting

model comprises a comprehensive range of explanatory variables, encompassing both linear and curvilinear relationships, as outlined in Eq. 2 (Figure A3.2).

$$Settlement\_success = gam(settle \sim s(days\ travelled) + ENSO * season + s(lon_{ini}, lat_{ini}) + s(id, bs = \mathrm{re})$$

*Equation 2*

In the Eq. 2, *ENSO* variable accounts for El Niño, La Niña and neutral conditions, while *season* encompasses the four seasons, both treated as factorial with their interaction included due to their impact on settlement. *Days travelled* represents the time elapsed since the kelp fragment's detachment, with *lon_ini* and *lat_ini* denoting initial coordinates. These, alongside *ID* are numerical factors with non-linear relationships modelled by splines. *ID* also controls for unexplained variance between fragments. This methodological approach facilitates an in-depth evaluation of settlement likelihood factors along the coastline.

All factors, including ENSO phase, season, initial coordinates, days travelled and ID, significantly influenced settlement outcomes ($p < 0.05$). The analysis underscored that winter (79.4% of the spores reached a settlement area, $p < 0.001$) and autumn (78.6%, $p < 0.001$) exhibited the highest number of kelp fragments arriving in settlement areas, displaying significant differences (Table A2.1 and A2.2). Conversely, the lowest kelp fragment counts in settlement areas were observed during spring (73.5%, $p < 0.001$), followed by summer (71.7%, $p < 0.001$). Regarding ENSO conditions, it was found that El Niño periods resulted in significantly higher numbers of kelp fragments reaching settlement areas (78.1%, $p < 0.001$), followed by neutral periods (76%, $p < 0.001$) and La Niña conditions exhibited the lowest (75,8%, $p < 0.001$; Table A2.1 and A2.2). Notably, the interaction between ENSO and season demonstrated an influence on kelp fragments dispersion. The highest kelp fragments settling rate was observed during El Niño in autumn (78.1%, $p < 0.001$) and the lowest was observed during La Niña in summer (74.1%, $p < 0.001$; Table A2.3). Summer, followed by spring were consistently the lowest through all the ENSO conditions. Autumn was higher during El Niño and La Niña, but not during neutral condition, which occurred in winter.

### Dispersal distance

Kelp fragments displayed a median dispersal distance of 48.94 km, ranging from a minimum of less than a metre (0.8 metres) to a maximum of 2051.33 kilometres. Long-distance dispersal, exceeding a thousand kilometres, was uncommon, with such events classified as outliers as it can be observed in Figure 9. Furthermore, it is improbable for a kelp fragment to travel such extensive distances, as it is likely to be carried into deep water or break down into detritus before reaching thousands of

kilometres. A positive relation was evident between travel duration and dispersal distance, kelp fragments averaged 18.58 km on the first day, extending up to 305.19 km by day 125. A directional trend was also observed: 52.2% of spore-releasing kelp fragments drifted northeast (Figure A4.3) and those travelling over 200 km exclusively followed this trajectory. Additionally, 25.1% moved northwest. It was noted that the further a kelp fragment travelled, the less likely it was to reach a settlement area.

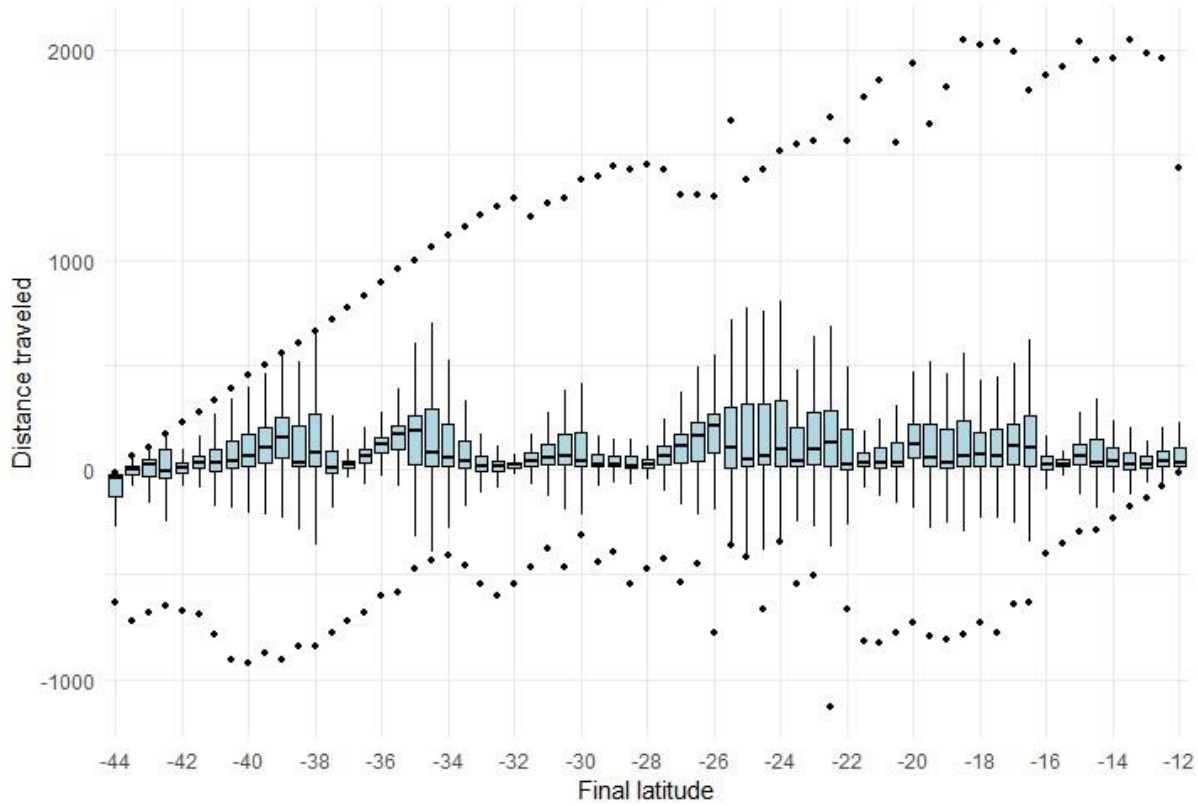


**Figure 9.** Boxplot of dispersal distances for kelp fragments by latitude: northward vs. southward settlement trajectories in the southeast Pacific (1997-2008). Positive values indicate northward travel, while negative values indicate southward travel. The black dots represent the minimum and maximum observed values (outliers).

The longest distances travelled by kelp fragments were recorded between 20 and 30°S from 1997 to 2000 (Figure 10), with a noted decrease in subsequent years. Peak average distances were in 1998, 1999, 2003 and 2007 at 90.3, 90.6, 90.8 and 95.1 km, respectively. In contrast, 2001, 2006 and 2008 show the shortest distances with 45.7, 48.9 and 52.6 km, respectively (Figure A5.4 and Table A5.4).

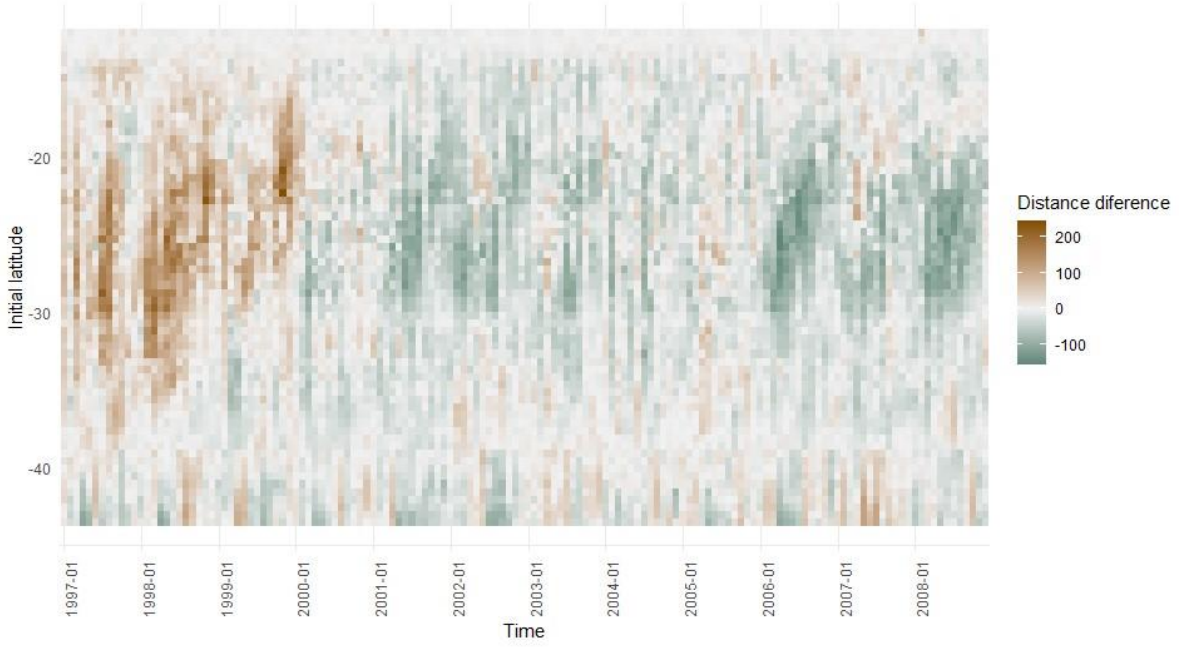


**Figure 10.** Temporal variation matrix of monthly kelp fragment dispersal distances in the southeast Pacific (1997-2008). This matrix illustrates the monthly deviations in average kelp fragment dispersal distance compared to the multi-year monthly average, highlighting increases or decreases in travel distances (km).

I found that ENSO phases and season at release influenced dispersal distance of kelp fragments. With kelp fragments covering greater distances during Spring (mean = 264.3, median = 256.3, SD = 155.3) followed by Summer (mean = 238, median = 218.7, SD = 152.4), winter (mean = 198.3, median = 166.7, SD = 145.1) and the shortest distance during Autumn (mean = 149.5, median = 121.2, SD = 119,3). El Niño recorded the longest dispersal distance (mean = 212,7, median = 183.5, SD = 151.8), followed by La Niña (mean = 198.1, median = 166.3, SD = 144.7) and neutral (mean = 182.4, median = 150.7, SD = 139.4). ENSO and season interactions also impact the distance travelled by kelp fragments, with the longest distances during neutral conditions in spring (mean = 284.9, median = 280.4, SD = 151.4). Autumn consistently displayed the shortest travel distances for kelp fragments across all ENSO conditions, while spring was associated with the longest distances during neutral and La Niña (mean = 294.1, median = 301, SD = 174.3) conditions, while during El Niño, the summer led to the longest fragments travels (mean = 294.9, median = 279.4, SD = 168.9).

## Discussion

I assessed the complex dispersal dynamics of the giant kelp, *Macrocystis pyrifera*, along the southeast Pacific coast through a coupling of hydrodynamic and individual-based modelling. This Chapter's decadal-scale analysis highlights the influence of travel duration on the settlement success of kelp spores, with shorter travel times increasing settlement likelihood. Moreover, my research has established a direct relationship between the length of travel and the distances covered, suggesting that while longer dispersal events are less common, they are crucial for maintaining the connectivity

among kelp populations along the South American coast. Nonetheless, the rarity of long-distance dispersal underscores the importance of localized processes in the persistence of kelp populations. These insights inform the necessity for conservation and management efforts to focus on local scales, such as implementing a spatial management unit of 50 km sections.

### Trajectory Patterns of Kelp Fragments

Kelp fragments predominantly showed a northward trajectory. This trend suggests an enhanced potential for connections with northern populations, a phenomenon also noted in other marine species in this region (Ospina-Alvarez et al., 2018, Blanco et al., 2019). Prevailing wind patterns and the HCS's northward flow likely drive this dispersion pattern. Nonetheless, southward movement was recorded below approximately 36°S, aligning with the northernmost range of the giant kelp's southern populations (Buschmann et al., 2004). This geographical demarcation also corresponds with a well-documented upwelling zone near 37°S (Aguirre et al., 2012). Here, the seasonal shift of the South Pacific anticyclone disrupts the prevailing southern winds during winter, leading to the emergence of seasonal upwelling (Aguirre et al., 2012). Such conditions increase the likelihood of southward transport during winter. Additionally, ENSO may amplify this effect when the anticyclone weakens (Montecinos and Gomez, 2010). Climate change further complicates these patterns by driving the Pacific Anticyclone southward, shifting the intense upwelling zone to around 34°S in spring (Weidberg et al., 2020). Over time, this could shrink the southern giant kelp population due to reduced southward dispersal.

This Chapter's results also highlighted the spatial variability in kelp fragment dispersal. I found that most of the kelp fragments might be originated from the southern region of Chile, where the kelp is more abundant. This pattern suggests a potential source-sink dynamic, where populations in the south might act as sources that supply kelp fragments to populations in the north. However, additional analysis is required to validate and comprehensively assess this pattern. While infrequent, the occurrence of long-distance dispersal events from this southern population to the north suggests a potential role in maintaining genetic diversity and potentially facilitating recovery in the event of local disturbances (Steinberg et al., 2016). Therefore, management strategies need to also consider the protection of these source populations in the southern region. Nevertheless, it is important to note that this pattern is primarily driven by the very high kelp density in the southern area. Hence, a finer spatial scale analyses to clearly understand the role of this area in relation to the rest of the population is needed.

### Influence of seasonal changes on kelp dispersal and settlement

This research has uncovered a significant link between seasonal changes and the dispersal and settlement patterns of kelp fragments in the Southeast Pacific. While my investigation primarily

focused on distinct seasonal periods, it is plausible that the transition between seasons may exhibit a more pronounced effect on these patterns. However, it's important to note that the model has not explicitly considered this transition period. I found that autumn and winter see increased settlement, coinciding with the intensification of the Westerlies and the weakening of the Pacific Anticyclone, which shifts north-westward during these seasons (Montecinos et al., 2011, Falvey and Garreaud, 2007). The dominance of westerly winds during this time propels the kelp fragments towards the land, enhancing settlement. Conversely, spring and summer bring stronger anticyclonic conditions and weaker Westerlies, giving rise to easterly trade winds. This shift, along with stronger southern winds, triggers upwelling and escalates Ekman transport, displacing surface waters—and thus kelp fragments—westward, away from the coast (Pérez-Santos et al., 2019).

The variations in kelp fragment dispersal distances across seasons are closely linked to the intensity of the Pacific Anticyclone. Kelp fragments tend to travel greater distances during spring (264.3 km) and summer (238 km), a trend that lessens in autumn (149.5 km) and winter (198.3 km). This seasonal pattern reflects the meteorological changes along the coastline, heavily influenced by the Pacific Anticyclone's varying strength (Falvey and Garreaud, 2007). In the warmer months, atmospheric conditions are marked by decreased wind turbulence and heightened stability, largely due to the anticyclone's fortification. As a high-pressure system, the Pacific Anticyclone suppresses storm formation (Montecinos and Aceituno, 2003) and strengthens southern winds, enhancing the northward movement of kelp fragments via the coastal jet (Garreaud and Falvey, 2009). This effect is augmented by surface currents responding to wind-induced stress and contributes to the formation of mesoscale eddies, which have been shown to facilitate long-distance dispersal (Adams and Flierl, 2010). The interplay of these meteorological and oceanic factors might be contributing to more kelp fragments moving north without encountering significant obstacles and reaching longer distances. However, it is important to note that while kelp fragments may travel greater distances during warmer months, shorter distances still present a higher likelihood of spores reaching settlement areas. In contrast, when the Pacific Anticyclone and the southern winds weaken and the coastal weather conditions become more turbulent and the northward transport decreases, kelp fragments experienced constrained dispersal. This is largely attributable to the emergence of disruptive weather events, such as storms and reduced formation of mesoscale eddies, which impede the fragments' progress and often cause them to accumulate in specific areas, thus limiting their capacity to travel longer distances. Although high-energy events like storms have often been associated with anomalous long-distance dispersal in other systems (Monzón-Argüello et al., 2012, Gillespie et al., 2012, Waters et al., 2018), the findings from Chapter 2 suggest a different mechanism along the Chilean coast, where reduced southern winds and diminished mesoscale eddy activity may limit dispersal capacity. This

contrast in dispersal dynamics across different seasons underscores the significant impact of meteorological and oceanic factors on the dispersal behaviour of kelp fragments in the Southeast Pacific.

### Influence of ENSO Events on Kelp Dispersal and Settlement

I also observed a robust influence of ENSO conditions on both settlement probability and dispersal distance of kelp fragments. Notably, during El Niño conditions, there is a higher likelihood of kelp fragments arriving at settlement areas (78.1%) and longer distance travelled (183.54 km), compared to La Niña conditions showing the lowest likelihood of fragments reaching settlement areas (75.8%) and shorter dispersion distance (166.32 km). The differential settlement rates and distance dispersal during ENSO phases can be attributed to the intensified oceanic and atmospheric patterns (Wang et al., 2017). Specifically, La Niña conditions result in a notable intensification of the trade winds at the HCS (Wang et al., 2017, Vargas et al., 2007, Alheit and Niquen, 2004), leading to extended and more intense upwelling, especially in central and southern Chile (Montecinos and Gomez, 2010). This could result in kelp fragments being dispersed offshore, away from kelp forest areas, as well as restrict the dispersion and thus the travel distance of buoyant particles, as they are more likely to become entrapped within nearshore water masses. In contrast, El Niño weakens the trade winds, enhancing westerly winds and reducing upwelling (Tsonis et al., 2005), thereby a larger proportion of fragments might be retained in coastal areas and disperse more extensively. Moreover, the longest dispersal distances were observed in the early years of the study, particularly during the significant El Niño event around 1998. These findings align with prior research that demonstrates that during El Niño phases, reduced coastal winds and altered ocean dynamics, including enhanced poleward undercurrents, increased eddy kinetic energy and disrupted upwelling patterns, contribute to longer-distance travel of particles along the Southeast Pacific coast (Astudillo et al., 2019, Colas et al., 2008, Conejero et al., 2020, Strub et al., 2019).

With climate change potentially intensifying and increasing the frequency of ENSO events, along with the expected rise in sea temperatures (Timmermann et al., 1999, Cai et al., 2021, Cai et al., 2014, Le et al., 2022), adaptive management strategies must consider these variations, such as temporary harvesting closures, which vary depending on the ENSO phenomenon and the season. El Niño conditions, characterized by warmer sea temperatures and weakened upwelling, can disrupt the reproductive patterns of *M. pyrifera*, potentially leading to altered reproductive timing or even kelp mortality (Tegner et al., 1997, Dayton et al., 1992, Steneck et al., 2013). Conversely, La Niña conditions, with cooler waters and stronger upwelling, may support kelp reproduction but also present challenges in ensuring settlement due to localized dispersion (Tegner et al., 1997, Cai et al., 2015). Understanding these effects is vital for predicting how kelp populations might respond to future climate changes

along the southeast Pacific coast. Conservation efforts should be informed by these insights, with a focus on preserving genetic diversity and protecting source populations through effective local management (Cowen et al., 2007, Balbar and Metaxas, 2019, Steinberg et al., 2016), emphasizing the implementation of spatial management units spanning 50 km sections. Future modelling efforts should also incorporate the interplay between kelp ecosystem conservation and human activities, thereby providing comprehensive guidance for integrative spatial management (Ospina-Alvarez et al., 2020b). Additionally, the development of detailed databases that specifically map out locations and features is crucial for generating more accurate assessments of the key processes underpinning social-ecological systems in coastal regions (e.g., kelp harvesting). Such integrated approaches are essential for ensuring the sustainability of these valuable ecosystems and the communities that depend on them.

## Conclusion

This Chapter provides valuable insights into the potential dispersal and settlement patterns of giant kelp in the southeast Pacific region. It revealed the influence of ENSO conditions and seasonal variations on dispersal distances and the probabilities of reaching a settlement area. Although kelp fragments dispersal is not the main source of spore dispersal, other important factors such as successful spore release, spore viability, transportation to the seafloor, sediment composition, texture and flow velocity also influence kelp dispersal and settlement (Gaylord et al., 2004). Nonetheless, these findings provide an important insight in the giant kelp dispersal dynamics and could have implications for the management and conservation of this ecologically important species. Looking ahead, there is potential to improve the model resolution by integrating more detailed hydrodynamic data and using nested models to better capture finer-scale processes. This is particularly important for areas like Patagonia, which, although not included in the study, host significant kelp populations. If models with higher resolution are incorporated, increasing the frequency of output measurements would help capture finer-scale dispersal dynamics and avoid missing important short-term variations. To ensure the resilience of giant kelp populations in the face of environmental changes, it is essential to prioritise the protection of nearshore areas where most of the kelp is located, consider the influence of ENSO conditions and seasonal variations and promote connectivity between populations in the southern and northern regions of the ecosystem.

# Chapter 3: Incorporating giant kelp connectivity into management strategies in the southeast Pacific[2]


## Abstract

Intensive harvesting and climate change affect the delivery of multiple ecosystem services provided by giant kelp, *Macrocystis pyrifera,* in the Southeast Pacific region. Amid these threats, dispersal and connectivity are crucial processes that support the replenishment and recovery of giant kelp, yet they remain poorly understood. In Chapter 3, I assess the connectivity of giant kelp in the Southeast Pacific to inform its conservation and management. To achieve this, I use the outputs of Chapter 2 and network analysis to identify critical source and sink areas and key connectivity corridors at multiple spatial and temporal scales. I also assess the influence of seasonal and El Niño Southern Oscillation (ENSO) variability on connectivity in the region. I found that the southern population (36 to 43°S) is the highest priority for management (e.g. no-take zone) as it serves as a crucial source-sink area, playing a fundamental role in propagule dissemination, local retention and non-local retention. I also identified changes on the connectivity within the central population (28 to 35°S), influenced by both ENSO events and seasonal variability. Adaptive management strategies, including temporal harvest closures, are recommended to address both inter and intra-annual fluctuations in connectivity. Additionally, through the delineation of management units based on population connectivity, I identify key source areas within each unit that warrant protection. The outputs of Chapter 3 underscore the importance of integrating connectivity and regional environmental dynamics into conservation frameworks to enhance the resilience of kelp forests in the Southeast Pacific and elsewhere.



Keywords: giant kelp, marine connectivity, Humboldt Current System, ENSO (El Niño-Southern Oscillation), adaptative management, conservation


[2] Published as:
Thompson-Saud, G., Grech, A., Choukroun, S., Vásquez, S. I., & Ospina-Alvarez, A. (2025). Incorporating giant kelp connectivity into management strategies in the southeast Pacific. Ocean & Coastal Management, 266, 107661.

## Introduction

Connectivity is a fundamental process in terrestrial and marine systems that promotes the persistence and recovery of populations through dispersal (Balbar and Metaxas, 2019). It influences the resilience of individual populations to environmental disturbances and the dynamics of entire ecosystems. In the marine realm, oceanic and wind driven currents are the main agents of dispersal, especially during the early life stages of many organisms. The early pelagic stage, in particular, can be the only opportunity for dispersal for some species, including marine plants. Consequently, understanding connectivity patterns of organisms is essential for effective management (Van der Stocken et al., 2019b, Steneck et al., 2009) and enhancement of their population viability (Beger et al., 2010).

Assessing connectivity in early life stages often involves tracking the movement and age of drifting individuals (Macaya et al., 2005, Shanks, 2009), studying larval behaviour (Paris et al., 2008, Castorani et al., 2015) and analysing genetic markers (Hedgecock, 2017, Castorani et al., 2015, Palumbi, 2003, Weersing and Toonen, 2009). However, these methods have limitations in capturing the full species distribution and are typically short-term (Abesamis et al., 2016). To address this, indirect approaches like biophysical models have emerged, combining Individual Based Models (IBMs) with hydrodynamic models. IBMs typically advect particles, forced by flow fields from hydrodynamic models, while incorporating biological parameters of the organism (e.g. size, buoyancy, vertical movement, orientation, reproductive time and mortality). The hydrodynamic model typically resolves the circulation including currents, tides and winds information. These coupled biophysical models generate dispersal pathways used to computed connectivity matrices and network analysis, revealing key insights into the dynamics of habitat patches (discrete areas of suitable habitat for a species within a larger landscape), dispersal routes and overall population connectivity (Werner et al., 2007, Treml et al., 2008, Rayfield et al., 2011, Ospina-Alvarez et al., 2020b). While connectivity analyses using biophysical model have been performed in several species (Ospina-Alvarez et al., 2020b, Grech et al., 2018, Abecasis et al., 2023, Treml et al., 2008, Pastor et al., 2023, Blanco et al., 2019), there is a noticeable bias towards animals, with limited research on plants or algae (Bryan-Brown et al., 2017).

*Macrocystis pyrifera*, commonly known as giant kelp (or “huiro negro” in Chile or “sargazo gigante” In Peru), has a keystone role along the Southeast Pacific coastline, spanning from 6°S (northern Peru) to 55°S (Patagonia, Chile), covering approximately 6,600 km (Hoffmann and Santelices, 1997) (Figure 11.b). *M. pyrifera* reproduces through spores, which typically disperse over short distances using their flagella, travelling a few tens of kilometres within hours to days (Kinlan, Graham, Sala, & Dayton, 2003). However, detached kelp fragments containing viable spores can be transported over much greater distances, sometimes exceeding 100 or even 1000 kilometres, particularly under severe

weather conditions, connecting distant populations (Bernardes-Batista et al., 2018, Gaines et al., 2007). Once the spores are attached to the substrate, the kelp grows rapidly, reaching harvestable sizes in approximately 1 to 3 years, depending on environmental conditions. Most kelp individuals will naturally degrade around this time, though new sporophytes will be recruited. Spores are typically released during the cooler months, from winter to early spring. Understanding the dynamics of giant kelp ecosystems is particularly relevant in the Southeast Pacific region, where these underwater forests hold both ecological and economic significance. *M. pyrifera* serves as an ecosystem engineer, forming dense kelp forests that serve as essential habitats and shelter for many species (Graham et al., 2007, Pérez-Matus et al., 2017). Furthermore, the species holds substantial economic value, being harvested for alginate extraction and serving as a food source for the abalone industry, primarily targeting *Haliotis rufescens* (Villegas et al., 2019).

Over the past two decades, there has been a notable surge in the extraction of kelp in the Southeast Pacific, driven by the rising global demand for raw seaweed (Villegas et al., 2019). Most of this seaweed collection is conducted by small-scale fisheries, collected from natural kelp forests (Porras, 2019). Most of the harvesting occurs in the northern part of the region (around 10 to 32°S), where the kelp forest is perennial (available year-round), unlike the southern population that is annual, with harvesting season occurring in December (Vásquez, 2009, Gutierrez et al., 2007). The over-exploitation of the northern population has led to fragmentation and a significant decline in abundance (Buschmann et al., 2006b). This increased exploitation has occurred in the absence of regulations, raising concerns about the sustainability of these ecosystems (Porras and Vásquez, 2020). Compounding these pressures, climate change poses an additional threat to kelp forests, potentially altering ocean temperatures and currents, which are crucial for kelp growth and dispersal (Smale, 2020, Beas-Luna et al., 2020). The early life stages of *M. pyrifera* are particularly vulnerable to rising ocean temperatures, with spore settlement and germling development significantly declining beyond 21.7°C to 23.8°C (Le et al., 2022). The combined effects of over-exploitation and climate-driven changes could further degrade these ecosystems, reducing their resilience and capacity to recover. In addition to direct temperature-driven stress, climate change can also shift herbivore populations, leading to increased grazing pressure on kelp forests (Norderhaug and Christie, 2009). In areas where kelp is not harvested, widespread declines have been observed due to the combined effects of ocean warming and intensified herbivory, particularly from sea urchins and other grazers (Norderhaug and Christie, 2009, Filbee-Dexter et al., 2016). The loss of kelp in these regions highlights the broader vulnerability of these ecosystems, as over-exploitation and climate-driven changes together could further degrade their resilience and capacity to recover.

In response to these growing threats, Chile introduced legislation in 2013 governing kelp extraction along its coast. Kelp forest harvesting is now regulated through TURFs (Territorial Use Rights in Fisheries), which aim to sustainably extract and protect common resources in Chile through a co-management strategy (Albornoz and Glückler, 2020). Similarly, in Peru, giant kelp has been regulated since 2009, prohibiting the removal of kelp without the necessary permits (Avila-Peltroche and Padilla-Vallejos, 2020). This shift towards sustainable extraction represents a significant step towards curbing the indiscriminate exploitation of *M. pyrifera*. Nevertheless, a more thorough understanding of ecosystem processes is required to enhance conservation strategies across various scales. Understanding the connectivity patterns of giant kelp is crucial for spatial prioritisation in conservation and management efforts. Specifically, this knowledge enables the identification of key dispersal pathways and source populations, which are essential for designing effective TURFs. By focusing conservation and sustainable harvesting efforts on these critical areas, it is possible to maintain the ecological integrity and resilience of kelp forests to extraction and environmental changes, ensuring that these habitats continue to support biodiversity and provide economic benefits. This strategic approach aims to optimize conservation outcomes while balancing the needs of local fisheries, promoting a sustainable coexistence between resource use and ecosystem preservation.

The goal of Chapter 3 is to evaluate the dispersal and connectivity of giant kelp forests in the Southeast Pacific to inform effective management strategies. I approach this by integrating the outputs of Chapter 2 with network analysis and graph theory, identifying critical areas that significantly contribute to the connectivity of *M. pyrifera*. Furthermore, I examine how connectivity patterns shift under varying ENSO conditions and across different seasons, aiming to determine the key areas that sustain connectivity within giant kelp forests over time. I discuss how the insights gained from this Chapter can be used to guide future management strategies, including the conservation and sustainable harvesting of these marine ecosystems.

## Methods

To study the connectivity dynamics of kelp populations in the Southeast Pacific region, connectivity matrices were constructed computed using biophysical model outputs as described in the work of Thompson-Saud et al. (2024) (Chapter 2), which applied a biophysical model to the region between 6 to 43°S. South of 43°S, the area around the fjords exhibits highly complex dynamics due to its intricate topography. Adequately representing these dynamics would have required the inclusion of nested models with finer resolution and technical specifications for this ecosystem, which represents a challenge for future research. In Chapter 2, I constructed a kelp density map based on hexagonal cells that were used to discretise the kelp distribution along coastal areas, with cell value corresponding to

giant kelp density within each cell. The kelp density data, representing the average kelp coverage from 2015 to 2019, was sourced from a dataset developed by Mora-Soto et al. (2020) using satellite imagery from Google Earth Engine (Figure 11.a) (Gorelick et al., 2017). Ocean circulation was simulated using a Regional Ocean Modelling System (ROMS)-based hydrodynamic model with a 10 km horizontal resolution and 10 $m^2s^{-1}$ horizontal dispersion. A customized version of Ichthyop, an IBM modified to be used in the Southeast Pacific region, was incorporated to simulate kelp dispersal (Lett et al., 2008). Ichthyop considered parameters like maximum length of individual simulations, reproductive timing and decay rate capturing fertility reduction over time (Table B1.1). Each particle represents a floating fertile kelp fragment initially carrying 11,200 spores. The number of spores decreases over time as governed by a decay rate, with further details provided in Chapter 2. 5,000 particles were released weekly from 1997 to 2008, guided by a density map reflecting kelp distribution. This release rate was chosen for computational efficiency and to represent general connectivity patterns within the model. Consequently, areas of high kelp density released more particles compared to areas of lower density. A total of 8,158,121 spore arrived to kelp forests patches between 1997 to 2008. Particle positions were recorded at specific days (1, 5, 10, 15, 20, 30, 45, 60, 90 and 125) and distances they travelled were measured. In my study, outputs of the biophysical model of Chapter 2 were used to compute connectivity matrices, where nodes represent habitat patches of kelp and links between nodes representing the cumulative number of particles (fragments and spores) that moved between nodes. Connectivity matrices were constructed by calculating the number of particles moving between different areas, facilitating subsequent network analyses.

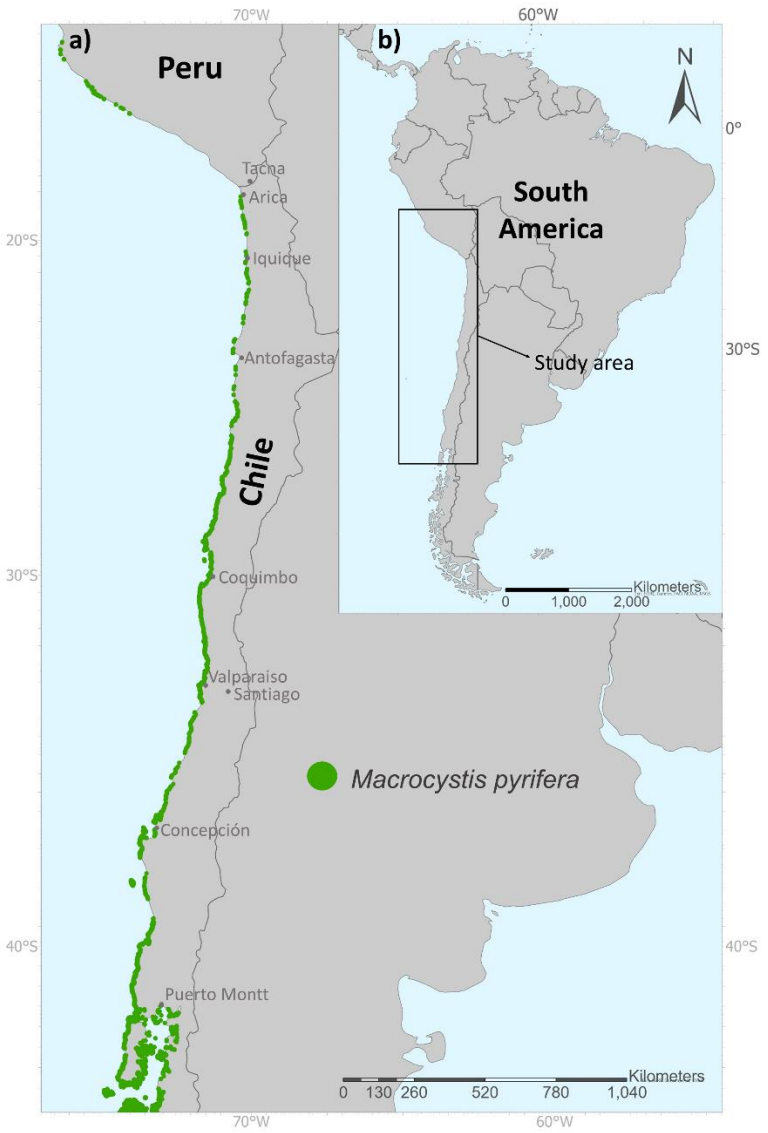


**Figure 11.** Distribution of *Macrocystis pyrifera* in the Southeast Pacific. a) Kelp distribution along the Chilean and Peruvian coast. The kelp distribution was obtained from Mora-Soto et al. (2020). b) South America with the Southeast Pacific region in the left side. The maps are in Transverse Cylindrical Equal Area projection.

My methodology encompassed a comprehensive temporal analysis from 1997 to 2008, allowing me to evaluate the influence of seasonal and inter-annual variability on the connectivity patterns, including assessments during various El Niño Southern Oscillation (ENSO) phases (El Niño, La Niña and neutral) as well as seasonal variations (summer, autumn, winter and spring). ENSO's influence was assessed by months (NOAA, 2024) and seasonal periods were categorized as follows: summer from January to March, autumn from April to June, winter from July to September and spring from October to December. The ROMS hydrodynamic model incorporates variations in oceanographic conditions driven by ENSO phases. This is because both atmospheric forcings (NCEP2 reanalysis; Kanamitsu et al. (2002)) and lateral boundary oceanic forcings (ECCO; Stammer et al. (1999)) are realistic and capture a wide range of temporal scales, from daily to interannual, including ENSO variability. Consequently,

the circulation dynamics simulated by ROMS are intrinsically influenced by ENSO conditions. Since the model successfully captured these dynamics during the study period, it enabled an assessment of kelp dispersal under El Niño, La Niña and neutral conditions. Given the significant influence of ENSO events and seasonal changes on the Southeast Pacific's dynamics, this approach provided a thorough representation of kelp dispersal patterns under varying climatic conditions.

Network analysis and graph theory, which model systems as a collection of interconnected units called graphs, were employed to measure connectivity patterns and to identify subpopulations/units within the giant kelp forest system. In graph theory, a graph consisted of nodes, which in this case, represent habitat patches of kelp in the form of hexagons, that are connected by edges, which represent the potential dispersal routes between these patches. Weights were assigned to the nodes and links to provide information about the strength of the connections. This was achieved by normalizing the connectivity matrices using the maximum and minimum values to ensure that the weights accurately reflect the relative strength of the connections. The network analysis was conducted using the "tidyverse" and “igraph” packages (Wickham et al., 2019, Csardi and Nepusz, 2006) within the R language. Network visualizations were generated using the following R packages: “ggplot2” v.3.2.1, “ggmap” v.3.0.0 and “ggraph” v.2.0.0 (Kahle and Wickham, 2013, Pedersen, 2021, Hadley, 2016).

To assess the overarching population patterns, I calculated a range of network measures (Table 2) applied to the habitat graph, enabling the quantification of diverse structural aspects of the population. I performed network measures for the entire period, different ENSO conditions and seasons, using key metrics, including total edges, network density, network diameter, connected components and modularity. The calculations were made for different times using the graph for each ENSO and season, but I did not account for variability within ENSO phases or seasonal periods in these metrics. By conducting network measures, this Chapter’s primary aim was not to focus on individual metrics but rather to evaluate how the graph changes across different seasons and ENSO phases, thereby providing a broader understanding of temporal connectivity patterns. Additionally, various node level and centrality measures (Table 2) were utilized to gain insights into the distinct roles of individual kelp patches relative to others and infer the attributes of the connectivity of the ecosystem. For instance, out-strength and in-strength were evaluated to determine the directionality (source or sink, respectively) and strength of connections between patches, providing a weighted degree to quantify the contribution of different patches to the overall population structure. These measures help identify areas that export a large number of propagules (sources) and those that primarily receive propagules (sinks). The mathematical formulation can be found in Appendix B2 of the Supporting Information.

The modularity measure was employed to evaluate the interconnectivity among nodes and potential boundaries in metapopulation for the giant kelp, aiding in the identification of areas exhibiting stronger connectivity among themselves compared to the broader population. This analysis enables the delineation of management units, highlighting regions that are more closely connected and thus essential for effective conservation and resource management. I utilized cluster infomap algorithm that works by using random walks to identify groups or communities in a network by maximizing the flow of information within communities and minimizing the flow between communities (Rosvall and Bergstrom, 2008). The Infomap algorithm produces communities that optimize the information-theoretic map equation and detect hierarchical community structures (Rosvall et al., 2009). Utilizing these units, the out-strength measure was applied to delineate key areas serving as sources of kelp fragments per unit. This was done by analysing the connectivity matrices for the entire study area and then normalizing the out-strength values within each unit to obtain relative measures. This normalization allows for a comparative assessment of the importance of each unit in terms of its contribution to kelp fragment dispersal.

**Table 2.** Network measures of the habitat graph and node level that were used to assess connectivity of the giant kelp.

| Measure | Function | Ecological and management relevance |
|---|---|---|
| Total edges | Indicates the number of pairs of immediately connected nodes | Shows how many connections are formed in the population |
| Network density[1] | Measures how close the network is to be completed. A complete graph has all possible edges and is equal to 1 | Describes the extent to which a population is connected through interactions. It is a ratio of the number of realized interactions to the total number of possible interactions |
| Network diameter[1] | The maximum number of steps required to traverse the network. Indicates compactness of the graph and overall traversability of the network | Provides insights into the overall efficiency of propagules flow within the population. A small network diameter indicates that the graph is compact, meaning nodes are relatively close to each other in terms of the number of edges that need to be traversed to move from one node to another |
| Connected components[1] | Number of connected subgraphs (or components). Components are sets of nodes connected to each other by paths (edges) | Provides insights into the structure of the ecosystem. Helps to identify areas that have direct or indirect paths between every pair of nodes within that component |
| Number of clusters (modularity)[2] | The number of clusters measures the count of distinct groups (or subgraphs) identified within a network. Modularity quantifies the strength of division of the network into these groups by comparing the density of connections within groups to that expected in a random network | Identifies possible metapopulation boundaries |
| Out-degree[3] | Represents the number of connections or edges going out from a particular node to other nodes in the graph (regardless of their weight) | Indicates how many different nodes a given node can directly influence or interact with. If applied over time, it can be used to infer how the connectivity and dispersal patterns of the population change over time |
| Out-strength[4] | Is the sum of the weights of all outgoing edges from a node | Indicates the total influence or output a node exerts on its neighbours. It highlights nodes or patches that act as sources, providing significant individuals |

| | | |
|---|---|---|
| In-strength[4] | Is the sum of the weights of all incoming edges to a node. | Indicates the total influence or input a node receives from its neighbours. It highlights nodes or patches that act as sinks (possible settlement areas), receiving significant individuals |
| Closeness centrality[5] | Measures how central a node is in terms of its average distance to all other nodes in the network. It is the reciprocal of the sum of the shortest path distances from the node to all other nodes | Measures how quickly information or any influence (e.g. disease or resources) can spread from a particular node to all other nodes in the network |
| Betweenness centrality[6] | Calculates a node's influence over the flow of information in a graph. A higher value indicates nodes that have greater control of the information flow in the network | Indicates patches that serve as steppingstones and highlights important dispersal routes |
| Eigenvector centrality[7] | Evaluates the importance of a node within a network by considering both the number of outgoing and incoming connections it has and the importance of those connections. It assigns higher centrality scores to nodes that are connected to other highly central nodes | Highlights key nodes or patches that are not only well-connected but are also connected to other important patches. Serves to determine highly resilient areas. |
| Local retention | Shows the ratio of locally produced settlement to local production | Reflects the proportion of propagules that recruit in the same area that they were released |
| Non-local retention | Shows the ratio of non-locally produced settlement to local production | Reflects the proportion of propagules that recruit in different areas that they were released |

[1]Newman (2018), [2]Rosvall et al. (2009), [3]Cantwell and Forman (1993), [4]Barrat et al. (2008), [5]Freeman (2002), [6]Freeman (1977) and [7]Bonacich (1987)

Generalized additive models (GAMs) were employed to assess the influence of season and ENSO variability on nodes using various node level measures. The dataset consisted of node differences across seasons and ENSO conditions, aiming to discern whether these changes were statistically significant. The analysis utilized the "mgcv" package (Wood, 2017) in the R language and environment for statistical computing (R Core Team, 2019). Several model families and configurations were tested to identify the best fit for the data. The "performance" package (Lüdecke et al., 2021) was applied to assess overdispersion, aiding in the selection of the family that effectively addressed this issue. Model performance was evaluated by assessing the deviance explained, ensuring convergence and utilizing the Akaike Information Criteria (AIC) from the "MuMIn" package (Barton and Barton, 2015).

To assess changes in connectivity across various temporal scales, encompassing the entire study duration (1997-2008) and considering distinct seasons and ENSO conditions, I utilized out-degree distribution and node degree measures. Out-degree distribution was employed to visually evaluate habitat connectivity and identify hotspots of outgoing connection of nodes, regardless of kelp density. This approach allowed me to detect structural changes in connectivity patterns over time and identify influential kelp habitats during specific seasons and ENSO phases. By analysing out-degree distributions, I aimed to understand how environmental variability influences connectivity dynamics in the studied ecosystem. On the other hand, node degree distribution was employed for quantitative assessment, enabling me to quantify the connectivity of individual nodes within the graph. This

measure involved counting the edges incident to a specific node, offering insights into the extent of its connections with other nodes.

## Results

From 1997 to 2008, the cumulative habitat graph, which represents the network of habitat patches and their connections over the entire period, comprised 104 nodes and 4,461 edges, capturing the connectivity of the population under study. While the number of nodes remained consistent across various habitat graphs during ENSO events and seasonal changes, the number of edges varied, indicating dynamic connectivity. Specifically, the edge count ranged from 3,238 during La Niña to 4,644 during El Niño and from 3,123 in spring to 4,330 in autumn (Table 3). Overall, the connectivity observed in the habitat graphs follows a south to north pathway which is consistent with oceanic currents in the region. However, from 36°S and beyond particles are also travelling southward.

### Network measure of the habitat graph and temporal variability

The network's connectivity and structure were influenced by seasonal dynamics and ENSO phases (Table 3). During El Niño, the network showed increased connectivity, evidenced by a higher number of edges, resulting in greater network density and a reduced network diameter, suggesting shorter average paths between nodes. In contrast, La Niña phases were marked by decreased connectivity, with fewer edges, lower network density and an expanded network diameter, indicating a more disconnected network structure. El Niño phases were also characterized by a lower number of clusters, indicating fewer distinct network modules and higher inter-node connections, as the population was divided into fewer clusters. Conversely, neutral conditions followed by La Niña exhibited a higher number of clusters, suggesting a greater degree of node segregation into distinct communities and reduced interconnections within the entire population. The clusters formed do not appear to be random, as all the community structures exhibit relatively high modularity (around 0.5), indicating well-defined communities.

Seasonal variations also had an impact on the network. Autumn was identified as the season with the highest connectivity, characterized by the most edges, greatest network density and smallest network diameter, indicating robust connectivity and dependency among kelp patches. In contrast, spring showed the opposite pattern with the lowest number of edges and smallest network density. Notably, spring also showed the highest number of clusters, further underscoring it as the least connected network. Winter and summer exhibited similar patterns, with summer having a slightly higher edge count. Remarkably, throughout all seasons and ENSO conditions, the network maintained three connected components, highlighting the structural resilience of the kelp population network despite environmental fluctuations.

**Table 3.** Network measures of the habitat graphs of the giant kelp in the southeast Pacific region, encompassing the entire study period (1997-2008), ENSO conditions (El Niño, La Niña and neutral) and seasons (summer, winter, autumn and spring).

| Measure | All | El Niño | La Niña | Neutral | Summer | Autumn | Winter | Spring |
|---|---|---|---|---|---|---|---|---|
| Total edges | 4841 | 4644 | 3238 | 3994 | 3680 | 4330 | 3675 | 3123 |
| Network density | 0.45 | 0.43 | 0.3 | 0.37 | 0.34 | 0.4 | 0.34 | 0.29 |
| Network diameter | 3 | 3 | 4 | 4 | 4 | 3 | 4 | 4 |
| Connected components | 3 | 3 | 3 | 3 | 3 | 3 | 3 | 3 |
| Number of clusters (modularity) | 9 (0.54) | 7 (0.58) | 8 (0.55) | 9 (0.54) | 8 (0.58) | 8 (0.54) | 8 (0.54) | 9 (0.54) |

## Node level network measures

The region spanning 36 to 43°S demonstrated significant movement of kelp fragments, both incoming and outgoing. Notably, the nodes around 41°S showed the highest out-strength and in-strength values (Figure 12.a and b). This suggests that the area around 41°S is a key hub in the network, with the most extensive outgoing and incoming connections to other nodes. Not surprisingly, the nodes with the highest non-local retention (76%) and highest local retention (67%) were both located in the region around 41°S (Figure 12.f). This insight highlights its potential as a critical focal point for exporting propagules and serving as a settlement area in kelp population dynamics and management strategies.

The geographical region spanning latitudes 36 to 43°S also exhibits the highest closeness centrality, indicating that the propagules in this area are spreading faster to the rest of the population (Figure 12.c). Specifically, habitat patches around 37°S are where propagules are spreading the fastest to the rest of the population. Consequently, any factor affecting this area will have a greater impact on the rest of the population compared to other areas. The area around 41°S also exhibited the highest eigenvector centrality, indicating that this area is well-connected and linked to other important areas of the population (Figure 12.e). Consequently, the southern region showed a notable degree of connectivity and resilience to disturbances. As a result, the central part of the population displayed higher betweenness centrality compared to those located at the extremes (Figure 12.d). This indicates that a significant number of areas within this central part acted as crucial steppingstones for connectivity. Particularly noteworthy is the region around 29°S, the population's midpoint, which demonstrates the highest betweenness centrality.

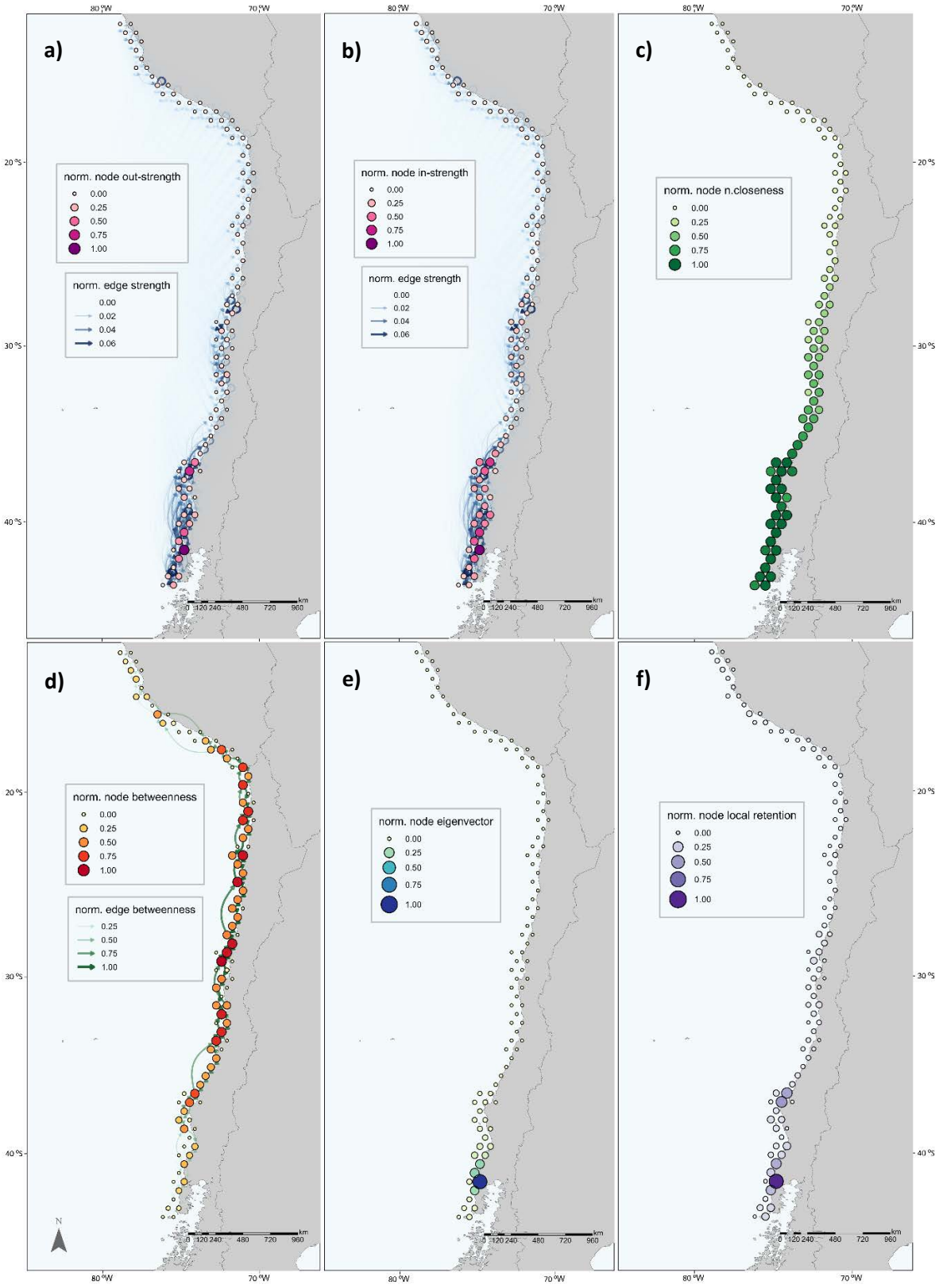


**Figure 12.** Maps of kelp fragment displaying node-level connectivity metrics. a) out-strength (source areas), b) In-strength (sink areas), c) closeness (fragments spread velocity), d) betweenness (bridge areas), e) eigenvector (influential areas) and f) local retention (fragment retention) in the southeast Pacific. Circles indicate settlement density of kelp fragments across the region, with the size and colour gradient representing the normalized concentration from low (small, light pink (a and b), light green (c), yellow (d), light blue (e) and light purple (f)) to high (large, dark purple (a and b), green (c), red (d), blue (e)

and purple (f)). Arrows illustrate the normalized flux of kelp fragments, with direction and thickness indicating the movement and relative quantity of fragments travelling from their release points to settlement areas.

In analysing temporal changes in node measurements, I selected the most parsimonious statistical model based on criteria including the lowest Akaike Information Criterion (AIC), highest explained deviance and optimal model fit. The chosen model incorporated a wide range of explanatory variables, as specified in Eq. 3.

$$Nodes\_changes = gam(Netwok\_measure \sim Time\ (ENSO\ or\ season) + s(Node, \quad bs =' re')$$

*Equation 3*

In Eq. 3, *gam* refers to the Generalized Additive Model. *Network_measure* refers to the various network metrics analysed, excluding betweenness centrality due to its incompatibility with any model family. The *Time* variable represents either ENSO phases (El Niño, La Niña and neutral) or seasons (summer, autumn, winter and spring), treated as factorial. s(*Node*, bs='re') represents a random effect smoothing term to account for unexplained variance among individual nodes. The model family for each network measure is specified in supplementary information (Table B3.2 and 3).

Analysis during different ENSO phases uncovered notable shifts in network measure patterns across nodes (Table B3.2). Seasonal effects demonstrate diverse impacts on network metrics (Table B3.3). For instance, degree and closeness centrality exhibit considerable variability across seasons, contrasting with out-strength and local retention, which show minimal seasonal variation. In-strength (i.e., settlement) and non-local retention exhibit similar patterns during spring and summer, as well as autumn and winter. Additionally, eigenvector centrality notably differs primarily during the spring season.

The out-degree, indicative of the number of outgoing connections each node has, was used to visualize variations across distinct ENSO phases and seasons (Figure 13). I found that nodes are connected to between 4 (weakly connected) and 90 (highly connected) other nodes out of a total of 125 nodes. Overall, the connectivity and structure of the population appear to be consistent in the north, somewhat less so in the south, but with notable variability observed in the region between 28 and 35°S across different seasons and ENSO conditions. During El Niño, this area shows high connectivity with around 50-75 connections per node, which decreases during neutral conditions and further decreases during La Niña to between 24 and 40 connections. Autumn appears to have the highest connectivity in this area with around 50 to 75 connections per node, followed by summer, winter and spring with around 5 to 25 connections per node.

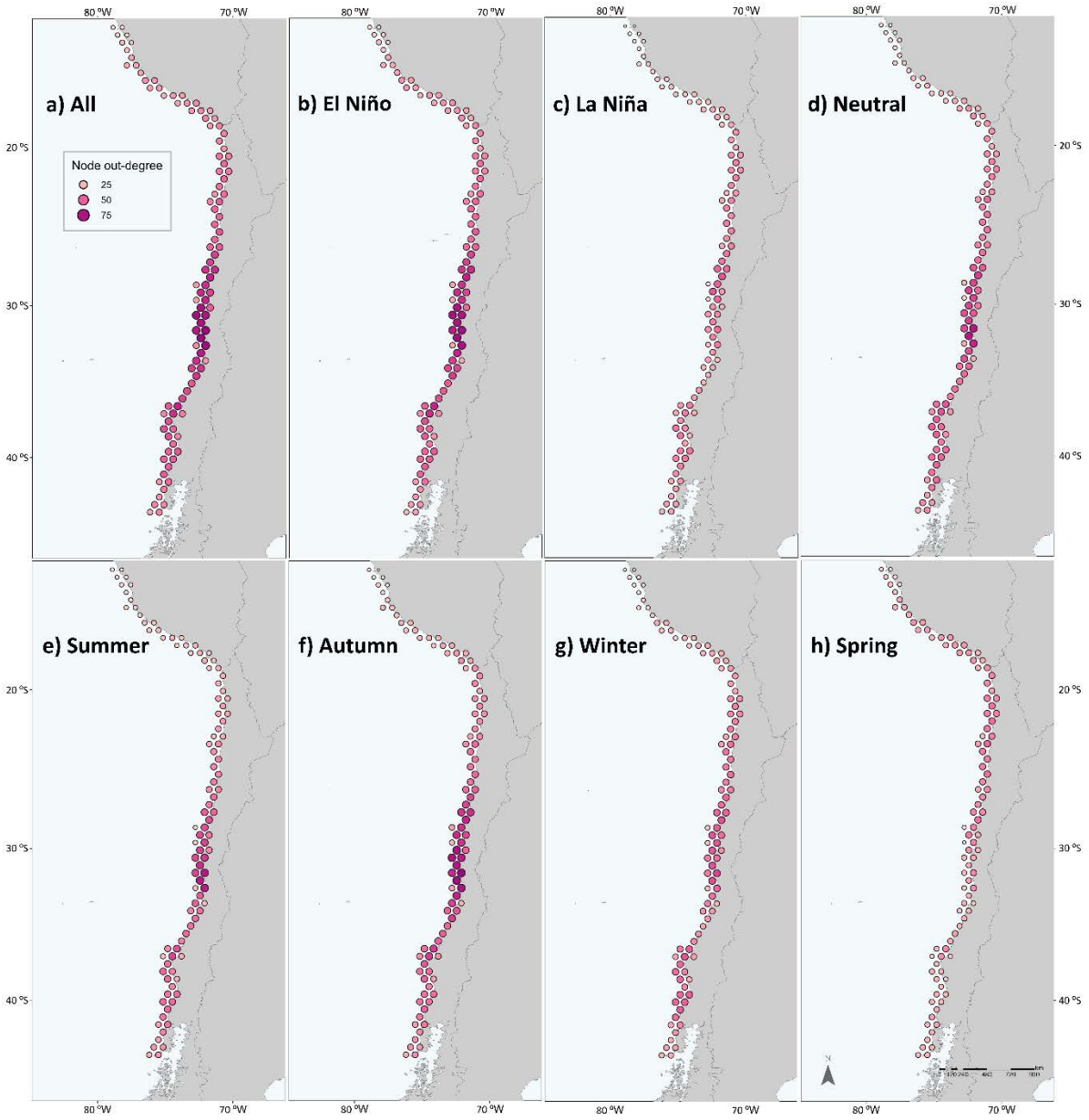


**Figure 13.** Maps of kelp fragments showing out-degree (number of connected nodes) centrality in the southeast Pacific during the entire period, different ENSO conditions and seasons. Circles indicate settlement density of kelp fragments across the region, with the size and colour gradient representing the normalized concentration from low (small, light pink) to high (large, dark purple). Map showing out-degree during a) the entire study period, b) El Niño, c) La Niña, d) neutral condition, e) summer, f) autumn, g) winter and h) spring.

All habitat graphs except spring showed properties of a random graph, with degree distribution similar to a Gaussian bell-shaped curve (Figure B4.1). This bell-shaped distribution suggests most nodes have a similar number of connections, with fewer nodes at the extreme high or low end of connections. A normal distribution of node degrees suggests a certain level of regularity and uniformity in the connectivity patterns of nodes. In contrast, spring's node degree distribution appeared more homogeneous, indicating a more even spread of node degrees across the range, excluding highly

connected nodes. This pattern implies a structurally different connectivity pattern during spring, lacking the regularity observed in other seasons.

### Identifying communities for management

A comprehensive cluster analysis of the habitat graph was conducted using the previously mentioned cluster Infomap algorithm, covering the period from 1997 to 2008. This analysis identified nine distinct clusters (Figure 14.a), which are important not as biological communities, but as potential metapopulation boundaries that inform strategic management decisions. These clusters are arranged in a south-to-north gradient according to their ecological significance. Notably, Unit 6 emerges as the most extensive management unit, spanning nearly 1000 km, whereas Unit 9 is the most compact, encompassing approximately 260 km. On average, the dimensions of these management units are approximately 400 km in length north to south. The considerably higher population density in the southern extremity has unmasked critical areas in other parts of the population where density is lower. Therefore, the identified management units were used to determine key source areas within each unit. This approach identified key supply areas within each unit, prioritised for management to ensure the preservation of connectivity both within and across the broader region (Figure 14.b).

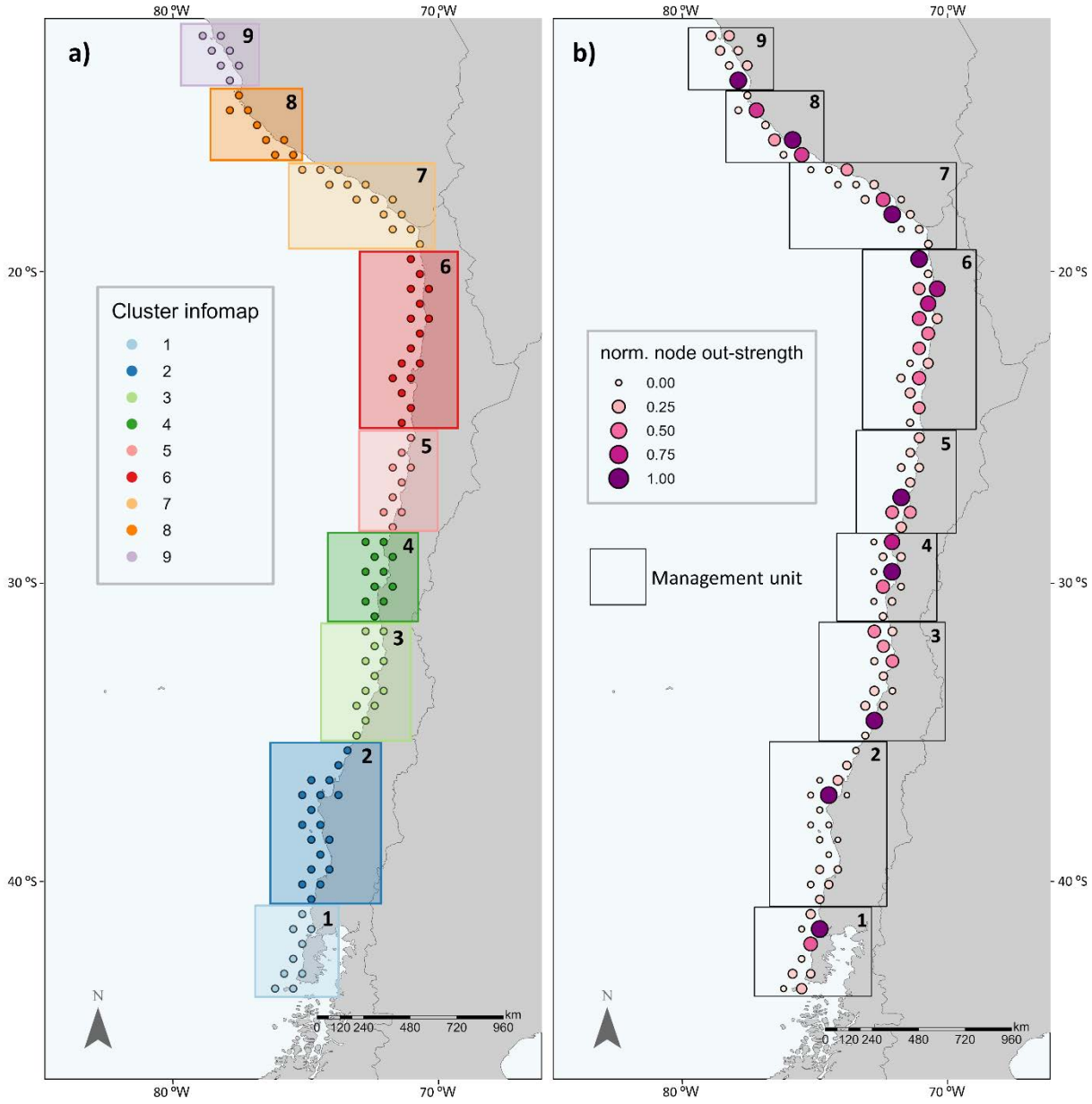


**Figure 14.** Maps of kelp fragment showing units (areas that are more connected) and out-strength (source areas) per unit in the southeast Pacific during 1997 to 2008. a) Map showing the management units determined by the cluster Infomap algorithm. Different colours represent different units and their numbers represent their importance. b) Map showing out-strength applied to each management unit.

## Discussion

### Network connectivity: Regional and temporal variability

This Chapter on the connectivity dynamics of *Macrocystis pyrifera*, giant kelp, along the southeast Pacific coast underscores the critical significance of the southern giant kelp population (36 to 43°S) as a fundamental source-sink area. This region, particularly the nodes situated around 41°S where alongshore wind stress is considerably lower throughout the year, plays a key role in propagule retention, as the reduced wind stress allows propagules to remain in the area for longer periods, promoting local persistence and connectivity. This area emerges as a key hub for connectivity,

propagule dissemination, local retention and non-local retention, indicating a heightened propensity for self-persistence and an important area for the persistence of the entire population as it is significantly contributing to the overall population structure. In contrast, the remaining populations manifest low resilience and connectivity, as the stochastic loss of nodes could induce significant disruptions in the network. However, the findings also reveal the central population's key role as a bridge, fostering connectivity across the entire population and facilitating linkages between the southern and northern extremes. Consequently, the potential disconnection of a central node poses a substantial risk, as it could lead to the isolation of the entire population.

The region between 28 and 35°S, regardless of kelp abundance, exhibits high connectivity, serving as a key hub influenced by seasonal upwelling patterns associated with fluctuations in the Southeast Pacific Subtropical Anticyclone (SPSA; Figure B5.2, 4 and 5) (Sobarzo et al., 2001, Letelier et al., 2009). During autumn, increased connectivity is observed in this central area, attributed to the northward displacement of the SPSA, which halts upwelling activity and reduces offshore dispersion associated with Ekman transport (Muñoz et al., 2023, Rahn et al., 2015). These changes result in the retention of particles in coastal areas, enhancing interaction and connectivity but potentially reducing nutrient availability due to decreased upwelling, which could impact kelp settlement (Hollarsmith et al., 2020). Connectivity decreases during winter due to the resurgence of upwelling in early August, which intensifies in spring and peaks in early January (the beginning of summer) (Muñoz et al., 2023). This enhanced upwelling activity drives westward particle movement, facilitated by increased Ekman transport, ultimately reducing connectivity in the central area. Despite the reduction in connectivity, increased upwelling enriches the environment, promoting favourable conditions for settlement and growth (Vásquez et al., 2007). Similar phenomena could explain the differences associated with ENSO dynamics, with weaker southerly winds during El Niño (Figure B5.3, 4 and 5) leading to a shorter and weaker upwelling season, thereby increasing connectivity between nodes. Conversely, La Niña intensifies southerly winds, strengthening upwelling and reducing connectivity associated with greater east-west activity.

Remarkably, the southern population, characterized by high connectivity and population density, remains more stable over time. The southern region experiences a more stable and weaker upwelling pattern due to the SPSA is just above this area (Montecino et al., 2006). This stability, along with nutrient inputs from coastal runoff, creates an environment conducive to kelp reproduction, settlement and growth. However, the potential southward shift of the Pacific Anticyclone induced by climate change poses a threat to the stability and reduction in size of this productive area (Weidberg et al., 2020). Understanding these intricate seasonal variations and stability dynamics is crucial for

anticipating the potential impacts of climate-induced shifts on *M. pyrifera* populations in the southeast Pacific.

## Management of *Macrocystis pyrifera* in the Southeast Pacific

This Chapter delineates effective management units for the extensive *M. pyrifera* population, with a pronounced focus on the southern region, particularly around 41°S, recognised for its essential role in overall population connectivity. While kelp in this region thrives due to high connectivity and favourable conditions, its protection is crucial as it serves as a source population, supporting the recovery of degraded or overexploited areas in the north. This connectivity is vital, as rapid natural colonization from source populations can significantly enhance recruitment success in areas affected by extraction pressures (Reed et al., 2024). Conservation initiatives such as the establishment of no-take zones in the kelp harvesting, specifically within the identified units 1 and 2, are a key strategy to fortify resilience and protect the integrity of the entire population. No-take zones have demonstrated effectiveness in supporting the resilience and biodiversity of marine ecosystems, including kelp forests, by promoting habitat protection and species recovery (Castilla and Bustamante, 1989).

The system of Territorial Use Rights in Fisheries (TURFs), which has been successfully implemented in Chile, offers a robust foundation for these conservation efforts (Moreno and Revenga, 2014). Leveraging existing TURFs, managers can strategically restrict harvesting in critical source areas such as those around 41°S, ensuring their protection while fostering community involvement in resource management. Studies have shown that kelp density is higher within TURFs compared to open-access areas, reinforcing their role in sustainable resource management (González-Roca et al., 2021). To strengthen this approach, we recommend policy integration at the local and national levels, ensuring that these areas are formally recognised in national conservation strategies and supported by enforcement mechanisms. Implementing this approach involves prohibiting extraction activities within the different TURFs situated in these critical areas. The historical data showcasing lower harvesting in this area provides a compelling rationale for its designation as a no-take zone (Porras and Vásquez, 2020). Meanwhile, it is noteworthy that the concentration of extraction activities for *M. pyrifera* spans from 12 to 32°S along the Peruvian and Chilean continental coast, with the arid climatic conditions contributing to cost efficiencies in raw material drying and processing (Vásquez, 2009, ARCE, 2021). Balancing conservation in high-connectivity areas in the south with sustainable harvesting practices in the north mitigates overexploitation risks while maintaining economic viability (Vásquez, 2009). Adaptive harvesting practices informed by connectivity patterns and co-management frameworks, which emphasize local participation, accommodate multiple stakeholder value judgments and equitable benefit-sharing (Gelcich et al., 2010, De Juan et al., 2017), ensure ecological and economic goals are met simultaneously.

Furthermore, my analysis identified key source areas within each management unit, revealing critical patches that may be overlooked due to the high population density in southern Chile. Recognising and safeguarding these areas within existing management frameworks is essential for effective conservation. In Chile, marine conservation practices emphasize the importance of aligning conservation goals with governance structures (Fernández and Castilla, 2005). Embedding these management units in national conservation plans would enhance their long-term protection and integration into broader restoration strategies. In particular, incorporating these key source areas, into existing TURFs would help enforce targeted restrictions in disproportionately important regions within each unit. Additionally, the centrality of certain nodes is key for maintaining connectivity across the population. Prioritising the protection of the area around 29°S mitigates the risk of disconnection and strengthens overall resilience of the kelp network.

The areas around 28 and 35°S stand out as critical hubs with consistently high connectivity. However, their connectivity patterns are influenced by seasonal upwelling, dictated by the intensity of Southerly winds during different seasons and ENSO conditions. With the expected intensification of ENSO events due to climate change (Cai et al., 2015, Cai et al., 2014, Timmermann et al., 1999), management strategies must consider seasonal variations in connectivity. To ensure resilience against climate change, adaptive management policies should be flexible, enabling dynamic response to ENSO forecasts. To this end, management strategies should not only recognise but also actively address these seasonal variations in connectivity. For instance, during periods of strong upwelling (spring and La Niña), targeted conservation measures or seasonal adjustments to activities impacting the kelp habitat, such as temporarily forbidding kelp extraction, could mitigate potential negative impacts and promote self-recruitment.

The resilience of *M. pyrifera* populations to extreme warming events is a critical aspect of connectivity and conservation in the context of climate change. While kelp-dominated ecosystems are often perceived as highly vulnerable to marine heatwaves, some studies have shown that certain populations can persist despite extreme warming events, possibly due to local oceanographic buffering (Reed et al., 2016, Arafeh-Dalmau et al., 2019). However, this resilience is not uniform, as other populations have experienced significant declines under similar conditions (Arafeh-Dalmau et al., 2019). A comparable effect may be occurring in the Humboldt Current System, where limited warming in recent decades could have provided some protection. However, with ongoing climate change, warming trends are expected to intensify posing new challenges for kelp forest resilience (Smale, 2020). To better understand and mitigate these impacts, incorporating climate variables into connectivity analyses can offer insights into population persistence under future scenarios (Frazão Santos et al., 2020). Additionally, transboundary conservation efforts (Mason et al., 2020, Mazor et

al., 2013) could play a crucial role in protecting *M. pyrifera* populations across Chile and Peru, ensuring regional ecological connectivity and enhance the resilience of kelp forests, ensuring their long-term sustainability. Integrating these perspectives into marine spatial planning (Buenafe et al., 2023) and conservation prioritisation (Dabalà et al., 2023) can help identify key areas for protection, optimize resource allocation and develop adaptive strategies that enhance the resilience of kelp forests amid changing climatic conditions.

In the Southeast Pacific, trophic cascades significantly shape *M. pyrifera* ecosystems. Herbivory by sea urchins (*Loxechinus albus*) threatens kelp forests, particularly where predator populations like lobsters (*Jasus frontalis*) and fish species have declined due to overfishing (Vásquez and Buschmann, 1997, Graham et al., 2007). Management strategies that integrate predator conservation into marine spatial planning, such as establishing Marine Protected Areas (MPAs), are critical for maintaining trophic interactions and preventing ecological degradation (Almanza and Buschmann, 2013, Katsanevakis et al., 2011). These strategies should include incentives for fisheries adopting sustainable practices and prioritise multi-species conservation to maintain kelp forest resilience. Protecting these trophic interactions is crucial to maintaining kelp forest resilience, especially as climate change and human pressures exacerbate ecological vulnerabilities in the region. Socioeconomic trade-offs of predator protection must also be addressed, balancing conservation goals with local livelihoods. Involving communities in designing and implementing management strategies fosters long-term ecological and economic sustainability (Gelcich et al., 2010).

## Conclusion

Chapter 3 provides a nuanced foundation for adaptive and targeted management strategies, emphasizing the importance of the southern population, key source areas, central nodes and seasonal management practices in sustaining the overall connectivity and resilience of the *M. pyrifera* population along the southeast Pacific coast. Furthermore, it encourages an integrated approach that acknowledges the concentration of extraction activities in the northern region and suggests collaboration between conservation efforts in the south and sustainable harvesting practices in the north. While our study offers valuable insights, there are several limitations that could be addressed in future research. Although the model captures the effects of oceanographic conditions, further research on the interplay of other ecological factors—such as trophic interactions and the influence of fisheries— would provide a more nuanced understanding on the resilience and connectivity of giant kelp. Moreover, expanding the bioavailability data for giant kelp across the entire study region could improve the model's accuracy, particularly in under-sampled or ecologically unique areas. To further refine connectivity assessment future research could involve running nested models with higher resolution. This approach would offer a more granular exploration of the connectivity and will help to

test the efficacy of current TURFs configurations to protect the giant kelp. Lastly, it would be valuable to investigate the long-term effects of climate change on *M. pyrifera* populations, especially in the context of more frequent and intense ENSO events and shifting oceanographic conditions. Overall, the findings of this Chapter and recommendations provide a comprehensive foundation for informed decision-making, emphasizing the urgency of proactive and adaptive management strategies in the conservation of this marine ecosystem.

# Chapter 4: Factors influencing the early growth and dispersal potential of mangrove propagules[3]


## Abstract

Mangrove dispersal, characterised by propagule movement across complex coastal habitats, is essential for maintaining genetic diversity and ecological resilience. A comprehensive understanding of these processes requires information on the influence of mangrove propagule traits on dispersal potential. However, relatively few studies have investigated the behaviour of propagules in the water column, particularly their responses to different salinities and the duration of their buoyancy. The goal of this Chapter is to enhance the understanding of mangrove dispersal potential by using an experimental approach to assess buoyancy and morphological attributes of 13 mangrove species in the central Great Barrier Reef (GBR) region of Queensland, Australia. Over 90 days, I measured the buoyancy of mangrove propagules and recorded changes in root and stem growth under different salinity conditions, tracking the progression of these traits over time. I found evidence for interspecies variation in buoyancy and diverse responses to salinity treatments, with propagule positioning in the water column changing over time, and for some species, also influenced by salinity. Most of the species showed potential for long-distance dispersal as they stayed afloat for part or most of the experiment. Additionally, I developed species-specific parameters that can be implemented in biophysical models to assess dispersal trajectories of mangroves. The findings of Chapter 4 highlight the importance of integrating mangrove propagule traits in dispersal modelling given the variability in buoyancy behaviours observed among different species.



Keywords: mangrove propagules, dispersion, propagules traits, conservation, management, salinity, buoyancy


[3] Submitted for publication as:
Thompson-Saud, G., Robertson, A. I., Choukroun, Ospina-Alvarez, Logan, M & A. Grech, A. Factors influencing the early growth and dispersal potential of mangrove propagules. Regional Studies in Marine Science.

## Introduction

Seed dispersal is a fundamental ecological process for the survival, reproduction and spatial distribution of plant communities (Schupp et al., 2010, Howe and Smallwood, 1982, Howe and Miriti, 2004). It supports genetic diversity, colonization of new habitats and ecological resilience to environmental and anthropogenic change. For many coastal and marine plants, dispersal mechanisms are intricately linked to water movement. Mangroves, which play a vital role in coastal ecology, climate regulation and human livelihoods, rely on the oceanic dispersal of their propagules to maintain genetic diversity and ecological stability across different habitats (Balbar and Metaxas, 2019, Cowen et al., 2007, Steinberg et al., 2016, Van der Stocken et al., 2019b). This dispersal may be influenced by coastal ocean, tidal and wind and wave dynamics, all of which can interact differently with propagules depending on their position in the water column. Understanding these potential dispersal pathways requires information on mangrove propagule traits, such as post-detachment viability, positive buoyancy duration and position of the propagule within the water column. This knowledge is crucial for effective mangrove population management and conservation, offering insights into their resilience and adaptive strategies in the face of environmental change.

Mangroves inhabit the coastal intertidal zones of tropical and subtropical regions, which are characterised by dynamic environmental conditions driven by tidal cycles, extreme weather and varying salinity levels (Duke et al., 1998). The reproductive seasons generally occur during the warmer months when conditions are favourable for seed germination and establishment (Tomlinson, 2016). Mangroves produce flowers that undergo pollination by insects, birds, mammals or wind. Depending on the mangrove type, the seed may either remain attached to the tree until it germinates into a propagule (viviparous and crypto viviparous) or germinate independently from the parental tree (non-viviparous) (Tomlinson and Cox, 2000). Following detachment, the propagule may settle near the parental tree or travel on a passive journey covering small (e.g. within estuary or bays) or extensive distances (e.g. transoceanic) before reaching a suitable location to settle (Van der Stocken et al., 2019a, Sousa et al., 2007, Robertson and Alongi, 1995). Long-distance dispersal in mangroves is facilitated by positively buoyant propagules that remain afloat for extended periods (e.g. *Xylocarpus granatum, Rhizophora stylosa* and *Ceriops tagal*), drifting with ocean surface currents, winds and waves, until reaching an appropriate settling location or becoming non-viable (Van der Stocken et al., 2019a).

Salinity and exposure time to ocean water can influence buoyancy, dispersal and survival of mangrove propagules (Clarke et al., 2001, Tonné et al., 2017, Rabinowitz, 1978). For instance, higher salinity increases water density, which may enhance propagule buoyancy and potentially extend dispersal distances. However, mangrove propagules can also undergo physiological changes influenced by

salinity, such as water uptake and tissue softening (Smith and Snedaker, 1995, Aziz and Khan, 2001), which can further affect their buoyancy and floating orientation. For example, lower salinities may increase water intake, making propagules heavier and reducing positive buoyancy. Since propagules are exposed to varying salinity levels during dispersal, species with broader salinity tolerance are more likely to establish in a wider range of habitats. Previous work by Clarke et al. (2001) demonstrated interspecific variation in buoyancy and in some species in response to salinity concentration. However, these experiments were limited to 15 days, a duration likely too short to capture the full dispersal window. While some studies suggest that mangrove propagules can stay afloat, on average, for approximately 75 days (Van der Stocken et al., 2019a), no study to date has examined how long a broad range of mangrove species can stay alive and buoyant over extended periods.

Information on the survival, buoyancy and aerodynamics of mangrove propagules are crucial for the development of biophysical models of mangrove dispersal. Biophysical models of mangroves integrate biological information with hydrodynamic models to predict dispersal pathways of propagules and habitat connectivity (Van der Stocken et al., 2019a, Hamilton et al., 2017, Di Nitto et al., 2013, Van der Stocken and Menemenlis, 2017, Gouvêa et al., 2023, Ngeve et al., 2016, Proisy et al., 2016, Zainol et al., 2022). While the utilization of biophysical models has significantly enhanced our understanding of mangrove dispersal, there is an urgent need to develop more robust biological parameters to better inform biophysical models. Information, such as propagule morphology and buoyancy properties (Van der Stocken et al., 2015) is critical because these factors directly influence parameters like windage (the aerodynamic effect of wind on the exposed portion of the propagule, e.g. Breivik et al. (2011)) and drift factor (the effect of wind-driven drift current on the submerged portion, e.g. Wu (1983)), alongside the assessment of salinity concentration across various species to understand their capacity for dispersal and to determine the duration each species remains afloat while is still alive.

Like kelp in Chapter 2 and 3, mangrove propagules rely on oceanographic conditions to reach suitable habitats and both systems are influenced by dispersal dynamics that shape connectivity. The goal of Chapter 4 is to enhance the understanding of mangrove dispersal potential by measuring a series of propagule traits in 13 mangrove species from the central Great Barrier Reef (GBR) region of Queensland, Australia. Specifically, I aimed to: (1) assess the impact of salinity and time on propagule positive buoyancy; (2) evaluate root and stem development as key components influencing viability and dispersal; and (3) compute species-specific factors (drift factor and windage) to inform mangrove dispersal modelling. Through an experimental approach, Chapter 4 elucidated the complex interactions among time, salinity and morphological traits affecting mangrove propagule dispersal and identified which species possess the ability to float for an extended time and therefore have the potential for long-distance dispersal. These findings provide valuable insights into the factors driving

mangrove dispersal dynamics in the GBR region and can inform studies in other regions, given the comprehensive assessment of mangrove propagule morphologies evaluated here.

## Methods

### Study area

The Great Barrier Reef (GBR) region of Queensland, Australia (Figure 15) is a globally significant marine ecosystem, renowned for its rich biodiversity and complex habitats. The tropical climate, characterized by distinct wet and dry seasons. During the wet season, heavy rainfall and freshwater inflows from rivers can reduce salinity levels to as low as 15 PSU (Van Woesik, 1992), particularly near river mouths. In contrast, the dry season is associated with limited freshwater input and high evaporation rates, which can raise salinity levels to 37 PSU (Andutta et al., 2011). This range is relatively large when compared to typical open ocean salinity, which remains around 33–37 PSU (NASA, 2025).

The tidal ranges in this area are substantial, typically ranging from around 2 and 7 metres, and play a critical role in the ecological dynamics and connectivity of reef habitats. The GBR host 41 species of mangroves, representing 50% of the world's mangrove species.

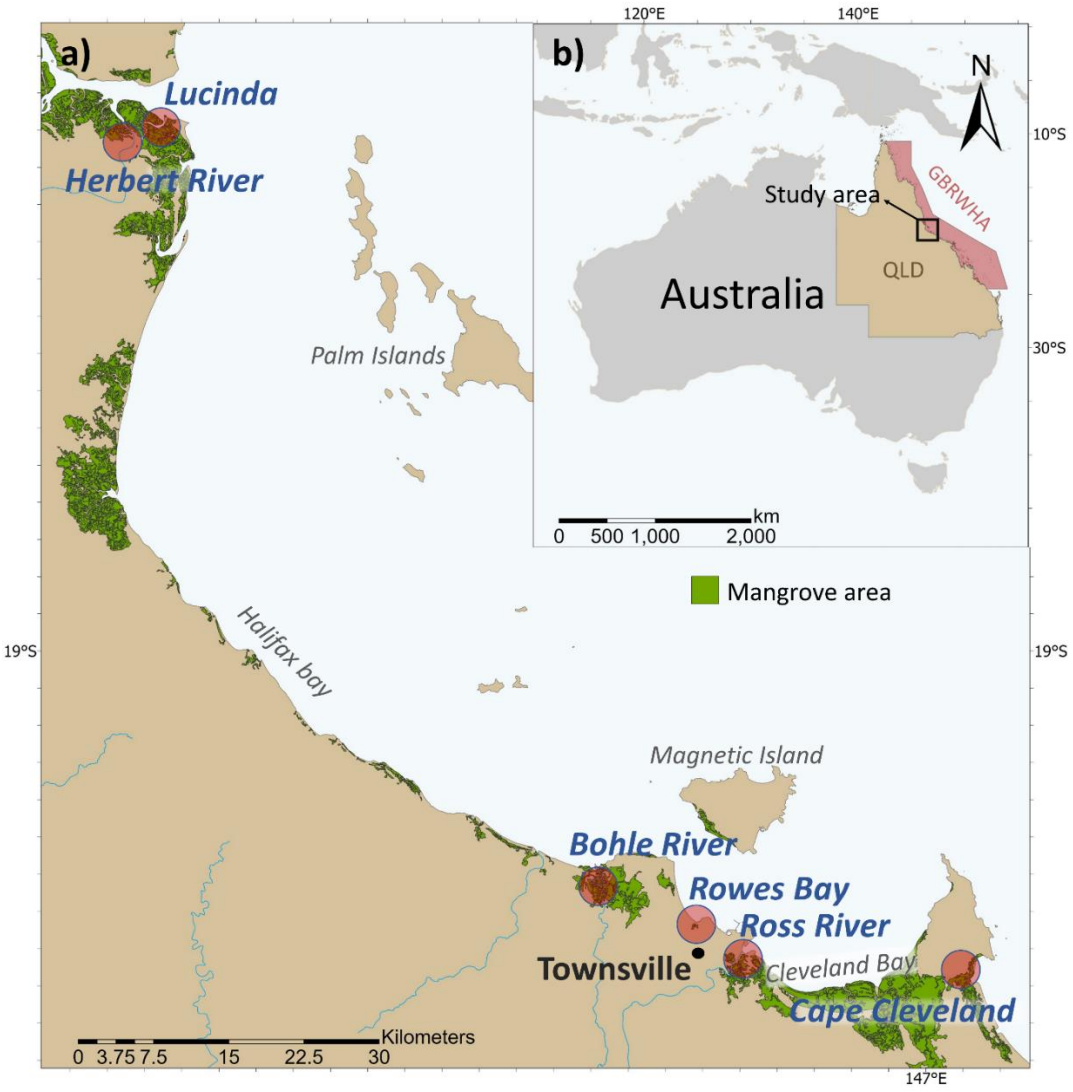


**Figure 15.** a) Mangroves' geographic distribution of the study area. Areas coloured green are mangrove habitats and light blue lines are rivers. The red circles and their corresponding names in blue are the locations where propagules were collected. b) Map of Australia, with Queensland (QLD) coloured brown and the Great Barrier Reef World Heritage Area (GBRWHA) shown in red. The study area is indicated by a black square.

## Field collection

During this study conducted in the central GBR, I collected propagules from 13 different mangrove species (Table 4). Each species was represented with 15 samples, obtained from six locations: Cape Cleveland (19°S, 147°E); Ross River, Rowes Bay and Bohle River in Townsville (19°S, 146°E); and Lucinda and Herbert River (18°S, 146°E; Figure 15). The propagules were collected from different locations because the species are distributed across various coastal areas. This approach covered a variety of species, each characterized by distinct morphologies, buoyancy traits and dispersal capacities (Table 4). To maintain the condition of the propagules, mature specimens were harvested directly from the trees to prevent prolonged contact with saltwater, thereby minimizing the risk of altering osmotic processes before the experiments. It is noteworthy that *Heritiera littoralis*, the only exception to this

practice, was sourced from the soil surrounding the parental tree, as no specimens where found attached to the tree. Due to the inherent difficulty in ascertaining the duration these propagules spent on the soil and in contact with saltwater before collection, this variable remained a consideration in the study as it could influence their viability and buoyancy. To ensure uniformity in my measurement procedures, all propagules underwent assessment (measuring length, width, weight, etc.) on the day immediately following their collection.

**Table 4.** General information about the mangrove species collected and the area from which they were collected. Vivipary refers to the method of seed germination specific to mangroves where the seed begins to develop while still attached to the parental tree; germination describes whether the seed germinates above (epigeal) or below (hypogeal) the ground; and the dates are formatted as DD/MM/YYYY.

| Species | Family | Vivipary | Propagule type | Germination | Area collected | Date of collection |
|---|---|---|---|---|---|---|
| *Nypa fruticans* | Arecaceae | Crypto viviparous | Seed | Epigeal | Herbert River | 12/01/2023 |
| *Bruguiera gymnorhiza* | Rhizophoraceae | Viviparous | Seedling | Epigeal | Lucinda | 26/01/2023, 8/03/2023 |
| *Xylocarpus granatum* | Meliaceae | Non-viviparous | Seed | Hypogeal | Lucinda | 26/01/2023 |
| *Ceriops australis* | Rhizophoraceae | Viviparous | Seedling | Epigeal | Lucinda | 26/01/2023 |
| *Ceriops tagal* | Rhizophoraceae | Viviparous | Seedling | Epigeal | Lucinda | 26/01/2023 |
| *Luminitzera racemosa* | Combretaceae | Non-viviparous | One-seeded fruit | Epigeal | Bohle River | 8/02/2023 |
| *Rhizophora stylosa* | Rhizophoraceae | Viviparous | Seedling | Epigeal | Ross River and Lucinda | 30/01/2023, 8/03/2023 |
| *Heritiera littoralis* | Malvaceae | Non-viviparous | One-seeded fruit | Hypogeal | Lucinda | 8/02/2023 |
| *Bruguiera exaristata* | Rhizophoraceae | Viviparous | Seedling | Epigeal | Cape Cleveland | 8/02/2023 |
| *Avicennia marina* | Acanthaceae | Crypto viviparous | Seed | Epigeal | Rowes Bay | 10/02/2023 |
| *Sonneratia alba* | Lythraceae | Non-viviparous | One-seeded fruit | Epigeal | Rowes Bay | 8/02/2023, 10/02/2023 |
| *Excoecaria agallocha* | Euphorbiaceae | Non-viviparous | One-seeded fruit | Epigeal | Cape Cleveland | 30/01/2023 |
| *Aegialitis annulata* | Plumbaginaceae | Crypto viviparous | One-seeded fruit | Epigeal | Rowes Bay | 29/03/2023 |

## Laboratory-Based Assessment of Propagule Dynamics

The experiment involved placing propagules in water tanks with varying salinity levels of 35, 22.5 and 10 practical salinity units (PSU) for a total of 90 days. These salinity levels likely represent conditions that propagules might encounter as they move through different environments, from estuarine areas to open ocean waters with varying freshwater input. Each tank contained five propagules of a single species, constituting three distinct treatment groups for each species. The tanks were situated in the Marine and Aquaculture Research Facility (MARFU) laboratory at James Cook University, Townsville, where a constant temperature of 25°C was maintained using an air conditioner. To ensure uniform conditions, the water in the tanks underwent stirring every three days, with salinity measurements

taken at five-day intervals. Additional freshwater was introduced as needed to compensate for changes in salinity concentrations resulting from evaporation. Propagules were measured daily for the initial five days and subsequently at five-day intervals until day 90. The comprehensive set of measurements included weight, length, width, buoyancy (considering both overall buoyancy and the specific length of the portion of the propagule outside the water), orientation, as well as root and stem initiation, length and quantity. Propagules were kept under ambient indoor lighting, with overhead fluorescent lights turned on during measurement periods. While light exposure was not systematically controlled, propagules were not kept in complete darkness for extended periods. This detailed monitoring approach aimed to capture the changing physical characteristics of the propagules throughout the 90-day experimental period.

### Data analysis

Bayesian hierarchical models were used to examine two aspects of mangrove propagule buoyancy in response to salinity over time: (1) propensity of propagules to float and (2) percentage of propagule above the water surface. These models were selected for their ability to handle small sample sizes and incorporate prior knowledge, thereby enhancing the robustness and interpretability of the model. To determine the percentage above water, the portion of each propagule protruding above and below the waterline was measured using a ruler. This measurement was taken in a two-dimensional manner, reflecting the linear distance above and below water. Each model was fitted separately for each of the 13 mangrove species and included population effects of salinity (levels: 35, 22.5 and 10 PSU), time (1-90 days) and their interactions. Models also included the varying effect of propagule ID to account for the dependency structure introduced by repeated measurements of the same sampling units. In the buoyancy propensity, time was scaled (mean: 0, standard deviation (sd): 1) to assist model convergence.

All models employed weakly informative priors across all parameters (Table C1.1). More specifically, normal priors were used for the intercept and all population effects, while half student t-distributions (3 degrees of freedom (df)) were applied to the varying (sd) parameters. Where required, priors on shape parameters were based on gamma distributions.

All models were fit using the R “brms” package (Bürkner, 2017) within the R Statistical and Graphical Environment (R Code Team, 2019) and included a total of 5,000 iterations after a warmup of 1,000, thinning to a rate of five across three chains. Markov chain Monte Carlo (MCMC) chain mixing and convergence were confirmed from a series of diagnostics (trace plots, autocorrelation plots, r-hat and effective sample size statistics). Model validations, including goodness of fit, heteroscedasticity and overdispersion, were performed using posterior predictive checks and simulated residuals (DHARMa)

(Hartig, 2020). If there were multiple potential valid candidate models per species, leave-one-out information criterion (loo) (Yao et al., 2017) was used to select the best model.

The buoyancy propensity models (binary data) were fitted against a binomial (logit link) family (Eq. 4). Days 2, 3 and 4 were excluded prior to modelling as they did not provide additional information and their exclusion helped to regularize the temporal covariate.

$$y_{ij} \sim Bin(\pi_{ij}, 1)$$

$$\log(\frac{\pi_{ij}}{1 - \pi_{ij}}) = \beta_0 + \sum_{s=1}^{n} \beta_s S_i \; x \; \beta_t scale(T_i) + \; \gamma_j Z_i$$

$$\gamma_j \sim N(0, \sigma_j)$$
$$\beta_j \sim N(n, v)$$
$$\beta_{[1,n],t} \sim N(0, v)$$
$$\sigma_j \sim t(3,0, v)$$

*Equation 4*

Flotation $\gamma_{ij}$ of the $j_{th}$ propagule at the $i_{th}$ time point was assumed to be drawn from a binomial distribution parameterised by the probability of floating ($\pi_{ij}$). The (natural log of the odds of) probabilities were described by a linear model that included the varying effects of ID ($\gamma_j$) as well as an intercept ($\beta_0$) and the population effects ($\beta_{[1,n],t}$) of salinity ($S_i$) crossed with scaled time ($scale(T_i)$). Constants $n$ and $v$ above were calculated from the observed data.

The models for the percentage of propagule above water were fitted using a beta (logit link) family (Eq. 5). Instead of scaling the time covariate, it was transformed to a logarithmic scale and then rescaled to the range [0-1] to ensure that the model intercepts represented the expected percentage above water at the start of the experiment. This transformation was performed to maintain interpretability of the intercepts despite variations in the duration each propagule remained buoyant throughout the time series. The percentage of propagule above water was modelled for several species (*N. fruticans, B. gymnorhiza, X. granatum, H. littoralis* and *S. alba*). Other species exhibited minimal variation across salinity and time, hindering model stability. Therefore, these species were excluded from these models.

$$y_{ij} \sim beta(\mu_{ij}, \emptyset)$$

$$\log(\frac{\mu_{ij}}{1 - \mu_{ij}}) = \beta_0 + \sum_{s=1}^{n} \beta_s S_i \, x \, \beta_t scale(T_i) + \gamma_j Z_i$$

$$\emptyset \sim T(0.01, 0.01)$$
$$\gamma_j \sim N(0, \sigma_j)$$
$$\beta_0 \sim N(n, v)$$
$$\beta_{[1,n],t} \sim N(0, v)$$
$$\sigma_j \sim t(3,0, v)$$

*Equation 5*

For the buoyancy models, days at which the propagules are most likely to sink were calculated as -$\beta_0/\beta_t$ (conditional on salinity level) from the full posteriors before being summarised to median and lower/upper highest probability density intervals (rounded to integer days).

Percentage above water ($y$) of the $j_{th}$ propagule at the $i_{th}$ time was assumed to be drawn from a beta distribution parameterised respectively by the probability of floating ($\pi_{ij}$) and a dispersion (∅) parameter. The (natural log of the odds of) probabilities were described by a linear model that included the varying effects of ID ($\gamma_j$) as well as an intercept ($\beta_0$) and the population effects ($\beta_{[1,n],t}$) of salinity ($S$) crossed with rescaled logarithm transformed time ($T$). Constants $n$ and $v$ above were calculated from the observed data.

Once the models were run and validated, for each species, pairwise contrasts between each of the salinity levels were conducted across the posteriors marginalising over time. Evidence for differences was thereafter based on Bayesian exceedance probabilities. Finally, for the buoyancy models (binomial) and root growth models, days at which propagules are most likely to sink were calculated using LD50, which represents the time when 50% of the seeds are expected to sink.

In addition to the statistical analyses, a quantitative metric was developed to account for root growth observed during the experiment. Specifically, a "root energy" index was calculated as the product of the number of roots and the length of the longest root, as defined in Eq. 6. This metric allowed for a simple comparative assessment of root development across species and salinity treatment. Among the species studied, only *B. gymnorhiza, X. granatum, C. australis, B. exaristata, A. marina* and *E. agallocha* developed roots at some point during the 90-day experiment.

$$Root\ energy = Root\ number * Longest\ root$$

*Equation 6*

## Factors for species-specific mangrove modelling

A common approach to incorporate wind effects on propagules, such as seeds and fragments, in biophysical dispersal models is to add 3% of the wind speed to the velocity of virtual particles (Tsanis, 1989). However, this approach may not always represent what happens, as the buoyancy of the propagules also influences the wind's effect. To address this, I developed a species-specific parametrization for Lagrangian particle tracking models to improve simulations of mangrove dispersal. Instead of using the standard 3%, I calculated the drift factor ($\vec{u}_{drift}$) and windage ($\vec{u}_{windage}$). These parameters can be added to the current velocity ($\vec{u}_{current}$) to more accurately represent the wind's impact on propagule dispersal. Drift factor and windage were determined based on propagule morphology, specifically assessing the proportion submerged and exposed. The drift factor, representing the effect of the wind-driven drift current on the submerged portion of the propagule, was calculated using Eq. 8 (Van der Mheen et al., 2020). Windage, which accounts for the effect of wind on the exposed portion of the propagule, was calculated using Eq. 9.

$$\vec{u}_{drift} = \left[\alpha - \left(\frac{1}{k\sqrt{\frac{\rho_a + C_d}{\rho_w}}}\right) log\left(\frac{z}{z_0}\right)\right] * \vec{u}_{10}$$

*Equation 8*

where $\alpha$ is 0.03, $k$ is von Karman's constant (0.41), $\rho_a$ is the air density (1.2 kg/m$^3$), $\rho_w$ is the water density, which was approximated to 1025 kg/m$^3$ across all salinity treatments, given the relatively small variation in water density among them. $C_d$ is the drag coefficient (0.00105 for wind speed under 7m/s), $z_0$ is the roughness length of the ocean side (assumed to be a small non-zero value, −0.001 m) (Pugh, 1987), $z$ is the depth, representing the length of the propagule submerged in water and $\vec{u}_{10}$ is the wind speed at 10 m.

$$\vec{u}_{windage} = \sqrt{\frac{\rho_a\ C_{Da}\ A_a}{\rho_w\ C_{Dw}\ A_w}} * \vec{u}_{10}$$

*Equation 9*

where $\rho$ represents the fluid density, $C_D$ is the drag coefficient of the object, $A$ stands for the effective exposed area and the subscripts $a$ and $w$ denote the parameters on the air and water sides, respectively. $\frac{\rho_a}{\rho_w}$ is equal to $1.17 \cdot 10^{-3}$, $\frac{C_{Da}}{C_{Dw}}$ assumed to be equal to 1 (Isobe et al., 2011) and the $\frac{A_a}{A_w}$ is calculating for each species using the length of the propagule that is outside of the water, divided by the length that is inside of the water. Although $A$ represents the area, this ratio can be simplified by using lengths instead of areas because the proportional relationship holds true for both

measurements since the propagules are approximately symmetrically shaped for most mangrove species.

To guide the determination of which species require consideration of salinity and time variations when calculating these factors, I employed the outputs of the statistical analysis, which assessed whether the percentage of propagules above the water surface was influenced by salinity and time. For species that developed roots and/or stem, I also considered the length of the longest root and the length of the stem. The only exception was *A. marina*, as their irregular shape and orientation made it difficult to identify what was above and what was below the waterline.

## Results

The morphological characteristics of mangrove propagules exhibited substantial variation across different species. Sizes and shapes ranged from small and rounded, like *Excoecaria agallocha*, to long and elongated, such as *Rhizophora stylosa* (Table 5). The orientation of the propagules in the water column also showed variability, influenced by the propagule shape and the time of measurement. For instance, elongated species like *Bruguiera gymnorhiza* predominantly maintained a vertical position, while other elongated species such as *Ceriops tagal, R. stylosa* and *Aegialitis annulata* were predominantly in a horizontal position (Figure 16). However, certain species with elongated propagules, like *Ceriops australis* and *Bruguiera exaristata*, exhibited a similar amount of time spent in both vertical and horizontal positions. Both root and stem development were observed in some propagules, including *B. exaristata, Xylocarpus granatum* and *Avicennia marina*. In contrast, other species, such as *Nypa fruticans, C. tagal, Luminitzera racemose, R. stylosa, Heritiera littoralis* and *Sonneratia alba,* did not exhibit any development of roots or stems during the 90-day experimental period. Root initiation ranged from 26 to 82 days, while stem initiation occurred between 63 and 70 days across various species.

**Table 5.** Mangrove propagules characteristics, including mean mass, length, width, shape, predominant orientation, percentage of propagules that developed root and stem during the 90-day experiment and the average day that this happened.

| Species | Mean weight (g) | Mean length (cm) | Mean width (cm) | Shape | Predominant orientation | Seeds that developed roots (%) | Day of root initiation | Seeds that developed stem (%) | Day of stem initiation |
|---|---|---|---|---|---|---|---|---|---|
| *Nypa fruticans* | 42.56 | 6.98 | 4.41 | Oblong ellipsoid | Horizontal | 0 | n/a | 0 | n/a |
| *Bruguiera gymnorhiza* | 27.23 | 20.2 | 1.53 | Cigar shaped | Vertical | 93 | 58 | 93 | 66 |
| *Xylocarpus granatum* | 23.44 | 4.5 | 4.3 | Angular and tetrahedral | Horizontal | 93 | 30 | 27 | 63 |
| *Ceriops australis* | 2.01 | 13.65 | 0.59 | Pencil like but tapered | Vertical | 100 | 50 | 0 | n/a |
| *Ceriops tagal* | 6.3 | 19.69 | 0.92 | Pencil like but tapered | Horizontal | 0 | n/a | 0 | n/a |
| *Luminitzera racemosa* | 0* | 1.71 | 0.46 | Oblong ellipsoid | Horizontal | 0 | n/a | 0 | n/a |
| *Rhizophora stylosa* | 35.1 | 37.59 | 1.37 | Elongate | Horizontal | 0 | n/a | 0 | n/a |
| *Heritiera littoralis* | 19.11 | 5.24 | 3.35 | Slightly flattered ellipsoidal | Horizontal | 0 | n/a | 0 | n/a |
| *Bruguiera exaristata* | 4.26 | 11.73 | 0.84 | Cigar shaped | Vertical | 100 | 28 | 100 | 70 |
| *Avicennia marina* | 4.38 | 2.22 | 2.1 | Rounded | Horizontal | 100 | 26 | 100 | 69 |
| *Sonneratia alba* | 20.74 | 2.76** | 2.76** | Sickle shaped | Vertical | 0 | n/a | 0 | n/a |
| *Excoecaria agallocha* | 0* | 0.4** | 0.4** | Spherical | n/a | 80 | 27 | 0 | n/a |
| *Aegialitis annulata* | 0.38 | 6.55 | 0.3 | Elongated | Horizontal | 67 | 82 | 0 | n/a |

*Imperceptible to the scale

** Diameter

## Propagule buoyancy

The 13 species exhibited diverse responses in buoyancy to the salinity treatment and time after detachment (Figure 16). For instance, *A. marina* submerged during the early stages of the experiments but subsequently resurfaced after a few days (Figure 16.j). Conversely, species like *S. alba* and *A. annulata* sank initially and did not undergo re-floating (Figure 16.k and m). Notably, propagules of *R. stylosa* sank only in the treatment with a salinity of 10 PSU, while those in the other treatments remained afloat (Figure 16.g). In the case of *S. alba*, one propagule in the 22.5 PSU salinity treatment exhibited a unique behaviour by opening on the second day releasing over 100 seeds. Initially buoyant,

these seeds gradually started sinking on day five, with approximately half of them floating by day 90. Certain species either consistently exhibited minimal sinking throughout the study or sank most of their propagules in the initial days of experiments, making statistical measurement impractical due to limited observable changes. The buoyancy of *N. fruticans, L. racemose, H. littoralis* and *E. agallocha* in relation to salinity and time was statistically tested. Importantly, once a propagule sank for the first time, it was considered to remain submerged, even if subsequent re-floating occurred. This methodology was chosen both for statistical purposes and to align with the ecological realism of mangrove dispersal dynamics, where propagules are likely to become attached to the substrate after an initial sinking event.

The results of the statistical analyses conducted across all species indicate that there was evidence of differences in propagule positive buoyancy across all salinity concentrations. In general, propagules became less positively buoyant at lower salinity, with an 86% decrease at 22.5 PSU and by 90% decrease at 10 PSU compared to 35 PSU (Table C1.2). This trend was consistently observed in *N. fruticans, H. littoralis* and *E. agallocha*. However, *L. racemosa* exhibited a decline in positive buoyancy only between 10 and 35 PSU. Notably, positive buoyancy changed over time across all propagules. In addition, expected sinking times varied among species and salinity treatments, with each species displaying distinct patterns in the number of days before becoming negatively buoyant (Table C1.3).

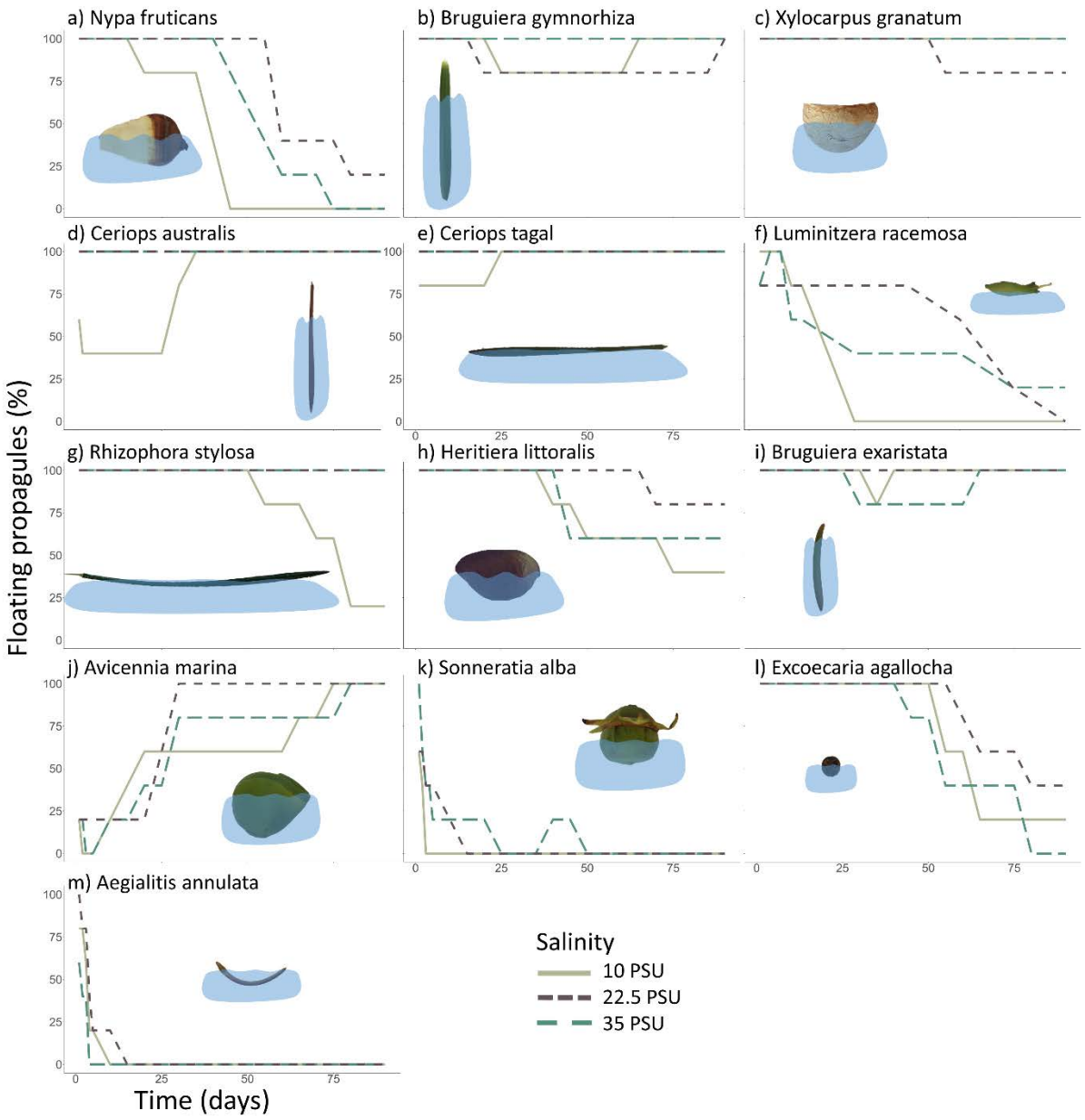


**Figure 16.** Mean percentage of propagules that are floating at different salinities: 10 (solid light green line), 22.5 (dashed brown line) and 35 (dashed green line). Each treatment contains five replicates. The lines represent the percentages of propagules floating at each salinity level. The propagule diagram is a representation and not based on data.

## Percentage of propagule above the water surface

Overall, I found that, among the species tested, the proportion of propagule remaining above the water surface declined more rapidly at lower salinities. Specifically, the decline was 51% greater at 10 PSU than 35 PSU (Table C1.4). This trend was consistent in *B. gymnorhiza* and *H. littoralis*. However, *S. alba* showed a different pattern, with the decline being 85% lower at 22.5 PSU compared to 35 PSU, indicating a slower loss of exposed surface area at intermediate salinity. Additionally, the proportion of the exposed area of the propagules varied over time for *N. fruticans, B. gymnorhiza* and *X. granatum*.

## Root growth

'Root energy', defined as the product of the number of roots and the length of the longest root, was calculated for *B. gymnorhiza, X. granatum, C. australis, B. exaristata, A. marina* and *E. agallocha,* the only species that developed roots at some point during the 90-day experiment (Figure 17).

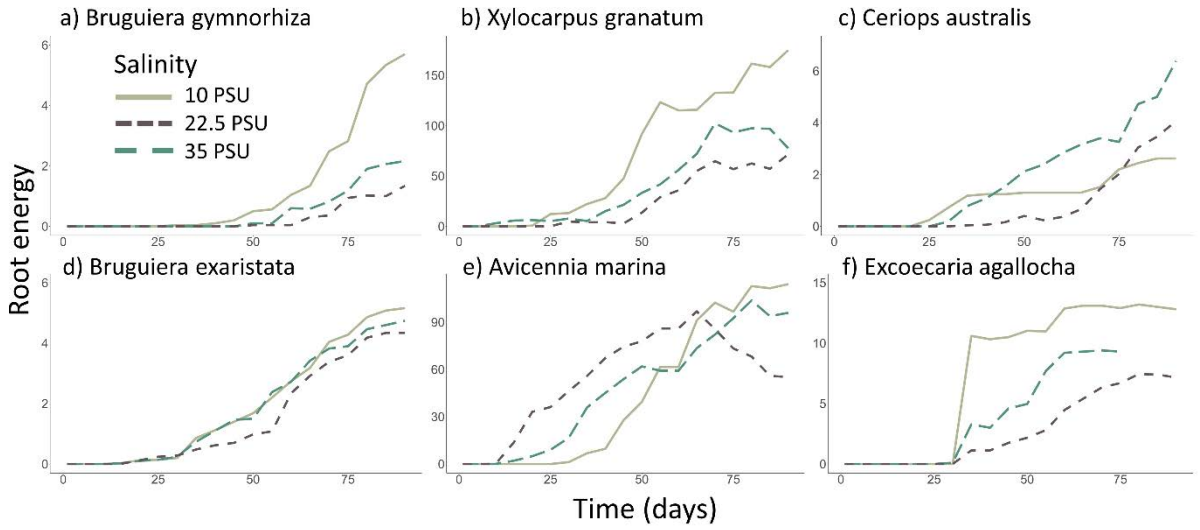


**Figure 17.** Root energy representing the number of roots multiplied by the longest root for the six species that developed roots during the experiment. The lines represent the salinity concentration: 10 (solid light green line), 22.5 (dashed brown line) and 35 (dashed green line).

Overall, root energy varied across species and salinity levels, with 10 PSU consistently having the highest root energy. In contrast, 22.5 PSU resulted in the lowest root energy across all species. Growth trends also differed among species. For instance, *B. gymnorhiza* and *X. granatum* exhibited a sharp increase in root energy after day 50, whereas *B. exaristata* displayed a more gradual and steady increase over time. Additionally, *X. granatum* and *A. marina* produced higher overall root energy compared to the other species that developed roots.

## Factors for species-specific mangrove modelling

The calculated values for drift factor and windage, derived from assessments of propagule morphology, including the proportion submerged and exposed, are presented in Table 6. I obtained values for drift factor and windage for each species and incorporated different salinities and time when appropriate. It is important to note that for some species, windage might not be suitable to include in the model. Even if the proportion above the waterline is high, if the length is negligible, the effect of the drift current is likely more significant than windage, which acts directly on the area of the object that protrudes from the water surface.

**Table 6.** Species-specific drift factor and windage values, detailing the salinity conditions, measurement times for areas above and below the water surface and corresponding values for drift factor and windage.

| Species | Salinity | Time | Above surface | Below surface | Drift factor | Windage |
|---|---|---|---|---|---|---|
| *Nypa fruticans* | All | 1 | 0.011 | 0.022 | 0.023547 | 0.024194 |
| | All | 30 | 0.007 | 0.027 | 0.022995 | 0.016788 |
| | All | 60 | 0.007 | 0.053 | 0.02118 | 0.012435 |
| *Bruguiera gymnorhiza* | 35 | 1 | 0.003 | 0.168 | 0.018075 | 0.004572 |
| | 35 | 30 | 0.012 | 0.182 | 0.01786 | 0.008601 |
| | 35 | 60 | 0.011 | 0.191 | 0.01773 | 0.008022 |
| | 22.5 | 1 | 0.004 | 0.013 | 0.024962 | 0.01898 |
| | 22.5 | 30 | 0.014 | 0.186 | 0.017801 | 0.009387 |
| | 22.5 | 60 | 0.021 | 0.19 | 0.017744 | 0.011375 |
| | 10 | 1 | 0.013 | 0.155 | 0.018292 | 0.009909 |
| | 10 | 30 | 0.016 | 0.164 | 0.018148 | 0.010535 |
| | 10 | 60 | 0.027 | 0.18 | 0.01789 | 0.013252 |
| *Xylocarpus granatum* | All | 1 | 0.004 | 0.019 | 0.023941 | 0.015699 |
| | All | 30 | 0.002 | 0.021 | 0.023672 | 0.010559 |
| | All | 60 | 0.002 | 0.025 | 0.023203 | 0.009678 |
| *Ceriops australis* | All | All | 0.001 | 0.1185 | 0.019015 | 0.003143 |
| *Ceriops tagal* | All | All | 0.001 | 0.009 | 0.025952 | 0.011405 |
| *Luminitzera racemosa* | All | All | 0.001 | 0.004 | 0.028135 | 0.017108 |
| *Rhizophora stylosa* | All | All | 0.003 | 0.011 | 0.025412 | 0.017869 |
| *Heritiera littoralis* | 35 | All | 0.01 | 0.021 | 0.023672 | 0.023611 |
| | 22.5 | All | 0.01 | 0.022 | 0.023547 | 0.023068 |
| | 10 | All | 0.01 | 0.024 | 0.023312 | 0.022086 |
| *Bruguiera exaristata* | All | All | 0.002 | 0.089 | 0.019785 | 0.005129 |
| *Avicennia marina* | All | All | 0.001 | 0.021 | 0.023672 | 0.007467 |
| *Sonneratia alba* | 35 | All | 0.003 | 0.031 | 0.022624 | 0.010644 |
| | 10 | All | 0.003 | 0.037 | 0.022184 | 0.008955 |
| | 22.5 | All | 0.001 | 0.036 | 0.022221 | 0.005703 |
| *Excoecaria agallocha* | All | All | 0.002 | 0.002 | 0.03 | 0.034216 |
| *Aegialitis annulata* | All | All | 1.00E-04 | 0.003 | 0.029 | 0.006354 |

## Discussion

The findings of Chapter 4 reveal substantial variability among different species of mangrove propagules in terms of buoyancy, exposure above and below the waterline and root growth characteristics. Moreover, intraspecies differences were observed when propagules were subjected to varying salinity levels, with behaviours showing considerable variation over time. These results have significant implications for predicting mangrove dispersal and connectivity, as the duration of

buoyancy and responses to salinity conditions were found to differ across species, demonstrating a higher complexity in biological parameters than what has been incorporated in biophysical models of mangrove dispersal. Additionally, I found that propagule exposure above and below the water surface also varies among species and salinity levels. Therefore, these factors must also be considered in modelling, as they impact aspects such as windage and drift factor, thereby influencing dispersal dynamics.

The morphology and behaviour in the water column of the mangrove propagules varied notably among the 13 species assessed here. Some species, such as *B. gymnorhiza, X. granatum, C. australis, C. tagal, R. stylosa* and *B. exaristata*, remained buoyant throughout the 90-day experiment, indicating their potential for prolonged dispersal via currents, tides and winds. Others, like *N. fruticans, L. racemosa, H. littoralis* and *E. agallocha*, were also buoyant but for shorter durations. While it is true that some literature reports extensive floating periods for species like *H. littoralis* (Clarke et al., 2001), it is worth noting that *H. littoralis* was the only species collected from the soil surrounding the parental tree, so the exact duration of its buoyancy prior to collection is uncertain. There was also a group of species, including *A. marina, S. alba* and *A. annulata*, which showed little potential for dispersal as they sank within the first days of the experiment. These findings align with those of Clarke et al. (2001), who conducted a similar experiment although over a shorter timeframe, obtaining similar patterns.

Intraspecies variations in buoyancy were also apparent with changes in salinity concentration. Specifically, for *N. fruticans* and *E. agallocha*, notable differences were observed across different salinity treatments, indicating that salinity should be considered a crucial parameter when modelling the dispersal of these species. Additionally, buoyancy of all propagules that were tested changed throughout the experiment, including *N. fruticans, L. racemose, H. littoralis* and *E. agallocha*. While previous mangrove dispersal models have considered the impact of time (Van der Stocken and Menemenlis, 2017), it was determined that the maximum floating period of 75 days post-detachment does not hold true universally across all species. This underscores the necessity of incorporating species-specific information when evaluating mangrove dispersal, given the observed variability among different species. It is worth noting that *N. fruticans* seeds in this study were relatively small compared to specimens from core populations, where seeds can float for extended periods and disperse over hundreds of kilometres (Robertson and Alongi, 1995). This suggests that the findings for *N. fruticans* in this experiment may represent the lower end of the species' dispersal capabilities.

In the case of *R. stylosa*, statistical analysis for buoyancy was not feasible due to insufficient variation for testing. However, notable differences were observed between the 10 PSU treatment and the other treatments. Propagules in the 10 PSU treatment sank while those exposed to higher salinity remained

buoyant. These differences were likely attributable to the distinct collection sites. Propagules used in the 35 PSU and 22.5 PSU treatments were sourced from Ross River (Townsville), whereas those in the 10 PSU treatment were sourced from Lucinda. This sampling strategy was adopted because it was challenging to gather all necessary propagules from a single location. Additionally, propagules from the 10 PSU treatment were significantly smaller than those from the other sites, suggesting potential differences in developmental stage or environmental adaptation. Consequently, I cannot definitively conclude that the treatment itself influences the buoyancy of *R. stylosa*. It is plausible that variability in species buoyancy could also be linked to the geographical origin of the propagule. Propagule traits such as buoyancy, size and establishment time can vary and are often shaped by the typical position of the adult trees within the intertidal zone, with landward species generally producing smaller propagules that require longer periods free from inundation to establish (Rabinowitz, 1978). One possible explanation for this observation is that propagules from Lucinda (10 PSU) may have had different structural or physiological traits influencing their buoyancy, such as smaller size, reduced internal air cavities or increased water uptake, possibly due to local environment. Further investigations are needed to clarify the extent and causes of intraspecific variability in propagule traits across different locations.

I also observed that some propagules initially sank during the first days but later resurfaced, indicating that the dispersal capacity is lower for these species, as they are more likely to settle near the parental tree. Specifically, all propagules of *A. marina* sank during the initial period, while some of the propagules of *C. australis* in the 10 PSU salinity treatment experienced a similar phenomenon. In the case of *A. marina*, which is considered a pioneer species in mangrove ecosystems and the most widespread mangrove species (Osborne and Berjak, 1997), its rapid sinking behaviour suggests a different dispersal strategy compared to other species. Our results show that *A. marina* sinks quickly within the first few days of the experiment, forming roots early on, indicating its capacity for swift establishment rather than relying on long-distance dispersal through buoyancy. Consequently, the potential dispersal capabilities of *A. marina* may be overestimated in some biophysical models, which often emphasize buoyancy and long-distance dispersal. Our findings suggest that these species may employ a more localized strategy for establishment, which could be important for refining models of mangrove dispersal and connectivity. In previous studies, an early sink of *A. marina* seeds has also been observed (Clarke et al., 2001). Research on *A. marina* dispersal in southeastern Australia indicates that inter-population dispersal is infrequent due to the limited number of floating propagules, leading to restricted gene flow between populations (Clarke, 1993). However, it is important to note that while dispersal becomes less likely, it is still possible, as propagules might not be able to settle or they might be able to disperse under water. Instances of *A. marina* propagules

found outside mangrove forests suggest that some propagules might not settle immediately and could disperse upon refloating (Minchinton, 2006).

As buoyancy alone does not solely determine propagule transport, I also examined propagule morphology, specifically assessing the proportion submerged and exposed. This information is essential for calculating windage (the effect of wind on the exposed portion of the propagule) and drift factor (the effect of wind-driven drift current on the submerged portion) (Van der Mheen et al., 2020). The analysis revealed differences in salinity treatments for *B. gymnorhiza, H. littoralis* and *S. alba*. Therefore, when applying windage and drift factor to these species in biophysical models, it is crucial to consider the salinity of the areas where the propagules are travelling. Furthermore, *N. fruticans, B. gymnorhiza* and *X. granatum* changed over time. Thus, the time propagules remain afloat should be considered when modelling the dispersal of these species as it has been previously described (Tonné et al., 2017). Moreover, in the case of *B. gymnorhiza*, it is also important to account for root and stem development, which occur around days 45 and 66 of the experiments, respectively, as they introduce additional drag. Given that the *B. gymnorhiza* propagules were mostly in a vertical position, root and stem lengths were incorporated into the drift factor and windage calculations to better represent the influence of wind-driven currents on their dispersal.

Climate change is likely to affect the dispersal of mangrove propagules, primarily through alterations in salinity, currents and wind patterns (Alongi, 2015, Van der Stocken et al., 2022). Rising sea levels, changes in temperature, precipitation and evaporation rates are expected to alter coastal salinity regimes, potentially impacting the buoyancy and viability of mangrove propagules. Evidence indicates that warmer and less saline ocean conditions, attributed to increased freshwater input, could alter the dispersal paths of mangrove propagules and elevate sinking rates in less suitable offshore areas, potentially impacting the resilience of mangrove forests (Van der Stocken et al., 2022). In some areas the opposite might be true, higher salinity levels may enhance positive buoyancy, allowing propagules to travel greater distances; however, excessively high salinities could exceed the tolerance thresholds of certain species by affecting seed viability, metabolism or osmotic balance, leading to reduced dispersal success (Alongi, 2022). Moreover, it has been found that germination rates of some mangrove species decline significantly or fail to germinate at high salinity levels, such as *Xylocarpus mekongensis* and *X. granatum* at 40 ppt and *Heritiera fomes* and *Anisoptera cucullata*, which cease germination at 35 ppt and 20 ppt, respectively (Mahmood Hossain et al., 2014). Additionally, extreme salinity conditions, such as 50 ppt, have been shown to completely inhibit mangrove growth (MDPI, 2023). Further research is needed to quantify the extent to which extreme salinity levels impact propagule viability, which is an essential trait of propagules, significantly influences the success of mangrove species in colonizing suitable habitats. In addition to changes in salinity, other variables such

as changes in ocean currents, driven by shifting temperature gradients and altered wind patterns, can further transform dispersal dynamics. Enhanced or altered currents may facilitate longer dispersal distances, potentially aiding in the colonisation of new habitats or reduce dispersal distances and potentially hinder connectivity between mangrove populations, reducing genetic exchange and resilience (Alongi, 2015). Additionally, intensified wind patterns (Greene et al., 2010), including more frequent and severe storms (Brooks, 2013), could influence propagules dispersal patterns. Increased wind strength might enhance or reduce dispersal distances for floating propagules but also poses the risk of depositing them in unsuitable environments, thereby reducing overall establishment success. Understanding these climate-induced changes is crucial for developing accurate predictive models and effective conservation strategies to maintain mangrove ecosystems in a rapidly changing world. Integrating species-specific responses to salinity, current alterations and wind patterns into these predictions will be essential for forecasting future dispersal patterns and ensuring the resilience of mangrove forests.

## Conclusion

Chapter 4 highlights the variable influence of mangrove propagule traits on dispersal potential, which are shaped not only by buoyancy but also morphological characteristics. Future investigations can improve the parametrisation of biophysical models by integrating this Chapter's findings on how long propagules remain afloat, salinity effects and propagule positioning within the water column. This comprehensive approach will improve the accuracy of mangrove dispersal modelling, crucially important in dynamic environments such as the Great Barrier Reef, where salinity variations fluctuate between seasons, as well as in other regions with more stable environmental conditions. The data generated from this research can refine and validate biophysical models, ultimately providing valuable insights into mangrove population connectivity.

# Chapter 5: Operationalising connectivity in the spatial management of mangroves[4]


## Abstract

Mangroves form highly interconnected ecosystems, yet their connectivity is often overlooked in spatial planning. Management strategies that operationalise connectivity are particularly important within the context of blue carbon initiatives, which seek to enhance carbon sequestration through ecosystem protection and restoration. Successful restoration relies on propagule dispersal to recolonise previously disconnected areas, making connectivity a key factor in long-term ecosystem recovery. To address this gap, in Chapter 5, I developed a biophysical model to predict propagule dispersal and transport dynamics for two important mangrove species in the central Great Barrier Reef, *Rhizophora stylosa* and *Bruguiera gymnorhiza.* Additionally, network analysis was employed to assess the centrality of their sub-populations across different coastal areas and to identify key dispersal routes contributing to connectivity processes. I mapped habitat patches based on five connectivity-driven management objectives and combined this information with mangrove health data to develop an urgency index for prioritising spatial management. I identify central areas, like the Hinchinbrook Channel and the region below Mission Beach, as important replenishment sources or connectivity corridors that also coincide with degraded mangrove habitats. By focusing on these areas, the findings of Chapter 5 support targeted management efforts that enhance mangrove resilience against climate change and coastal development in a cost-effective manner.



Key words: blue carbon, Great Barrier Reef (GBR), urgency index, spatial management, connectivity, *Rhizophora stylosa* and *Bruguiera gymnorhiza*


[4] In preparation for submission as:
Thompson-Saud, G., A. I., Choukroun, Hanuise, D., Canning, A., Ospina-Alvarez, & A. Grech, A. Operationalising connectivity in the spatial management of mangroves. Global Change Biology.

## Introduction

Marine connectivity is important for the conservation and restoration of mangroves because it influences the interactions between species and their habitats (Hilty et al., 2020). It governs the movement and dispersal of organisms across landscapes and seascapes, influencing ecological processes and the resilience of populations. For conservation and management strategies, particularly in the design of protected areas and active restoration, incorporating connectivity is necessary to maintain viable populations and preserve ecosystem functions (Balbar and Metaxas, 2019, Carr et al., 2017). Research has shown that protecting well-connected dispersal corridors enhances biodiversity and resilience to environmental pressures, while networks of no-take marine reserves can stabilize ecological processes by buffering fluctuations in recruitment and larval supply (Fontoura et al., 2022, Harrison et al., 2020). Moreover, considering ecological connectivity is vital for the effective design of marine protected areas and networks, ensuring the long-term conservation of ecosystem integrity, biodiversity and ecosystem services (Gardner et al., 2024). Despite growing recognition of the importance of marine connectivity, there remains a significant knowledge gap regarding the connectivity of marine plants, particularly mangroves, and their implications for management (Bryan-Brown et al., 2017).

Mangroves forests are coastal ecosystems that occupy the niche between mean and high sea level alongside saltmarsh, with the ratio of the two depending on long-term rainfall (Saintilan et al., 2009). These forests consist of unique plants that have evolved salt tolerance to thrive in these environments (Tomlinson, 2016). Mangroves provide a range of ecosystem services, from protecting shorelines to supporting biodiversity and sequestering carbon (Sievers et al., 2023, Lee et al., 2014). Recognising their role in carbon sequestration, global blue carbon initiatives have gained significant attention, with substantial financial investments aimed at protecting and restoring mangrove ecosystems. These initiatives are part of broader climate mitigation strategies, underscoring the importance of mangroves in addressing global carbon emissions and achieving climate targets (Hamilton and Friess, 2018). For mangroves to provide these services, they need to be healthy, which refers to the ecosystem's condition and vitality, including the growth of mangrove species and habitat quality. A critical component of maintaining mangrove health is their connectivity through propagule dispersal, which links geographically distant habitats and enhances resilience to disturbances (Van der Stocken et al., 2019b). However, the role of propagule connectivity in mangrove ecosystems is often overlooked in conservation design due to the inherent challenges in assessing it (Van der Stocken et al., 2019b).

Recent advances in biophysical models, such as higher-resolution hydrodynamic simulations, along with developments in network graph theory, including weighted connectivity metrics, have facilitated

the exploration of connectivity between marine habitats, offering tools for identifying dispersal pathways, as previously applied in Chapter 2 (Van der Stocken et al., 2019a, Hamilton et al., 2017, Di Nitto et al., 2013, Van der Stocken and Menemenlis, 2017, Gouvêa et al., 2023, Ngeve et al., 2016, Proisy et al., 2016, Zainol et al., 2022). Connectivity has been effectively integrated into decision-making for marine reserve design, where models have informed the placement of reserves to maximize larval dispersal and fishery sustainability (Gaines et al., 2003, McCook et al., 2009b, Almany et al., 2009, Treml et al., 2008, Treml and Halpin, 2012, Ospina-Alvarez et al., 2020b). Demonstrating that by considering the movement patterns of species across marine landscapes, spatial planning can be optimized to ensure connectivity between key habitats, which enhances biodiversity conservation and sustains ecosystem services (Ospina-Alvarez et al., 2020b). However, mangrove ecosystems present challenges for incorporating connectivity into management. Unlike coral reefs and other marine systems, mangrove propagule dispersal is heavily influenced by buoyancy duration and the interaction of propagules with coastal geomorphology as they occupy the interface between terrestrial and marine systems (Spencer et al., 2016). These complexities highlight the need for new frameworks tailored to mangrove ecosystems. To make connectivity actionable for mangrove management, it is essential to integrate these dispersal dynamics into robust biophysical models. Linking these findings to management goals will help ensure that connectivity directly informs spatial planning and conservation strategies (Keeley et al., 2021, Beger et al., 2022).

Similar to the approach in Chapters 2 and 3, Chapter 5 examines population connectivity of two mangrove species, *Rhizophora stylosa* and *Bruguiera gymnorhiza*, which are widely distributed across Queensland's mangrove ecosystems. These species were selected for their broad distribution in the region, their contrasting propagule traits that influence drift dynamics and the availability of detailed distribution maps, which facilitate the analysis of their connectivity patterns. The primary goal of this Chapter is to enhance mangrove management by integrating connectivity metrics that align directly with management objectives. To achieve this, I refined the accuracy of biophysical models by adjusting their parameters to reflect species-specific traits, such as propagule buoyancy and morphology. The questions driving this research are: (1) what are the dispersal patterns and connectivity characteristics of *R. stylosa* and *B. gymnorhiza* propagules?; (2) how do windage and drift factors influence the dispersal patterns of their propagules?; (3) how can connectivity metrics be aligned with management objectives to enhance the resilience of mangroves through dispersal?; and (4) how can a new framework that incorporates impact assessments and connectivity metrics be developed to prioritise management actions? By advancing the understanding of mangrove connectivity, this research not only strengthens management practices but also aligns with global climate initiatives such as the Blue Carbon Initiative (BCI, 2019) and supports national programs like Australia’s Emission Reduction Fund

(ERF, 2014). Protecting connectivity directly contributes to these programs' goals, as maintaining well-connected mangrove ecosystems enhances their capacity for carbon sequestration and emission reduction, reinforcing their role in climate mitigation.

## Methods

### Species description and distribution

In Chapter 5, I focus on two mangrove species in the central Great Barrier Reef (GBR): *Rhizophora stylosa* and *Bruguiera gymnorhiza*. *R. stylosa*, or the stilt-rooted mangrove, is typically found in the seaward zone of the intertidal area, where it thrives in regularly inundated conditions. It is noted for its aerial roots that support its growth in waterlogged soils. It produces elongated, viviparous propagules that develop while still attached to the parental tree. These propagules have a slender shape and a pointed tip, allowing them to embed in soft substrates upon stranding. They are characterized by long floating periods, which facilitate long-distance dispersal (Duke, 2006). *B. gymnorhiza*, commonly known as the large-leaved or orange mangrove, is more commonly found in the mid-to-upper intertidal zone, where it experiences less frequent tidal inundation. It is distinguished by its buttress roots and large, thick leaves, helping to protect the coastline and providing habitat for various marine organisms. This species produces large, robust propagules with a characteristic blunt, cigar-like shape, exhibiting a shorter floating duration (Duke, 2006). Both species are particularly common in the central GBR, where they contribute significantly to the stability, productivity and resilience of mangrove ecosystems. Understanding their dispersal dynamics and connectivity patterns is crucial for effective conservation and management of these coastal forests.

The distribution maps of mangrove species used in Chapter 5 were developed by Dunning (2010) as part of the Queensland Coastal Wetlands dataset, covering the period from 1987 to 1997 (Figure 18). These were the only publicly available maps that showed mangrove distribution by genera, rather than general distribution. This mapping includes mangrove communities, saltpans and samphire with mangrove areas classified by genera, including *Bruguiera* and *Rhizophora*. It was created through automatic classification of 25 metres resolution Landsat TM images, supplemented by colour aerial photography and ground truthing. The dataset provides a positional accuracy of 100 metres and a classification accuracy of approximately 80%. Since mangroves typically grow in estuarine areas that are usually not included in hydrodynamic models, I created polygons in the first cell of the hydrodynamic model, where oceanic conditions are represented, to depict mangrove distribution and quantities, covering the central GBR area from around Bowen to Cairns.

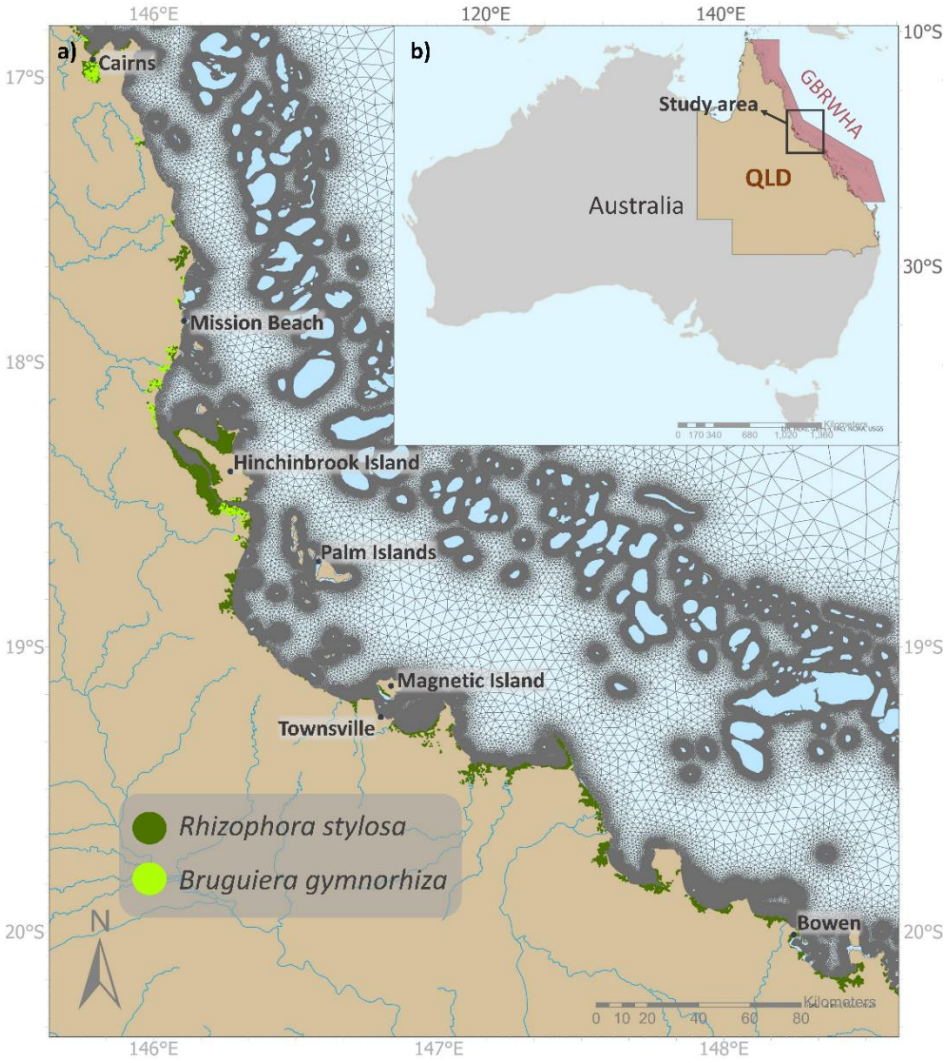


**Figure 18.** Study region. a) Areas coloured dark green are *Rhizophora stylosa* habitats and light green are *Bruguiera gymnorhiza* habitats. The light blue lines are rivers. The dark grey polygons represent the mesh grid of the hydrodynamic model. b) Map of Australia, with Queensland (QLD) coloured brown and the Great Barrier Reef World Heritage Area (GBRWHA) shown in red. The study area is indicated by a black square.

## Coastal conditions

The coastal hydrodynamics in the central GBR are characterized by complex interactions between tidal currents, river inflows and oceanic forces (Wolanski and Kingsford, 2024). Inflows from major rivers, such as the Burdekin and Herbert, contribute significant volumes of freshwater. These freshwater inputs also deliver sediments and nutrients that support the development of estuarine habitats (Day Jr et al., 2012), but they can also negatively affect these ecosystems, for example, through root burial by sediment or the promotion of algal blooms, which can degrade water quality and mangrove health (Feller et al., 1999). Oceanic forces, including wave action and coastal currents, further shape the coastal landscape by contributing to energy processes, sediment transport and deposition. These forces influence the location and stability of suitable habitats for mangrove seedlings, affecting their establishment and growth. The interplay between these hydrodynamic factors determines the

distribution and health of mangrove communities, highlighting the importance of understanding and modelling these processes accurately for effective mangrove management.

### Coupled Hydrodynamic-Individual Based model

Ocean circulation along the GBR was modelled using the finite-element, unstructured-mesh ocean model SLIM (Second-generation Louvain-la-Neuve Ice-ocean Model; SLIM (2025)). The 2D barotropic version of the model was employed, as the coastal areas of the GBR are considered well-mixed and shallow, where vertical current variations are minimal (Luick et al., 2007). The mesh used in the model has a horizontal resolution between 250 metres, near the coast, while reaching up to 5 kilometres near the coral sea, covering the extent of the whole GBR from 10.08 to 25.29°S. SLIM2D simulates sea surface elevation and depth-averaged current velocity (Lambrechts et al., 2008). The model was forced with wind, tides and current data. Bathymetric data, sourced from the Australian Government at a resolution of 30 metres (Beaman, 2017), were used to define seafloor contours. Simulations were conducted over the period from 2015 to 2016, providing hourly output data.

The SLIM model incorporates an Individual-Based Model (IBM) tool that simulates the physical and biological influences on the floating propagules of *R. stylosa* and *B. gymnorhiza* (Table 7). These propagules are represented as virtual particles within the model. The release location of the virtual particles for *R. stylosa* was specifically delimited within the coordinates 20.27 to 16.74°S, representing the central GBR (Figure 18). For *B. gymnorhiza*, release points were defined over a smaller area between 18.71 to 16.74°S, as this species is not found in the southern part of the central GBR. To accurately reflect the physical characteristics of these propagules, I included parameters such as windage (the aerodynamic effect of wind on the exposed portion of the propagule) and drift factor (the effect of wind-driven drift current on the submerged portion) (Van der Mheen et al., 2020). These factors were added to the hydrodynamic velocities to account for their influence in their dispersal velocity. These parameters were obtained from Chapter 4, where they were calculated by measuring the exposed and submerged areas of 15 propagules for each species over 90 days. Although salinity concentration can affect propagule buoyancy, with evidence from Chapter 4 showing that *B. gymnorhiza* changes buoyancy in response to varying salinity levels, this factor was not included in the model due to SLIM's lack of salinity incorporation. As a result, I recalculated the parameters for *B. gymnorhiza* by focusing only on temporal variation, excluding the effects of varying salinity, rather than directly using the factors from Chapter 4. For *B. gymnorhiza*, I used three different drift factors and windage values, as the propagules demonstrated changes in orientation over time. In contrast, for *R. stylosa*, I used a single drift factor, as there was no evidence of positional changes over time and the portion above the waterline was too small for windage to have an effect without exaggerating the influence of wind. For both species, I also ran the models without any drift factor and windage

adjustments to evaluate whether including these factors significantly affects the results of the biophysical model and subsequent analyses.

**Table 7.** Summary of the input parameters used in the biophysical model of *R. stylosa* and *B. gymnorhiza* in the central Great Barrier Reef.

| Category | Parameters | State / Description |
|---|---|---|
| *Particle-tracking model* | Total number of particles released | ~ 1,000,000 for each release |
| | Particle types/classes | Particles representing floating mangrove propagules |
| *Initiation of pelagic phase* | Release location | Known location of *R. stylosa* and *B. gymnorhiza* forests (Figure 18) |
| | Release events coverage | From 2015 to 2016 |
| | Frequency of release events | Once a week from January to February (known reproductive period) (Duke, 2006) |
| *Transport and movement* | Maximum length of pelagic phase | 90 days |
| | Buoyancy | Positive |
| | Windage | *R. stylosa:* no windage – the proportion of the propagule above the waterline was too small that windage effects were negligible |
| | | *B. gymnorhiza*: 0.0183 (day 1-30), 0.0179 (day 31-60) and 0.0096 (day 61-90) – varies over time as the propagule's position with respect to the waterline changes over time |
| | Drift factor | *R. stylosa:* 0.0254 (day 1-90) – this value remained constant as the propagule position did not vary over time |
| | | *B. gymnorhiza*: 0.0073 (day 1-30), 0.0096 (day 31-60) and 0.0112 (day 61-90) – varies over time as the propagule's position with respect to the waterline changes over time |
| *Settlement* | Settlement rate | No settlement rate |

Each virtual particle remained afloat for the entire 90-day simulation, even when touching coastal areas, where they bounced back into the ocean, or connecting with mangrove zones. This approach was chosen because the experiments in Chapter 4 did not show any clear pattern of sinking for these species' propagules. As a result, the exact timing of sinking was unknown; however, it is confirmed that the propagules remained afloat at least for 90 days. From 2015 to 2016, approximately eighteen million particles were released in each model for each mangrove species. This number does not represent the actual propagule count but is used to ensure that the model's results are not overly influenced by the number of particles. A higher number of particles helps to smooth out variability, leading to more stable and reliable outcomes. I adjusted the model to dynamically release virtual particles based on local density conditions, with higher mangrove densities leading to the release of more particles. To determine local density, I measured the area of each mangrove patch and

normalizing particle release accordingly, ensuring that larger areas released more particles to reflect increased dispersal in crowded areas. This density-dependent particle release provided a more realistic representation of the dispersal dynamics observed in natural mangrove populations.

### Connectivity analysis

Given the highly dynamic and rapidly changing coastal conditions in the GBR, the biophysical model outputs were assessed on an hourly basis to ensure that critical information was not overlooked. Similar network analysis and graph theory measures, as used in Chapters 3, were employed to assess connectivity patterns and to identify subpopulations within the mangrove population. The networks consisted of nodes, which represent habitat patches separated by approximately 100 metres, that are connected by edges, which represent the potential dispersal routes. Weights were assigned to the nodes and links to provide information about the strength of the connections. The network analysis was conducted using "tidyverse" and “igraph” packages (Wickham et al., 2019, Csardi and Nepusz, 2006) within the R language. Network visualizations were generated using the following R packages: “ggplot2” v.3.2.1, “ggmap” v.3.0.0 and “ggraph” v.2.0.0 (Hadley, 2016, Kahle and Wickham, 2013, Pedersen, 2019).

To evaluate the overarching population patterns, I applied network measures to the habitat graph (Table 8), allowing me to quantify various structural aspects of the population, focusing on overall connectivity patterns. Using binary metrics for this assessment provides a clear and simplified view of the network structure by focusing on the presence or absence of connections. I used these network analyses for models with and without drift factor and/or windage, facilitating comparisons across different scenarios. Metrics, such as total edges, network density, network diameter, connected components and modularity, were used to assess overall network structure. I also employed the modularity measure to assess the interconnectivity among nodes and identify potential boundaries within the metapopulation of mangrove species. This approach helps to identify areas that exhibit stronger internal connectivity compared to the broader population, aiding in the definition of possible subpopulations that can be used as management units. By doing so, we can better focus conservation efforts on areas with more cohesive ecological structures, ensuring that interventions are applied to regions of the population with greater connectivity. To identify groups within the network, I used the cluster Infomap algorithm, which operates by performing random walks to maximize information flow within communities while minimizing it between communities (Rosvall and Bergstrom, 2008). The Infomap algorithm identifies communities that optimize the map equation from an information-theoretic perspective and can detect hierarchical community structures (Rosvall et al., 2009). The Infomap algorithm has been successfully applied in dispersal ecology to identify oceanic provinces that

are highly connected internally while exhibiting minimal particle exchange with other regions (Pastor et al., 2022).

**Table 8.** Network measures of the habitat graph that were used to assess connectivity of mangroves.

| Measure | Function | Ecological relevance |
|---|---|---|
| Total edges | Indicates the number of pairs of immediately connected nodes | Shows how many connections are formed in the population |
| Network density | Measures how close the network is to be completed. A complete graph has all possible edges and is equal to 1 | Describes the extent to which a population is connected through interactions. It is a ratio of the number of realized interactions to the total number of possible interactions |
| Network diameter | The maximum number of steps required to traverse the network. Indicates compactness of the graph and overall traversability of the network | Provides insights into the overall efficiency of propagules flow within the population. A small network diameter indicates that the graph is compact, meaning nodes are relatively close to each other in terms of the number of edges that need to be traversed to move from one node to another |
| Connected components | Number of connected subgraphs (or components). Components are sets of nodes connected to each other by paths (edges) | Provides insights into the structure of the ecosystem. Helps to identify areas that have direct or indirect paths between every pair of nodes within that component |
| Number of clusters (modularity) | The number of clusters measures the count of distinct groups (or communities) identified within a network. Modularity quantifies how strongly these groups are organised, by comparing the density of connections within groups to that expected in a random network | Identifies possible metapopulation boundaries |

For the models incorporating drift factor alone and drift factor with windage, I employed various weighted node-level and centrality measures to understand the distinct roles of mangrove patches within the network and to infer the connectivity attributes of the ecosystem (Table 9). The weighted measures reflect the number of propagules moving between each habitat patch, providing a more accurate representation of connectivity than binary connections. One such measure was self-recruitment—calculated here by dividing the number of individuals recruited to the same population where they were spawned or produced by the total number of individuals recruited to that population. I defined management objectives for each of the node-level measures (Table 9) and mapped management priority at the scale of mangrove habitat patches. Using satellite imagery analysed with NDVI (Normalized Difference Vegetation Index), I mapped the condition of mangrove areas, highlighting variations in mangrove health across the study area (Figure D1.1). I then employed an Impact, Priority and Urgency Framework, a decision-making tool to prioritise management actions. While this specific framework was developed for this study, it builds upon existing approaches in conservation planning that integrate ecological importance, threat level and connectivity to guide action (e.g. Game et al. (2013), Schwartz et al. (2018), Carwardine et al. (2012), Carwardine et al. (2019)). In this framework, *impact* reflects the current state of the area, *priority* corresponds to node-

level connectivity measures and *urgency* is an index derived by combining *impact* and *priority* (Figure 19).

**Table 9.** Node-level network measures, along with their associated management objectives and rationale for understanding mangrove connectivity.

| Measure | Description | Management objective | Rationale |
|---|---|---|---|
| Out-strength | The total weight of all outgoing connections from a node, representing the strength and volume of dispersal to other connected nodes in the network | Maintain key dispersal and export zones (source) | Areas with high out-strength are critical as they are major sources of seeds for the ecosystem. |
| In-strength | The total weight of all incoming connections to a node, representing the strength of propagule recruitment received from other connected nodes in the network | Safeguard key recruitment and nursery areas (sink) | Areas with high in-strength are crucial for seed deposition and recruitment. |
| Self-recruitment rate | The proportion of individuals recruited to the same population where they were produced, relative to the total recruitment at that population | Protect isolated and self-sufficient habitats | Areas with high self-recruitment support populations that are largely independent, maintaining resilience and adaptability within specific environments without significant reliance on propagule input from other regions. |
| PageRank | A measure of a node's importance based on its connectivity and influence within the network, considering both direct and indirect connections. | Enhance connectivity resilience by protecting highly connected and influential areas | Areas with high PageRank centrality maintain strong indirect connections and contribute significantly to the overall connectivity of the ecosystem. |
| Betweenness | A measure of a node's role as a connector or stepping stone, calculated as the number of shortest paths passing through the node | Protect and manage key connectivity corridors to ensure ecosystem linkage | Stepping stones serve as pathways that connect different parts of the network, facilitating the flow of propagules across the ecosystem. |

I calculated an urgency score for each management objective by multiplying the normalized values of impact and priority and then categorized these scores into five urgency levels using natural breaks: very high (requiring immediate action), high (prompt intervention recommended), medium (necessitating near-term intervention), low (requiring attention, but no immediate action) and very low (minimal or no action required at this time; Figure 19). Additionally, I calculated the urgency scores for all combined objectives and assessed the variance in these scores to determine whether any individual objective contributed disproportionately to the overall urgency (Table D1.1 and D1.2). This decision-making tool allowed me to evaluate and prioritise management areas by, for example, identifying regions of high connectivity importance that are also degraded mangrove zones. By targeting these regions, we can ensure that management efforts are focused on areas that are not only in poor condition but also strategically important for ecological resilience and success. I identified the most critical nodes for management intervention because they are important for multiple measure of connectivity and are highly degraded and then evaluated stressors in each area and distinguishing between manageable and unmanageable factors (Table D1.1 and D1.2). This approach enabled me to prioritise conservation areas cost-effectively, focusing resources on locations where

interventions could yield the greatest ecological benefits and where managing specific stressors was most feasible.

| | | Impact | | | | |
|---|---|---|---|---|---|---|
| | **Urgency** | Very low | Low | Medium | High | Very high |
| Priority | Very high | Medium | High | Very high | Very high | Very high |
| | High | Low | Medium | High | Very high | Very high |
| | Medium | Very low | Low | Medium | High | Very high |
| | Low | Very low | Very low | Low | Medium | High |
| | Very Low | Very low | Very low | Very low | Low | Medium |

**Figure 19.** Impact, Priority and Urgency index. Table showing the scoring process used to determine the urgency for management actions based on impact and priority levels.

## Results

### Outputs of the biophysical model

The outputs of the biophysical models exhibit significant variation depending on the factors incorporated into each model. For *Rhizophora stylosa*, the model that included drift factor shows that most particles (61.8%) connected with mangrove areas travelled northward, while only 24.6% travelled northward in the model without drift factor. When comparing dispersal distances, the model with drift factor shows median distances of 5.9 metres after one day, 42.5 metres after one week, 157.2 metres after one month and 411.4 metres after 90 days. In contrast, the model without drift factor shows slightly shorter distances initially: 4 metres after one day, 27.8 metres after one week, 168.6 metres after one month and 730.3 metres at the end of the 90-day period. These results suggest that while the model with drift factor initially allows for greater dispersal, the model without drift factor ultimately results in particles travelling longer distances by the end of the simulation. The total number of connections with mangrove areas was 11.57 billion with drift factor and 10.94 billion without drift factor, representing a 5.7% increase in connectivity due to the wind factor.

For *Bruguiera gymnorhiza*, the model that incorporated drift factor and windage showed that 49.2% of particles connected to mangrove areas were travelling southward, while in the model without

them, 44.5% of particles moved northward. This suggests that while the main movement direction shifted, the changes were less pronounced compared to those observed in the *R. stylosa* models. In terms of dispersal distance, the model with drift factor and windage showed that particles travelled 7.3 metres on the first day, 45.4 metres after a week, 160.6 metres after a month and 425.2 metres at the end of the 90-day period. Meanwhile, the model without drift factor and windage exhibited 7.7 metres on day one, 54.6 metres after a week, 234.6 metres after a month and 865.8 metres after 90 days. Although the initial distances were similar between the models, the model without drift factor and windage showed a greater increase in dispersal distance after a month, particularly at the end of the simulation. The total number of particles connected to mangrove areas was 5.65 billion with drift factor and windage and 5.92 billion without them, representing a 4.5% decrease due to the effect of wind.

### Network measures

For *R. stylosa*, the model incorporating drift factor demonstrated greater connectivity compared to the model without it. This is evident from the nearly doubled number of edges, leading to a higher network density and a reduction in the number of clusters by more than half (Table 10). However, the modularity of the drift factor model was slightly lower, indicating that even with fewer clusters, the communities formed were less cohesive than those in the model without drift. Despite these differences, the network diameter and the number of connected components remained unchanged between the models, suggesting that the overall compactness and structural integrity of the network were unaffected by the inclusion of the drift factor.

In contrast, the model for *B. gymnorhiza* that includes both drift factor and windage showed slightly reduced connectivity compared to the model without them. This reduction is evident from the lower number of edges and the corresponding decrease in network density. Despite these differences, both models shared the same network diameter and number of connected components, similar to *R. stylosa*. However, the model with drift factor and windage formed fewer and less cohesive clusters, as indicated by the lower modularity. In comparison, the model without windage produced more clusters with higher modularity, reflecting the formation of more communities that have stronger internal connections.

**Table 10.** Network measures of the habitat graphs of *Rhizophora stylosa* and *Bruguiera gymnorhiza* in the central Great Barrier Reef. For *R. stylosa*, only the drift factor was included, as the effect of windage was negligible.

| **Species** | ***Rhizophora stylosa*** | | ***Bruguiera gymnorhiza*** | |
|---|---|---|---|---|
| **Measure** | **Drift factor** | **No wind added** | **Drift factor and windage** | **No wind added** |
| Total edges | 41018 | 28533 | 1348 | 1608 |
| Network density | 0.43 | 0.3 | 0.47 | 0.56 |
| Network diameter | 4 | 4 | 3 | 3 |
| Connected components | 3 | 3 | 3 | 3 |
| Number of clusters (modularity) | 11 (0.44) | 23 (0.65) | 5 (0.33) | 8 (0.61) |

## Node level network measures

For *R. stylosa*, Hinchinbrook Island emerged as a critical hub in the network, exhibiting the highest levels of both incoming and outgoing connections (Figure 20.a and b). The Hinchinbrook channel showed significant movement of *R. stylosa* propagules, marked by the highest levels of both in-strength and out-strength. This indicates that this area acts as both a major source and sink area within the central Great Barrier Reef (GBR). The high out-strength on the eastern side of Hinchinbrook underscores its importance as a key source area, contributing significantly to the dispersal of propagules across the network. Furthermore, high self-recruitment rate in the Hinchinbrook Island (Figure 20.c), indicate that this dense area effectively retains a substantial number of propagules, thereby playing an important role in promoting local population stability. North of Hinchinbrook, around Mission Beach, also shows elevated in-strength, highlighting it as an important sink area for propagules. Moreover, while there was bidirectional movement of propagules across the network, a notable pattern of long-distance dispersal predominantly towards the north was observed.

PageRank analysis identified several key nodes across the population (Figure 20.d). Notably, influential nodes were found in both the central and southern parts of the GBR, underscoring the widespread connectivity that extends beyond the immediate vicinity of Hinchinbrook. In the southern region, these nodes contribute significantly to maintaining network cohesion and ensuring the effective dispersal of propagules throughout the population. The distribution of high PageRank nodes suggests that while Hinchinbrook is a central hub, other areas also play vital roles in sustaining the overall network dynamics. Betweenness centrality analysis revealed critical nodes and connections distributed throughout the entire population, with the most significant ones located in the Hinchinbrook Channel and extending along the southern part of the population (Figure 20.e). These nodes serve as connectors within the network, acting as bridges for propagule dispersal between different regions. The high betweenness centrality observed in the Hinchinbrook Channel underscores

its role as a corridor in the network. Similarly, the nodes in the southern region demonstrate their significance in maintaining connectivity within the population.

The Infomap algorithm identified eleven distinct clusters (Figure 20.f), highlighting a modular network structure with a modularity score of 0.44, indicating a moderate level of network partitioning. In this structure, connectivity is generally stronger within clusters than between them. For instance, Cluster 5 is particularly extensive, spanning from Cape Cleveland to halfway along the Hinchinbrook Channel—covering approximately 120 km. This cluster also includes distant nodes extending both north and south, integrating spatially separate regions. On the other hand, smaller clusters, such as Cluster 6, which contains only two nodes, and Cluster 8, comprising six nodes that span just a few kilometres, illustrate more localized connectivity patterns. The distinct variation in cluster size and distribution reflects the complex and heterogeneous nature of connectivity within the region, where some areas are more tightly interconnected over large distances, while others exhibit more isolated and compact connectivity dynamics.

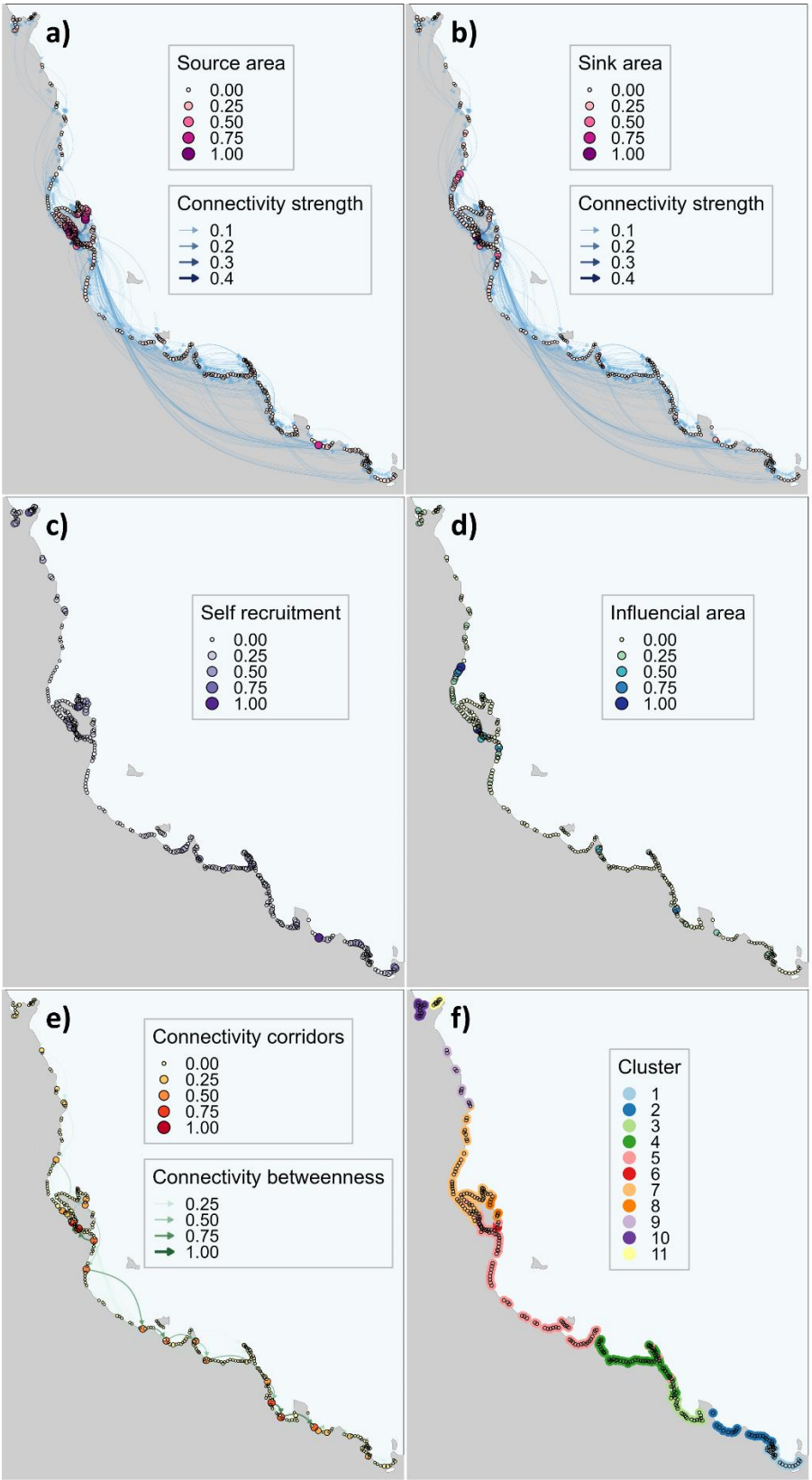


**Figure 20.** Maps showing *R. stylosa* displaying node-level connectivity metrics. a) out-strength (source), b) In-strength (sink), c) Self recruitment, d) PageRank (influential), e) betweenness centrality (connectivity corridors), f) Community detection (different colours represent different communities/clusters). For the maps from a) to e), circles indicate settlement density of mangrove propagules across the region, with the size and colour gradient representing the normalized concentration from low (small, light pink (a and b), light purple (c), light blue (d) and yellow (e) to high (large, dark purple (a and b), purple (c),

blue (d) and red (e)). Arrows illustrate the normalized flux of mangrove propagules, with direction and thickness indicating the movement and relative quantity of fragments travelling from their release points to settlement areas. Due to the resolution and the high number of arrows, only the larger arrows are visible, representing the most significant propagule movements. Place names for these maps are provided in Figure 18.

For *B. gymnorhiza*, I identified a critical hub for connectivity located just below Mission Beach. This area exhibited high levels of both outgoing and incoming connections, reflected in its elevated out-strength and in-strength (Figure 21.a and b). Furthermore, the nodes in this region had the highest PageRank scores (Figure 21.d), indicating their significant influence on the overall network. These nodes help to maintain the connectivity, resilience and cohesion of the population, supporting the broader network structure. This central hub also emerged as the most important stepping stone within the network (Figure 21.e), facilitating the movement of propagules across different regions. Additionally, other nodes, particularly those located near Cairns, act as stepping stones, helping to maintain the overall connectivity of the population. Areas with high self-recruitment are located at the northern and southern extremes of the population. These zones effectively retain their propagules but show limited connectivity to the broader network, indicating they are somewhat isolated from other parts of the population (Figure 21.c). It is worth noting that areas with high self-recruitment are also low source-sink areas. The population of *B. gymnorhiza* forms five distinct clusters (Figure 21.f) with a modularity of 0.33, indicating moderately distinct communities within the network. Two of these clusters (clusters 2 and 5) demonstrate high self-recruitment, suggesting that they are resilient and capable of maintaining their populations independently of changes elsewhere in the network. In contrast, clusters 1, 3 and 4 may be more reliant on external connections for their persistence.

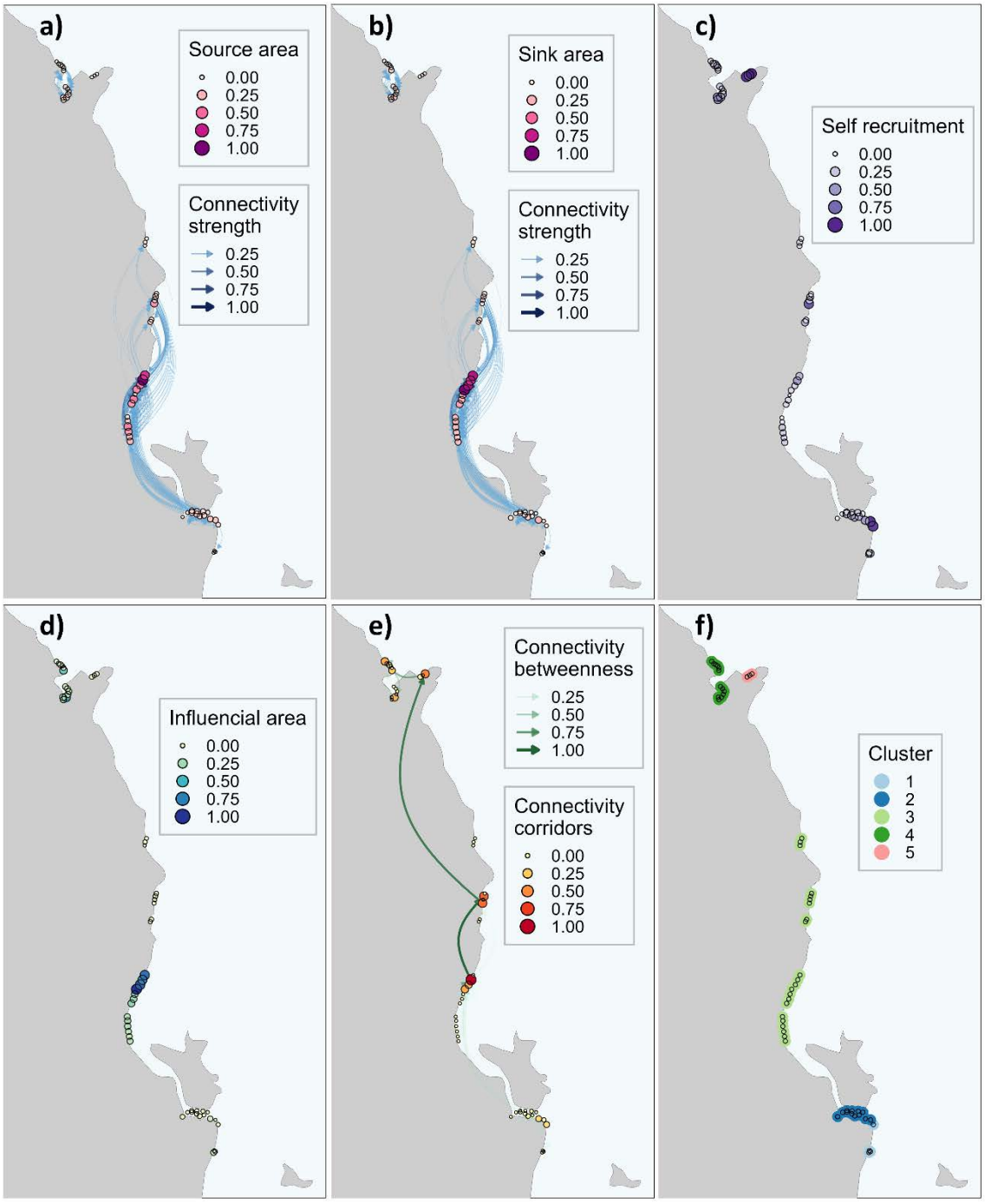


**Figure 21.** Maps *B. gymnorhiza* displaying node-level connectivity metrics. a) out-strength (source), b) In-strength (sink), c) Self recruitment, d) PageRank (influential), e) betweenness centrality (connectivity corridors), f) Community detection (different colours represent different communities/clusters). For the maps from a) to e), circles indicate settlement density of mangrove propagules across the region, with the size and colour gradient representing the normalized concentration from low (small, light pink (a and b), light purple (c), light blue (d) and yellow (e) to high (large, dark purple (a and b), purple (c), blue (d) and red (e)). Arrows illustrate the normalized flux of mangrove propagules, with direction and thickness indicating the movement and relative quantity of fragments travelling from their release points to settlement areas. Place names for these maps are provided in Figure 18.

## Prioritising management

The spatial distribution of management urgency for *R. stylosa* (Figure 22) and *B. gymnorhiza* (Figure 23) were mapped to highlight key areas for management. To achieve this, a mangrove health map (Figure D1.1) was developed using satellite imagery analysed with NDVI. This information was then combined with the connectivity analysis (Figures 20 and 21) to identify areas where management urgency is highest. For *R. stylosa*, very high urgency areas are concentrated in regions of significant connectivity and poor mangrove health, particularly in the Hinchinbrook Channel (Figure 22). All five management objectives indicated very high urgency in this area, highlighting it as a key area for intervention. However, the node consistently scoring very high urgency (node 206; Table D1.1) faces primarily unmanageable stressors, such as storm damage, which limits the types of interventions that can be applied. Regarding the management objective to maintain key source areas (out-strength), one node in the south (node 42) was identified as very high urgency, where altered hydrology is a major threat. In such areas, management interventions like restoring natural tidal flow could be implemented to improve mangrove health. For other objectives, such as protecting stepping stone areas (betweenness), several nodes were highlighted as high urgency, including node 141, which faces multiple manageable stressors, such as structural loss, altered hydrology, encroachment and access tracks. Management interventions in these areas could focus on addressing these stressors to improve ecosystem resilience.

Conversely, the urgency map for *B. gymnorhiza* (Figure 23) shows that the Mission Beach area, particularly nodes 26 to 29 (Table D1.2), exhibits very high urgency across all management objectives. This area faces a variety of manageable stressors, including structural loss, altered hydrology and encroachment, making it a key focus for management and restoration, as these stressors can be addressed effectively. Additionally, some high urgency nodes are located in the northern part of the population, such as node 48 (stepping stone areas) and node 40 (influential areas). Both nodes are affected by manageable stressors, including structural loss, altered hydrology, encroachment and access tracks, highlighting them as priority areas for targeted interventions.

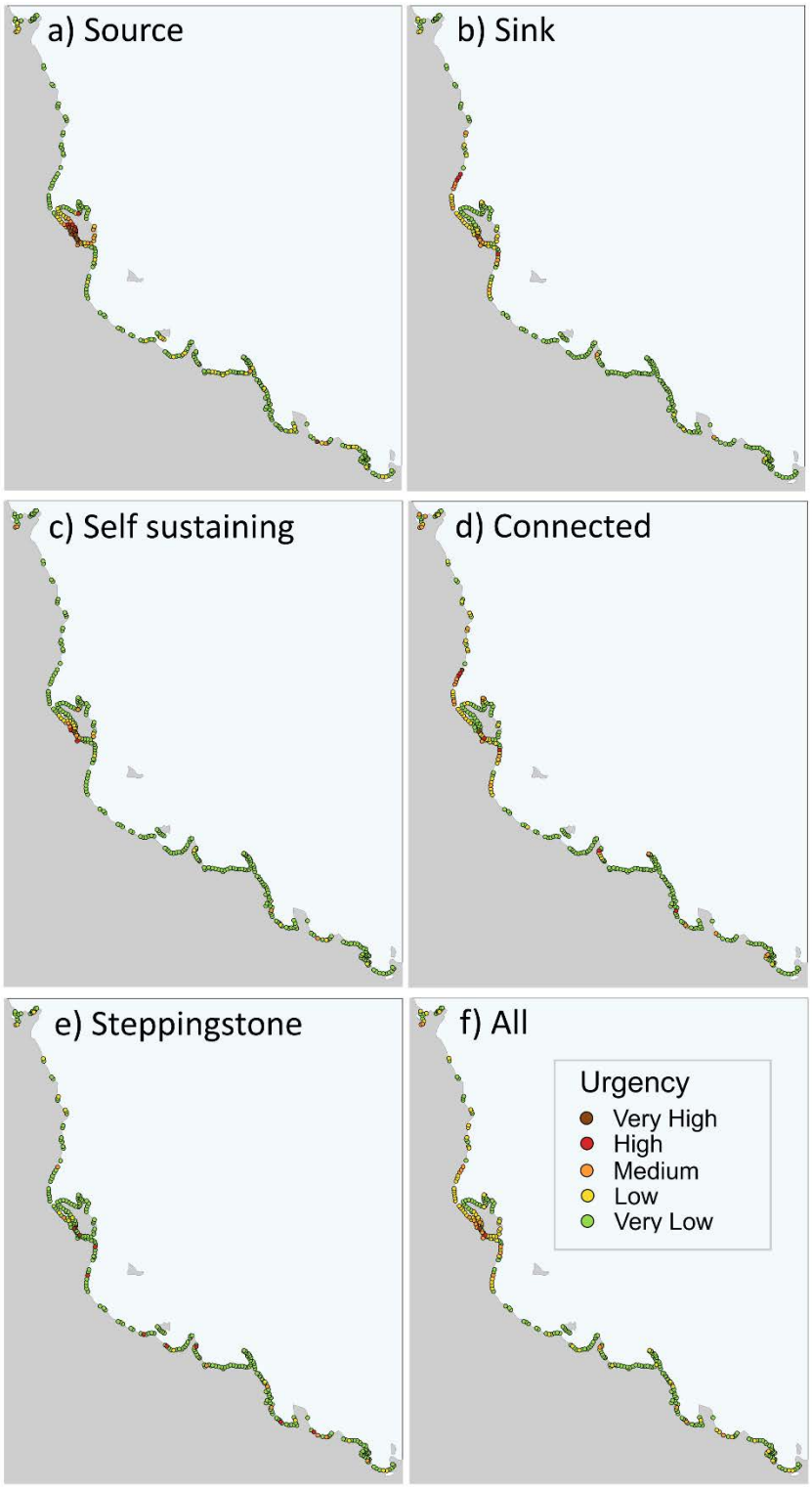


**Figure 22.** Urgency index results for *R. stylosa* across various network measures. (a) Source (out-strength), highlighting key recruitment and nursery areas to be safeguarded; (b) Sink (in-strength), identifying dispersal and export zones to be maintained; (c) Self-sustaining (self-recruitment), indicating isolated and self-sustaining habitats; (d) Connected (PageRank), underscoring highly connected and influential areas to enhance connectivity resilience; and (e) Steppingstones (betweenness), marking key connectivity corridors essential for maintaining ecosystem linkages. Place names for these maps are provided in Figure 18.

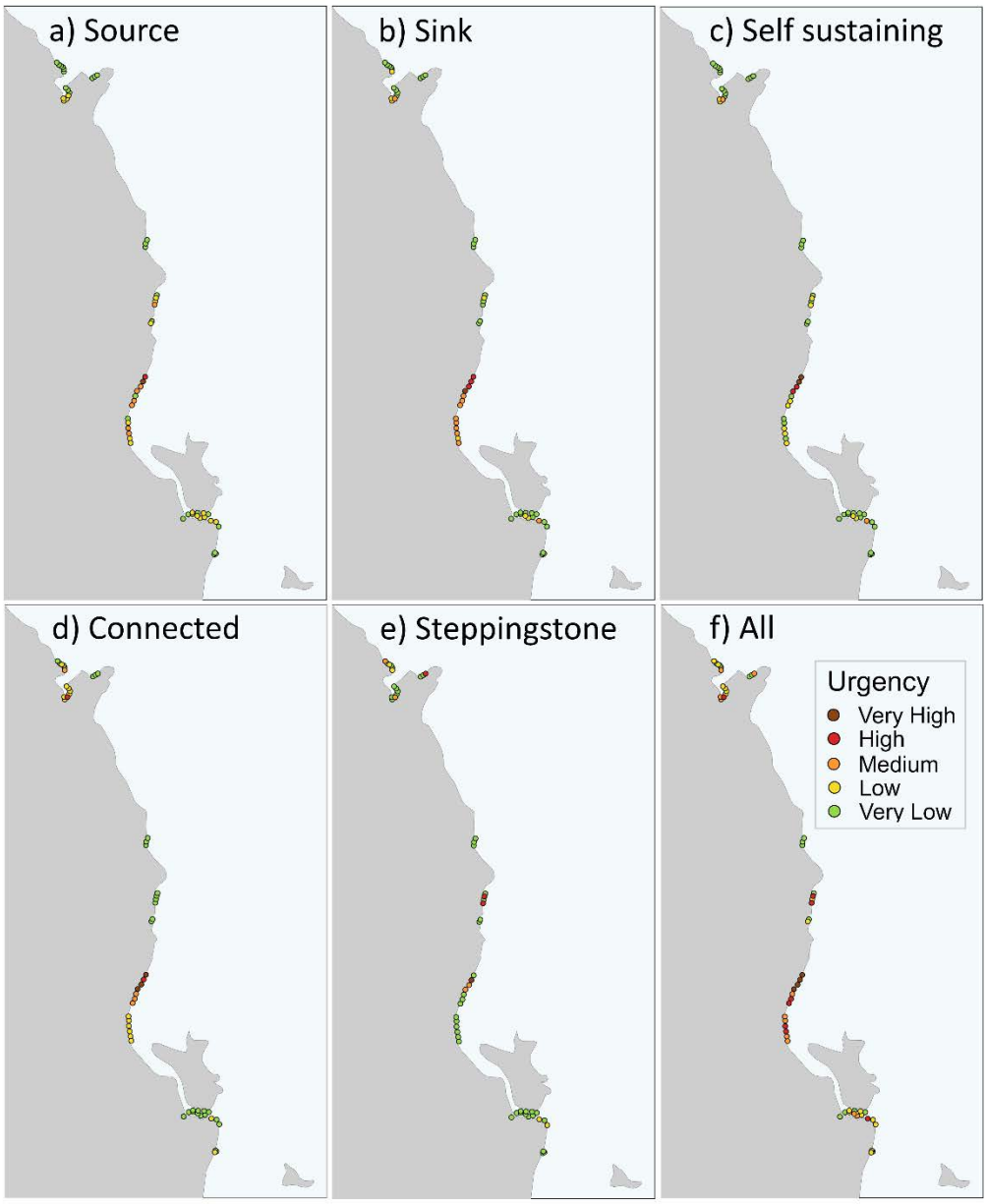


**Figure 23.** Urgency index results for *B. gymnorhiza* across various network measures. (a) Source (out-strength), highlighting key recruitment and nursery areas to be safeguarded; (b) Sink (in-strength), identifying dispersal and export zones to be maintained; (c) Self-sustaining (self-recruitment), indicating isolated and self-sustaining habitats; (d) Connected (PageRank), underscoring highly connected and influential areas to enhance connectivity resilience; and (e) Steppingstones (betweenness), marking key connectivity corridors essential for maintaining ecosystem linkages. Place names for these maps are provided in Figure 18.

## Discussion

While marine connectivity is increasingly recognised as a critical component of ecosystem resilience, there remains a significant gap in the integration of quantitative connectivity objectives into conservation planning. This research addresses this gap by successfully integrating quantitative connectivity metrics into a prioritisation framework. This approach not only works towards enhancing the management of mangrove species but also provides a scalable model that can be applied to other ecosystems. For instance, similar hydrodynamic modelling approaches and connectivity analyses have

been successfully applied to seagrass meadows, coral reefs, salt marshes and kelp forest (Grech et al., 2016, Thompson-Saud et al., 2024, Ospina-Alvarez et al., 2020a, Pastor et al., 2023, Pastor et al., 2022). By adapting this urgency framework to different ecosystems, the same principles can guide conservation strategies and strengthen ecosystem resilience across various coastal habitats. The implications of this work extend beyond mangroves, offering a framework for incorporating connectivity into planning processes that support biodiversity and ecosystem services in a changing climate. By demonstrating how specific connectivity objectives can directly inform management strategies, I offer a pathway for improving resilience in ecosystems facing increasing anthropogenic pressures.

Using coupled hydrodynamic and individual-based models along with connectivity analysis, I assessed the dispersal and connectivity dynamics of *Rhizophora stylosa* and *Bruguiera gymnorhiza* in the Central Great Barrier Reef (GBR). This approach allowed me to identify critical areas for targeted management. For *R. stylosa*, the Hinchinbrook Channel emerged as a fundamental source-sink area, helping maintain the connectivity and resilience of the entire population, and is also notably affected by degraded mangrove health. However, this area presents limited management actions, therefore, while it remains an important source-sink area, many of the challenges it faces are largely unmanageable. In contrast, for *B. gymnorhiza*, the key connectivity area appears to be slightly north, around Mission Beach. This area shows poor mangrove health and was highlighted as very high urgency across all management objectives. Alongside its connectivity importance and poor health, the presence of manageable stressors, like structural loss, altered hydrology and encroachment, makes it an area for targeted management efforts. Although my model accounts for dispersal based on release density and area, it does not explicitly incorporate fecundity, which could influence source strength. This means that a location with a small mangrove extent but high fecundity may still function as an important source, potentially altering connectivity patterns. Similarly, sink areas may persist due to high influx, even if local propagule production is low.

The inclusion of drift factor significantly influenced the connectivity dynamics of *R. stylosa*. The addition of this factor nearly doubled the number of total connections, increasing from 28,533 to 41,018. This increase, adding to the increase in network density and decrease in the number of clusters, indicates a substantial enhancement in the overall connectivity of the network, revealing that the exclusion of this factor, which is essential for properly modelling the dynamics of *R. stylosa,* might result in underestimating connectivity, potentially leading to inaccurate modelling of the species and, consequently, misguided management decisions. In contrast, the dispersal patterns of *B. gymnorhiza* were less affected by the inclusion of windage and drift factor. In this case, the opposite effect occurred: adding these factors led to a slight decrease in the number of edges and network density.

Additionally, there was a reduction in the number of clusters, from 8 to 5, indicating some decrease in fragmentation, though not as dramatically as observed for *R. stylosa*. Despite these minor changes and considering that the network diameter and number of connected components remained constant, the overall structure and extent of connectivity appear to be relatively stable. These findings underscore the importance of incorporating species-specific parameters in connectivity modelling for species like *R. stylosa*, where these factors influence dispersal pathways and connectivity outcomes. However, for *B. gymnorhiza*, the relatively minor impact of these factors suggests that its connectivity dynamics are more stable and less dependent on these parameters, indicating that the model's accuracy may not be significantly compromised if these factors are excluded. Nevertheless, including these factors in the model, even for *B. gymnorhiza*, ensures a more robust and comprehensive understanding, minimizing the risk of potential oversights in the modelling process.

The results of the connectivity analysis underscore the need for targeted management strategies to enhance the connectivity and resilience of mangrove ecosystems in the Central GBR. Chapter 5 identifies areas that require focused management efforts, particularly the Hinchinbrook Channel for *R. stylosa* and Mission Beach for *B. gymnorhiza*. While the Hinchinbrook Channel plays a significant role in maintaining connectivity, its restoration options are limited due to unmanageable stressors, such as storm damage. As a result, conservation efforts may be less impactful compared to areas with more manageable stressors. However, interventions like replanting could still be considered to address the existing damage. Mission Beach, on the other hand, represents a critical area for *B. gymnorhiza* connectivity and is a viable target for a range of management actions due to the presence of manageable stressors, such as structural loss and altered hydrology. Effective interventions, such as restoring the hydrodynamic conditions through the rehabilitation of tidal flows and sediment transport processes, can support both connectivity and the long-term health of the mangrove population.

To protect these mangrove populations, it is key to establish and enforce protected zones with clear management objectives and priorities (Carter et al., 2015). Restoration initiatives should be implemented in areas where natural regeneration is insufficient (Lewis III et al., 2019), particularly in regions identified as very high or high urgency. For example, areas with low sink rates that do not show natural recovery may benefit the most from targeted restoration efforts, such as tree planting. At the same time, preservation of existing mangrove forests and careful land-use management helps to mitigate human impacts (Ashton, 2022). In some areas of the Hinchinbrook Channel, for instance, while storm damage and shoreline erosion are major threats, encroachment and hydrological alterations due to agricultural and urban development also pose significant risks (Canning and Duke,

2013). Striking a balance between the needs for coastal development and the conservation of mangrove habitats helps to reduce these impacts. Sustainable development practices, such as implementing zoning laws that restrict urban expansion and agricultural activities in critical mangrove areas and establishing buffer zones to prevent land degradation and reduce runoff are necessary to address this challenge effectively (Carter et al., 2015).

Several measures have already been implemented to improve the health of mangrove ecosystems, including the removal of bund walls, more common in the southern regions, and floodgates, frequently found in the north. A notable example of this is in Trinity Inlet, just north of Cairns, where a bund wall was removed as part of a blue carbon initiative (Luke et al., 2017). Some areas have shown significant recovery of mangrove populations, while others have not, likely due to variations in dispersal patterns within the inlet. This highlights the need for future models to consider the influence of freshwater inputs and local hydrodynamics on propagule movement and establishment. However, not all restoration efforts have seen even partial success. In places like Mungalla in Ingham, the removal of a bund wall did not produce the expected positive outcomes, as the area showed little improvement in mangrove health (Abbott et al., 2020). This failure is often attributed to insufficient research and planning prior to the removal. For projects supported by blue carbon programs, it is important to assess whether bund wall removal will also enhance carbon storage while minimizing the release of stored carbon. This requires thorough sediment analysis to determine carbon dynamics and hydrological assessments to understand how removing the walls will impact water flow and ecosystem function.

The initiatives to remove bund walls are often driven by local communities, motivated by economic incentives that align with broader environmental objectives. Community involvement is crucial for successful mangrove management, particularly in areas where local livelihoods are closely linked to the health of mangrove ecosystems (Schmitt, 2012, Forkam et al., 2020). Community-based management and education programs help for the long-term conservation of these ecosystems (Berkes, 2007, Reid, 2016). Additionally, the inclusion of traditional knowledge from Indigenous communities, who have a long history of sustainably managing and utilizing mangrove resources, is increasingly recognised as an important aspect of conservation and management efforts (Saravanan, 2005, Datta et al., 2012, Vierros, 2017). For example, in cyclone-affected areas along the GBR, like the Hinchinbrook Channel, local community involvement could be critical for restoring damaged mangrove habitats and ensuring resilience. This is particularly important as it has shown that some of these areas have not naturally recovered even after more than a decade after the cyclone event (Duke et al., 2024).

Another significant threat to the mangroves of the GBR is climate change, which has been consistently identified as a greater threat than other localized human impacts (Canning and Duke, 2013). By 2100, the central GBR is projected to experience conditions that are less suitable for sustaining and growing mangrove populations due to factors such as sea level rise and increased precipitation (Martinez-Diaz and Reef, 2023). Rising sea levels pose a significant threat to seaward mangroves, but their ability to trap sediment and elevate the forest floor through root growth may help them persist in some areas (Lovelock et al., 2015, Krauss et al., 2014). However, other climate-driven changes, such as rising temperatures and greater freshwater inputs are expected to lower ocean water density, causing mangrove propagules to float for shorter periods (Van der Stocken et al., 2022). This reduced buoyancy will likely limit their long-distance dispersal, while also altering their position in the water column, further hindering their ability to reach suitable habitats. These challenges make adaptive management strategies necessary for conserving mangrove populations (Chow, 2018, Ellison, 2014). Building resilience will involve protecting existing forests, restoring degraded areas and considering the potential for inland migration of infrastructure as sea levels rise (Chow, 2018, Azevedo de Almeida and Mostafavi, 2016). For example, planning for sea level rise by relocating roads, ports and urban areas further inland can provide the space needed for the natural expansion of mangroves.

Recent advancements in climate-smart conservation planning are increasingly relevant to the management of mangrove ecosystems, particularly in light of climate change impacts on their dispersal and connectivity. Rising ocean temperatures and shifting currents (Wu et al., 2012) are likely to influence the movement patterns of mangrove propagules, potentially altering dispersal pathways and connectivity between key habitats. In addition, more frequent and intense cyclones, driven by climate change, may also generate stronger winds (Knutson et al., 2020) that further impact propagule transport and settlement. This could affect the ability of mangroves to establish in new areas, particularly if climate-induced shifts limit propagule buoyancy and long-distance dispersal (Van der Stocken et al., 2022). In this context, integrating climate change projections into connectivity models is essential for understanding how future environmental conditions might disrupt or enhance connectivity across the broader mangrove network (Coleman et al., 2017). This approach, applied to ocean planning frameworks, provides a valuable means of anticipating shifts and designing adaptive management strategies that prioritise areas maintaining or improving connectivity under changing conditions (Frazão Santos et al., 2020). Additionally, the metric-based framework for climate-smart conservation proposed by Buenafe et al. (2023) could be applied to evaluate and prioritise mangrove habitats that are both ecologically significant and resilient to future climate shifts. Protecting and restoring these habitats is crucial, as mangroves offer significant economic and biodiversity benefits while safeguarding coastal communities from flooding (Dabalà et al., 2023). Integrating these climate-

smart strategies with connectivity analysis will ensure that mangrove management plans not only address current threats but also anticipate future challenges, helping to sustain the resilience of these ecosystems across the central GBR and beyond.

Incorporating connectivity into conservation planning is essential for the long-term success of restoration and blue carbon initiatives. Well-connected habitats support genetic diversity, population stability, and ecosystem recovery following disturbances (Balbar and Metaxas, 2019, Cowen et al., 2007, Steinberg et al., 2016). In mangrove ecosystems, connectivity enhances resilience by facilitating propagule dispersal and species movement, which helps maintain habitat stability and expansion (Van der Stocken et al., 2019b). This, in turn, strengthens their role in coastal protection and carbon sequestration, making connected mangrove forests more effective for blue carbon financing initiatives that prioritise long-term carbon storage (Saavedra-Hortua et al., 2023, Adame et al., 2024). Projects that account for connectivity are better positioned to deliver these benefits, ensuring that restored or conserved areas are not isolated patches but part of a larger, functional network. This is particularly important as global blue carbon initiatives receive increasing attention and funding, with substantial financial investments aimed at protecting and restoring mangrove ecosystems.

## Conclusion

Chapter 5 highlights the significant role of connectivity in managing mangrove ecosystems in the central Great Barrier Reef (GBR), with a specific emphasis on *Rhizophora stylosa* and *Bruguiera gymnorhiza*. The results demonstrate that targeted management strategies, particularly in areas like Mission Beach, are important for enhancing the resilience of these species. The connectivity analysis provides a foundation for identifying urgency areas where conservation efforts should be focused to ensure the long-term survival of these ecosystems. Looking ahead, applying a similar approach that incorporates the mapping of ecosystem services could further refine and focus conservation initiatives, providing an even more solid framework for decision making. Additionally, incorporating longer-term simulations to account for interannual variability, such as the influence of the El Niño-Southern Oscillation (ENSO), would enhance the model's ability to capture temporal fluctuations in dispersal patterns. Furthermore, genetic analysis to validate these outputs would be a valuable area for future research, as it could provide insights into genetic diversity and connectivity patterns that complement the spatial model. By leveraging these approaches, future research can contribute to a more comprehensive understanding of mangrove dynamics across different geographical scales, ultimately supporting more effective and informed management decisions. As I move forward, it is

imperative to refine our models, expand their application and ensure that they are used to guide policy and management actions that protect these ecosystems for generations to come.

# Chapter 6: General Discussion

In the face of climate change and increasing human pressure, dispersal and connectivity play crucial roles in maintaining the resilience of kelp and mangrove forests (Cowen et al., 2007, Balbar and Metaxas, 2019, Carr et al., 2017). These ecosystems support biodiversity, carbon sequestration and coastal protection (Sievers et al., 2023, Lee et al., 2014, Bayley et al., 2021), yet their long-term health is at risk. Integrating information on connectivity into management frameworks is essential for preserving their ecological function (Beger et al., 2022, Keeley et al., 2021). However, this task is often complicated by the challenges of collecting sufficient data and establishing management goals that effectively protect or maintain connectivity. The aim of this thesis was to inform management by enhancing the accuracy of dispersal and connectivity estimates in marine and coastal ecosystems, achieved by integrating species-specific traits into biophysical models. The outputs of these models were used to inform management decisions, particularly in accounting for environmental variability and the need for targeted, species-specific conservation strategies.

Both giant kelp (*Macrocystis pyrifera*) and mangrove species, such as *Rhizophora stylosa* and *Bruguiera gymnorhiza*, play important ecological roles. Giant kelp serves as an ecosystem engineer species by creating extensive underwater forests that offer habitat and shelter to a diversity of marine organisms. Additionally*, M. pyrifera* holds significant economic importance, as it is used for alginate extraction and serves as a primary food source for the abalone in the aquaculture industry (Villegas et al., 2019). Mangroves are also known for their role at stabilizing coastlines, protecting against storm surges and sequestering carbon (Sievers et al., 2023, Lee et al., 2014). Moreover, both ecosystems, but especially mangroves, contribute significantly to the Blue Carbon Initiative, which emphasizes the conservation of coastal ecosystems as carbon sinks that aid in climate change mitigation, with substantial financial investments aimed at protecting and restoring these ecosystems (Alongi, 2020, Bayley et al., 2021, Zeng et al., 2021).

Using a 12-year long dataset, I demonstrated that the dispersal and connectivity of giant kelp in the Southeast Pacific are largely shaped by ocean currents, wind patterns and seasonal changes, with the added complexity of El Niño-Southern Oscillation (ENSO) events. Chapter 2 revealed that shorter dispersal distances for kelp fragments significantly enhance settlement success, underscoring the importance of local environmental conditions in driving kelp population dynamics. While some fragments dispersed over very long distances (above 1,000 km), these were mostly outliers. The median dispersal distance, approximately 50 km, further emphasizes the need for localized management efforts. A key finding of Chapter 3 was the identification of the southern population as a critical source area, supplying propagules to the northern population. Preserving the southern

population is, therefore, critical for sustaining kelp harvesting in northern areas. Notably, the southern region experiences less harvesting pressure compared to the north making it easier to protect. I also identified regions where dispersal distance and connectivity fluctuated significantly between seasons and ENSO conditions. These areas would benefit from adaptive management strategies that can better protect ecosystems during periods of lower connectivity, when reduced replenishment is expected. These findings offer valuable insights for the conservation of giant kelp, suggesting that the protection of key areas can help maintain a sustainable kelp population, promote genetic diversity and ensure ecosystem resilience in the face of ongoing environmental changes.

Building on the insights from the giant kelp study, I applied a similar biophysical approach in Chapter 5 to analyse the dispersal and connectivity patterns of mangroves in the central Great Barrier Reef (GBR). I found significant interspecies variation in buoyancy, which directly affects the dispersal potential of each mangrove species. By integrating these species-specific traits from Chapter 4 into the biophysical models, I was able to improve the accuracy of dispersal trajectory predictions, underscoring the importance of incorporating biological parameters unique to each species in these models. The connectivity analysis for mangroves revealed critical areas within the central GBR that act as replenishment sources and connectivity corridors. By combining this data with satellite imagery of mangrove health, I developed an urgency index to prioritise spatial management. This index enabled me to identify areas that are both important for maintaining connectivity and show signs of unhealthy mangrove conditions. I also used findings from a condition survey to categorize the stressors in each area as either manageable or unmanageable, allowing for a more targeted focus in intervention efforts. Protecting these areas forms the foundation for effective management, ensuring that efforts are directed where they are most needed and most likely to succeed. These findings provide a strong basis for targeted management actions aimed at enhancing the resilience of mangrove ecosystems, which are increasingly threatened by coastal development and climate change.

## Advances in biophysical modelling

In this thesis, several methodological advances in biophysical model were introduced, improving our ability to predict dispersal and connectivity in marine and coastal ecosystems. These advancements are key for generating accurate management insights, particularly in ecosystems like mangroves and giant kelp, where species-specific traits and local hydrodynamic factors influence dispersal and connectivity.

A strength of this work is the incorporation of new biological traits into the biophysical models. By integrating empirical species-specific traits into these models, the accuracy of connectivity predictions improves significantly, as demonstrated in my work with both giant kelp and mangroves. For instance,

In Chapter 4, variations in buoyancy among mangrove species offered insights into their dispersal potential. I identified which species had propagules capable of long-term buoyancy and dispersal and those that did not, refining our understanding of species-specific dispersal behaviour. Additionally, I determined how these propagules position in the water column, which allowed me to calculate more accurate parameters, such as windage and drift factor, to inform the biophysical models. As a result, the biophysical model of Chapter 5 offered more precise management information. This precision ensures that conservation strategies are not only better informed but also more likely to succeed, as they are grounded in a deeper understanding of species-specific dispersal mechanisms and local hydrodynamic conditions. By improving the accuracy of these predictions, management interventions can be better targeted, increasing their overall effectiveness.

Moreover, the advances in modelling mangrove ecosystems are attributed to the high-resolution hydrodynamic modelling approach used in this research, which employs a spatial resolution ranging from 250 metres near the coast and reefs to 5 kilometres further offshore. The model captures the complex dynamics critical for understanding mangrove dispersal and connectivity. This fine resolution is especially important in coastal areas, where hydrodynamic processes and biological interactions are intensified, providing a clearer picture of how factors like currents affect mangrove resilience. Higher resolution models can lead to more accurate predictions of dispersal patterns and population dynamics, ultimately guiding targeted conservation efforts. By refining the spatial granularity of the simulations, I enhance our ability to make informed management decisions that protect mangrove habitats and their associated ecosystem services.

Beyond species-specific traits and high-resolution models, it is also critical to run simulations over longer time periods to capture the influence of climate variability. Events such as the El Niño-Southern Oscillation (ENSO) significantly impact oceanographic conditions and understanding how these fluctuations affect dispersal and connectivity is vital. In Chapter 2, I addressed this by running a 12-year simulation to assess the connectivity of giant kelp. This extended model run allowed for the evaluation of interannual variability, ensuring that both typical conditions and extreme climate events were included in the analysis. In highly dynamic systems like the Southeast Pacific region, where ocean currents and weather patterns are heavily influenced by climate cycles, incorporating these long-term effects is essential. The ability to capture shifts in connectivity patterns during events like El Niño and La Niña, as demonstrated in Chapter 3, provides a more comprehensive understanding of dispersal mechanisms. This insight allows for the formulation of adaptive management practices that better protect this important ecosystem.

## Implications for conservation and management

Connectivity is widely recognised as a critical factor for biodiversity conservation, promoting ecosystem resilience and supporting species persistence in the face of environmental changes (Olds et al., 2016, Balbar and Metaxas, 2019). Without effective connectivity, isolated populations are vulnerable to genetic bottlenecks, reduced ecosystem function and even local extinction (Balbar and Metaxas, 2019). This is particularly important for species with limited adult mobility, such as mangroves and giant kelp, where dispersal during early life stages, driven by ocean currents and wind patterns, is often the primary mechanism connecting distant populations. For instance, in Chapter 3, the study on giant kelp identified the southern population as a key source for the northern population, where most harvesting occurs. This highlights the importance of connectivity for replenishing distant populations. Protecting the southern population, where harvesting pressure is lower, could increase productivity and ensure long-term ecosystem resilience. This finding aligns with broader conservation strategies, which suggest that identifying and protecting key source areas is vital for maintaining overall population health (Rodrigues and Rouyer, 2023).

The role of connectivity in sustaining ecosystem services—such as carbon sequestration, biodiversity conservation and resilience to climate change—has become a focal point in blue carbon initiatives (Pendleton et al., 2012). For instance, one of the aims of Australia's Emission Reduction Fund program is to recover mangrove habitats to increase carbon sequestration. However, enhancing the effectiveness of such initiatives can be greatly improved by including pre-analytical assessments to better understand these ecosystems. By developing frameworks like the urgency index, introduced in Chapter 5, insights can be gained into identifying key areas for connectivity that are in poor mangrove health. This approach not only aids in prioritising conservation efforts but also ensures that interventions are strategically focused where they are most needed. Protecting these areas provides a strategic foundation for successful management interventions that enhance ecosystem resilience in the face of ongoing development pressures. Additionally, having clear connectivity-driven objectives for management can further sharpen the focus of these efforts. For instance, understanding whether the goal is to protect critical connectivity corridors, source populations or enhance resilience can influence how priorities are set. By aligning management objectives with specific connectivity functions conservation efforts can be even more targeted and effective (Beger et al., 2022, Keeley et al., 2021). This focus ensures that interventions are strategic and likely to succeed in preserving connectivity functions critical to ecosystem health.

Environmental variability, particularly seasonal changes and large-scale events like El Niño-Southern Oscillation (ENSO), plays a significant role in shaping connectivity patterns (Gurdek-Bas et al., 2022). This becomes even more important in the context of climate change, as phenomena like ENSO are

expected to increase in both frequency and intensity. Incorporating such variability into management plans is essential to safeguard key species and maintain ecosystem resilience. In Chapter 2 and 3, the study demonstrated the substantial influence that different seasons and ENSO conditions can have on dispersal and connectivity in certain parts of the population of the giant kelp. While these effects may not be equally apparent across the entire population, there are critical areas where environmental variability is pronounced, underscoring the need for adaptive management strategies. In particular, during periods of low connectivity, when replenishment is reduced, measures such as seasonal protections or adjusting harvest restrictions could significantly enhance management efficacy, ensuring better support for population resilience.

## Limitations and future research

Despite the advancements made in this thesis, several limitations remain. While this thesis has focused primarily on the dispersal phase of kelp and mangrove species, the pre- and post-dispersal phases—such as propagule production, establishment success and seedling survival—have not been fully explored. These stages are critical in shaping connectivity outcomes and meta population dynamics, as they determine the number of propagules available for dispersal and their ability to survive in new habitats (Kinlan and Gaines, 2003, Burgess et al., 2014). Future research should incorporate experimental work that examines these phases in greater detail. For example, field studies could investigate how factors like predation, seed viability and substrate suitability influence propagule survival and establishment post-dispersal. Understanding these processes would provide a more holistic view of species connectivity and improve the predictive power of biophysical models, leading to more effective management strategies (Cowen et al., 2000).

For giant kelp, the model resolution could be enhanced by incorporating more detailed hydrodynamic data and employing nested models to capture finer-scale processes. Modelling the nearshore environment presents significant challenges due to the complexity of factors influencing organism dispersal, such as tides, freshwater runoff and upwelling (Swearer et al., 2019). This is especially relevant for regions like Patagonia, which were not included in the study but are home to significant kelp populations. The omission is largely due to the complexity of hydrodynamics around the fjords in this area. Accurately understanding kelp dispersal and connectivity in the Southeast Pacific requires models that can address such intricacies. In this context, nested models would be key to resolving these finer-scale processes.

For mangroves, extending the model duration and including additional environmental variables, such as salinity, would provide a more comprehensive understanding of propagule dispersal (Leis, 2020). For instance, Chapter's 4 findings showed that the dispersal of certain propagules, such as *B.*

*gymnorhiza*, is influenced by salinity, affecting windage and drift factors beyond just time. Accounting for these factors could significantly alter dispersal outcomes. However, SLIM did not include salinity, limiting our ability to factor it in. Additionally, extending the model's duration would facilitate the evaluation of interannual variability, particularly regarding the impacts of ENSO events. These phenomena have significantly influenced the GBR and have been observed to affect connectivity in other ecosystems as well (Gurdek-Bas et al., 2022). Understanding these dynamics helps manage ecosystem resilience and mitigate the adverse effects of climate variability. Unfortunately, time and computing constraints prevented me from extending the model run.

Building on the findings of this thesis, future research should focus on identifying and assessing management actions that can effectively address areas of high urgency for intervention. For example, if the removal of barriers like walls or artificial structures is considered, it is important to evaluate how such actions could influence mangrove habitats and carbon sequestration (Ellison et al., 2020). In regions like the GBR, where bund walls and floodgates have been historically used to manage hydrology, understanding the ecological impacts of removing these structures is crucial. Such changes could significantly affect not only connectivity but also sediment composition, water flow and overall habitat recovery. By modelling the effects of hydrodynamic alterations on dispersal patterns, sediment transport and carbon storage, I could better predict the outcomes of these management interventions (Pradhan et al., 2018). This will enable more precise planning and allow conservation strategies to be fine-tuned for optimal ecological restoration.

Future research could build on the urgency index analysis presented in Chapter 5 by applying it to other regions within the GBR or globally. This would help identify areas where connectivity is compromised, allowing managers to prioritise them for restoration or intervention. Once these critical areas are identified, it would be valuable to simulate different management scenarios, such as the removal of barriers, to assess how hydrology and other ecological factors respond (Costa and Vieira, 2023). For instance, removing a bund wall might restore natural water flow, enhance sediment transport and boost propagule retention, ultimately improving connectivity. However, each site may respond differently based on local conditions, making it crucial to explore site-specific outcomes before implementing large-scale restoration efforts.

Integrating these findings into broader conservation strategies could help improve mangrove management globally. By incorporating climate change scenarios and anthropogenic impacts into these models, managers could also account for long-term shifts in hydrodynamics and connectivity patterns (Parmesan et al., 2022, Maskey et al., 2022). This would help guide targeted management

efforts that not only aim to restore mangrove habitats but also ensure the long-term resilience of these ecosystems under changing environmental conditions.

## Conclusion

Together, the chapters in this thesis build a cohesive understanding of how species-specific biological traits, local hydrodynamic conditions and environmental variability shape dispersal and connectivity in marine macrophytes. The empirical findings on buoyancy and drift traits in Chapter 4 directly informed the parameterization of the biophysical models in Chapter 5, enhancing the ecological realism of connectivity predictions for mangroves. Similarly, the long-term simulations for giant kelp in Chapters 2 and 3 demonstrated how interannual variability—particularly ENSO phases—drives substantial shifts in dispersal pathways and connectivity strength. These patterns are not unique to kelp or mangroves; rather, they highlight commonalities across macrophytes, such as the importance of early life-stage dispersal, sensitivity to oceanographic forcing and limited adult mobility. Insights from this work could inform broader management strategies for macrophytes like seagrasses, which also rely heavily on ocean-driven dispersal. For instance, identifying and protecting connectivity corridors and source populations is a unifying strategy across taxa. Looking ahead, with ENSO events predicted to become more intense and frequent under climate change, we can anticipate increasingly disrupted connectivity networks, potentially leading to mismatches between dispersal events and habitat suitability. Adaptive strategies, such as seasonal protections, dynamic spatial zoning and predictive modelling, will be essential to ensure the resilience of macrophyte ecosystems in a rapidly changing ocean.

This thesis underscores the critical role of integrating species-specific traits into biophysical models to enhance our understanding of dispersal and connectivity within marine and coastal ecosystems. By focusing on giant kelp and mangroves, I have generated valuable insights that inform management and conservation strategies for these ecosystems, which are essential for supporting biodiversity, facilitating carbon sequestration and enhancing ecosystem resilience. The central message of this work emphasizes that dispersal and connectivity are fundamental components of ecosystem health; their dispersal dynamics are complex and require robust modelling approaches; and their incorporation into conservation frameworks is crucial for the long-term sustainability of these ecosystems. By improving the accuracy of dispersal and connectivity models and identifying key areas for protection, this research contributes to the broader literature on connectivity and provides practical applications for management strategies that align with efforts like the Blue Carbon Initiative. By applying a similar approach across different areas and ecosystems, I conclude that both the hydrodynamics of a location and the biological characteristics of the species being studied are crucial. To thoroughly understand an ecosystem's connectivity, biophysical models must be developed to

account for these specific traits, as the outcomes are highly site- and species-specific. Ultimately, this thesis highlights the importance of maintaining connectivity in marine and coastal ecosystems to ensure biodiversity, resilience to natural and anthropogenic stressors and species persistence. The findings establish a robust foundation for management approaches that can effectively mitigate the impacts of climate change and human activities on these critical habitats, paving the way for more adaptive, species-specific conservation strategies that support ecosystem resilience.

# References


ABBOTT, B. N., WALLACE, J., NICHOLAS, D. M., KARIM, F. & WALTHAM, N. J. 2020. Bund removal to re-establish tidal flow, remove aquatic weeds and restore coastal wetland services—North Queensland, Australia. *PLoS One,* 15**,** e0217531.

ABECASIS, D., FRAGKOPOULOU, E., CLARO, B. & ASSIS, J. 2023. Biophysical modelling and graph theory identify key connectivity hubs in the Mediterranean marine reserve network. *Frontiers in Marine Science,* 9**,** 1000687.

ADAME, M., CORMIER, N., TAILLARDAT, P., IRAM, N., ROVAI, A., SLOEY, T., YANDO, E., BLANCO-LIBREROS, J., ARNAUD, M. & JENNERJAHN, T. 2024. Deconstructing the mangrove carbon cycle: Gains, transformation, and losses. *Ecosphere,* 15**,** e4806.

ADAME, M. F. & REEF, R. 2020. Potential pollution sources from agricultural activities on tropical forested floodplain wetlands revealed by soil eDNA. *Forests,* 11**,** 892.

ADAMS, D. K. & FLIERL, G. R. 2010. Modeled interactions of mesoscale eddies with the East Pacific Rise: Implications for larval dispersal. *Deep Sea Research Part I: Oceanographic Research Papers,* 57**,** 1163-1176.

AGUIRRE, C., PIZARRO, Ó., STRUB, P. T., GARREAUD, R. & BARTH, J. A. 2012. Seasonal dynamics of the near-surface alongshore flow off central Chile. *Journal of Geophysical Research: Oceans,* 117.

ALBERTO, F., RAIMONDI, P. T., REED, D. C., WATSON, J. R., SIEGEL, D. A., MITARAI, S., COELHO, N. & SERRAO, E. A. 2011. Isolation by oceanographic distance explains genetic structure for Macrocystis pyrifera in the Santa Barbara Channel. *Molecular Ecology,* 20**,** 2543-2554.

ALBORNOZ, C. & GLÜCKLER, J. 2020. Co-Management of Small-Scale Fisheries in Chile From a Network Governance Perspective. *Environments,* 7**,** 104.

ALHEIT, J. & NIQUEN, M. 2004. Regime shifts in the Humboldt Current ecosystem. *Progress in Oceanography,* 60**,** 201-222.

ALMANY, G., CONNOLLY, S., HEATH, D., HOGAN, J., JONES, G., MCCOOK, L., MILLS, M., PRESSEY, R. & WILLIAMSON, D. 2009. Connectivity, biodiversity conservation and the design of marine reserve networks for coral reefs. *Coral reefs,* 28**,** 339-351.

ALMANZA, V. & BUSCHMANN, A. H. 2013. The ecological importance of Macrocystis pyrifera (Phaeophyta) forests towards a sustainable management and exploitation of Chilean coastal benthic co-management areas. *International Journal of Environment and Sustainable Development,* 12**,** 341-360.

ALONGI, D. M. 2015. The impact of climate change on mangrove forests. *Current Climate Change Reports,* 1**,** 30-39.

ALONGI, D. M. 2020. Global significance of mangrove blue carbon in climate change mitigation. *Sci,* 2**,** 67.

ALONGI, D. M. 2022. Climate change and mangroves. *Mangroves: Biodiversity, Livelihoods and Conservation.* Springer.

ANDUTTA, F. P., RIDD, P. V. & WOLANSKI, E. 2011. Dynamics of hypersaline coastal waters in the Great Barrier Reef. *Estuarine, Coastal and Shelf Science,* 94**,** 299-305.

ARAFEH-DALMAU, N., MONTAÑO-MOCTEZUMA, G., MARTÍNEZ, J. A., BEAS-LUNA, R., SCHOEMAN, D. S. & TORRES-MOYE, G. 2019. Extreme marine heatwaves alter kelp forest community near its equatorward distribution limit. *Frontiers in Marine Science,* 6**,** 499.

ARCE, J. M. 2021. Anuario Científico Tecnológico IMARPE 2020.

ASARI, N., SURATMAN, M. N., MOHD AYOB, N. A. & ABDUL HAMID, N. H. 2021. Mangrove as a natural barrier to environmental risks and coastal protection. *Mangroves: Ecology, Biodiversity and Management***,** 305-322.

ASHTON, E. C. 2022. Threats to mangroves and conservation strategies. *Mangroves: Biodiversity, Livelihoods and Conservation.* Springer.

ASTUDILLO, O., DEWITTE, B., MALLET, M., RUTLLANT, J., GOUBANOVA, K., FRAPPART, F., RAMOS, M. & BRAVO, L. 2019. Sensitivity of the near-shore oceanic circulation off Central Chile to coastal wind profiles characteristics. *Journal of Geophysical Research: Oceans,* 124**,** 4644-4676.

AVILA-PELTROCHE, J. & PADILLA-VALLEJOS, J. 2020. The seaweed resources of Peru. *Botanica marina,* 63**,** 381-394.

AZEVEDO DE ALMEIDA, B. & MOSTAFAVI, A. 2016. Resilience of infrastructure systems to sea-level rise in coastal areas: Impacts, adaptation measures, and implementation challenges. *Sustainability,* 8**,** 1115.

AZIZ, I. & KHAN, M. A. 2001. Effect of Seawater on the Growth, Ion Content and Water Potential of Rhizophora mucronata Lam. *Journal of Plant Research,* 114**,** 369.

BALBAR, A. C. & METAXAS, A. 2019. The current application of ecological connectivity in the design of marine protected areas. *Global ecology and conservation,* 17**,** e00569.

BARRAT, A., BARTHELEMY, M. & VESPIGNANI, A. 2008. *Dynamical processes on complex networks*, Cambridge university press.

BARTON, K. & BARTON, M. K. 2015. Package 'mumin'. *Version,* 1**,** 439.

BAYLEY, D., BRICKLE, P., BREWIN, P., GOLDING, N. & PELEMBE, T. 2021. Valuation of kelp forest ecosystem services in the Falkland Islands: A case study integrating blue carbon sequestration potential. *One Ecosystem,* 6**,** e62811.

BCI. 2019. *The Blue Carbon Initiative* [Online]. Available: https://www.thebluecarboninitiative.org/ [Accessed February 15, 2025].

BEAMAN, R. J. 2017. AusBathyTopo (Great Barrier Reef) 30m 2017 - A regional-scale depth model (20170025C). *In:* AUSTRALIA, G. (ed.).

BEAS-LUNA, R., MICHELI, F., WOODSON, C. B., CARR, M., MALONE, D., TORRE, J., BOCH, C., CASELLE, J. E., EDWARDS, M. & FREIWALD, J. 2020. Geographic variation in responses of kelp forest communities of the California Current to recent climatic changes. *Global Change Biology,* 26**,** 6457-6473.

BEGER, M., LINKE, S., WATTS, M., GAME, E., TREML, E., BALL, I. & POSSINGHAM, H. P. 2010. Incorporating asymmetric connectivity into spatial decision making for conservation. *Conservation Letters,* 3**,** 359-368.

BEGER, M., METAXAS, A., BALBAR, A. C., MCGOWAN, J. A., DAIGLE, R., KUEMPEL, C. D., TREML, E. A. & POSSINGHAM, H. P. 2022. Demystifying ecological connectivity for actionable spatial conservation planning. *Trends in ecology & evolution,* 37**,** 1079-1091.

BERKES, F. 2007. Community-based conservation in a globalized world. *Proceedings of the National academy of sciences,* 104**,** 15188-15193.

BERNARDES-BATISTA, M., BATISTA ANDERSON, A., FRANZAN SANCHES, P., SIMIONATTO POLITO, P., CESAR LIMA SILVEIRA, T., VELEZ-RUBIO, G. M., SCARABINO, F., CAMACHO, O., SCHMITZ, C. & MARTINEZ, A. 2018. Kelps' long-distance dispersal: role of ecological/oceanographic processes and implications to marine forest conservation. *Diversity,* 10**,** 11.

BLANCO, M., OSPINA-ÁLVAREZ, A., NAVARRETE, S. A. & FERNÁNDEZ, M. 2019. Influence of larval traits on dispersal and connectivity patterns of two exploited marine invertebrates in central Chile. *Marine Ecology Progress Series,* 612**,** 43-64.

BONACICH, P. 1987. Power and centrality: A family of measures. *American journal of sociology,* 92**,** 1170-1182.

BOUILLON, S., BORGES, A. V., CASTAÑEDA-MOYA, E., DIELE, K., DITTMAR, T., DUKE, N. C., KRISTENSEN, E., LEE, S. Y., MARCHAND, C. & MIDDELBURG, J. J. 2008. Mangrove production and carbon sinks: a revision of global budget estimates. *Global biogeochemical cycles,* 22.

BREIVIK, Ø., ALLEN, A. A., MAISONDIEU, C. & ROTH, J. C. 2011. Wind-induced drift of objects at sea: The leeway field method. *Applied Ocean Research,* 33**,** 100-109.

BROOKS, H. E. 2013. Severe thunderstorms and climate change. *Atmospheric research,* 123**,** 129-138.

BRYAN-BROWN, D. N., BROWN, C. J., HUGHES, J. M. & CONNOLLY, R. M. 2017. Patterns and trends in marine population connectivity research. *Marine Ecology Progress Series,* 585**,** 243-256.

BUENAFE, K. C. V., DUNN, D. C., EVERETT, J. D., BRITO-MORALES, I., SCHOEMAN, D. S., HANSON, J. O., DABALÀ, A., NEUBERT, S., CANNICCI, S. & KASCHNER, K. 2023. A metric-based framework for climate-smart conservation planning. *Ecological Applications,* 33**,** e2852.

BURGESS, S. C., NICKOLS, K. J., GRIESEMER, C. D., BARNETT, L. A., DEDRICK, A. G., SATTERTHWAITE, E. V., YAMANE, L., MORGAN, S. G., WHITE, J. W. & BOTSFORD, L. W. 2014. Beyond connectivity: how empirical methods can quantify population persistence to improve marine protected-area design. *Ecological Applications,* 24**,** 257-270.

BÜRKNER, P.-C. 2017. brms: An R package for Bayesian multilevel models using Stan. *Journal of statistical software,* 80**,** 1-28.

BUSCHMANN, A., VÁSQUEZ, J., OSORIO, P., REYES, E., FILÚN, L., HERNÁNDEZ-GONZÁLEZ, M. & VEGA, A. 2004. The effect of water movement, temperature and salinity on abundance and reproductive patterns of Macrocystis spp.(Phaeophyta) at different latitudes in Chile. *Marine Biology,* 145**,** 849-862.

BUSCHMANN, A. H., MORENO, C., VÁSQUEZ, J. A. & HERNÁNDEZ-GONZÁLEZ, M. C. 2006a. Reproduction strategies of Macrocystis pyrifera (Phaeophyta) in Southern Chile: the importance of population dynamics. *Journal of Applied Phycology,* 18**,** 575-582.

BUSCHMANN, A. H., MORENO, C., VÁSQUEZ, J. A. & HERNÁNDEZ-GONZÁLEZ, M. C. 2006b. Reproduction strategies of Macrocystis pyrifera (Phaeophyta) in Southern Chile: the importance of population dynamics. *Journal of Applied Phycology,* 18**,** 575-582.

CAI, W., BORLACE, S., LENGAIGNE, M., VAN RENSCH, P., COLLINS, M., VECCHI, G., TIMMERMANN, A., SANTOSO, A., MCPHADEN, M. J. & WU, L. 2014. Increasing frequency of extreme El Niño events due to greenhouse warming. *Nature climate change,* 4**,** 111-116.

CAI, W., SANTOSO, A., COLLINS, M., DEWITTE, B., KARAMPERIDOU, C., KUG, J.-S., LENGAIGNE, M., MCPHADEN, M. J., STUECKER, M. F. & TASCHETTO, A. S. 2021. Changing El Niño–Southern oscillation in a warming climate. *Nature Reviews Earth & Environment,* 2**,** 628-644.

CAI, W., WANG, G., SANTOSO, A., MCPHADEN, M. J., WU, L., JIN, F.-F., TIMMERMANN, A., COLLINS, M., VECCHI, G. & LENGAIGNE, M. 2015. Increased frequency of extreme La Niña events under greenhouse warming. *Nature Climate Change,* 5**,** 132-137.

CANNING, A. & DUKE, N. 2013. Southern Great Barrier Reef Mangrove and Saltmarsh Condition Survey 2023 (report 23/70). *Townsville, Australia: TropWATER, James Cook University*.

CANTWELL, M. D. & FORMAN, R. T. 1993. Landscape graphs: ecological modeling with graph theory to detect configurations common to diverse landscapes. *Landscape Ecology,* 8**,** 239-255.

CARNEY, L. T. & EDWARDS, M. S. 2010. ROLE OF NUTRIENT FLUCTUATIONS AND DELAYED DEVELOPMENT IN GAMETOPHYTE REPRODUCTION BY MACROCYSTIS PYRIFERA (PHAEOPHYCEAE) IN SOUTHERN CALIFORNIA 1. *Journal of Phycology,* 46**,** 987-996.

CARR, M. H., ROBINSON, S. P., WAHLE, C., DAVIS, G., KROLL, S., MURRAY, S., SCHUMACKER, E. J. & WILLIAMS, M. 2017. The central importance of ecological spatial connectivity to effective coastal marine protected areas and to meeting the challenges of climate change in the marine environment. *Aquatic Conservation: Marine and Freshwater Ecosystems,* 27**,** 6-29.

CARTER, H. N., SCHMIDT, S. W. & HIRONS, A. C. 2015. An international assessment of mangrove management: incorporation in integrated coastal zone management. *Diversity,* 7**,** 74-104.

CARWARDINE, J., MARTIN, T. G., FIRN, J., REYES, R. P., NICOL, S., REESON, A., GRANTHAM, H. S., STRATFORD, D., KEHOE, L. & CHADÈS, I. 2019. Priority Threat Management for biodiversity conservation: A handbook. *Journal of Applied Ecology,* 56**,** 481-490.

CARWARDINE, J., O'CONNOR, T., LEGGE, S., MACKEY, B., POSSINGHAM, H. P. & MARTIN, T. G. 2012. Prioritizing threat management for biodiversity conservation. *Conservation Letters,* 5**,** 196-204.

CASTILLA, J. C. & BUSTAMANTE, R. H. 1989. Human exclusion from rocky intertidal of Las Cruces, Central Chile: Effects on Durvillaea antarctica(Phaeophyta, Durvilleales). *Marine ecology progress series. Oldendorf,* 50**,** 203-214.

CASTORANI, M. C., REED, D. C., ALBERTO, F., BELL, T. W., SIMONS, R. D., CAVANAUGH, K. C., SIEGEL, D. A. & RAIMONDI, P. T. 2015. Connectivity structures local population dynamics: a long-term empirical test in a large metapopulation system. *Ecology,* 96**,** 3141-3152.

CHAIGNEAU, A. & PIZARRO, O. 2005. Eddy characteristics in the eastern South Pacific. *Journal of Geophysical Research: Oceans,* 110.

CHAMBERLAIN, D., PHINN, S. & POSSINGHAM, H. 2020. Remote sensing of mangroves and estuarine communities in central Queensland, Australia. *Remote Sensing,* 12**,** 197.

CHOW, J. 2018. Mangrove management for climate change adaptation and sustainable development in coastal zones. *Journal of Sustainable Forestry,* 37**,** 139-156.

CLARKE, P. J. 1993. Dispersal of grey mangrove (Avicennia marina) propagules in southeastern Australia. *Aquatic Botany,* 45**,** 195-204.

CLARKE, P. J., KERRIGAN, R. A. & WESTPHAL, C. J. 2001. Dispersal potential and early growth in 14 tropical mangroves: do early life history traits correlate with patterns of adult distribution? *Journal of Ecology***,** 648-659.

COLAS, F., CAPET, X., MCWILLIAMS, J. C. & SHCHEPETKIN, A. 2008. 1997–1998 El Niño off Peru: A numerical study. *Progress in Oceanography,* 79**,** 138-155.

COLEMAN, M. A., CETINA-HEREDIA, P., ROUGHAN, M., FENG, M., VAN SEBILLE, E. & KELAHER, B. P. 2017. Anticipating changes to future connectivity within a network of marine protected areas. *Global Change Biology,* 23**,** 3533-3542.

CONEJERO, C., DEWITTE, B., GARÇON, V., SUDRE, J. & MONTES, I. 2020. ENSO diversity driving low-frequency change in mesoscale activity off Peru and Chile. *Scientific Reports,* 10**,** 17902.

COSTA, F. & VIEIRA, A. 2023. Stream Barrier Removal: Are New Approaches Possible in Small Rivers? The Case of the Selho River (Northwestern Portugal). *Hydrology,* 10**,** 163.

COWEN, R. K., GAWARKIEWICZ, G., PINEDA, J., THORROLD, S. R. & WERNER, F. E. 2007. Population connectivity in marine systems an overview. *Oceanography,* 20**,** 14-21.

COWEN, R. K., LWIZA, K. M., SPONAUGLE, S., PARIS, C. B. & OLSON, D. B. 2000. Connectivity of marine populations: open or closed? *Science,* 287**,** 857-859.

CSARDI, G. & NEPUSZ, T. 2006. The igraph software. *Complex syst,* 1695**,** 1-9.

DABALÀ, A., DAHDOUH-GUEBAS, F., DUNN, D. C., EVERETT, J. D., LOVELOCK, C. E., HANSON, J. O., BUENAFE, K. C. V., NEUBERT, S. & RICHARDSON, A. J. 2023. Priority areas to protect mangroves and maximise ecosystem services. *Nature communications,* 14**,** 5863.

DATTA, D., CHATTOPADHYAY, R. & GUHA, P. 2012. Community based mangrove management: A review on status and sustainability. *Journal of environmental management,* 107**,** 84-95.

DAY JR, J. W., YÁÑEZ-ARANCIBIA, A., KEMP, W. M. & CRUMP, B. C. 2012. Introduction to estuarine ecology. *Estuarine ecology***,** 1-18.

DAYTON, P. K., TEGNER, M. J., PARNELL, P. E. & EDWARDS, P. B. 1992. Temporal and spatial patterns of disturbance and recovery in a kelp forest community. *Ecological Monographs,* 62**,** 421-445.

DE JUAN, S., GELCICH, S. & FERNANDEZ, M. 2017. Integrating stakeholder perceptions and preferences on ecosystem services in the management of coastal areas. *Ocean & coastal management,* 136**,** 38-48.

DI NITTO, D., ERFTEMEIJER, P., VAN BEEK, J., DAHDOUH-GUEBAS, F., HIGAZI, L., QUISTHOUDT, K., JAYATISSA, L. & KOEDAM, N. 2013. Modelling drivers of mangrove propagule dispersal and restoration of abandoned shrimp farms. *Biogeosciences,* 10**,** 5095-5113.

DUKE, N. 2006. *Australia's mangroves: the authoritative guide to Australia's mangrove plants*, MER.

DUKE, N., BALL, M. & ELLISON, J. 1998. Factors influencing biodiversity and distributional gradients in mangroves. *Global Ecology & Biogeography Letters,* 7**,** 27-47.

DUKE, N., LAWN, P., ROELFSEMA, C., PHINN, S., ZAHMEL, K., PEDERSEN, D., HARRIS, C., STEGGLES, N. & TACK, C. 2003. Assessing Historical Change in Coastal Environments. Port Curtis, Fitzroy River Estuary and Moreton Bay Regions.

DUKE, N. C., CANNING, A. D. & MACKENZIE, J. R. 2024. More Intense Severe Tropical Cyclones in Recent Decades Cause Greater Impacts on Mangroves Bordering Australia's Great Barrier Reef. *Oceanographic Processes of Coral Reefs.* CRC Press.

DUNNING, M. D. 2010. Queensland Coastal Wetlands (Mangroves, saltpans, samphire), 1987 - 1997 (DEEDI). eAtlas.

DUTTA ROY, A., KARPOWICZ, D. A., HENDY, I., ROG, S. M., WATT, M. S., REEF, R., BROADBENT, E. N., ASBRIDGE, E. F., GEBRIE, A. & ALI, T. 2024. Current status of remote sensing for studying the impacts of hurricanes on mangrove forests in the coastal United States. *Remote Sensing,* 16**,** 3596.

ELLISON, A. M., FELSON, A. J. & FRIESS, D. A. 2020. Mangrove rehabilitation and restoration as experimental adaptive management. *Frontiers in Marine Science,* 7**,** 327.

ELLISON, J. C. 2014. Climate change adaptation: Management options for mangrove areas. *Mangrove Ecosystems of Asia: Status, Challenges and Management Strategies***,** 391-413.

ERF. 2014. *Review of the Emissions Reduction Fund* [Online]. Available: https://www.climatechangeauthority.gov.au/review-emissions-reduction-fund [Accessed January 8, 2025].

FALVEY, M. & GARREAUD, R. 2007. Wintertime precipitation episodes in central Chile: Associated meteorological conditions and orographic influences. *Journal of Hydrometeorology,* 8**,** 171-193.

FELLER, I. C., WHIGHAM, D. F., O'NEILL, J. P. & MCKEE, K. L. 1999. Effects of nutrient enrichment on within-stand cycling in a mangrove forest. *Ecology,* 80**,** 2193-2205.

FERNÁNDEZ, M. & CASTILLA, J. C. 2005. Marine conservation in Chile: historical perspective, lessons, and challenges. *Conservation Biology,* 19**,** 1752-1762.

FILBEE-DEXTER, K., FEEHAN, C. J. & SCHEIBLING, R. E. 2016. Large-scale degradation of a kelp ecosystem in an ocean warming hotspot. *Marine Ecology Progress Series,* 543**,** 141-152.

FONTOURA, L., D'AGATA, S., GAMOYO, M., BARNECHE, D. R., LUIZ, O. J., MADIN, E. M., EGGERTSEN, L. & MAINA, J. M. 2022. Protecting connectivity promotes successful biodiversity and fisheries conservation. *Science,* 375**,** 336-340.

FORKAM, D. C., AJONINA, G. N., AJONINA, P. U. & TCHAMBA, M. N. 2020. Framework for assessing the level of stakeholders involvement and governance in mangrove management: case of selected local communities in the south west coastal Atlantic Region, Cameroon. *Journal of Ecology and The Natural Environment,* 12**,** 150-164.

FRAZÃO SANTOS, C., AGARDY, T., ANDRADE, F., CALADO, H., CROWDER, L. B., EHLER, C. N., GARCÍA-MORALES, S., GISSI, E., HALPERN, B. S. & ORBACH, M. K. 2020. Integrating climate change in ocean planning. *Nature Sustainability,* 3**,** 505-516.

FREEMAN, L. C. 1977. A set of measures of centrality based on betweenness. *Sociometry***,** 35-41.

FREEMAN, L. C. 2002. Centrality in social networks: Conceptual clarification. *Social network: critical concepts in sociology. Londres: Routledge,* 1**,** 238-263.

GAINES, S. D., GAYLORD, B., GERBER, L. R., HASTINGS, A. & KINLAN, B. P. 2007. Connecting places: the ecological consequences of dispersal in the sea. *Oceanography,* 20**,** 90-99.

GAINES, S. D., GAYLORD, B. & LARGIER, J. L. 2003. Avoiding current oversights in marine reserve design. *Ecological Applications,* 13**,** 32-46.

GAME, E. T., KAREIVA, P. & POSSINGHAM, H. P. 2013. Six common mistakes in conservation priority setting. *Conservation Biology,* 27**,** 480-485.

GARDNER, J. P., LAUSCHE, B., PITTMAN, S. J. & METAXAS, A. 2024. Marine connectivity conservation: Guidance for MPA and MPA network design and management. *Marine Policy,* 167**,** 106250.

GARREAUD, R. D. & FALVEY, M. 2009. The coastal winds off western subtropical South America in future climate scenarios. *International Journal of Climatology: A Journal of the Royal Meteorological Society,* 29**,** 543-554.

GAYLORD, B., REED, D. C., WASHBURN, L. & RAIMONDI, P. T. 2004. Physical–biological coupling in spore dispersal of kelp forest macroalgae. *Journal of Marine Systems,* 49**,** 19-39.

GELCICH, S., HUGHES, T. P., OLSSON, P., FOLKE, C., DEFEO, O., FERNÁNDEZ, M., FOALE, S., GUNDERSON, L. H., RODRÍGUEZ-SICKERT, C. & SCHEFFER, M. 2010. Navigating transformations in governance of Chilean marine coastal resources. *Proceedings of the National Academy of Sciences,* 107**,** 16794-16799.

GILLESPIE, R. G., BALDWIN, B. G., WATERS, J. M., FRASER, C. I., NIKULA, R. & RODERICK, G. K. 2012. Long-distance dispersal: a framework for hypothesis testing. *Trends in ecology & evolution,* 27**,** 47-56.

GONZÁLEZ-ROCA, F., GELCICH, S., PÉREZ-RUZAFA, Á., VEGA, J. A. & VÁSQUEZ, J. A. 2021. Exploring the role of access regimes over an economically important intertidal kelp species. *Ocean & Coastal Management,* 212**,** 105811.

GORELICK, N., HANCHER, M., DIXON, M., ILYUSHCHENKO, S., THAU, D. & MOORE, R. 2017. Google Earth Engine: Planetary-scale geospatial analysis for everyone. *Remote sensing of Environment,* 202**,** 18-27.

GOUDKAMP, K. & CHIN, A. 2006. Mangroves and saltmarshes.

GOUVÊA, L. P., FRAGKOPOULOU, E., CAVANAUGH, K., SERRÃO, E. A., ARAÚJO, M. B., COSTELLO, M. J., WESTERGERLING, E. T. & ASSIS, J. 2023. Oceanographic connectivity explains the intra-specific diversity of mangrove forests at global scales. *Proceedings of the National Academy of Sciences,* 120**,** e2209637120.

GRAHAM, M. H., VASQUEZ, J. A. & BUSCHMANN, A. H. 2007. Global ecology of the giant kelp Macrocystis: from ecotypes to ecosystems. *Oceanography and Marine Biology,* 45**,** 39.

GRECH, A., HANERT, E., MCKENZIE, L., RASHEED, M., THOMAS, C., TOL, S., WANG, M., WAYCOTT, M., WOLTER, J. & COLES, R. 2018. Predicting the cumulative effect of multiple disturbances on seagrass connectivity. *Global change biology,* 24**,** 3093-3104.

GRECH, A., WOLTER, J., COLES, R., MCKENZIE, L., RASHEED, M., THOMAS, C., WAYCOTT, M. & HANERT, E. 2016. Spatial patterns of seagrass dispersal and settlement. *Diversity and Distributions,* 22**,** 1150-1162.

GREENE, S., MORRISSEY, M. & JOHNSON, S. E. 2010. Wind climatology, climate change, and wind energy. *Geography Compass,* 4**,** 1592-1605.

GURDEK-BAS, R., BENTHUYSEN, J. A., HARRISON, H. B., ZENGER, K. R. & VAN HERWERDEN, L. 2022. The El Niño Southern Oscillation drives multidirectional inter-reef larval connectivity in the Great Barrier Reef. *Scientific Reports,* 12**,** 21290.

GUTIERREZ, A., CORREA, T., MUNOZ, V., SANTIBANEZ, A., MARCOS, R., CÁCERES, C. & BUSCHMANN, A. H. Farming of the giant kelp Macrocystis pyrifera in southern Chile for development of novel food products. Eighteenth International Seaweed Symposium: Proceedings of the Eighteenth International Seaweed Symposium, held in Bergen, Norway, 20–25 June 2004, 2007. Springer, 33-41.

HADLEY, W. 2016. *Ggplot2: Elegrant graphics for data analysis*, Springer.

HAMILTON, J. F., OSMAN, R. W. & FELLER, I. C. 2017. Modeling local effects on propagule movement and the potential expansion of mangroves and associated fauna: Testing in a sub-tropical lagoon. *Hydrobiologia,* 803**,** 173-187.

HAMILTON, S. E. & FRIESS, D. A. 2018. Global carbon stocks and potential emissions due to mangrove deforestation from 2000 to 2012. *Nature Climate Change,* 8**,** 240-244.

HAMYLTON, S., KELLEWAY, J., ROGERS, K., MCLEAN, R., TYNAN, Z. N. & REPINA, O. 2023. Mangrove expansion on the low wooded islands of the Great Barrier Reef. *Proceedings of the Royal Society B,* 290**,** 20231183.

HARRISON, H. B., BODE, M., WILLIAMSON, D. H., BERUMEN, M. L. & JONES, G. P. 2020. A connectivity portfolio effect stabilizes marine reserve performance. *Proceedings of the National Academy of Sciences,* 117**,** 25595-25600.

HARTIG, F. 2020. DHARMa: residual diagnostics for hierarchical (multi-level/mixed) regression models. *R package version 0.3,* 3.

HEDGECOCK, D. SECOND-GENERATION LINKAGE MAPS REVEAL ERRORS IN THE ASSEMBLY OF THE PACIFIC OYSTER (Crassostrea gigas) GENOME AND FACTORS AFFECTING MAP LENGTHS AND MARKER ORDERS. AQUACULTURE, 2017. ELSEVIER SCIENCE BV PO BOX 211, 1000 AE AMSTERDAM, NETHERLANDS, 101-101.

HERNÁNDEZ-CARMONA, G., HUGHES, B. & GRAHAM, M. H. 2006. Reproductive longevity of drifting kelp Macrocystis pyrifera (Phaeophyceae) in Monterey bay, USA 1. *Journal of Phycology,* 42**,** 1199-1207.

HILTY, J., WORBOYS, G. L., KEELEY, A., WOODLEY, S., LAUSCHE, B. J., LOCKE, H., CARR, M., PULSFORD, I., PITTOCK, J. & WHITE, J. W. 2020. Guidelines for conserving connectivity through ecological networks and corridors.

HOBDAY, A. J. 2000. Abundance and dispersal of drifting kelp Macrocystis pyrifera rafts in the Southern California Bight. *Marine Ecology Progress Series,* 195**,** 101-116.

HOFFMANN, A. & SANTELICES, B. 1997. Flora marina de Chile central. *Flora marina de Chile central.*

HOLLARSMITH, J. A., BUSCHMANN, A. H., CAMUS, C. & GROSHOLZ, E. D. 2020. Varying reproductive success under ocean warming and acidification across giant kelp (Macrocystis pyrifera) populations. *Journal of Experimental Marine Biology and Ecology,* 522**,** 151247.

HOUSTON, W. 1999. Severe hail damage to mangroves at Port Curtis, Australia. *Mangroves and Salt Marshes,* 3**,** 29-40.

HOWE, H. F. & MIRITI, M. N. 2004. When seed dispersal matters. *BioScience,* 54**,** 651-660.

HOWE, H. F. & SMALLWOOD, J. 1982. Ecology of seed dispersal. *Annual review of ecology and systematics,* 13**,** 201-228.

HUGHES, T. P., BELLWOOD, D. R., FOLKE, C., STENECK, R. S. & WILSON, J. 2005. New paradigms for supporting the resilience of marine ecosystems. *Trends in ecology & evolution,* 20**,** 380-386.

ISOBE, A., HINATA, H., KAKO, S. I. & YOSHIOKA, S. 2011. Formulation of leeway-drift velocities for sea-surface drifting-objects based on a wind-wave flume experiment. *Interdisciplinary studies on environmental chemistry-marine environmental modeling and analysis. Terrapub., Tokyo***,** 239-249.

KAHLE, D. J. & WICKHAM, H. 2013. ggmap: spatial visualization with ggplot2. *R J.,* 5**,** 144.

KANAMITSU, M., EBISUZAKI, W., WOOLLEN, J., YANG, S.-K., HNILO, J., FIORINO, M. & POTTER, G. 2002. Ncep–doe amip-ii reanalysis (r-2). *Bulletin of the American Meteorological Society,* 83**,** 1631-1644.

KATSANEVAKIS, S., STELZENMÜLLER, V., SOUTH, A., SØRENSEN, T. K., JONES, P. J., KERR, S., BADALAMENTI, F., ANAGNOSTOU, C., BREEN, P. & CHUST, G. 2011. Ecosystem-based marine spatial management: review of concepts, policies, tools, and critical issues. *Ocean & coastal management,* 54**,** 807-820.

KEELEY, A. T., BEIER, P. & JENNESS, J. S. 2021. Connectivity metrics for conservation planning and monitoring. *Biological Conservation,* 255**,** 109008.

KENNEDY, J. P., GARAVELLI, L., TRUELOVE, N. K., DEVLIN, D. J., BOX, S. J., CHÉRUBIN, L. M. & FELLER, I. C. 2017. Contrasting genetic effects of red mangrove (Rhizophora mangle L.) range expansion along West and East Florida. *Journal of Biogeography,* 44**,** 335-347.

KINLAN, B. P. & GAINES, S. D. 2003. Propagule dispersal in marine and terrestrial environments: a community perspective. *Ecology,* 84**,** 2007-2020.

KINLAN, B. P., GRAHAM, M. H., SALA, E. & DAYTON, P. K. 2003a. Arrested development of giant kelp (Macrocystis pyrifera, Phaeophyceae) embryonic sporophytes: a mechanism for delayed recruitment in perennial kelps? *Journal of Phycology,* 39**,** 47-57.

KINLAN, B. P., GRAHAM, M. H., SALA, E. & DAYTON, P. K. 2003b. ARRESTED DEVELOPMENT OF GIANT KELP (MACROCYSTIS PYRIFERA, PHAEOPHYCEAE) EMBRYONIC SPOROPHYTES: A MECHANISM FOR DELAYED RECRUITMENT IN PERENNIAL KELPS? 1. *Journal of Phycology,* 39**,** 47-57.

KNUTSON, T., CAMARGO, S. J., CHAN, J. C., EMANUEL, K., HO, C.-H., KOSSIN, J., MOHAPATRA, M., SATOH, M., SUGI, M. & WALSH, K. 2020. Tropical cyclones and climate change assessment: Part II: Projected response to anthropogenic warming. *Bulletin of the American Meteorological Society,* 101**,** E303-E322.

KRAUSS, K. W., MCKEE, K. L., LOVELOCK, C. E., CAHOON, D. R., SAINTILAN, N., REEF, R. & CHEN, L. 2014. How mangrove forests adjust to rising sea level. *New Phytologist,* 202**,** 19-34.

LAMBRECHTS, J., HANERT, E., DELEERSNIJDER, E., BERNARD, P.-E., LEGAT, V., REMACLE, J.-F. & WOLANSKI, E. 2008. A multi-scale model of the hydrodynamics of the whole Great Barrier Reef. *Estuarine, Coastal and Shelf Science,* 79**,** 143-151.

LE, D. M., DESMOND, M. J., PRITCHARD, D. W. & HEPBURN, C. D. 2022. Effect of temperature on sporulation and spore development of giant kelp (Macrocystis pyrifera). *Plos one,* 17**,** e0278268.

LEE, S. Y., PRIMAVERA, J. H., DAHDOUH-GUEBAS, F., MCKEE, K., BOSIRE, J. O., CANNICCI, S., DIELE, K., FROMARD, F., KOEDAM, N. & MARCHAND, C. 2014. Ecological role and services of tropical mangrove ecosystems: a reassessment. *Global ecology and biogeography,* 23**,** 726-743.

LEIS, J. M. Perspectives on larval behaviour in biophysical modelling of larval dispersal in marine, demersal fishes. Oceans, 2020. MDPI, 1-25.

LETELIER, J., PIZARRO, O. & NUÑEZ, S. 2009. Seasonal variability of coastal upwelling and the upwelling front off central Chile. *Journal of Geophysical Research: Oceans,* 114.

LETT, C., VERLEY, P., MULLON, C., PARADA, C., BROCHIER, T., PENVEN, P. & BLANKE, B. 2008. A Lagrangian tool for modelling ichthyoplankton dynamics. *Environmental Modelling & Software,* 23**,** 1210-1214.

LEWIS III, R. R., BROWN, B. M. & FLYNN, L. L. 2019. Methods and criteria for successful mangrove forest rehabilitation. *Coastal wetlands.* Elsevier.

LOVELOCK, C. E., ADAME, M. F., BENNION, V., HAYES, M., REEF, R., SANTINI, N. & CAHOON, D. R. 2015. Sea level and turbidity controls on mangrove soil surface elevation change. *Estuarine, Coastal and Shelf Science,* 153**,** 1-9.

LOVELOCK, C. E. & REEF, R. 2020. Variable impacts of climate change on blue carbon. *One Earth,* 3**,** 195-211.

LÜDECKE, D., BEN-SHACHAR, M. S., PATIL, I., WAGGONER, P. & MAKOWSKI, D. 2021. performance: An R package for assessment, comparison and testing of statistical models. *Journal of Open Source Software,* 6.

LUICK, J. L., MASON, L., HARDY, T. & FURNAS, M. J. 2007. Circulation in the Great Barrier Reef Lagoon using numerical tracers and in situ data. *Continental Shelf Research,* 27**,** 757-778.

LUKE, H., MARTENS, M. A., MOON, E. M., SMITH, D., WARD, N. J. & BUSH, R. T. 2017. Ecological restoration of a severely degraded coastal acid sulfate soil: A case study of the East Trinity wetland, Queensland. *Ecological Management & Restoration,* 18**,** 103-114.

MACAYA, E. C., BOLTANA, S., HINOJOSA, I. A., MACCHIAVELLO, J. E., VALDIVIA, N. A., VASQUEZ, N. R., BUSCHMANN, A. H., VASQUEZ, J. A., ALONSO VEGA, J. & THIEL, M. 2005. Presence of sporophylls in floating kelp rafts of Macrocystis spp. (Phaeophyceae) along the Chilean Pacific Coast. *Journal of Phycology,* 41**,** 913-922.

MACAYA, E. C. & ZUCCARELLO, G. 2010. Genetic structure of the giant kelp Macrocystis pyrifera along the southeastern Pacific. *Marine Ecology Progress Series,* 420**,** 103-112.

MAGRIS, R. A., PRESSEY, R. L., WEEKS, R. & BAN, N. C. 2014. Integrating connectivity and climate change into marine conservation planning. *Biological Conservation,* 170**,** 207-221.

MAHMOOD HOSSAIN, M. H., SANJOY SAHA, S. S., SERAJIS SALEKIN, S. S., ABDULLAH-AL-MAMUN, A.-A.-M., SIDDIQUE, M. & ABDULLAH, S. 2014. Salinity influence on germination of four important mangrove species of the sundarbans, Bangladesh.

MAROIS, D. E. & MITSCH, W. J. 2015. Coastal protection from tsunamis and cyclones provided by mangrove wetlands–a review. *International Journal of Biodiversity Science, Ecosystem Services & Management,* 11**,** 71-83.

MÁRQUEZ PORRAS, R. 2019. La fiebre de las algas. Forma y dinámicas del extractivismo en la costa chilena. *Revista Andaluza de Antropología, 17, 52-71.*

MARTINEZ-DIAZ, M. & REEF, R. 2023. *Mangrove biogeography under climate change scenarios and urbanisation.* Monash University.

MASKEY, M. L., FACINCANI DOURADO, G., RALLINGS, A. M., RHEINHEIMER, D. E., MEDELLÍN-AZUARA, J. & VIERS, J. H. 2022. Assessing hydrological alteration caused by climate change and reservoir

operations in the San Joaquin River Basin, California. *Frontiers in Environmental Science,* 10**,** 765426.
MASON, N., WARD, M., WATSON, J. E., VENTER, O. & RUNTING, R. K. 2020. Global opportunities and challenges for transboundary conservation. *Nature ecology & evolution,* 4**,** 694-701.
MAZA, M., LARA, J. L. & LOSADA, I. J. 2021. Predicting the evolution of coastal protection service with mangrove forest age. *Coastal Engineering,* 168**,** 103922.
MAZOR, T., POSSINGHAM, H. P. & KARK, S. 2013. Collaboration among countries in marine conservation can achieve substantial efficiencies. *Diversity and Distributions,* 19**,** 1380-1393.
MCCOOK, L., ALMANY, G., BERUMEN, M. L., DAY, J., GREEN, A., JONES, G., LEIS, J., PLANES, S., RUSS, G. & SALE, P. 2009a. Management under uncertainty: guide-lines for incorporating connectivity into the protection of coral reefs. *Coral Reefs,* 28**,** 353-366.
MCCOOK, L., ALMANY, G., BERUMEN, M. L., DAY, J., GREEN, A., JONES, G., LEIS, J., PLANES, S., RUSS, G. & SALE, P. 2009b. Management under uncertainty: guide-lines for incorporating connectivity into the protection of coral reefs. *Coral reefs,* 28**,** 353-366.
MCKILLUP, S. & MCKILLUP, R. 1997. An outbreak of the moth Achaea serva (Fabr.) on the mangrove Excoecaria agallocha (L.).
MINCHINTON, T. E. 2006. Consequences of pre-dispersal damage by insects for the dispersal and recruitment of mangroves. *Oecologia,* 148**,** 70-80.
MONTECINO, V. & LANGE, C. B. 2009. The Humboldt Current System: Ecosystem components and processes, fisheries, and sediment studies. *Progress in Oceanography,* 83**,** 65-79.
MONTECINO, V., STRUB, P. T., CHAVEZ, F., THOMAS, A., TARAZONA, J. & BAUMGARTNER, T. 2006. Bio-physical interactions off western South America. *The sea,* 14**,** 329-390.
MONTECINOS, A. & ACEITUNO, P. 2003. Seasonality of the ENSO-related rainfall variability in central Chile and associated circulation anomalies. *Journal of climate,* 16**,** 281-296.
MONTECINOS, A. & GOMEZ, F. 2010. ENSO modulation of the upwelling season off southern-central Chile. *Geophysical Research Letters,* 37.
MONTECINOS, A., KURGANSKY, M. V., MUÑOZ, C. & TAKAHASHI, K. 2011. Non-ENSO interannual rainfall variability in central Chile during austral winter. *Theoretical and Applied Climatology,* 106**,** 557-568.
MONZÓN-ARGÜELLO, C., DELL'AMICO, F., MORINIERE, P., MARCO, A., LÓPEZ-JURADO, L. F., HAYS, G. C., SCOTT, R., MARSH, R. & LEE, P. L. 2012. Lost at sea: genetic, oceanographic and meteorological evidence for storm-forced dispersal. *Journal of the Royal Society Interface,* 9**,** 1725-1732.
MORA-SOTO, A., PALACIOS, M., MACAYA, E. C., GÓMEZ, I., HUOVINEN, P., PÉREZ-MATUS, A., YOUNG, M., GOLDING, N., TORO, M. & YAQUB, M. 2020. A high-resolution global map of giant kelp (Macrocystis pyrifera) forests and intertidal green algae (Ulvophyceae) with Sentinel-2 imagery. *Remote Sensing,* 12**,** 694.
MORENO, A. & REVENGA, C. 2014. The system of territorial use rights in fisheries in Chile. *Arlington, Virginia, USA: The Nature Conservancy*.
MUÑOZ, R., VERGARA, O. A., FIGUEROA, P. A., MARDONES, P., SOBARZO, M. & SALDÍAS, G. S. 2023. On the phenology of coastal upwelling off central-southern Chile. *Dynamics of Atmospheres and Oceans,* 104**,** 101405.
NASA. 2025. *Salinity overview* [Online]. Available: https://salinity.oceansciences.org/overview-faqs.htm?utm_source=chatgpt.com [Accessed April 12, 2025].
NEWMAN, M. 2018. *Networks*, Oxford university press.
NGEVE, M. N., VAN DER STOCKEN, T., MENEMENLIS, D., KOEDAM, N. & TRIEST, L. 2016. Contrasting effects of historical sea level rise and contemporary ocean currents on regional gene flow of Rhizophora racemosa in Eastern Atlantic mangroves. *PLoS One,* 11**,** e0150950.
NOAA 2024. ENSO Cold & Warm Episodes by Season.
NORDERHAUG, K. M. & CHRISTIE, H. C. 2009. Sea urchin grazing and kelp re-vegetation in the NE Atlantic. *Marine Biology Research,* 5**,** 515-528.

OLDS, A. D., CONNOLLY, R. M., PITT, K. A., PITTMAN, S. J., MAXWELL, P. S., HUIJBERS, C. M., MOORE, B. R., ALBERT, S., RISSIK, D. & BABCOCK, R. C. 2016. Quantifying the conservation value of seascape connectivity: a global synthesis. *Global Ecology and Biogeography,* 25**,** 3-15.

OSBORNE, D. J. & BERJAK, P. 1997. The making of mangroves: the remarkable pioneering role played by seeds of Avicennia marina. *Endeavour,* 21**,** 143-147.

OSPINA-ALVAREZ, A., DE JUAN, S., ALÓS, J., BASTERRETXEA, G., ALONSO-FERNÁNDEZ, A., FOLLANA-BERNÁ, G., PALMER, M. & CATALÁN, I. A. 2020a. MPA network design based on graph theory and emergent properties of larval dispersal. *Marine Ecology Progress Series,* 650**,** 309-326.

OSPINA-ALVAREZ, A., DE JUAN, S., DAVIS, K. J., GONZÁLEZ, C., FERNÁNDEZ, M. & NAVARRETE, S. A. 2020b. Integration of biophysical connectivity in the spatial optimization of coastal ecosystem services. *Science of The Total Environment,* 733**,** 139367.

OSPINA-ALVAREZ, A., WEIDBERG, N., AIKEN, C. M. & NAVARRETE, S. A. 2018. Larval transport in the upwelling ecosystem of central Chile: The effects of vertical migration, developmental time and coastal topography on recruitment. *Progress in Oceanography,* 168**,** 82-99.

OTHMAN, M. A. 1994. Value of mangroves in coastal protection. *Hydrobiologia,* 285**,** 277-282.

PALUMBI, S. R. 2003. Population genetics, demographic connectivity, and the design of marine reserves. *Ecological applications,* 13**,** 146-158.

PARIS, C. B., GUIGAND, C. M., IRISSON, J.-O., FISHER, R. & D'ALESSANDRO, E. 2008. Orientation with no frame of reference (OWNFOR): a novel system to observe and quantify orientation in reef fish larvae. *Caribbean connectivity: Implications for marine protected area management***,** 52-62.

PARMESAN, C., MORECROFT, M. D. & TRISURAT, Y. 2022. *Climate change 2022: Impacts, adaptation and vulnerability.* GIEC.

PASTOR, A., CATALÁN, I. A., TERRADOS, J., MOURRE, B. & OSPINA-ALVAREZ, A. 2023. Connectivity-based approach to guide conservation and restoration of seagrass Posidonia oceanica in the NW Mediterranean. *Biological Conservation,* 285**,** 110248.

PASTOR, A., OSPINA-ALVAREZ, A., LARSEN, J., HANSEN, F. T., KRAUSE-JENSEN, D. & MAAR, M. 2022. A network analysis of connected biophysical pathways to advice eelgrass (Zostera marina) restoration. *Marine Environmental Research,* 179**,** 105690.

PEDERSEN, T. 2019. Package 'ggraph': An Implementation of Grammar of Graphics for Graphs and Networks. CRAN.

PEDERSEN, T. L. 2021. Package 'ggraph': An Implementation of Grammar of Graphics for Graphs and Networks. *Retrieved January,* 1.

PENDLETON, L., DONATO, D. C., MURRAY, B. C., CROOKS, S., JENKINS, W. A., SIFLEET, S., CRAFT, C., FOURQUREAN, J. W., KAUFFMAN, J. B. & MARBÀ, N. 2012. Estimating global "blue carbon" emissions from conversion and degradation of vegetated coastal ecosystems.

PÉREZ-MATUS, A., OSPINA-ALVAREZ, A., CAMUS, P. A., CARRASCO, S. A., FERNANDEZ, M., GELCICH, S., GODOY, N., OJEDA, F. P., PARDO, L. M. & ROZBACZYLO, N. 2017. Temperate rocky subtidal reef community reveals human impacts across the entire food web. *Marine Ecology Progress Series,* 567**,** 1-16.

PÉREZ-SANTOS, I., SEGUEL, R., SCHNEIDER, W., LINFORD, P., DONOSO, D., NAVARRO, E., AMAYA-CÁRCAMO, C., PINILLA, E. & DANERI, G. 2019. Synoptic-scale variability of surface winds and ocean response to atmospheric forcing in the eastern austral Pacific Ocean. *Ocean Science,* 15**,** 1247-1266.

PORRAS, R. M. 2019. LA FIEBRE DE LAS ALGAS. FORMA Y DINÁMICAS DEL EXTRACTIVISMO EN LA COSTA CHILENA. *Revista Andaluza de Antropología***,** 52-71.

PORRAS, R. M. & VÁSQUEZ, J. A. 2020. El extractivismo de las algas pardas en el norte de Chile. *European Review of Latin American and Caribbean Studies/Revista Europea de Estudios Latinoamericanos y del Caribe***,** 101-121.

PRADHAN, S., SAMAL, R. N., CHOUDHURY, S. B. & MOHANTY, P. K. 2018. Hydrodynamic and cohesive sediment transport modeling in chilika lagoon. *ISPRS Annals of the Photogrammetry, Remote Sensing and Spatial Information Sciences,* 4**,** 141-149.

PROISY, C., SIDIK, F., PROSPÉRI, M.-J. & TRANCHANT, B. Connectivity of mangroves in the indonesian archipelago through dispersal pathways of propagules using an ocean circulation model. 2016. INRA.

PUGH, D. T. 1987. Tides, surges and mean sea level.

R CODE TEAM 2019. R: A language and environment for statistical computing. *(No Title)*.

RABINOWITZ, D. 1978. Dispersal properties of mangrove propagules. *Biotropica***,** 47-57.

RAHN, D. A., ROSENBLÜTH, B. & RUTLLANT, J. A. 2015. Detecting subtle seasonal transitions of upwelling in North-Central Chile. *Journal of Physical Oceanography,* 45**,** 854-867.

RAMIREZ-ROMERO, E., AMORES, A., DIAZ, D., MUÑOZ, A., CATALAN, I. A., MOLINERO, J. C. & OSPINA-ALVAREZ, A. 2023. Atmospheric–ocean coupling drives prevailing and synchronic dispersal patterns of marine species with long pelagic durations. *Scientific reports,* 13**,** 2366.

RAYFIELD, B., FORTIN, M.-J. & FALL, A. 2011. Connectivity for conservation: a framework to classify network measures. *Ecology,* 92**,** 847-858.

REED, D., WASHBURN, L., RASSWEILER, A., MILLER, R., BELL, T. & HARRER, S. 2016. Extreme warming challenges sentinel status of kelp forests as indicators of climate change. *Nature Communications,* 7**,** 13757.

REED, D. C., AMSLER, C. D. & EBELING, A. W. 1992. Dispersal in kelps: factors affecting spore swimming and competency. *Ecology,* 73**,** 1577-1585.

REED, D. C., SCHROETER, S. C., HUANG, D., WEISMAN, D., BEHESHTI, K. M. & SMITH, R. S. 2024. The ecology of giant kelp colonization and its implications for kelp forest restoration. *Journal of Phycology*.

REEF, R. & LOVELOCK, C. E. 2015. Regulation of water balance in mangroves. *Annals of botany,* 115**,** 385-395.

REID, H. 2016. Ecosystem-and community-based adaptation: learning from community-based natural resource management. *Climate and development,* 8**,** 4-9.

ROBERTSON, A. I. & ALONGI, D. M. 1995. Role of riverine mangrove forests in organic carbon export to the tropical coastal ocean: a preliminary mass balance for the Fly Delta (Papua New Guinea). *Geo-Marine Letters,* 15**,** 134-139.

RODRIGUES, A. S. & ROUYER, M.-M. 2023. Measuring the ecological benefits of protected areas. Nature Publishing Group UK London.

ROSVALL, M., AXELSSON, D. & BERGSTROM, C. T. 2009. The map equation. *The European Physical Journal Special Topics,* 178**,** 13-23.

ROSVALL, M. & BERGSTROM, C. T. 2008. Maps of random walks on complex networks reveal community structure. *Proceedings of the national academy of sciences,* 105**,** 1118-1123.

ROTHÄUSLER, E., GOMEZ, I., HINOJOSA, I. A., KARSTEN, U., TALA, F. & THIEL, M. 2009. Effect of temperature and grazing on growth and reproduction of floating Macrocystis spp.(phaeophyceae) along a latitudinal gradient 1. *Journal of Phycology,* 45**,** 547-559.

SAAVEDRA-HORTUA, D., NAGELKERKEN, I., ESTUPINAN-SUAREZ, L. M. & GILLIS, L. G. 2023. Effects of connectivity on carbon and nitrogen stocks in mangrove and seagrass ecosystems. *Science of the Total Environment,* 896**,** 164829.

SAINTILAN, N., ROGERS, K. & MCKEE, K. 2009. Salt marsh-mangrove interactions in Australasia and the Americas.

SARAVANAN, K. 2005. A study on the diversity and management of Pondicherry mangroves. *Department of Science, Technology and Environment, Government of Pondicherry*.

SCHMITT, K. 2012. Mangrove planting, community participation and integrated management in Soc Trang Province, Viet Nam. *Sharing lessons on mangrove restoration***,** 205.

SCHUPP, E. W., JORDANO, P. & GÓMEZ, J. M. 2010. Seed dispersal effectiveness revisited: a conceptual review. *New phytologist,* 188**,** 333-353.

SCHWARTZ, M. W., COOK, C. N., PRESSEY, R. L., PULLIN, A. S., RUNGE, M. C., SALAFSKY, N., SUTHERLAND, W. J. & WILLIAMSON, M. A. 2018. Decision support frameworks and tools for conservation. *Conservation Letters,* 11**,** e12385.

SHANKS, A. L. 2009. Pelagic larval duration and dispersal distance revisited. *The biological bulletin,* 216**,** 373-385.

SIEVERS, M., BROWN, C. J., MCGOWAN, J., TURSCHWELL, M. P., BUELOW, C. A., HOLGATE, B., PEARSON, R. M., ADAME, M. F., ANDRADI-BROWN, D. A. & ARNELL, A. 2023. Co-occurrence of biodiversity, carbon storage, coastal protection, and fish and invertebrate production to inform global mangrove conservation planning. *Science of the Total Environment,* 904**,** 166357.

SLIM. 2025. *SLIM: a multi-scale model of the land-sea continuum* [Online]. Available: https://www.slim-ocean.be [Accessed April 3, 2025].

SMALE, D. A. 2020. Impacts of ocean warming on kelp forest ecosystems. *New Phytologist,* 225**,** 1447-1454.

SMITH, S. M. & SNEDAKER, S. C. 1995. Salinity responses in two populations of viviparous Rhizophora mangle L. seedlings. *Biotropica***,** 435-440.

SOBARZO, M., FIGUEROA, M. & DJURFELDT, L. 2001. Upwelling of subsurface water into the rim of the Biobıo submarine canyon as a response to surface winds. *Continental Shelf Research,* 21**,** 279-299.

SOUSA, W. P., KENNEDY, P. G., MITCHELL, B. J. & ORDÓÑEZ L, B. M. 2007. Supply-side ecology in mangroves: do propagule dispersal and seedling establishment explain forest structure? *Ecological monographs,* 77**,** 53-76.

SPENCER, T., MÖLLER, I. & REEF, R. 2016. Mangrove systems and environments. *Reference Module in Earth Systems and Environmental Sciences.* Elsevier.

STAMMER, D., DAVIS, R., FU, L. L., FUKUMORI, I., GIERING, R., LEE, T., MAROTZKE, J., MARSHALL, J., MENEMENLIS, D., NIILER, P., WUNSCH, C. & ZLOTNICKI., V. 1999. The consortium for estimating the circulation and climate of the ocean (ECCO) - Science goals and task plan - Report No1. Techical report, Jet Propulsion Laboratory - Massachusetts Institute of Technology - Scripps Institution of Oceanography.

STEINBERG, R., VAN DER MEER, M., WALKER, E., BERUMEN, M. L., HOBBS, J.-P. A. & VAN HERWERDEN, L. 2016. Genetic connectivity and self-replenishment of inshore and offshore populations of the endemic anemonefish, Amphiprion latezonatus. *Coral Reefs,* 35**,** 959-970.

STENECK, R., PARIS, C., ARNOLD, S., ABLAN-LAGMAN, M., ALCALA, A. C., BUTLER, M., MCCOOK, L., RUSS, G. & SALE, P. 2009. Thinking and managing outside the box: coalescing connectivity networks to build region-wide resilience in coral reef ecosystems. *Coral Reefs,* 28**,** 367-378.

STENECK, R. S., GRAHAM, M. H., BOURQUE, B. J., CORBETT, D., ERLANDSON, J. M., ESTES, J. A. & TEGNER, M. J. 2002. Kelp forest ecosystems: biodiversity, stability, resilience and future. *Environmental conservation,* 29**,** 436-459.

STENECK, R. S., JOHNSON, C. R., BERTNESS, M., BRUNO, J., SILLIMAN, B. & STACHOWICZ, J. 2013. Dynamic patterns, processes and feedbacks. *Marine community ecology***,** 315-336.

STRUB, P. T., JAMES, C., MONTECINO, V., RUTLLANT, J. A. & BLANCO, J. L. 2019. Ocean circulation along the southern Chile transition region (38–46 S): Mean, seasonal and interannual variability, with a focus on 2014–2016. *Progress in Oceanography,* 172**,** 159-198.

SWEARER, S. E., TREML, E. A. & SHIMA, J. S. 2019. A review of biophysical models of marine larval dispersal. *Oceanography and Marine Biology*.

TEAM, R. D. C. 2010. R: A language and environment for statistical computing. *(No Title)*.

TEGNER, M., DAYTON, P., EDWARDS, P. & RISER, K. 1997. Large-scale, low-frequency oceanographic effects on kelp forest succession: a tale of two cohorts. *Marine Ecology Progress Series,* 146**,** 117-134.

THOMPSON-SAUD, G., GRECH, A., CHOUKROUN, S., VÁSQUEZ, S., SALAS, C. & OSPINA-ALVAREZ, A. 2024. The biophysical dynamics of giant kelp, Macrocystis pyrifera: Seasonal patterns and dispersal mechanisms in the southeast Pacific. *Journal of Biogeography*.

TIMMERMANN, A., OBERHUBER, J., BACHER, A., ESCH, M., LATIF, M. & ROECKNER, E. 1999. Increased El Niño frequency in a climate model forced by future greenhouse warming. *Nature,* 398**,** 694-697.

TOMLINSON, P. B. 2016. *The botany of mangroves*, Cambridge University Press.

TOMLINSON, P. B. & COX, P. A. 2000. Systematic and functional anatomy of seedlings in mangrove Rhizophoraceae: vivipary explained? *Botanical Journal of the Linnean Society,* 134**,** 215-231.

TONNÉ, N., BEECKMAN, H., ROBERT, E. M. & KOEDAM, N. 2017. Towards an unknown fate: The floating behaviour of recently abscised propagules from wide ranging Rhizophoraceae mangrove species. *Aquatic botany,* 140**,** 23-33.

TREML, E. A. & HALPIN, P. N. 2012. Marine population connectivity identifies ecological neighbors for conservation planning in the Coral Triangle. *Conservation Letters,* 5**,** 441-449.

TREML, E. A., HALPIN, P. N., URBAN, D. L. & PRATSON, L. F. 2008. Modeling population connectivity by ocean currents, a graph-theoretic approach for marine conservation. *Landscape Ecology,* 23**,** 19-36.

TSANIS, I. K. 1989. Simulation of wind-induced water currents. *Journal of Hydraulic Engineering,* 115**,** 1113-1134.

TSONIS, A., ELSNER, J., HUNT, A. & JAGGER, T. 2005. Unfolding the relation between global temperature and ENSO. *Geophysical Research Letters,* 32.

VAN DER MHEEN, M., PATTIARATCHI, C., COSOLI, S. & WANDRES, M. 2020. Depth-dependent correction for wind-driven drift current in particle tracking applications. *Frontiers in Marine Science,* 7**,** 305.

VAN DER STOCKEN, T., CARROLL, D., MENEMENLIS, D., SIMARD, M. & KOEDAM, N. 2019a. Global-scale dispersal and connectivity in mangroves. *Proceedings of the National Academy of Sciences,* 116**,** 915-922.

VAN DER STOCKEN, T. & MENEMENLIS, D. 2017. Modelling mangrove propagule dispersal trajectories using high-resolution estimates of ocean surface winds and currents. *Biotropica,* 49**,** 472-481.

VAN DER STOCKEN, T., VANSCHOENWINKEL, B., CARROLL, D., CAVANAUGH, K. C. & KOEDAM, N. 2022. Mangrove dispersal disrupted by projected changes in global seawater density. *Nature Climate Change,* 12**,** 685-691.

VAN DER STOCKEN, T., VANSCHOENWINKEL, B., DE RYCK, D. J., BOUMA, T. J., DAHDOUH-GUEBAS, F. & KOEDAM, N. 2015. Interaction between water and wind as a driver of passive dispersal in mangroves. *PLoS One,* 10**,** e0121593.

VAN DER STOCKEN, T., WEE, A. K., DE RYCK, D. J., VANSCHOENWINKEL, B., FRIESS, D. A., DAHDOUH-GUEBAS, F., SIMARD, M., KOEDAM, N. & WEBB, E. L. 2019b. A general framework for propagule dispersal in mangroves. *Biological Reviews,* 94**,** 1547-1575.

VAN WOESIK, R. 1992. *Ecology of coral assemblages on continental islands in the southern section of the Great Barrier Reef, Australia.* James Cook University.

VARGAS, G., PANTOJA, S., RUTLLANT, J. A., LANGE, C. B. & ORTLIEB, L. 2007. Enhancement of coastal upwelling and interdecadal ENSO-like variability in the Peru-Chile Current since late 19th century. *Geophysical Research Letters,* 34.

VÁSQUEZ, J. A. Production, use and fate of Chilean brown seaweeds: re-sources for a sustainable fishery. Nineteenth International Seaweed Symposium: Proceedings of the 19th International Seaweed Symposium, held in Kobe, Japan, 26-31 March, 2007., 2009. Springer, 7-17.

VÁSQUEZ, J. A. & BUSCHMANN, A. H. 1997. Herbivore-kelp interactions in Chilean subtidal. *Revista Chilena de Historia Natural,* 70**,** 52.

VÁSQUEZ, J. A., VEGA, J. A. & BUSCHMANN, A. H. Long term variability in the structure of kelp communities in northern Chile and the 1997–98 ENSO. Eighteenth International Seaweed

Symposium: Proceedings of the Eighteenth International Seaweed Symposium, held in Bergen, Norway, 20–25 June 2004, 2007. Springer, 279-293.
VIERROS, M. 2017. Communities and blue carbon: the role of traditional management systems in providing benefits for carbon storage, biodiversity conservation and livelihoods. *Climatic Change,* 140**,** 89-100.
VILLEGAS, M., LAUDIEN, J., SIELFELD, W. & ARNTZ, W. 2019. Effect of foresting barren ground with Macrocystis pyrifera (Linnaeus) C. Agardh on the occurrence of coastal fishes off northern Chile. *Journal of Applied Phycology,* 31**,** 2145-2157.
WANG, C., DESER, C., YU, J.-Y., DINEZIO, P. & CLEMENT, A. 2017. El Niño and southern oscillation (ENSO): a review. *Coral reefs of the eastern tropical Pacific: Persistence and loss in a dynamic environment***,** 85-106.
WANNER, M. S., WALTER, J. A., REUMAN, D. C., BELL, T. W. & CASTORANI, M. C. 2024. Dispersal synchronizes giant kelp forests. *Ecology***,** e4270.
WATERS, J. M., KING, T. M., FRASER, C. I. & CRAW, D. 2018. Crossing the front: contrasting storm-forced dispersal dynamics revealed by biological, geological and genetic analysis of beach-cast kelp. *Journal of the Royal Society Interface,* 15**,** 20180046.
WEERSING, K. & TOONEN, R. J. 2009. Population genetics, larval dispersal, and connectivity in marine systems. *Marine Ecology Progress Series,* 393**,** 1-12.
WEIDBERG, N., OSPINA-ALVAREZ, A., BONICELLI, J., BARAHONA, M., AIKEN, C. M., BROITMAN, B. R. & NAVARRETE, S. A. 2020. Spatial shifts in productivity of the coastal ocean over the past two decades induced by migration of the Pacific Anticyclone and Bakun's effect in the Humboldt Upwelling Ecosystem. *Global and Planetary Change,* 193**,** 103259.
WERNER, F. E., COWEN, R. K. & PARIS, C. B. 2007. Coupled biological and physical models: present capabilities and necessary developments for future studies of population connectivity. *Oceanography,* 20**,** 54-69.
WHITE, J. W., RASSWEILER, A., SAMHOURI, J. F., STIER, A. C. & WHITE, C. 2014. Ecologists should not use statistical significance tests to interpret simulation model results. *Oikos,* 123**,** 385-388.
WICKHAM, H., AVERICK, M., BRYAN, J., CHANG, W., MCGOWAN, L. D. A., FRANÇOIS, R., GROLEMUND, G., HAYES, A., HENRY, L. & HESTER, J. 2019. Welcome to the Tidyverse. *Journal of open source software,* 4**,** 1686.
WOLANSKI, E. & KINGSFORD, M. J. 2024. *Oceanographic processes of coral reefs: physical and biological links in the Great Barrier Reef*, CRC Press.
WOOD, S. N. 2017. *Generalized additive models: an introduction with R*, CRC press.
WU, J. 1983. Sea-surface drift currents induced by wind and waves. *Journal of Physical Oceanography,* 13**,** 1441-1451.
WU, L., CAI, W., ZHANG, L., NAKAMURA, H., TIMMERMANN, A., JOYCE, T., MCPHADEN, M. J., ALEXANDER, M., QIU, B. & VISBECK, M. 2012. Enhanced warming over the global subtropical western boundary currents. *Nature Climate Change,* 2**,** 161-166.
YAO, Y., VEHTARI, A., SIMPSON, D. & GELMAN, A. 2017. 1 When is leave-one-out cross validation appropriate?
ZAINOL, Z., PERIS, A. D., AKHIR, M. F., RAHIM, N. H. A., SATYANARAYANA, B. & DAHDOUH-GUEBAS, F. 2022. Mangrove propagule dispersal in a shallow and narrow coastal lagoon: a simulation-based assessment of the Setiu Wetlands, Malaysia. *Forests,* 13**,** 1525.
ZENG, Y., FRIESS, D. A., SARIRA, T. V., SIMAN, K. & KOH, L. P. 2021. Global potential and limits of mangrove blue carbon for climate change mitigation. *Current Biology,* 31**,** 1737-1743. e3.

# Appendix A. Supplementary information for Chapter 2

## Appendix A1. Oceanographic conditions

The Humboldt Current System (HCS) is a cold, low-salinity, nutrient-rich ocean current that flows northward along the western coast of South America. It originates from the South Pacific Current and extends from southern Chile (~42°S), where the West Winds Drift intersects the South American continent, to northern Peru and Ecuador (~4°S), where cool, nutrient rich upwelled waters collide with warm tropical waters forming the Equatorial Front. In the upper ocean, the HCS also known as the Peru-Chile Current System (PCCS) is characterized by equatorward flow of fresh, cooler Sub-Antarctic Surface Water (SASW) northward of 45°S along the eastern rim of the subtropical gyre (Figure 3.b). The main flow of the HCS veers offshore in southern Peru and a weaker coastal limb continues equatorward (Chaigneau and Pizarro, 2005, Montecino and Lange, 2009). The SASW mix with the saltier and warmer Subtropical Surface Water (SSW) beginning at ~18°S and is partially subducted. At the northern end of the HCS, the cool and saltier coastal upwelled waters collide with the fresher and warmer Tropical Surface Waters (TSW) (Montecino and Lange, 2009). Below the surface circulation, the Equatorial Undercurrent (EUC) flows eastward along the equator and feeds the poleward Peru–Chile Undercurrent (PCUC). This poleward undercurrent lies over the slope and continental shelf from northern Peru to about 42°S off Chile and is associated with the transport of Equatorial Sub-surface Waters (ESSW). The PCCS is significantly influenced by the south-eastern Pacific atmospheric anticyclone, which triggers intense upwelling in the region and brings nutrient-rich waters from the deep ocean to the surface, leading to high productivity.

During the study period, from 1997 to 2008, the southeast Pacific coast experienced notable oceanographic conditions. The most significant influence on the region's oceanography was the occurrence of El Niño and La Niña events (Figure A1.1). The trade winds, which typically exhibit an east-to-west flow, experience a weakening during El Niño conditions and a strengthening during La Niña conditions. Conversely, the prevailing westerly winds, the Westerlies, strengthened during El Niño and weakened during La Niña. El Niño events, characterized by the warming of surface waters in the central and eastern equatorial Pacific, led to altered oceanographic patterns along the Chilean and Peruvian coasts, such as a weakening of the HCS and upwelling. The most prominent El Niño event during the study period was from 1997 to 1998. Conversely, La Niña events, marked by the cooling of surface waters in the region, led to the enhancement of the Humboldt Current and upwelling along the coasts. The cooler ocean temperatures during La Niña also contributed to more stable weather patterns and a decrease in rainfall in the region. Several La Niña events were present during the study period, with the most significant one occurring in 2007.

The ocean currents and upwelling patterns vary significantly throughout the seasons, primarily driven by shifts in atmospheric circulation and oceanic conditions, particularly the strength and position of the South Pacific Anticyclone. Seasonal periods in Chapter 2 were defined as follows: summer from January to March, autumn from April to June, winter from July to September and spring from October to December. During spring and summer, there is a weakening of the HCS, attributed to the strengthening and southward movement of the South Pacific Anticyclone, resulting in reduced upwelling and warmer surface waters in north HCS and the opposite in central and south HCS, increase upwelling and colder surface waters. In contrast, autumn and winter witness the intensification of the HCS as the South Pacific Anticyclone undergoes a weakening phase, concurrently shifting its position to a slightly northwestward location. As a result of this atmospheric transition, the Westerlies become more dominant, blowing in from the west and transporting moisture-laden air masses from the Pacific Ocean towards the western coastal regions of Chile. This leads to strengthened upwelling, bringing cold, nutrient-rich waters to the surface in north HCS and the opposite in central and south HCS. Winter is typically when the Humboldt Current is at its strongest.

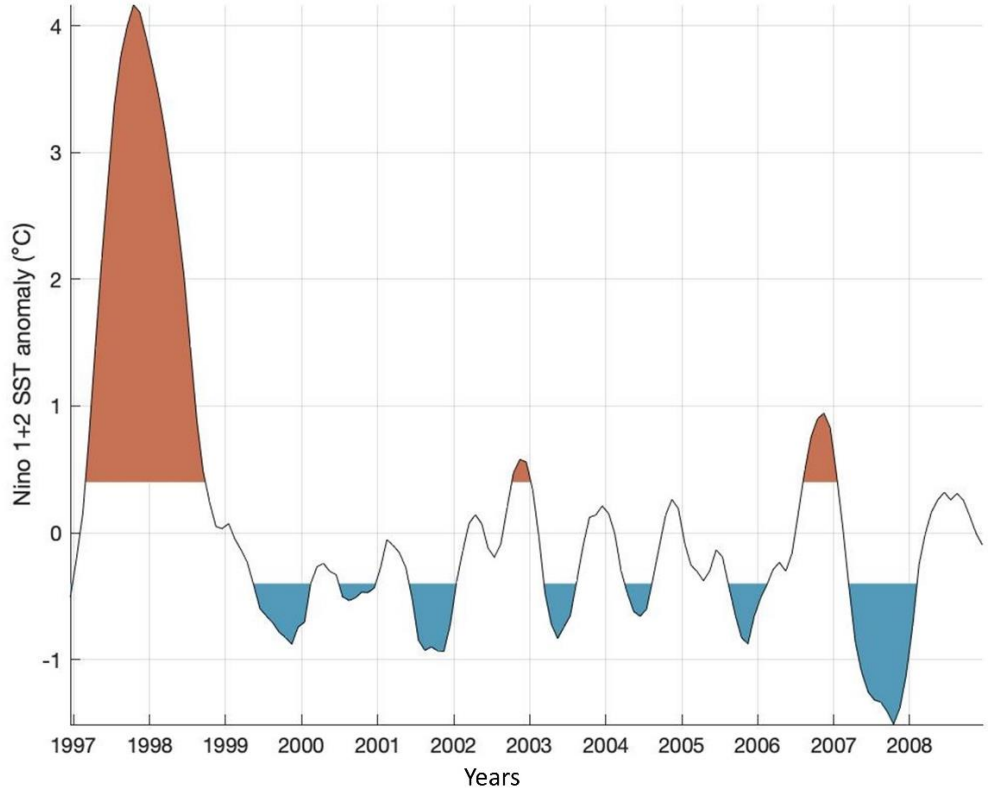


**Figure A1.1.** El Niño Southern Oscillation (ENSO) events from 1997-2008: This figure illustrates the occurrences of ENSO events spanning from 1997 to 2008. Within the graph, red peaks signify El Niño conditions, blue peaks indicate La Niña conditions and uncoloured peaks denote neutral ENSO conditions.

## Appendix A2. Statistical outputs of the settlement success model

**Table A2.1.** Summary of GAM results for the settlement success. The explanatory variables are ENSO (El Niño, La Niña and neutral), season (spring, autumn, winter and summer), days travelling (days since the particle was released) and initial longitude and initial latitude (release location).

| Model | Family | Explanatory Variables | Type of variable | Estimate | p-value | Deviance explained |
|---|---|---|---|---|---|---|
| Settlement success | Binomial | Intercept | | 1.28 | $< 2 \times 10^{-16}$ | 26.4% |
| | | El Niño | Factorial | 0.47 | $< 2 \times 10^{-16}$ | |
| | | La Niña | Factorial | -0.09 | $< 2 \times 10^{-16}$ | |
| | | Spring | Factorial | 0.13 | $< 2 \times 10^{-16}$ | |
| | | Autumn | Factorial | 0.93 | $< 2 \times 10^{-16}$ | |
| | | Winter | Factorial | 1.00 | $< 2 \times 10^{-16}$ | |
| | | El Niño * Spring | Factorial | -0.02 | 0.02 | |
| | | La Niña * Spring | Factorial | -0.90 | $< 2 \times 10^{-16}$ | |
| | | El Niño * Autumn | Factorial | 0.24 | $< 2 \times 10^{-16}$ | |
| | | La Niña * Autumn | Factorial | -0.11 | $< 2 \times 10^{-16}$ | |
| | | El Niño * Winter | Factorial | -0.24 | $< 2 \times 10^{-16}$ | |
| | | La Niña * Winter | Factorial | -0.23 | $< 2 \times 10^{-16}$ | |
| | | s(days travelling) | numerical non-linear distributions | | $< 2 \times 10^{-16}$ | |
| | | s(release lon and lat) | numerical non-linear distributions | | $< 2 \times 10^{-16}$ | |
| | | s(ID) | numerical non-linear distributions | | $< 2 \times 10^{-16}$ | |

**Table A2.2.** Summary of GAM results for the settlement success, showing the estimate of marginal means for seasons and ENSO variable. The explanatory variables are ENSO (El Niño, La Niña and neutral), season (spring, autumn, winter and summer), days travelling (days since the particle was released) and initial longitude and initial latitude (release location).

| Model | Family | Variable | Contrast | Estimate | p-value |
|---|---|---|---|---|---|
| Settlement success | Binomial | Season | Summer - spring | -0.0213 | < 0.0001 |
| | | | Summer - Autumn | -0.1835 | < 0.0001 |
| | | | Summer - Winter | -0.1635 | < 0.0001 |
| | | | Spring - Autumn | -0.1622 | < 0.0001 |
| | | | Spring - Winter | -0.1422 | < 0.0001 |
| | | | Autumn - Winter | 0.0200 | < 0.0001 |
| | | ENSO | Neutral - El Niño | -0.0823 | < 0.0001 |
| | | | Neutral - La Niña | 0.0411 | < 0.0001 |
| | | | El Niño - La Niña | 0.1234 | < 0.0001 |

**Table A2.3.** Summary of GAM results for the settlement success, showing the estimate of marginal means for season variable, considering the levels of the ENSO. The explanatory variables are ENSO (El Niño, La Niña and neutral), season (spring, autumn, winter and summer), days travelling (days since the particle was released) and initial longitude and initial latitude (release location).

| Model | Variables compared | Contrast | Neutral | El Niño | La Niña | p-value |
|---|---|---|---|---|---|---|
| Settlement success | ENSO * season | Summer - spring | -0.03043 | -0.02225 | -0.00938 | < 0.0001 |
| | | Summer - Autumn | -0.18756 | -0.17303 | -0.17520 | < 0.0001 |
| | | Summer - Winter | -0.19760 | -0.12594 | -0.16600 | < 0.0001 |
| | | Spring - Autumn | -0.15713 | -0.15078 | -0.16582 | < 0.0001 |
| | | Spring - Winter | -0.16717 | -0.10369 | -0.15661 | < 0.0001 |
| | | Autumn - Winter | -0.01005 | 0.04708 | 0.00920 | < 0.0001 |

## Appendix A3. GAM graphs of the settlement success and dispersal distance models

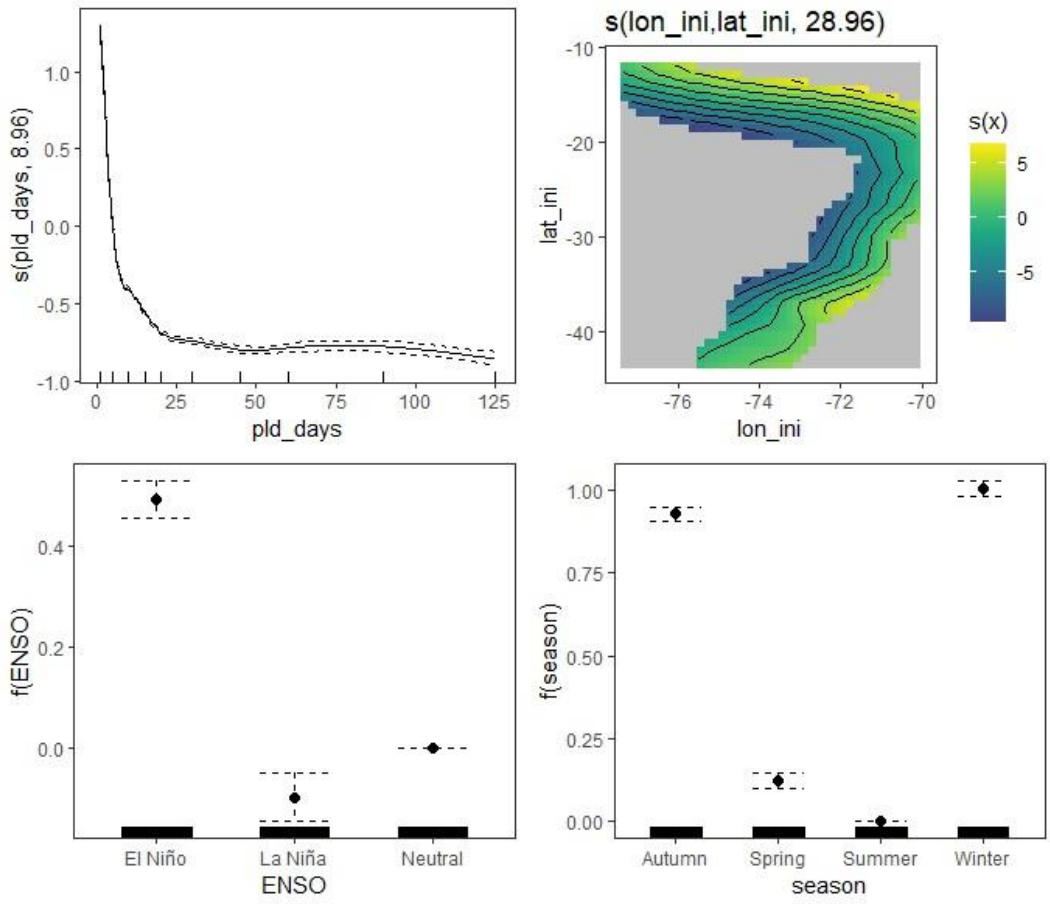


**Figure A3.2.** Gam graphs of the settlement model. The top-left plot shows the effect of time (pld_days) on the response variable with a confidence interval, depicting how the likelihood of kelp fragment settlement decreases over time. The top-middle contour plot represents the spatial effect of initial longitude and latitude (lon_ini, lat_ini) on the response variable. The colour scale indicates the strength and direction of the effect (e.g., likelihood of settlement). The bottom plots show the categorical effects of ENSO conditions and season on the response variable, allowing for an easy comparison of their impact.

Appendix A4. Polar graph with the dispersal distances and directions of kelp fragments

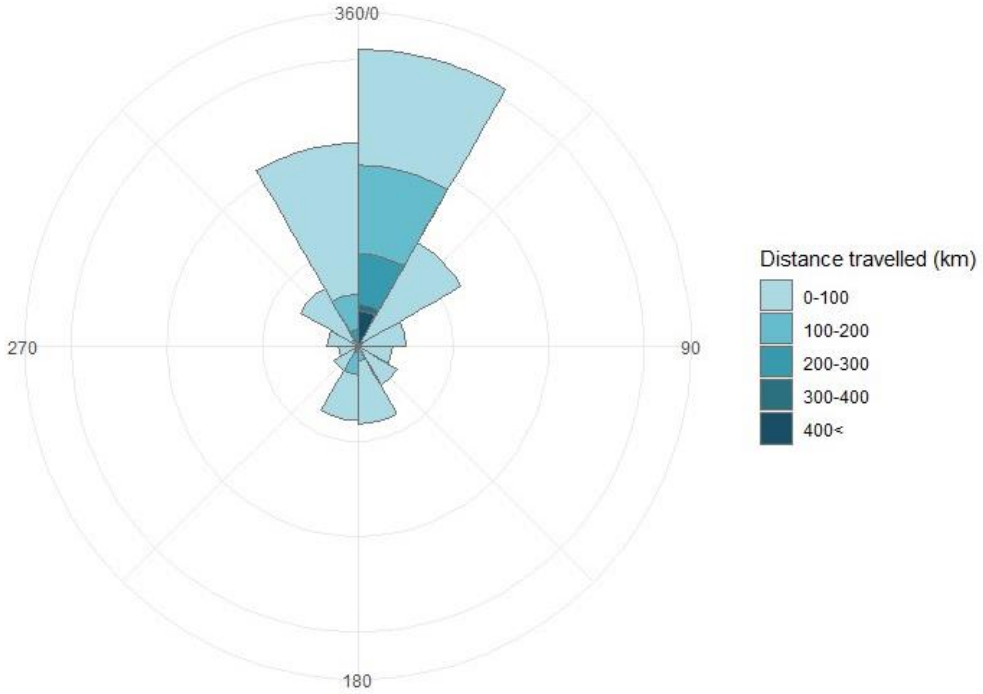


**Figure A4.3.** Polar representation of kelp fragment dispersal distances and directions in the southeast Pacific (1997-2008). This graph showcases the distribution of travel distances and directional tendencies of kelp fragments, categorized by distance in km intervals and directions displayed in degrees from the origin point.

Appendix A5. Settlement success and dispersal distance by year

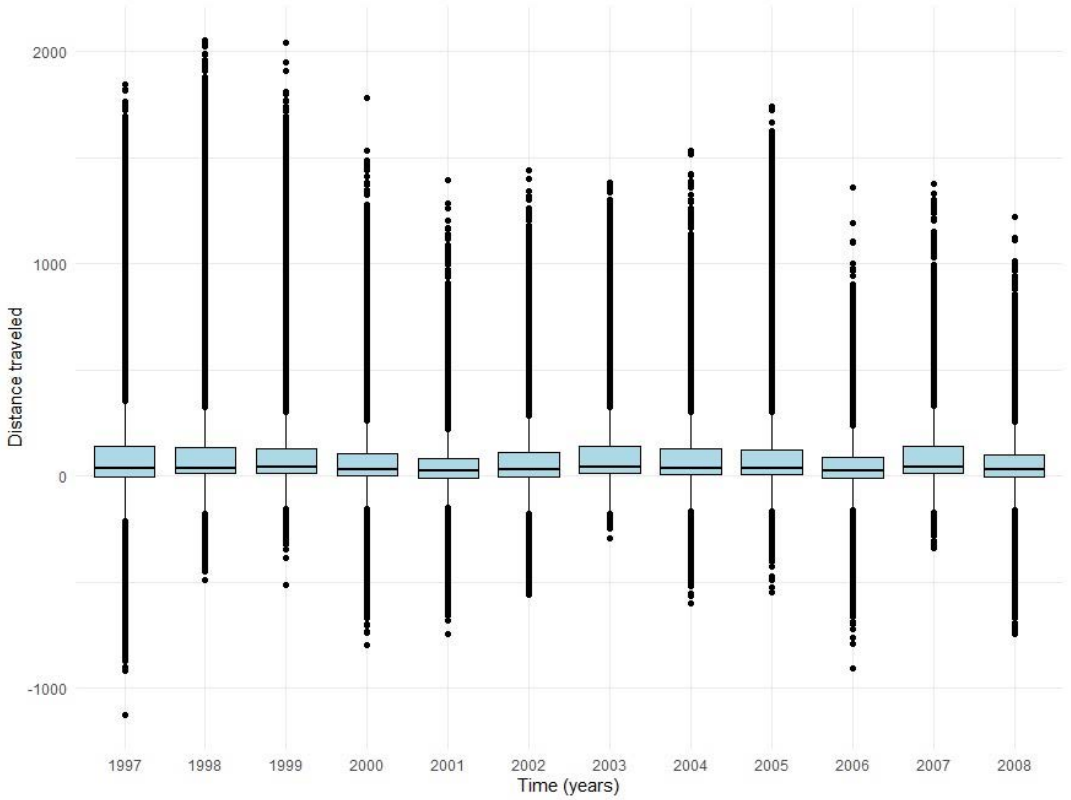


**Figure A5.4.** Boxplot illustrating the dispersal distances covered by kelp fragments that reach settlement areas by year (1997-2008) in the southeast Pacific. Positive values indicate northward travel, while negative values indicate southward travel. The box represents the middle 50% of the data. The middle line inside the box represents the median. The whiskers extend from the edges of the box to the highest and lowest data points within 1.5 times the middle 50% of the data from the upper and lower quartiles, respectively. The black dots are outliers.

**Table A5.4.** Average distance travelled per year by kelp fragments in the Southeast Pacific.

| Year | Mean distance (km) |
|---|---|
| 1997 | 82.6 |
| 1998 | 90.3 |
| 1999 | 90.6 |
| 2000 | 60 |
| 2001 | 45.7 |
| 2002 | 64.7 |
| 2003 | 90.8 |
| 2004 | 75.5 |
| 2005 | 74.3 |
| 2006 | 48.9 |
| 2007 | 95.1 |
| 2008 | 52.6 |

References

CHAIGNEAU, A. & PIZARRO, O. 2005. Eddy characteristics in the eastern South Pacific. Journal of Geophysical Research: Oceans, 110.

MONTECINO, V. & LANGE, C. B. 2009. The Humboldt Current System: Ecosystem components and processes, fisheries, and sediment studies. Progress in Oceanography, 83, 65-79.

# Appendix B. Supplementary information for Chapter 3

## Appendix B1. Parameters used for the biophysical model of kelp forest in the Southeast Pacific region (Thompson-Saud et al. (2024) – **Chapter 2**).

**Table B1.1.** Summary of the main input parameters used for the biophysical model of *M. pyrifera* in the Southeast Pacific region.

| Category | Parameters | State / Description |
|---|---|---|
| *Particle-tracking model* | Total number of particles released | 5000 for each release |
| | Particle types/classes | Particles representing floating fronds/fragments releasing spores |
| *Initiation of pelagic phase* | Release location | Known location of *M. pyrifera* forests (Mora-Soto et al., 2020) |
| | Release events coverage | From 1997 to 2008 |
| | Frequency of release events | Once a week all year round |
| *Transport and movement* | Maximum length of pelagic phase | 125 days (Hernández-Carmona et al., 2006) |
| | Horizontal dispersion | 10 $m^2s^{-1}$ |
| | Buoyancy | Positive |
| | Vertical migration | No |
| | Direct wind drift | Yes, included as forcing |
| *Settlement* | Settlement rate | Decay rate ($N_{(t)} = 13{,}321.2 \times e^{-0.000509 \times t} - 2121.1$)* |

* where: *N(t)* is the number of spores at time, *t* (hours), 13321.17 is the initial number of spores (adjusted for the decay curve), 0.000509 is the decay rate, −2121.06 is the constant to fit the curve to the data.

## Appendix B2. Mathematical formulation of the network measures of the habitat graph and node level.

**Total Edges**: the total number of edges in the network is simply a count of the edges.

**Network Density**:

$$D = \frac{2m}{n(\mathrm{n}-1)}$$

where $n$ is the number of nodes and $m$ is the number of edges in the network.

**Network Diameter**: the longest shortest path between any pair of nodes in the network.

**Connected Components**: the count of maximal subgraphs in which any two vertices are connected to each other by paths and which are connected to no additional vertices in the supergraph.

**Number of Clusters (Modularity)**:

$$Q = \frac{1}{2m}\sum_{i,j}\left(A_{ij} - \frac{k_i k_j}{2m}\right)\delta(c_i c_j)$$

where $A_{ij}$ is the element in the adjacency matrix, $k_i$ is the degree of node $i$, $m$ is the total number of edges, and $\delta(c_i c_j)$ is 1 if nodes $i$ and $j$ are in the same cluster and 0 otherwise.

**Out degree**:

$$k_{out}(i) = \sum_j A_{ij}$$

where $k_i$ is the degree centrality of node $i$ and $A_{ij}$ is the adjacency matrix element.

**In Strength**:

$$S_{out}(i) = \sum_j w_{ji}$$

where $w_{ji}$ is the weight of the edge from node $j$ to node $i$.

**Out Strength**:

$$S_{out}(i) = \sum_j w_{ij}$$

where $w_{ij}$ is the weight of the edge from node $i$ to node $j$.

**Betweenness Centrality**:

$$C_B(i) = \sum_{s \neq i \neq t} \left( \frac{\sigma_{st}(i)}{\sigma_{st}} \right)$$

where $\sigma_{st}$ is the total number of shortest paths from node $s$ to node $t$, and $\sigma_{st}(i)$ is the number of those paths that pass through node $i$.

**Eigenvector Centrality**:

$$v = \frac{1}{\boldsymbol{\lambda}} A v$$

where $A$ is the adjacency matrix of the network, $v$ is the eigenvector corresponding to the largest eigenvalue $\boldsymbol{\lambda}$.

**Closeness Centrality**:

$$C_c(i) = \frac{1}{\sum_j d(i,j)}$$

where $d(i,j)$ is the shortest path distance between nodes $i$ and $j$.

**Local Retention**: the proportion of the total out-strength of the node that remains within the node itself.

**Non-Local Retention**: the proportion of the total in-strength of the node that comes from nodes outside of itself.

## Appendix B3. Statistical outputs of the network measure changes in nodes.

**Table B3.2.** Summary of the GAM results for the network measures changes in nodes. The explanatory variable is TIME which represents ENSO (El Niño, La Niña and neutral).

| Model | Family | Explanatory Variables | Estimate | p-value | Deviance explained |
|---|---|---|---|---|---|
| In-strength | Gamma(link = 'log') | Intercept | 175 | $< 2 \times 10^{-16}$ | 64.9% |
| | | La Niña | 3.16 | $1.76 \times 10^{-3}$ | |
| | | Neutral | 9.85 | $< 2 \times 10^{-16}$ | |
| Out-strength | Gamma(link = 'log') | Intercept | 118.4 | $< 2 \times 10^{-16}$ | 52.3% |
| | | La Niña | 2.13 | $3.37 \times 10^{-2}$ | |
| | | Neutral | 6.69 | $1.06 \times 10^{-10}$ | |
| Degree | Gaussian | Intercept | 53.24 | $< 2 \times 10^{-16}$ | 29.6% |
| | | El Niño | -11.4 | $< 2 \times 10^{-16}$ | |
| | | La Niña | -5.27 | $2.57 \times 10^{-7}$ | |
| Eigenvector | Gamma(link = 'log') | Intercept | 38.73 | $< 2 \times 10^{-16}$ | 87.6% |
| | | El Niño | -16.27 | $< 2 \times 10^{-16}$ | |
| | | La Niña | -14.13 | $< 2 \times 10^{-16}$ | |
| Closeness | Gamma(link = 'log') | Intercept | -87.27 | $< 2 \times 10^{-16}$ | 92.6% |
| | | El Niño | -18.83 | $< 2 \times 10^{-16}$ | |
| | | La Niña | -11.18 | $< 2 \times 10^{-16}$ | |
| Local retention | Gamma(link = 'log') | Intercept | 89.96 | $< 2 \times 10^{-16}$ | 45.5% |
| | | El Niño | 2.02 | $4.38 \times 10^{-2}$ | |
| | | La Niña | 5.91 | $8.98 \times 10^{-9}$ | |
| Non local retention | Gamma(link = 'log') | Intercept | 189.64 | $< 2 \times 10^{-16}$ | 65% |
| | | El Niño | 0.17 | $1.29 \times 10^{-3}$ | |
| | | La Niña | 0.82 | $< 2 \times 10^{-16}$ | |

**Table B3.3.** Summary of the GAM results for the network measures changes in nodes. The explanatory variable is TIME which represents the different seasons (spring, autumn, winter and summer).

| Model | Family | Explanatory Variables | Estimate | p-value | Deviance explained |
|---|---|---|---|---|---|
| In-strength | Gamma(link = 'log') | Intercept | 189.84 | $< 2 \times 10^{-16}$ | 59.5% |
| | | Spring | -2.11 | $3.59 \times 10^{-2}$ | |
| | | Summer | -2.85 | $4.62 \times 10^{-3}$ | |
| | | Winter | 0.21 | 0.83 | |
| Out-strength | Gamma(link = 'log') | Intercept | 138.65 | $< 2 \times 10^{-16}$ | 49% |
| | | Spring | -1.51 | 0.15 | |
| | | Summer | -2.1 | $4.85 \times 10^{-2}$ | |
| | | Winter | -0.06 | 0.96 | |
| Degree | Gamma(link = 'log') | Intercept | 152.91 | $< 2 \times 10^{-16}$ | 81.6% |
| | | Spring | -15.85 | $< 2 \times 10^{-16}$ | |
| | | Summer | -8.31 | $2.87 \times 10^{-15}$ | |
| | | Winter | -7.77 | $1.08 \times 10^{-13}$ | |
| Eigenvector | Gamma(link = 'log') | Intercept | 25.51 | $< 2 \times 10^{-16}$ | 89% |
| | | Spring | -5.89 | $7.98 \times 10^{-9}$ | |
| | | Summer | -0.74 | 0.46 | |
| | | Winter | -1.7 | $8.92 \times 10^{-2}$ | |
| Closeness | Gamma(link = 'log') | Intercept | -85 | $< 2 \times 10^{-16}$ | 91.1% |
| | | Spring | -17.2 | $< 2 \times 10^{-16}$ | |
| | | Summer | -17.44 | $< 2 \times 10^{-16}$ | |
| | | Winter | -7.64 | $1.55 \times 10^{-13}$ | |
| Local retention | Gamma(link = 'log') | Intercept | 99.6 | $< 2 \times 10^{-16}$ | 41% |
| | | Spring | -1.11 | 0.27 | |
| | | Summer | -1.34 | 0.18 | |
| | | Winter | -0.15 | 0.89 | |
| Non local retention | Gamma(link = 'log') | Intercept | 202.51 | $< 2 \times 10^{-16}$ | 59.1% |
| | | Spring | -2.33 | $2.02 \times 10^{-2}$ | |
| | | Summer | -3.29 | $1.11 \times 10^{-3}$ | |
| | | Winter | 0.43 | 0.67 | |

Appendix B4. Node degree distribution

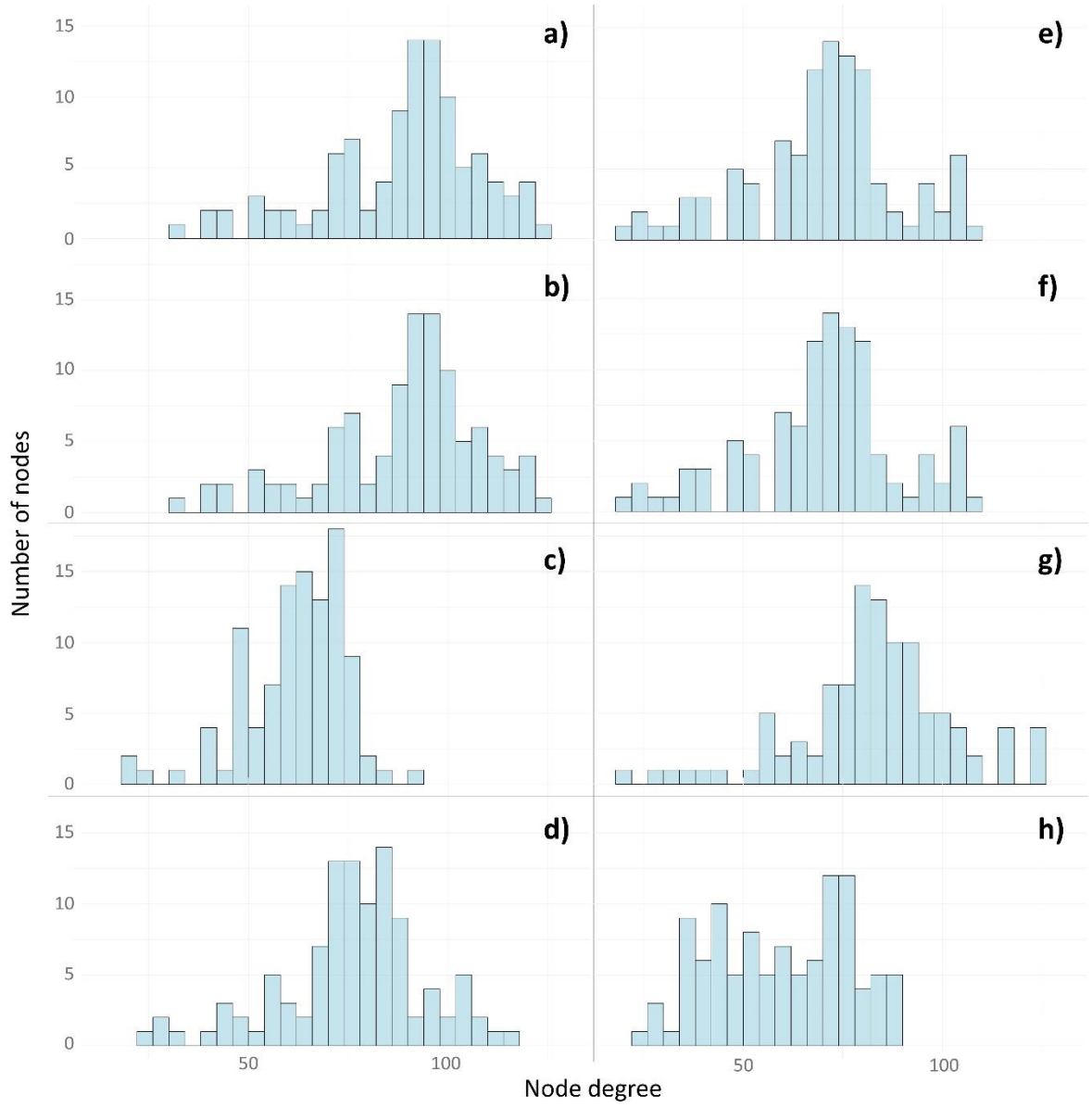


**Figure B4.1.** Graphs showing node degree in the southeast Pacific during the entire period, different ENSO conditions and seasons. Graph of a) the entire period, b) El Niño, c) La Niña, d) neutral, e) summer, f) winter, g) autumn and h) spring.

Appendix B5. Maps with wind direction and speed and their Pearson correlation matrices.

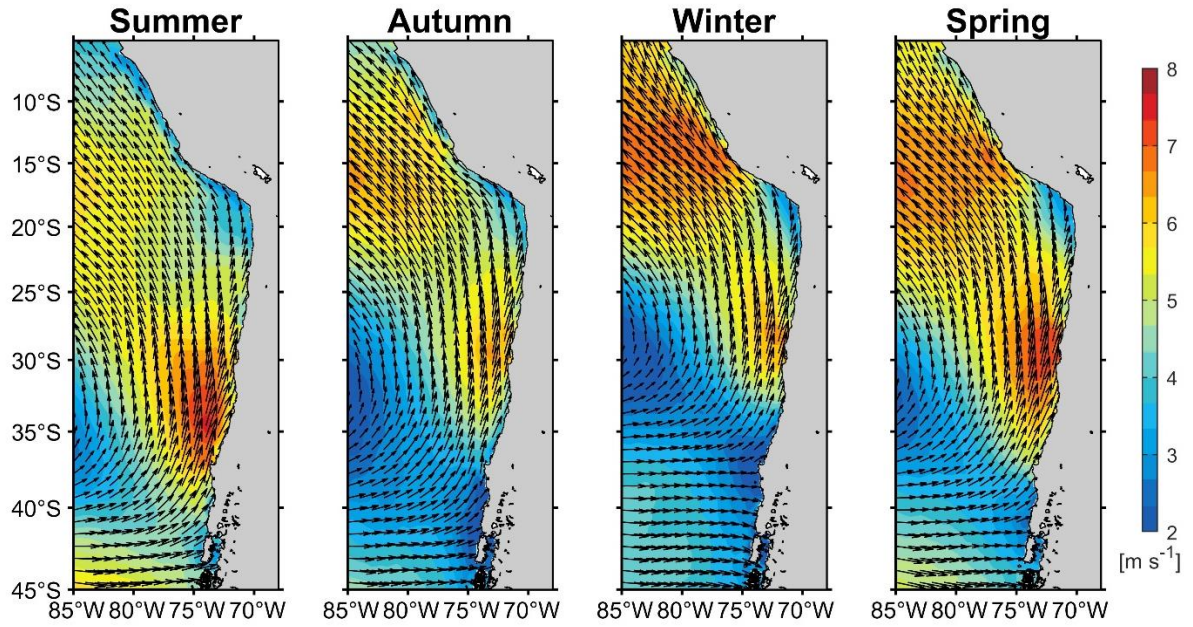


**Figure B5.2.** Average wind maps for season (summer, autumn, winter and spring) in the Southeast Pacific Region. Arrows indicate wind direction, with colour representing wind intensity (blue for low, red for high). The maps are generated using atmospheric forcings from the ROMS (NCEP2).

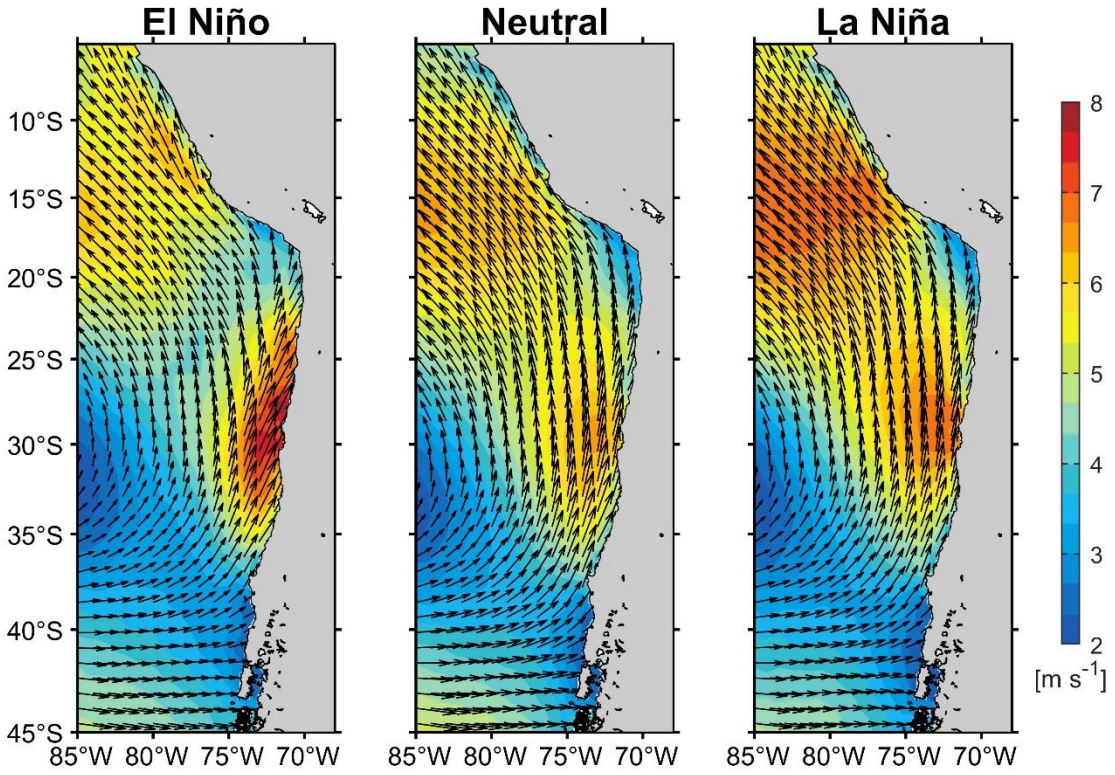


**Figure B5.3.** Average wind maps for ENSO (El Niño, neutral and La Niña Periods) in the Southeast Pacific Region. Arrows indicate wind direction, with colour representing wind intensity (blue for low, red for high). The maps are generated using atmospheric forcings from the ROMS (NCEP2).

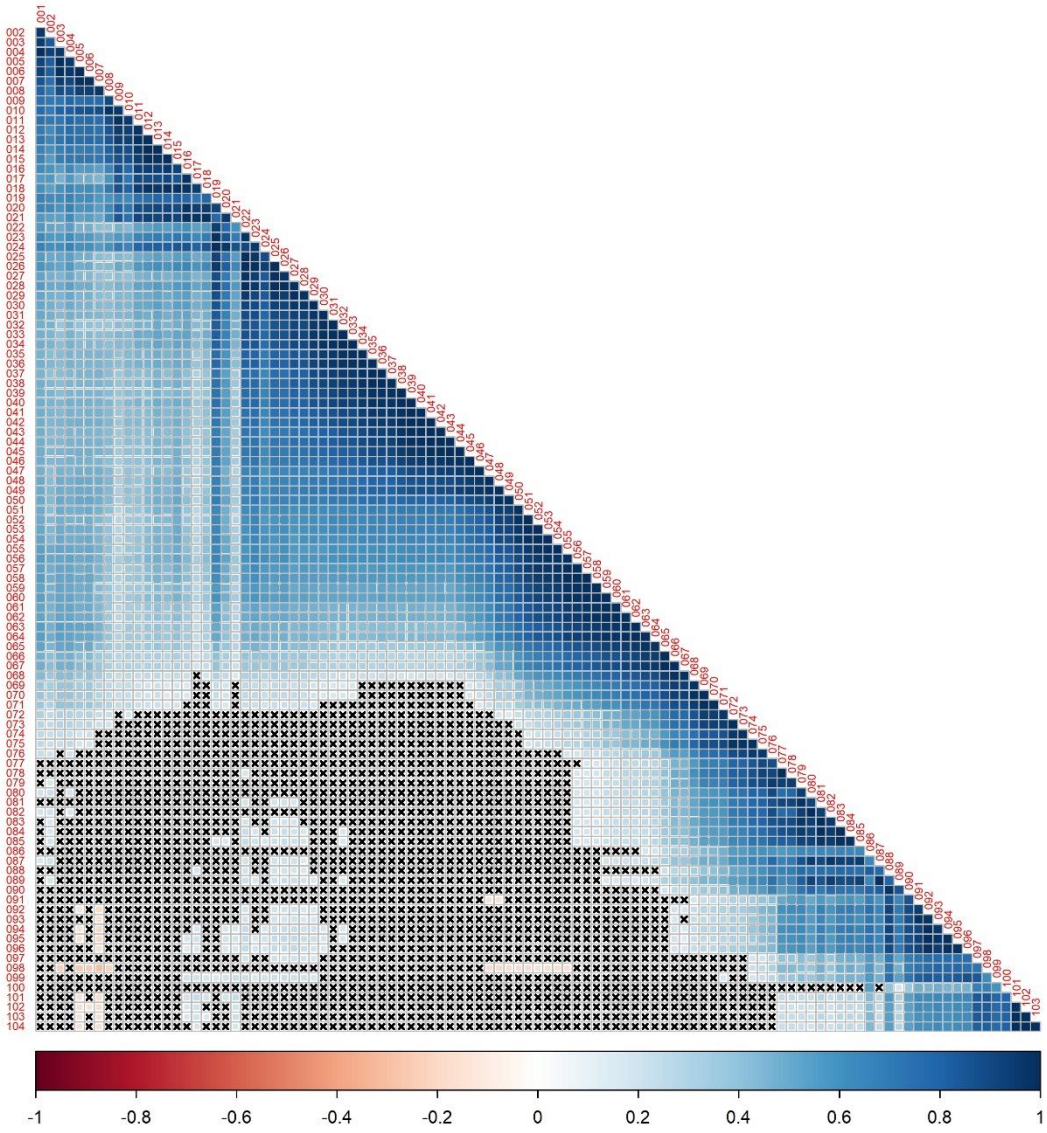


**Figure B5.4.** Pearson correlation matrix of wind direction among analysed nodes. The nodes are distributed from north (upper) to south (lower). Non-significant correlations are indicated by black arrows.

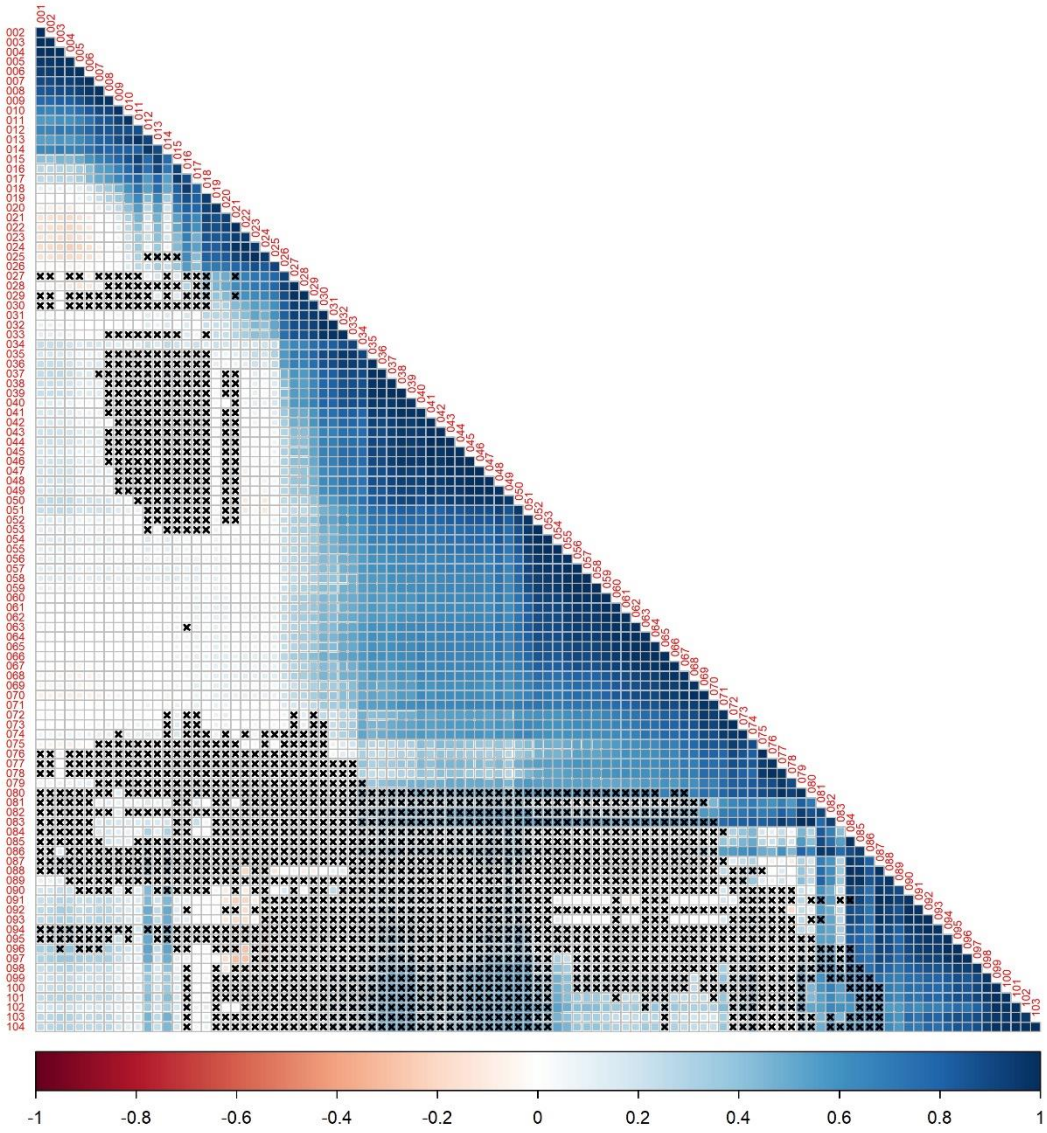


**Figure B5.5.** Pearson correlation matrix of wind magnitude (wind speed) among analysed nodes. The nodes are distributed from north (upper) to south (lower). Non-significant correlations are indicated by black arrows.

# Appendix C. Supplementary information for Chapter 4

## Appendix C1. Priors for Bayesian models and statistical outputs of the propagule's buoyancy and percentage of propagule outside of the water.

**Table C1.1.** Priors used for the statistical analysis of the propagule's buoyancy and percentage of propagule outside of the water.

| Family | Family | Intercept | b | sd | phi |
|---|---|---|---|---|---|
| *Nypa fruticans* | Binomial | 0,1 | 0, 1.5 | 3,0,1 | n/a |
| *Nypa fruticans* | Beta | 0,1 | 0,3 | 3,0,2 | 0.01, 0.01 |
| *Bruguiera gymnorhiza* | Beta | 0,1 | 0,3 | 3,0,2 | 0.01, 0.01 |
| *Xylocarpus granatum* | Beta | 0,1 | 0,3 | 3,0,2 | 0.01, 0.01 |
| *Luminitzera racemosa* | Binomial | 0,1 | 0,1.5 | 3,0,2 | n/a |
| *Heritiera littoralis* | Binomial | 0,2 | 0,0.5 | 3,0,2 | n/a |
| *Heritiera littoralis* | Beta | 0,1 | 0,3 | 3,0,2 | 0.01, 0.01 |
| *Sonneratia alba* | Beta | 0,1 | 0,3 | 3,0,2 | 0.01, 0.01 |
| *Excoecaria agallocha* | Binomial | 0,2 | 0,1.5 | 3,0,2 | n/a |
| All Species | Binomial | 0,1 | 0, 1.5 | 3,0,2 | n/a |
| All Species | Beta | 0,1 | 0, 3 | 3,0,2 | 0.01, 0.01 |

**Table C1.2.** Summary of the results of Bayesian models for the propagule's buoyancy. The explanatory variables are salinity (35, 22,5 and 10 PSU) and time (measured every 5 days until day 90). The median is in the response scale. Lower and upper represent ± 95% Highest Probability Density credibility intervals. P(<1) and P(>1) are the exceedance probability.

| Model | Family | Explanatory Variables | Median | Lower | Upper | P(<1) | P(>1) |
|---|---|---|---|---|---|---|---|
| All species | Binomial | Intercept | 3.65 | 0.06 | 22.5 | 0.12 | 0.88 |
| | | Salinity 22.5 | 0.62 | 0.01 | 5.54 | 0.64 | 0.36 |
| | | Salinity 10 | 0.62 | 0 | 6.41 | 0.62 | 0.38 |
| | | Time | 0 | 0 | 0 | 1 | 0 |
| | | Salinity 22.5 * time | 0.14 | 0.01 | 0.72 | 0.97 | 0.03 |
| | | Salinity 10 * time | 0.1 | 0 | 0.6 | 0.99 | 0.01 |
| *Nypa fruticans* | Binomial | Intercept | 5.46 | 0.09 | 24.1 | 0.03 | 0.97 |
| | | Salinity 22.5 | 0.94 | 0.02 | 0.64 | 0.52 | 0.48 |
| | | Salinity 10 | 0.08 | 0 | 0.68 | 0.98 | 0.02 |
| | | Time | 0.01 | 0 | 0.03 | 1 | 0 |
| | | Salinity 22.5 * time | 0.14 | 0 | 0.79 | 0.97 | 0.03 |
| | | Salinity 10 * time | 0.15 | 0 | 0.93 | 0.96 | 0.04 |
| *Luminitzera racemosa* | Binomial | Intercept | 0.61 | 0.03 | 2.59 | 0.71 | 0.29 |
| | | Salinity 22.5 | 0.31 | 0.01 | 2.73 | 0.81 | 0.19 |
| | | Salinity 10 | 0.31 | 0.01 | 2.75 | 0.81 | 0.19 |
| | | Time | 0.05 | 0 | 0.18 | 1 | 0 |
| | | Salinity 22.5 * time | 0.6 | 0.01 | 3.04 | 0.7 | 0.3 |
| | | Salinity 10 * time | 0.24 | 0.01 | 1.26 | 0.92 | 0.08 |
| *Heritiera littoralis* | Binomial | Intercept | 43 | 0.4 | 283 | 0 | 1 |
| | | Salinity 22.5 | 0.98 | 0.26 | 2.26 | 0.52 | 0.48 |
| | | Salinity 10 | 0.94 | 0.23 | 2.03 | 0.55 | 0.45 |
| | | Time | 0.17 | 0.07 | 0.31 | 1 | 0 |
| | | Salinity 22.5 * time | 0.54 | 0.18 | 1.08 | 0.93 | 0.07 |
| | | Salinity 10 * time | 0.43 | 0.14 | 0.85 | 0.98 | 0.02 |
| *Excoecaria agallocha* | Binomial | Intercept | 54 | 0.3 | 443 | 0 | 1 |
| | | Salinity 22.5 | 0.57 | 0.01 | 5.27 | 0.66 | 0.34 |
| | | Salinity 10 | 0.78 | 0.01 | 6.44 | 0.58 | 0.42 |
| | | Time | 0.1 | 0 | 0.04 | 1 | 0 |
| | | Salinity 22.5 * time | 0.14 | 0 | 0.83 | 1 | 0 |
| | | Salinity 10 * time | 0.22 | 0 | 1.22 | 0.93 | 0.07 |

**Table C1.3.** The median (± 95% credibility interval) day that propagules are most likely to sink at different salinities, calculated using the binomial model for buoyancy.

| Salinity | 35 | | | 22.5 | | | 10 | | |
|---|---|---|---|---|---|---|---|---|---|
| **Species/sink day** | **Median** | **Lower** | **Upper** | **Median** | **Lower** | **Upper** | **Median** | **Lower** | **Upper** |
| *Nypa fruticans* | 55 | 44 | 66 | 52 | 43 | 60 | 42 | 33 | 50 |
| *Luminitzera racemosa* | 13 | 7 | 20 | 10 | 3 | 17 | 11 | 6 | 17 |
| *Heritiera littoralis* | 104 | 66 | 151 | 88 | 59 | 122 | 84 | 60 | 113 |
| *Excoecaria agallocha* | 69 | 54 | 87 | 60 | 47 | 71 | 62 | 50 | 75 |
| All species | 50 | 41 | 59 | 48 | 41 | 56 | 48 | 40 | 56 |

**Table C1.4.** Summary of the results of Bayesian models for the percentage of propagule outside of the water. The explanatory variables are salinity (35, 22,5 and 10 PSU) and time (measured the first five days every day and then every five days until day 90). The median is in the response scale. Lower and upper represent ± 95% Highest Probability Density credibility intervals. P(<1) and P(>1) are the exceedance probability.

| Model | Family | Explanatory Variables | Median | Lower | Upper | P(<1) | P(>1) |
|---|---|---|---|---|---|---|---|
| All species | Beta | Intercept | 0.3 | 0.2 | 0.43 | 1 | 0 |
| | | Salinity 22.5 | 1.26 | 0.61 | 2.03 | 0.21 | 0.79 |
| | | Salinity 10 | 0.68 | 0.36 | 1.13 | 0.91 | 0.09 |
| | | Time | 0.36 | 0.3 | 0.42 | 1 | 0 |
| | | Salinity 22.5 * time | 1.03 | 0.79 | 1.33 | 0.41 | 0.59 |
| | | Salinity 10 * time | 1.51 | 1.11 | 1.93 | 0 | 1 |
| *Nypa fruticans* | Beta | Intercept | 0.67 | 0.46 | 0.91 | 0.99 | 0.01 |
| | | Salinity 22.5 | 0.92 | 0.57 | 1.39 | 0.64 | 0.36 |
| | | Salinity 10 | 0.74 | 0.42 | 1.16 | 0.89 | 0.11 |
| | | Time | 0.21 | 0.13 | 0.29 | 1 | 0 |
| | | Salinity 22.5 * time | 1.1 | 0.53 | 1.86 | 0.38 | 0.62 |
| | | Salinity 10 * time | 0.71 | 0.32 | 1.33 | 0.83 | 0.17 |
| *Bruguiera gymnorhiza* | Beta | Intercept | 1.04 | 0.05 | 0.17 | 1 | 0 |
| | | Salinity 22.5 | 1.82 | 0.58 | 3.43 | 0.08 | 0.92 |
| | | Salinity 10 | 0.6 | 0.22 | 1.19 | 0.91 | 0.09 |
| | | Time | 0.68 | 0.4 | 1.05 | 0.94 | 0.06 |
| | | Salinity 22.5 * time | 0.87 | 0.45 | 1.47 | 0.68 | 0.32 |
| | | Salinity 10 * time | 2.91 | 1.33 | 5.17 | 0 | 1 |
| *Xylocarpus granatum* | Beta | Intercept | 0.39 | 0.29 | 5.01 | 1 | 0 |
| | | Salinity 22.5 | 0.74 | 0.5 | 1.05 | 0.95 | 0.05 |
| | | Salinity 10 | 0.65 | 0.44 | 0.94 | 0.99 | 0.01 |
| | | Time | 0.23 | 0.16 | 0.29 | 1 | 0 |
| | | Salinity 22.5 * time | 1.05 | 0.69 | 1.54 | 0.4 | 0.6 |
| | | Salinity 10 * time | 0.95 | 0.62 | 1.36 | 0.61 | 0.39 |
| *Heritiera littoralis* | Beta | Intercept | 1.2 | 0.39 | 2.38 | 0.3 | 0.7 |
| | | Salinity 22.5 | 0.85 | 0.32 | 1.66 | 0.66 | 0.34 |
| | | Salinity 10 | 0.48 | 0.35 | 0.63 | 1 | 0 |
| | | Time | 0.88 | 0.48 | 1.42 | 0.69 | 0.31 |
| | | Salinity 22.5 * time | 1.07 | 0.64 | 1.57 | 0.38 | 0.62 |
| | | Salinity 10 * time | 1.49 | 0.92 | 2.22 | 0.03 | 0.97 |
| *Sonneratia alba* | Beta | Intercept | 0.09 | 0.03 | 0.26 | 1 | 0 |
| | | Salinity 22.5 | 2.57 | 0.14 | 7.72 | 0.12 | 0.88 |
| | | Salinity 10 | 0.46 | 0.01 | 1.43 | 0.86 | 0.14 |
| | | Time | 0.71 | 0.17 | 1.66 | 0.75 | 0.25 |
| | | Salinity 22.5 * time | 0.15 | 0.03 | 0.44 | 1 | 0 |
| | | Salinity 10 * time | 0.2 | 0 | 4.21 | 0.81 | 0.19 |

# Appendix D. Supplementary information for Chapter 5

## Appendix D1. Urgency index assessment.

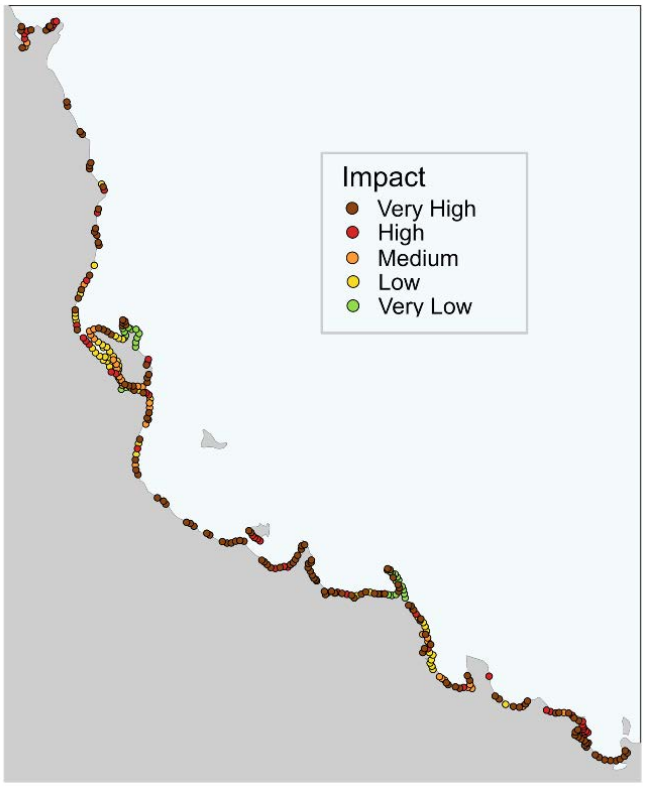


**Figure D1.1.** Impact status of mangrove areas, calculated using the Normalized Difference Vegetation Index (NDVI), highlighting variations in mangrove health across the study area.

**Table D1.1.** Urgency assessment for *Rhizophora stylosa*, including node number, latitude, longitude, manageable and unmanageable scores, combined objective score and variance across objectives.

| Node | Lat | Lon | Manageable | Unmanageable | All objectives | Node variance |
|---|---|---|---|---|---|---|
| 1 | -20.16 | 148.42 | 10 | 18 | 5 | 0.3 |
| 2 | -20.16 | 148.39 | 0 | 26 | 5 | 0.3 |
| 3 | -20.16 | 148.37 | 0 | 17 | 4 | 0 |
| 4 | -20.15 | 148.43 | 0 | 18 | 4 | 0 |
| 5 | -20.15 | 148.34 | 0 | 17 | 4 | 0 |
| 6 | -20.14 | 148.45 | 4 | 23 | 4 | 0 |
| 7 | -20.13 | 148.33 | 0 | 17 | 4 | 0 |
| 8 | -20.13 | 148.47 | 0 | 11 | 4 | 0 |
| 9 | -20.12 | 148.46 | 0 | 11 | 4 | 0 |
| 10 | -20.10 | 148.29 | 0 | 9 | 4 | 0 |
| 11 | -20.09 | 148.28 | 0 | 9 | 7 | 0.2 |
| 12 | -20.08 | 148.29 | 0 | 9 | 4 | 0 |
| 13 | -20.08 | 148.28 | 0 | 9 | 4 | 0 |
| 14 | -20.07 | 148.28 | 7 | 5 | 4 | 0 |

| | | | | | | |
|---|---|---|---|---|---|---|
| 15 | -20.06 | 148.26 | 7 | 5 | 4 | 0 |
| 16 | -20.05 | 148.25 | 7 | 5 | 4 | 0 |
| 17 | -20.05 | 148.24 | 7 | 5 | 5 | 0 |
| 18 | -20.04 | 148.28 | 7 | 5 | 4 | 0 |
| 19 | -20.03 | 148.29 | 7 | 5 | 4 | 0 |
| 20 | -20.03 | 148.28 | 15 | 4 | 4 | 0 |
| 21 | -20.03 | 148.24 | 15 | 4 | 7 | 0.5 |
| 22 | -20.03 | 148.28 | 15 | 4 | 4 | 0 |
| 23 | -20.02 | 148.26 | 15 | 4 | 4 | 0 |
| 24 | -20.02 | 148.25 | 15 | 4 | 7 | 0.5 |
| 25 | -20.02 | 148.27 | 15 | 4 | 4 | 0 |
| 26 | -20.01 | 148.27 | 15 | 4 | 4 | 0 |
| 27 | -20.01 | 148.27 | 15 | 4 | 4 | 0 |
| 28 | -20.00 | 148.27 | 15 | 4 | 4 | 0 |
| 29 | -19.99 | 148.27 | 15 | 4 | 4 | 0 |
| 30 | -19.98 | 148.25 | 8 | 8 | 4 | 0 |
| 31 | -19.97 | 148.23 | 8 | 8 | 4 | 0 |
| 32 | -19.96 | 148.22 | 8 | 8 | 4 | 0 |
| 33 | -19.95 | 148.21 | 3 | 20 | 5 | 0 |
| 34 | -19.95 | 148.15 | 4 | 30 | 5 | 0.3 |
| 35 | -19.95 | 148.19 | 4 | 30 | 5 | 0 |
| 36 | -19.95 | 148.16 | 4 | 30 | 4 | 0 |
| 37 | -19.94 | 148.12 | 4 | 30 | 4 | 0 |
| 38 | -19.94 | 148.11 | 4 | 30 | 4 | 0 |
| 39 | -19.92 | 147.99 | 12 | 9 | 7 | 0.3 |
| 40 | -19.92 | 147.96 | 12 | 9 | 5 | 0 |
| 41 | -19.92 | 148.00 | 12 | 9 | 4 | 0 |
| 42 | -19.91 | 147.93 | 9 | 17 | 10 | 0.2 |
| 43 | -19.91 | 148.01 | 12 | 9 | 4 | 0 |
| 44 | -19.89 | 148.02 | 8 | 14 | 4 | 0 |
| 45 | -19.89 | 147.90 | 3 | 17 | 4 | 0.5 |
| 46 | -19.87 | 147.88 | 3 | 17 | 8 | 0.3 |
| 47 | -19.84 | 147.78 | 0 | 4 | 4 | 0 |
| 48 | -19.84 | 147.72 | 4 | 7 | 4 | 0 |
| 49 | -19.83 | 147.74 | 0 | 7 | 5 | 0 |
| 50 | -19.83 | 147.76 | 0 | 7 | 4 | 0 |
| 51 | -19.83 | 147.70 | 4 | 7 | 4 | 0 |
| 52 | -19.82 | 147.67 | 8 | 4 | 5 | 0 |
| 53 | -19.82 | 147.77 | 1 | 2 | 5 | 0 |
| 54 | -19.81 | 147.66 | 14 | 7 | 8 | 0.3 |
| 55 | -19.80 | 147.77 | 0 | 4 | 5 | 0.3 |
| 56 | -19.80 | 147.65 | 14 | 7 | 4 | 0 |
| 57 | -19.79 | 147.64 | 14 | 7 | 4 | 0 |
| 58 | -19.79 | 147.63 | 14 | 7 | 4 | 0 |
| 59 | -19.78 | 147.85 | 5 | 21 | 4 | 0 |
| 60 | -19.78 | 147.76 | 0 | 4 | 4 | 0 |
| 61 | -19.75 | 147.60 | 0 | 9 | 4 | 0 |
| 62 | -19.74 | 147.60 | 0 | 9 | 4 | 0 |

| | | | | | | |
|---|---|---|---|---|---|---|
| 63 | -19.73 | 147.59 | 0 | 9 | 4 | 0 |
| 64 | -19.71 | 147.59 | 0 | 6 | 10 | 0.2 |
| 65 | -19.69 | 147.60 | 0 | 6 | 4 | 0 |
| 66 | -19.68 | 147.56 | 0 | 6 | 4 | 0 |
| 67 | -19.68 | 147.59 | 0 | 6 | 4 | 0 |
| 68 | -19.66 | 147.58 | 6 | 8 | 4 | 0 |
| 69 | -19.66 | 147.56 | 6 | 8 | 4 | 0 |
| 70 | -19.64 | 147.59 | 10 | 17 | 4 | 0 |
| 71 | -19.63 | 147.58 | 10 | 17 | 4 | 0 |
| 72 | -19.61 | 147.58 | 10 | 17 | 4 | 0 |
| 73 | -19.60 | 147.57 | 4 | 12 | 4 | 0 |
| 74 | -19.60 | 147.56 | 10 | 17 | 4 | 0 |
| 75 | -19.58 | 147.57 | 4 | 12 | 4 | 0 |
| 76 | -19.56 | 147.57 | 4 | 12 | 4 | 0.2 |
| 77 | -19.54 | 147.56 | 4 | 10 | 4 | 0 |
| 78 | -19.54 | 147.55 | 4 | 10 | 5 | 0 |
| 79 | -19.53 | 147.55 | 4 | 10 | 5 | 0.3 |
| 80 | -19.52 | 147.54 | 4 | 16 | 4 | 0 |
| 81 | -19.51 | 147.53 | 4 | 16 | 4 | 0 |
| 82 | -19.49 | 147.52 | 4 | 16 | 4 | 0 |
| 83 | -19.49 | 147.51 | 16 | 12 | 4 | 0 |
| 84 | -19.47 | 147.50 | 16 | 12 | 4 | 0 |
| 85 | -19.47 | 147.49 | 16 | 12 | 4 | 0 |
| 86 | -19.44 | 147.25 | 8 | 23 | 5 | 0 |
| 87 | -19.43 | 147.48 | 17 | 8 | 4 | 0 |
| 88 | -19.43 | 147.26 | 6 | 18 | 4 | 0 |
| 89 | -19.42 | 147.42 | 5 | 21 | 5 | 0 |
| 90 | -19.42 | 147.24 | 8 | 23 | 4 | 0 |
| 91 | -19.42 | 147.40 | 5 | 21 | 4 | 0 |
| 92 | -19.42 | 147.12 | 0 | 12 | 4 | 0 |
| 93 | -19.42 | 147.44 | 5 | 14 | 4 | 0 |
| 94 | -19.42 | 147.22 | 8 | 26 | 4 | 0 |
| 95 | -19.42 | 147.28 | 4 | 22 | 5 | 0 |
| 96 | -19.42 | 147.36 | 4 | 22 | 4 | 0 |
| 97 | -19.42 | 147.37 | 5 | 21 | 4 | 0 |
| 98 | -19.42 | 147.39 | 5 | 21 | 4 | 0 |
| 99 | -19.42 | 147.47 | 17 | 8 | 4 | 0 |
| 100 | -19.42 | 147.34 | 4 | 22 | 4 | 0 |
| 101 | -19.41 | 147.20 | 8 | 26 | 5 | 0 |
| 102 | -19.41 | 147.17 | 8 | 32 | 4 | 0 |
| 103 | -19.41 | 147.13 | 8 | 32 | 4 | 0.2 |
| 104 | -19.41 | 147.32 | 4 | 22 | 4 | 0 |
| 105 | -19.41 | 147.18 | 8 | 32 | 5 | 0 |
| 106 | -19.41 | 147.30 | 4 | 22 | 4 | 0 |
| 107 | -19.41 | 147.45 | 5 | 14 | 6 | 0.2 |
| 108 | -19.41 | 147.12 | 7 | 15 | 4 | 0 |
| 109 | -19.41 | 147.15 | 8 | 32 | 4 | 0 |
| 110 | -19.40 | 147.47 | 17 | 8 | 4 | 0 |

| | | | | | | |
|---|---|---|---|---|---|---|
| 111 | -19.39 | 147.45 | 5 | 14 | 5 | 0 |
| 112 | -19.38 | 147.46 | 7 | 14 | 5 | 0 |
| 113 | -19.38 | 147.45 | 0 | 20 | 4 | 0 |
| 114 | -19.36 | 147.44 | 0 | 20 | 4 | 0 |
| 115 | -19.36 | 147.08 | 7 | 15 | 4 | 0 |
| 116 | -19.36 | 147.45 | 7 | 14 | 4 | 0 |
| 117 | -19.35 | 147.08 | 7 | 15 | 4 | 0 |
| 118 | -19.35 | 147.08 | 7 | 15 | 4 | 0 |
| 119 | -19.35 | 147.07 | 7 | 15 | 4 | 0 |
| 120 | -19.34 | 147.43 | 0 | 20 | 4 | 0 |
| 121 | -19.34 | 147.44 | 7 | 14 | 4 | 0 |
| 122 | -19.33 | 147.06 | 7 | 15 | 5 | 0 |
| 123 | -19.33 | 147.43 | 7 | 14 | 4 | 0 |
| 124 | -19.32 | 147.42 | 2 | 16 | 4 | 0 |
| 125 | -19.32 | 147.41 | 2 | 16 | 4 | 0 |
| 126 | -19.32 | 147.06 | 0 | 12 | 5 | 0 |
| 127 | -19.31 | 147.40 | 2 | 16 | 4 | 0 |
| 128 | -19.31 | 147.41 | 2 | 16 | 4 | 0 |
| 129 | -19.30 | 147.40 | 2 | 16 | 6 | 0.2 |
| 130 | -19.30 | 146.90 | 7 | 14 | 5 | 0.3 |
| 131 | -19.30 | 147.05 | 0 | 12 | 7 | 0.5 |
| 132 | -19.30 | 146.88 | 7 | 14 | 4 | 0 |
| 133 | -19.30 | 146.92 | 7 | 14 | 4 | 0 |
| 134 | -19.30 | 146.96 | 7 | 15 | 4 | 0 |
| 135 | -19.29 | 146.94 | 7 | 16 | 4 | 0 |
| 136 | -19.29 | 146.97 | 7 | 15 | 5 | 0 |
| 137 | -19.29 | 146.86 | 17 | 23 | 4 | 0 |
| 138 | -19.28 | 147.05 | 0 | 12 | 10 | 0.3 |
| 139 | -19.28 | 146.98 | 7 | 15 | 5 | 0 |
| 140 | -19.28 | 147.06 | 0 | 12 | 4 | 0.5 |
| 141 | -19.27 | 146.85 | 17 | 23 | 4 | 0.5 |
| 142 | -19.27 | 146.84 | 20 | 4 | 4 | 0 |
| 143 | -19.27 | 147.06 | 0 | 12 | 4 | 0 |
| 144 | -19.26 | 146.99 | 0 | 7 | 4 | 0 |
| 145 | -19.25 | 147.00 | 0 | 7 | 4 | 0 |
| 146 | -19.22 | 147.02 | 0 | 7 | 4 | 0 |
| 147 | -19.20 | 147.02 | 0 | 7 | 4 | 0 |
| 148 | -19.20 | 147.03 | 0 | 7 | 4 | 0 |
| 149 | -19.19 | 146.69 | 0 | 5 | 4 | 0.5 |
| 150 | -19.19 | 146.70 | 0 | 5 | 5 | 0 |
| 151 | -19.18 | 146.66 | 6 | 4 | 4 | 0 |
| 152 | -19.18 | 146.76 | 0 | 6 | 4 | 0 |
| 153 | -19.18 | 146.72 | 0 | 15 | 4 | 0 |
| 154 | -19.18 | 146.83 | 0 | 6 | 5 | 0 |
| 155 | -19.18 | 146.74 | 0 | 15 | 4 | 0 |
| 156 | -19.17 | 146.82 | 0 | 6 | 5 | 0 |
| 157 | -19.17 | 146.81 | 0 | 6 | 5 | 0 |
| 158 | -19.16 | 146.80 | 0 | 6 | 4 | 0 |

| | | | | | | |
|---|---|---|---|---|---|---|
| 159 | -19.15 | 146.61 | 9 | 4 | 4 | 0 |
| 160 | -19.15 | 146.60 | 9 | 4 | 4 | 0 |
| 161 | -19.14 | 146.79 | 0 | 6 | 4 | 0 |
| 162 | -19.14 | 146.78 | 0 | 6 | 4 | 0 |
| 163 | -19.12 | 146.54 | 0 | 8 | 5 | 0 |
| 164 | -19.10 | 146.52 | 0 | 8 | 4 | 0 |
| 165 | -19.10 | 146.50 | 4 | 3 | 4 | 0 |
| 166 | -19.02 | 146.41 | 5 | 4 | 4 | 0 |
| 167 | -19.00 | 146.40 | 5 | 4 | 4 | 0 |
| 168 | -18.99 | 146.38 | 5 | 4 | 4 | 0 |
| 169 | -18.88 | 146.29 | 3 | 9 | 5 | 0 |
| 170 | -18.86 | 146.28 | 3 | 9 | 6 | 0.3 |
| 171 | -18.84 | 146.28 | 0 | 9 | 6 | 0.3 |
| 172 | -18.82 | 146.28 | 0 | 9 | 8 | 0.3 |
| 173 | -18.79 | 146.28 | 0 | 9 | 6 | 0.3 |
| 174 | -18.77 | 146.29 | 0 | 9 | 7 | 0.5 |
| 175 | -18.75 | 146.29 | 5 | 4 | 4 | 0 |
| 176 | -18.73 | 146.30 | 8 | 4 | 4 | 0 |
| 177 | -18.66 | 146.32 | 9 | 0 | 5 | 0 |
| 178 | -18.64 | 146.33 | 9 | 0 | 5 | 0 |
| 179 | -18.63 | 146.33 | 9 | 0 | 6 | 0.3 |
| 180 | -18.61 | 146.34 | 10 | 14 | 10 | 0.3 |
| 181 | -18.59 | 146.34 | 3 | 9 | 6 | 0.3 |
| 182 | -18.57 | 146.34 | 10 | 8 | 10 | 0.5 |
| 183 | -18.55 | 146.34 | 10 | 8 | 4 | 0 |
| 184 | -18.53 | 146.34 | 13 | 7 | 4 | 0 |
| 185 | -18.52 | 146.33 | 13 | 7 | 4 | 0 |
| 186 | -18.52 | 146.31 | 6 | 8 | 6 | 0.3 |
| 187 | -18.51 | 146.27 | 3 | 8 | 7 | 0.2 |
| 188 | -18.51 | 146.29 | 6 | 8 | 4 | 0 |
| 189 | -18.50 | 146.22 | 6 | 10 | 13 | 0.2 |
| 190 | -18.50 | 146.26 | 3 | 8 | 4 | 0 |
| 191 | -18.49 | 146.24 | 0 | 14 | 5 | 0 |
| 192 | -18.49 | 146.31 | 0 | 5 | 6 | 0.2 |
| 193 | -18.49 | 146.29 | 0 | 5 | 6 | 0.2 |
| 194 | -18.49 | 146.27 | 0 | 5 | 7 | 0.2 |
| 195 | -18.49 | 146.25 | 0 | 5 | 6 | 0.3 |
| 196 | -18.49 | 146.22 | 6 | 10 | 9 | 0.2 |
| 197 | -18.48 | 146.23 | 0 | 5 | 13 | 0.3 |
| 198 | -18.48 | 146.22 | 0 | 6 | 11 | 0.8 |
| 199 | -18.47 | 146.33 | 0 | 5 | 8 | 0.3 |
| 200 | -18.47 | 146.21 | 0 | 7 | 13 | 0.5 |
| 201 | -18.46 | 146.22 | 0 | 6 | 9 | 0.5 |
| 202 | -18.45 | 146.33 | 0 | 5 | 8 | 0.3 |
| 203 | -18.45 | 146.20 | 0 | 7 | 7 | 0.2 |
| 204 | -18.45 | 146.21 | 0 | 6 | 6 | 0.3 |
| 205 | -18.44 | 146.34 | 0 | 5 | 6 | 0.3 |
| 206 | -18.44 | 146.19 | 0 | 10 | 20 | 0 |

| | | | | | | |
|---|---|---|---|---|---|---|
| 207 | -18.43 | 146.20 | 0 | 10 | 10 | 0.2 |
| 208 | -18.43 | 146.17 | 0 | 10 | 12 | 0.2 |
| 209 | -18.42 | 146.20 | 0 | 10 | 9 | 0.2 |
| 210 | -18.41 | 146.20 | 0 | 10 | 9 | 0.2 |
| 211 | -18.40 | 146.16 | 0 | 16 | 10 | 0.7 |
| 212 | -18.40 | 146.20 | 0 | 10 | 7 | 0.5 |
| 213 | -18.40 | 146.33 | 0 | 5 | 6 | 0.2 |
| 214 | -18.39 | 146.19 | 0 | 16 | 10 | 0.8 |
| 215 | -18.39 | 146.33 | 0 | 5 | 6 | 0.3 |
| 216 | -18.38 | 146.15 | 0 | 16 | 11 | 0.2 |
| 217 | -18.38 | 146.20 | 0 | 10 | 7 | 0.5 |
| 218 | -18.37 | 146.13 | 0 | 16 | 8 | 0.3 |
| 219 | -18.37 | 146.18 | 0 | 16 | 7 | 0.2 |
| 220 | -18.37 | 146.34 | 0 | 5 | 5 | 0 |
| 221 | -18.36 | 146.16 | 0 | 16 | 8 | 0.8 |
| 222 | -18.36 | 146.14 | 0 | 16 | 8 | 0.8 |
| 223 | -18.36 | 146.18 | 0 | 10 | 7 | 0.8 |
| 224 | -18.36 | 146.12 | 0 | 19 | 9 | 0.3 |
| 225 | -18.34 | 146.10 | 4 | 19 | 8 | 0.3 |
| 226 | -18.34 | 146.16 | 0 | 10 | 6 | 0.2 |
| 227 | -18.32 | 146.09 | 4 | 19 | 8 | 0 |
| 228 | -18.32 | 146.13 | 0 | 10 | 4 | 0 |
| 229 | -18.32 | 146.15 | 0 | 10 | 6 | 0.2 |
| 230 | -18.32 | 146.28 | 0 | 10 | 4 | 0 |
| 231 | -18.31 | 146.13 | 0 | 10 | 5 | 0 |
| 232 | -18.30 | 146.07 | 10 | 23 | 7 | 0.2 |
| 233 | -18.30 | 146.28 | 0 | 10 | 4 | 0 |
| 234 | -18.29 | 146.11 | 0 | 5 | 5 | 0 |
| 235 | -18.29 | 146.06 | 10 | 23 | 6 | 0.3 |
| 236 | -18.28 | 146.22 | 0 | 3 | 9 | 0.2 |
| 237 | -18.28 | 146.09 | 0 | 5 | 5 | 0 |
| 238 | -18.28 | 146.20 | 0 | 3 | 5 | 0 |
| 239 | -18.28 | 146.05 | 10 | 23 | 6 | 0.3 |
| 240 | -18.28 | 146.23 | 0 | 3 | 4 | 0 |
| 241 | -18.28 | 146.29 | 0 | 3 | 4 | 0 |
| 242 | -18.27 | 146.19 | 0 | 3 | 4 | 0 |
| 243 | -18.26 | 146.23 | 0 | 3 | 4 | 0 |
| 244 | -18.26 | 146.08 | 8 | 10 | 5 | 0 |
| 245 | -18.26 | 146.17 | 0 | 3 | 4 | 0 |
| 246 | -18.26 | 146.29 | 0 | 3 | 4 | 0 |
| 247 | -18.25 | 146.23 | 0 | 3 | 4 | 0 |
| 248 | -18.25 | 146.15 | 0 | 3 | 4 | 0 |
| 249 | -18.25 | 146.07 | 8 | 10 | 5 | 0 |
| 250 | -18.24 | 146.02 | 14 | 19 | 8 | 0.3 |
| 251 | -18.24 | 146.13 | 0 | 3 | 4 | 0 |
| 252 | -18.24 | 146.26 | 0 | 3 | 4 | 0 |
| 253 | -18.24 | 146.28 | 0 | 3 | 4 | 0 |
| 254 | -18.24 | 146.09 | 5 | 12 | 5 | 0 |

| | | | | | | |
|---|---|---|---|---|---|---|
| 255 | -18.23 | 146.22 | 0 | 3 | 4 | 0 |
| 256 | -18.23 | 146.11 | 5 | 12 | 5 | 0 |
| 257 | -18.23 | 146.25 | 0 | 3 | 4 | 0 |
| 258 | -18.22 | 146.22 | 0 | 3 | 5 | 0 |
| 259 | -18.22 | 146.02 | 5 | 16 | 7 | 0.5 |
| 260 | -18.22 | 146.23 | 0 | 3 | 5 | 0 |
| 261 | -18.21 | 146.22 | 0 | 3 | 5 | 0 |
| 262 | -18.20 | 146.23 | 0 | 3 | 6 | 0.3 |
| 263 | -18.20 | 146.01 | 5 | 16 | 6 | 0.3 |
| 264 | -18.20 | 146.22 | 0 | 3 | 7 | 0.5 |
| 265 | -18.18 | 146.01 | 5 | 16 | 6 | 0.3 |
| 266 | -18.17 | 146.01 | 5 | 16 | 6 | 0.3 |
| 267 | -18.15 | 146.01 | 5 | 16 | 6 | 0.3 |
| 268 | -18.10 | 146.02 | 5 | 16 | 8 | 0.3 |
| 269 | -18.08 | 146.03 | 5 | 16 | 8 | 0.3 |
| 270 | -18.06 | 146.04 | 5 | 16 | 8 | 0.3 |
| 271 | -18.04 | 146.05 | 0 | 4 | 10 | 1.2 |
| 272 | -18.02 | 146.06 | 0 | 4 | 10 | 1.2 |
| 273 | -18.00 | 146.07 | 0 | 4 | 11 | 0.7 |
| 274 | -17.95 | 146.09 | 0 | 4 | 4 | 0 |
| 275 | -17.86 | 146.12 | 0 | 4 | 6 | 0.3 |
| 276 | -17.85 | 146.11 | 0 | 4 | 5 | 0 |
| 277 | -17.82 | 146.11 | 0 | 4 | 4 | 0 |
| 278 | -17.80 | 146.10 | 0 | 4 | 5 | 0 |
| 279 | -17.79 | 146.10 | 0 | 4 | 6 | 0.3 |
| 280 | -17.72 | 146.11 | 0 | 10 | 6 | 0.3 |
| 281 | -17.70 | 146.11 | 0 | 10 | 8 | 0.3 |
| 282 | -17.62 | 146.14 | 0 | 10 | 4 | 0 |
| 283 | -17.60 | 146.13 | 0 | 10 | 5 | 0.3 |
| 284 | -17.59 | 146.13 | 10 | 2 | 5 | 0.3 |
| 285 | -17.52 | 146.07 | 12 | 4 | 4 | 0 |
| 286 | -17.51 | 146.07 | 16 | 0 | 5 | 0 |
| 287 | -17.49 | 146.08 | 16 | 0 | 4 | 0 |
| 288 | -17.37 | 146.04 | 10 | 0 | 4 | 0 |
| 289 | -17.36 | 146.03 | 0 | 1 | 4 | 0 |
| 290 | -17.24 | 145.98 | 5 | 3 | 4 | 0 |
| 291 | -17.22 | 145.97 | 5 | 3 | 5 | 0.3 |
| 292 | -16.98 | 145.77 | 17 | 10 | 10 | 0.3 |
| 293 | -16.98 | 145.79 | 17 | 10 | 10 | 0.3 |
| 294 | -16.96 | 145.79 | 16 | 8 | 6 | 0.3 |
| 295 | -16.94 | 145.78 | 17 | 10 | 4 | 0 |
| 296 | -16.92 | 145.78 | 13 | 0 | 5 | 0 |
| 297 | -16.91 | 145.80 | 4 | 10 | 4 | 0 |
| 298 | -16.91 | 145.77 | 0 | 4 | 4 | 0 |
| 299 | -16.90 | 145.88 | 0 | 7 | 4 | 0 |
| 300 | -16.90 | 145.81 | 4 | 10 | 6 | 0.2 |
| 301 | -16.90 | 145.89 | 10 | 15 | 4 | 0 |
| 302 | -16.89 | 145.90 | 0 | 7 | 5 | 0.3 |

| | | | | | | |
|---|---|---|---|---|---|---|
| 303 | -16.89 | 145.77 | 0 | 4 | 7 | 0.5 |
| 304 | -16.89 | 145.89 | 10 | 15 | 4 | 0 |
| 305 | -16.89 | 145.90 | 0 | 7 | 4 | 0 |
| 306 | -16.88 | 145.91 | 0 | 13 | 4 | 0 |
| 307 | -16.87 | 145.92 | 0 | 13 | 4 | 0 |
| 308 | -16.86 | 145.93 | 0 | 13 | 4 | 0 |

**Table D1.2**. Urgency assessment for *Bruguiera gymnorhiza*, including node number, latitude, longitude, manageable and unmanageable scores, combined objective score and variance across objectives.

| Node | Lat | Lon | Manageable | Unmanageable | All objectives | Node variance |
|---|---|---|---|---|---|---|
| 1 | -18.64 | 146.32 | 10 | 18 | 5 | 0 |
| 2 | -18.64 | 146.33 | 0 | 26 | 4 | 0 |
| 3 | -18.64 | 146.33 | 0 | 17 | 4 | 0 |
| 4 | -18.54 | 146.34 | 0 | 18 | 4 | 0 |
| 5 | -18.52 | 146.33 | 0 | 17 | 5 | 0 |
| 6 | -18.52 | 146.31 | 4 | 23 | 10 | 0.5 |
| 7 | -18.51 | 146.21 | 0 | 17 | 4 | 0 |
| 8 | -18.51 | 146.27 | 0 | 11 | 7 | 0.2 |
| 9 | -18.51 | 146.29 | 0 | 11 | 5 | 0 |
| 10 | -18.50 | 146.26 | 0 | 9 | 7 | 0.2 |
| 11 | -18.50 | 146.23 | 0 | 9 | 4 | 0 |
| 12 | -18.49 | 146.30 | 0 | 9 | 4 | 0 |
| 13 | -18.49 | 146.24 | 0 | 9 | 5 | 0 |
| 14 | -18.49 | 146.28 | 7 | 5 | 5 | 0 |
| 15 | -18.49 | 146.26 | 7 | 5 | 4 | 0 |
| 16 | -18.49 | 146.24 | 7 | 5 | 5 | 0 |
| 17 | -18.24 | 146.02 | 7 | 5 | 9 | 0.2 |
| 18 | -18.22 | 146.02 | 7 | 5 | 7 | 0.2 |
| 19 | -18.20 | 146.01 | 7 | 5 | 10 | 0.2 |
| 20 | -18.18 | 146.01 | 15 | 4 | 10 | 0.2 |
| 21 | -18.16 | 146.01 | 15 | 4 | 8 | 0 |
| 22 | -18.15 | 146.01 | 15 | 4 | 7 | 0.2 |
| 23 | -18.10 | 146.02 | 15 | 4 | 11 | 0.7 |
| 24 | -18.08 | 146.03 | 15 | 4 | 11 | 0.7 |
| 25 | -18.06 | 146.04 | 15 | 4 | 8 | 0 |
| 26 | -18.05 | 146.04 | 15 | 4 | 17 | 0.3 |
| 27 | -18.03 | 146.06 | 15 | 4 | 16 | 0.3 |
| 28 | -18.01 | 146.06 | 15 | 4 | 18 | 0 |
| 29 | -17.99 | 146.07 | 15 | 4 | 18 | 0.3 |
| 30 | -17.80 | 146.09 | 8 | 8 | 5 | 0 |
| 31 | -17.79 | 146.10 | 8 | 8 | 4 | 0 |
| 32 | -17.73 | 146.11 | 8 | 8 | 7 | 0.7 |
| 33 | -17.72 | 146.11 | 3 | 20 | 5 | 0 |
| 34 | -17.71 | 146.11 | 4 | 30 | 7 | 0.7 |
| 35 | -17.70 | 146.11 | 4 | 30 | 4 | 0 |
| 36 | -17.52 | 146.07 | 4 | 30 | 4 | 0 |

| | | | | | | |
|---|---|---|---|---|---|---|
| 37 | -17.51 | 146.07 | 4 | 30 | 4 | 0 |
| 38 | -17.49 | 146.08 | 4 | 30 | 4 | 0 |
| 39 | -16.99 | 145.78 | 12 | 9 | 8 | 0 |
| 40 | -16.98 | 145.79 | 12 | 9 | 12 | 0.3 |
| 41 | -16.98 | 145.77 | 12 | 9 | 8 | 0 |
| 42 | -16.97 | 145.79 | 9 | 17 | 6 | 0.3 |
| 43 | -16.96 | 145.80 | 12 | 9 | 5 | 0 |
| 44 | -16.95 | 145.79 | 8 | 14 | 5 | 0 |
| 45 | -16.94 | 145.78 | 3 | 17 | 5 | 0 |
| 46 | -16.90 | 145.88 | 3 | 17 | 4 | 0 |
| 47 | -16.90 | 145.89 | 0 | 4 | 4 | 0 |
| 48 | -16.89 | 145.90 | 4 | 7 | 4 | 0.2 |
| 49 | -16.88 | 145.78 | 0 | 7 | 7 | 0 |
| 50 | -16.87 | 145.78 | 0 | 7 | 4 | 0 |
| 51 | -16.86 | 145.77 | 4 | 7 | 4 | 0 |
| 52 | -16.86 | 145.77 | 8 | 4 | 5 | 0.3 |
| 53 | -16.86 | 145.76 | 1 | 2 | 4 | 0 |
| 54 | -16.85 | 145.75 | 14 | 7 | 4 | 0.3 |

# Publications produced during my PhD candidature

**Publications**

Thompson-Saud, G., Grech, A., Choukroun, S., Vásquez, S. I., Salas, C., & Ospina-Alvarez, A. (2024). The biophysical dynamics of giant kelp, *Macrocystis pyrifera*: Seasonal patterns and dispersal mechanisms in the southeast Pacific. *Journal of Biogeography*, 51(11), 2198-2210. https://doi.org/10.1111/jbi.14980

Thompson-Saud, G., Grech, A., Choukroun, S., Vásquez, S. I., & Ospina-Alvarez, A. (2025). Incorporating giant kelp connectivity into management strategies in the southeast Pacific. Ocean & Coastal Management, 266, 107661. https://doi.org/10.1016/j.ocecoaman.2025.107661

Thompson-Saud, G., Robertson, A. I., Choukroun, Ospina-Alvarez, Logan, M & A. Grech, A. Factors influencing the early growth and dispersal potential of mangrove propagules. (Under review in *Regional Studies in Marine Science*).

Thompson-Saud, A. I., Choukroun, Hanuise, D., Canning, A., Ospina-Alvarez, & A. Grech, A. Operationalising connectivity in the spatial management of mangroves. (Target journal *Global Change Biology*).

**Conference presentation**

Thompson-Saud, G., (2022). Mangrove propagules dispersal and connectivity in the Great Barrier Reef. AMSA. Cairns, Queensland, Australia.

Thompson-Saud, G., (2022). Connectivity dynamics of giant kelp, *Macrocystis pyrifera*, in the southeast Pacific. IMEDEA. Esporles, Mallorca, Spain.

Thompson-Saud, G., (2023). Understanding the influence of propagule transport on the dispersal and connectivity of giant kelp, *Macrocystis pyrifera*, in the Southeast Pacific region. Conservation Biology. Kigali, Rwanda.

Thompson-Saud, G., (2024). Informing the prioritisation of mangrove management in the central Great Barrier Reef using biophysical modelling and network analysis. Australasian Saltmarsh and Mangrove Network Conference. Brisbane, Australia.